

Interfacial Activity of Star Polymers at Fluid Interfaces

Submitted in partial fulfillment of the requirements for

the degree of

Doctor of Philosophy

in

Chemical Engineering

Yun-Ru Huang

B.S., Chemical Engineering, National Taiwan University

M.S., Chemical and Biomolecular Engineering, University of Pennsylvania

Carnegie Mellon University
Pittsburgh, PA

December, 2018

© Yun-Ru Huang, 2018

All Rights Reserved

Acknowledgements

I owe my gratitude to many people who have helped me make this thesis a reality and this journey possible in the last few years.

First and foremost, I would like to express my appreciation to my thesis advisor, Professor Robert Tilton, for his relentless guidance and constant support throughout my graduate career. Bob has pushed me to achieve my full potential and inspired me to be a better researcher. One of the many things that he taught me when I just began my PhD was to never forget the big picture when I focus on the smallest detail of my research. Today I still find this piece of advice useful and applicable to many aspects of my life.

I sincerely thank my thesis committee members, Professor Lynn Walker, Professor James Schneider, Professor Todd Pyzybycien, and Professor Steve Garoff, for their insightful comments and constructive input to my work during the proposal exam and thesis defense. I would especially like to thank Steve for all of the discussions and suggestions that he has provided in our joint group meetings.

This work would not be possible without the collaboration with Professor Krzysztof Matyjaszewski's research group at CMU. Special thanks to Melissa Lamson and Yi Wang for providing well-synthesized star polymers. I owe a lot of my understanding of polymer synthesis to Melissa and benefit immensely from our interactions.

I am extremely grateful to work with a lot of talented colleagues both past and present in Tilton group. Many have influenced my life at CMU, but I particularly want to thank those whom I am fortunate to closely work with. Thanks to Alex Bertuccio, Brittany Nordmark,

Steven Iasella and Danish Iqbal for helping me get through some of the most stressful times during my graduate study. I have enjoyed all the great conversations (both scientific and non-scientific) we had, and appreciate the assistance and support that they have given to me along the way. Thanks to John Riley for being a great source of advice and helping me to start my laboratory work in my first year. Thanks to Amy Stetten, Ramankur Sharma, and Gunnar Duner for their help with getting me acquainted with the lab and graduate student life. Thanks to Bhagyashree Lele, Tsung-Lin Hsieh, Jingyi Pan and Henry Chu for all of the helpful conversations and for providing useful ideas towards the end of my study.

I am also thankful to all of the friendships that I have gained in the Department of Chemical Engineering. In particular, I would like to graciously acknowledge a few friends for making this journey far more pleasant. Thanks to Qin Gu for her support and feedback whenever I needed it. I have enjoyed all of the memories and adventures we had together in the past few years. Thanks to Pablo Garcia for his encouragement and sharing his “elder” wisdom. I always find our conversations interesting and inspiring (and maybe sometimes lengthy). Thanks to Ben Sauk and Michael Davidson for being fantastic friends. I cherish all of the wonderful times we have spent together exploring Pittsburgh and doing fun activities. Thanks to Xiaoxiao Yu and Akang Wang for being caring and loyal friends. I have enjoyed all of the fun events they have organized and introduced me into. Additional thanks go to Zixi Zhao, Burcu Karagoz, Nick Lamson, Kal Hajj, Chris Hanselman, Yajun Wang, Raj Sengupta, Bruce Yan, Naser Mahfouz, Kathy Fein, Charles Sharkey, Randy Gamble, Irem Sen, Steph Kirby, Travis Armiger, Blake Bleier and Justin Weinberg with whom I have fully enjoyed our interactions and from whom I have learned so much.

I would like to thank my Taiwanese friends in the Department of Physics and Statistics, Yen-Chi Chen, Hsiu-Hsien Lin, Hung-Jing Huang, Abel Sun, Chien-Hao Lin, Kuan-Wei Huang, and Yao-Yuan Mao. They are genuine and amazing friends who have helped ease my homesickness during my stay at CMU. I appreciate all of the conversations and the gatherings we have had in the past four years. I am also thankful to one of my closest undergrad friends, Hao Liu, for always being there to comfort me whenever I felt overwhelmed at work or with my life.

Above and beyond all, my words fail in truly expressing my gratitude to my parents for their unconditional love and sacrifice. Without their constant encouragement and persistent support, it would not have been possible to pursue my PhD abroad, let alone finish it. I also thank my sister, Yun-Wen, for her constant love, feedback and companionship through the good and the bad. I have enjoyed all of our late night secret sharing conversations and the great advice she has provided to me while growing up. Finally, if I could only pick one phrase to summarize my work after all these years of education and learning, it will be, “The more I learn, the more I realize how much I do not know.” I therefore dedicate this thesis to the memory of my grandfather, who never had a chance to go to school, but firmly believed in the power of education.

I would also like to thank my funding sources: the National Science Foundation under Grant CBET-1332836, the Carnegie Mellon University Department of Chemical Engineering and a PPG Graduate Fellowship. Thank you for your financial support for this research.

Abstract

This dissertation investigates the effect of composition and architecture of star polymers on their fundamental interfacial behavior at fluid interfaces and determines the contributions of important interfacial activity to the high foaming and emulsifying efficiency of star polymers. Star polymers are a novel class of surface active materials with a dense polymeric core and emanating polymer arms. Star polymers developed in this work are synthesized *via* atom transfer radical polymerization (ATRP) and are shown to be efficient foam and emulsion stabilizers. Three important dynamic interfacial processes: interfacial tension reduction, dynamic dilatational modulus and extent of adsorption are examined for star polymers with various structures and chemistries at air/water, xylene/water and cyclohexane/water interfaces. Adsorption on planar interfaces was monitored by ellipsometry, while interfacial tension and dilatational elasticity were measured separately by pendant drop tensiometry. Star polymers strongly reduce the interfacial tension, produce significant dynamic dilatational modulus and extent of adsorption due to the compact structure of star polymers compared to their linear counterparts. More mass is introduced per unit area of interface, and more interfacial penetration is achieved, upon their adsorption than for adsorption of linear polymers that adopt the conformation of loops, trains and tails. Star polymers with polyelectrolyte arms show pH-responsive interfacial behavior. The lateral electrostatic repulsions between the charged star polymers decrease the surface coverage but also enhance emulsion stability. Dynamic dilatational modulus and the ability of the star polymer adsorbed layer to resist ejection from the interface are identified to be correlated with high foaming and emulsifying efficiency. Finally, factors affecting the formation and stability of nanoemulsions stabilized by star polymers are examined.

Table of Contents

Acknowledgements	iii
Abstract	vi
Table of Contents	vii
List of Tables	x
List of Figures	xiii
1 Introduction	1
1.1 Motivation	1
1.2 Dissertation objectives	4
1.3 Outline of dissertation	5
1.4 Background	7
1.4.1 Emulsion classification – Macro-, nano- and microemulsions	7
1.4.2 Pickering emulsions	9
1.4.3 Nanoemulsions	12
1.4.4 Spontaneous emulsification	14
1.4.5 Interfacial tension reduction	15
1.4.6 Dilatational modulus	16
1.4.7 Polymer adsorption at fluid interfaces	18
2 Materials and Methods	21
2.1 Polymer brush nanoparticles	21
2.1.1 Multi-arm PEO star polymers	21
2.1.2 β -cyclodextrin core star polymers	21
2.2 Linear polymers, surfactants and solvents	23
2.3 Experimental methods and techniques	23
2.3.1 Foaming and emulsification	24
2.3.2 Pendant drop tensiometry	24
2.3.3 du Noüy ring tensiometry	29
2.3.4 Ellipsometry	30
2.3.5 Light scattering	32
3 Interfacial activity of PEO star polymers at fluid interfaces	35
3.1 Introduction	35
3.2 Linear PEO and PEO star polymers characterization	36

3.3	Interfacial behavior at air/water interface	37
3.3.1	Foaming efficiency and stability.....	37
3.3.2	Interfacial tension reduction	38
3.3.3	Dynamic dilatational elasticity	40
3.3.4	Large amplitude surface compression and expansion	45
3.3.5	Extent of adsorption.....	46
3.4	Interfacial behavior at oil/water interfaces.....	52
3.4.1	Emulsification efficiency and stability	52
3.4.2	Interfacial tension reduction	52
3.4.3	Dynamic dilatational elasticity	54
3.4.4	Large amplitude interfacial compression and expansion.....	59
3.4.5	Extent of adsorption.....	61
3.4.6	Path-dependent adsorption.....	62
3.5	Spontaneous emulsification with multi-arm PEO star polymers	66
3.6	Partition coefficient for PEO between xylene and water	70
3.7	Analysis for ellipsometric determination of surface excess concentration	72
3.8	Conclusions	75
4	Interfacial activity of β -cyclodextrin core star polymers at fluid interfaces.....	79
4.1	Introduction	79
4.2	β -cyclodextrin core star polymers characterization	80
4.3	Interfacial behavior at air/water interface	82
4.3.1	Foaming efficiency and stability.....	82
4.3.2	Surface tension reduction.....	83
4.3.3	Dynamic dilatational elasticity	87
4.3.4	Extent of adsorption.....	91
4.4	Interfacial behavior at oil/water interface	99
4.4.1	Emulsification efficiency and stability	99
4.4.2	Interfacial tension reduction	104
4.4.3	Dynamic dilatational elasticity	109
4.5	Conclusions	136
5	Nanoemulsion formation by spontaneous emulsification with star polymers.....	139
5.1	Introduction	139

5.2	Emulsion preparation methods.....	140
5.2.1	Nanoemulsions prepared by quiescent conditions.....	140
5.2.2	Macroemulsions prepared by high shear homogenization.....	141
5.3	PMEO ₂ MA star-stabilized nanoemulsions.....	141
5.4	Factors affecting nanoemulsion droplet size.....	144
5.4.1	Effect of temperature on nanoemulsion droplet size	144
5.4.2	Effect of polymer concentration on nanoemulsion droplet size	148
5.4.3	Effect of water volume fraction on nanoemulsion droplet size	150
5.5	Macroemulsions “break” into nanoemulsions.....	152
5.5.1	PMEO ₂ MA star polymers as emulsifiers.....	152
5.5.2	Triton X-100 as emulsifiers	157
5.6	Path-dependent PME ₂ MA star-stabilized nanoemulsions.....	158
5.7	Conclusions	162
6	Conclusions and future work.....	164
6.1	Summary of observations.....	164
6.2	Original contributions	166
6.3	Future work	167
6.3.1	Neutron scattering characterization of emulsions stabilized by star polymers.....	167
6.3.2	Interfacial exchange dynamics.....	168
	References.....	170

List of Tables

Table 1.1. Comparison of macroemulsions, nanoemulsions (also referred to as miniemulsions) and microemulsions with respect to size, shape, stability, method of preparation, polydispersity, and appearance. Nanoemulsions and microemulsions have a larger surface area per unit volume than macroemulsions because of their size. In addition, due to a strong kinetic stability, nanoemulsions are less sensitive to physical and chemical changes. Table is adapted from <i>Soft Matter</i> (2011) ³⁹ and <i>Soft Matter</i> (2016). ⁴⁷	8
Table 1.2. Differences between nanoemulsions and microemulsions	14
Table 2.1. Degree of polymerization and molecular weight of synthesized 14-arm star polymers	22
Table 2.2. Temperature effect on the hydrodynamic diameter of PMEO ₂ MA star polymers in water.....	22
Table 2.3. Drop volume and the corresponding drop radius, measured interfacial tension and calculated Bond number for 0.01 wt% PEO star polymers and 0.01 wt% diblock star polymers adsorbed at cyclohexane/water interface during small amplitude oscillation	28
Table 3.1. Number-average hydrodynamic radii for PEO stars and linear polymers	37
Table 3.2. Estimated change in the bulk concentrations upon polymer adsorption for PEO stars and linear PEO with a 10 μ L pendant drop at different bulk concentrations. The analysis is based on the assumptions of a spherical pendant drop and no polymer diffusion from the bulk reservoir to the pendant drop. The surface excess concentrations are obtained <i>via</i> ellipsometry using large glass petri dishes.	51
Table 3.3. Photographs of xylene/water with 0.1 wt% PEO stars initially dispersed in water (bottom phase), initially dispersed in xylene, and initially dispersed in both xylene and water phases with the same total amount of PEO stars (50/50 mass in each phase).....	68
Table 3.4. Change in refractive index of xylene and water phases in xylene/PEO-water system	71
Table 3.5. Change in refractive index of xylene and water phases in PEO-xylene/water system	71
Table 4.1. Number-average hydrodynamic diameters for various 14-arm star polymers in 1 mM NaCl aqueous solution at pH 5 and pH 9. Dynamic light scattering measurements were made at 20 °C with 0.1 wt% star polymer concentration.....	81
Table 4.2. Z-average hydrodynamic diameters and the polydispersity for various 14-arm star polymers in 1 mM NaCl aqueous solution at pH 5 and pH 9. Dynamic light scattering measurements were made at 20 °C with 0.1 wt% star polymer concentration.....	81

Table 4.3. Zeta potentials for various 14-arm star polymers in 1 mM NaCl aqueous solution at pH 5 and pH 9. Dynamic light scattering measurements were made at 20 °C with 0.1 wt% star polymer concentration	82
Table 4.4. Concentrations of star polymers to stabilize foams and the corresponding foam stability.....	83
Table 4.5. Estimated change in the bulk concentrations upon polymer adsorption for star polymers with an 8 μ L pendant drop at different bulk concentrations at pH 5. The analysis is based on the assumptions of a spherical pendant drop and no polymer diffusion from the bulk reservoir to the pendant drop. The surface excess concentrations are obtained <i>via</i> ellipsometry using large glass petri dishes.....	98
Table 4.6. Estimated change in the bulk concentrations upon polymer adsorption for star polymers with a 6 μ L pendant drop at different bulk concentrations at pH 9. The analysis is based on the assumptions of a spherical pendant drop and no polymer diffusion from the bulk reservoir to the pendant drop. The surface excess concentrations are obtained <i>via</i> ellipsometry using large glass petri dishes.....	99
Table 4.7. Minimum concentrations of star polymers to stabilize oil-in-water emulsions.....	101
Table 4.8. Interfacial pressure – interfacial area isotherms for various star polymer at the xylene/water interface with 0.001 wt% aqueous concentration.....	116
Table 4.9. Interfacial pressure – interfacial area isotherms for various star polymer at the cyclohexane/water interface with 0.001 wt% aqueous concentration	117
Table 4.10. Dependence of calculated quasi-static moduli on interfacial pressure for 0.001 wt% star polymers with 1 mM NaCl at the xylene/water interface	118
Table 4.11. Dependence of calculated quasi-static moduli on interfacial pressure for 0.001 wt% star polymers with 1 mM NaCl at the cylcohexane/water interface	119
Table 4.12. The trends of quasi-static modulus with increasing interfacial pressure during compression of the adsorbed layer for all three star polymers at xylene/water and cyclohexane/water interface with 0.001 wt% aqueous concentration at pH 5 and pH 9, 1 mM NaCl	120
Table 4.13. Interfacial pressure – interfacial area isotherms for various star polymer at the xylene/water interface with 0.1 wt% aqueous concentration.....	122
Table 4.14. Interfacial pressure – interfacial area isotherms for various star polymer at the cyclohexane/water interface with 0.1 wt% aqueous concentration	123

Table 4.15. Dependence of calculated quasi-static moduli on interfacial pressure for 0.1 wt% star polymers with 1 mM NaCl at the xylene/water interface	124
Table 4.16. Dependence of calculated quasi-static moduli on interfacial pressure for 0.1 wt% star polymers with 1 mM NaCl at the cyclohexane/water interface.....	125
Table 4.17. The trends of quasi-static modulus with increasing interfacial pressure during compression of the adsorbed layer for all three star polymers at xylene/water and cyclohexane/water interface with 0.1 wt% aqueous concentration at pH 5 and pH 9, 1 mM NaCl	126
Table 5.1. Derived count rate of nanoemulsions at different star polymer concentrations measured by dynamic light scattering. Xylene-in-water nanoemulsions were prepared using 50% water volume fraction at ambient temperature and left under quiescent conditions for 6 days before measurements. Higher derived count rate usually indicates higher concentration or larger droplets.....	150
Table 5.2. Photographs of xylene/water with 0.1 wt% PMEO ₂ MA stars initially dispersed in water (bottom phase), initially dispersed in xylene, and initially dispersed in both xylene and water phases with the same total amount of PMEO ₂ MA stars (50/50 mass in each phase).....	161

List of Figures

Figure 1.1. (upper) Position of a spherical particle at a planar oil/water interface for a contact angle $\theta < 90^\circ$ (left) and $\theta > 90^\circ$ (right). (lower) Corresponding type of emulsions based on particle wettability. For a particle with contact angle $\theta < 90^\circ$, the particle mostly resides in the aqueous phase and an oil-in-water emulsion forms (left). For a more hydrophobic particle $\theta > 90^\circ$, a water-in-oil emulsion (w/o) forms (right). 10

Figure 1.2. Types of interfacial deformation on a flat interface: shear, extension and dilatation. 17

Figure 1.3. Structure of (a) linear polymers and (b) nanoparticulate polymer brushes adsorbed to a fluid/fluid interface..... 19

Figure 2.1. The pendant drop geometry. An aqueous drop of polymer solution was created at the end of a needle and suspended in air or oil. The drop shape was recorded and the interfacial tension was determined by analysis according to the Young-Laplace equation. 25

Figure 2.2. The storage (filled symbols) and loss (empty symbols) dynamic dilatational modulus of 0.01 wt% (a) multi-arm PEO star polymers and (b) diblock star polymers adsorbed at cyclohexane/water interface as a function of frequency with different volume droplet. (a) Droplet volume: (\bullet, \circ) 15 μL (\blacksquare, \square) 5 μL and (\blacklozenge, \lozenge) 3 μL . The measured interfacial tensions before the dilatational experiments were 25.7 ± 0.05 , 25.1 ± 0.5 , and 25.6 ± 0.8 mN/m for droplet volume 15, 5, and 3 μL , respectively. (b) Droplet volume: (\bullet, \circ) 8 μL (\blacksquare, \square) 6 μL and (\blacklozenge, \lozenge) 4 μL . The measured interfacial tensions before the dilatational experiments were 10.6 ± 0.02 , 10.9 ± 0.03 , and 11.7 ± 0.09 mN/m for droplet volume 8, 6, and 4 μL , respectively..... 28

Figure 3.1. (a) Photographs of foams for varying concentrations of PEO stars 5 minutes after preparation. (b) Changes in foam height for different concentrations of PEO stars as a function of time: (\bullet) 0.1 (\blacksquare) 0.05 (\blacklozenge) 0.01 (\blacktriangle) 0.005 ($*$) 0.001 wt%. Lines serve to guide the eye. 38

Figure 3.2. Surface pressure isotherm of (\blacklozenge) PEO stars and linear (\square) PEO 1000k, (\circ) PEO 200k, and (Δ) PEO 6k adsorbed to the air/water interface. 39

Figure 3.3. Interfacial tension reduction for 0.05 wt% of PEO stars and linear PEO at air/water interface: (\blacklozenge) PEO stars and linear (\square) PEO 1000k, (\circ) PEO 200k, and (Δ) PEO 6k. 40

Figure 3.4. (a) The magnitude of the complex dynamic dilatational modulus of PEO stars adsorbed at the air/water interface as a function of frequency with 3% strain amplitude at different bulk concentrations: (\circ) 0.1 (\square) 0.05 (\lozenge) 0.01 (Δ) 0.005 ($*$) 0.001 ($+$) 0.0005 wt%. (b) The magnitude of the complex dynamic dilatational moduli averaged over all frequencies for PEO stars at the air/water interface. Schematic illustration showing how adsorbed (c) linear and (d) star polymers at the air/water interface differ in their response to the perturbation of surface

area. (The illustrated area change is exaggerated relative to the 3% strain amplitude imposed in the experiments.)..... 41

Figure 3.5. Surface tension and droplet area oscillation for 0.05 wt% of (a) PEO stars, linear (b) PEO 6k, (c) PEO 200k and (d) PEO 1000k at the air/water interface. The surface area oscillation frequency is 0.1 Hz. (e) Fast Fourier transform analysis of the surface tension data during forced surface area oscillations at the air/water interface confirms the lack of a dilatational elastic response for linear PEO, while PEO stars demonstrate a strong peak at the frequency of the forced area oscillation: (◆) PEO stars and linear (□) PEO 1000k, (○) PEO 200k, and (Δ) PEO 6k. 43

Figure 3.6. (a) Surface pressure versus area (mm^2) isotherm for PEO stars at air/water interface. The bulk concentration of PEO stars is 0.001 wt%. The surface area compression and expansion rate was kept in the range of 0.07 – 0.1 mm^2/s . Three cycles of surface compression and expansion were recorded. (b) Compression and expansion modulus for PEO stars at air/water interface as a function of surface pressure deduced from the surface pressure versus area isotherm. Three cycles of surface compression and expansion were recorded. 46

Figure 3.7. (a) Surface excess concentration and (b) apparent area fraction surface coverage for (◆) PEO stars and linear (□) PEO 1000k, (○) PEO 200k, and (Δ) PEO 6k adsorption to the air/water interface. 47

Figure 3.8. Surface pressure area isotherm for PEO stars adsorbed at air/water interface. Ellipsometry provided the static surface excess concentration for each PEO star concentration at which surface pressures were measured in independent experiments. Linear regression for the slope of π vs. $\ln(1/\Gamma)$ yields a static dilatational elasticity $E_d = 5.1 \text{ mN/m}$ 50

Figure 3.9. Effect of PEO star concentration on emulsion stability: (●) 0.1 (■) 0.05 (◆) 0.01 (▲) 0.005 (*) 0.001 wt%. Changes in height for (a) xylene-in-water and (b) cyclohexane-in-water emulsions at different concentrations of PEO stars as a function of time. Lines serve to guide the eye. 52

Figure 3.10. Interfacial pressure isotherm of (◆) PEO stars and linear (□) PEO 1000k, (○) PEO 200k, and (Δ) PEO 6k adsorbed from water to (a) xylene/water and (b) cyclohexane/water interfaces. 53

Figure 3.11. The magnitude of the complex dynamic dilatational modulus of PEO stars adsorbed at the (a) xylene/water interface and (b) cyclohexane/water interface as a function of frequency with 3% strain amplitude at different bulk concentrations: (○) 0.1 (□) 0.05 (◇) 0.01 (Δ) 0.005 (*) 0.001 wt%. Concentration dependence of the magnitude of the complex dynamic dilatational moduli, averaged over all tested frequencies, of PEO stars at the (c) xylene/water and (d) cyclohexane/water interface..... 56

Figure 3.12. Interfacial tension and droplet area oscillation for 0.05 wt% of (a) PEO stars, linear (b) PEO 6k, (c) PEO 200k and (d) PEO 1000k at the xylene/water interface. The oscillation frequency is 0.1 Hz. (e) Fast Fourier transform analysis of interfacial tension response in the dynamic dilatational modulus experiments at the xylene/water interface: (◆) PEO stars and linear (□) PEO 1000k, (○) PEO 200k, and (Δ) PEO 6k. No peak was detected for linear PEO at the forced oscillation frequency..... 57

Figure 3.13. Interfacial tension and droplet area oscillation for 0.05 wt% of (a) PEO stars, linear (b) PEO 6k, (c) PEO 200k and (d) PEO 1000k at the cyclohexane/water interface. The oscillation frequency is 0.1 Hz. (e) Fast Fourier analysis of interfacial tension response in the dynamic dilatational modulus experiments at the cyclohexane/water interface: (◆) PEO stars and linear (□) PEO 1000k, (○) PEO 200k, and (Δ) PEO 6k. No peak was detected for linear PEO at the forced oscillation frequency..... 58

Figure 3.14. Interfacial pressure versus area (mm^2) isotherm for PEO stars at (a) xylene/water and (b) cyclohexane/water interface. The concentration of PEO stars in water is 0.001 wt%. The interfacial compression and expansion rate was kept in the range of 0.07 – 0.1 mm^2/s . In (a), the second and third cycles are overlapping. Compression and expansion modulus for PEO stars at (c) xylene/water and (d) cyclohexane/water interface as a function of interfacial pressure deduced from the interfacial pressure versus area isotherm. Three cycles of interfacial compression and expansion were recorded..... 60

Figure 3.15. (a) Measured ellipsometric Δy as a function of bulk polymer concentration adsorbed from water to the xylene/water interface: (◆) PEO stars (□) PEO 1000k (○) PEO 200k (Δ) PEO 6k. (b) Theoretically predicted dependence of (●) x and (◆) y on the thickness of a homogeneous adsorbed layer with $n_f = 1.44$ at 42° angle of incidence. 62

Figure 3.16. Comparison of xylene/water interfacial pressure isotherms for linear (a) PEO 6k, (b) PEO 200k, (c) PEO 1000k and (d) PEO stars adsorbed from xylene (□), from water (●) or from both xylene and water phases with half the total mass of PEO stars dispersed in each phase (Δ). 63

Figure 3.17. Change in ellipsometric parameters (a) Δx and (b) Δy for PEO star adsorption to the xylene/water interface from xylene (□) or from water (●). 65

Figure 3.18. Photographs of xylene/water with 0.1 wt% PEO stars initially dispersed in xylene (top phase) at time = 0, 3, 24, and 96 h after sample preparation, (a) – (d), respectively. Microscope images of spontaneous emulsification commencing at the interface between a xylene droplet of 0.1 wt% PEO stars surrounded by water at (e) the initial stage and (f) 20 seconds after the two liquids were brought into contact. The microscope images were taken using a microtensiometer apparatus.^{24,159} 67

Figure 3.19. Optical density of the xylene phase of the xylene/water system 3.5 hours after sample preparation. PEO stars were initially dispersed in xylene. Turbidity increased with the

bulk concentration of PEO stars initially dispersed in xylene, indicating increasing spontaneous emulsification of water into xylene..... 67

Figure 3.20. Proposed hypothetical mechanism for the spontaneous emulsification occurring at the interface between a PEO star-rich xylene phase and a water phase. Each stage is explained in the text..... 70

Figure 3.21. Calculated surface excess concentration as a function of the guessed refractive index of the adsorbed PEO layer at the air/water interface, based on analysis of the ellipsometric γ parameter for the “true” adsorbed layer that has refractive index of 1.44 and thickness of 20 Å. The angle of incidence is 53° 73

Figure 3.22. Calculated surface excess concentration as a function of the guessed refractive index of the adsorbed PEO layer at the xylene/water interface, based on analysis of the ellipsometric γ parameter for the “true” adsorbed layer that has refractive index of 1.44 and thickness of 20 Å. The angle of incidence is 43° 74

Figure 3.23. Calculated surface excess concentration measured from both xylene and water phases as a function of the guessed refractive index of the adsorbed PEO layer at the xylene/water interface, based on analysis of the ellipsometric γ parameter for the “true” adsorbed layer that has refractive index of 1.44 and thickness of 20 Å. The angle of incidence measuring from xylene and water is 43° and 47°, respectively. 75

Figure 3.24. The observed dilatational elasticity of adsorbed PEO star polymer layers may be a key factor that distinguishes their good emulsifying and foaming performance from the poor performance of linear PEO. 78

Figure 4.1. Surface pressure isotherm of (●) PMEO₂MA, (▲) PDMAEMA and (■) diblock star polymers adsorbed to the air/water interface at (a) pH 5 and (b) pH 9. 84

Figure 4.2. Surface tension as a function of time for 0.1 wt% diblock star polymers at the air/water interface at (□) pH 5 and (○) pH 9..... 85

Figure 4.3. Surface tension reduction as a function of time for (a) PMEO₂MA star polymers at pH 5, (b) PMEO₂MA star polymers at pH 9 (c) PDMAEMA star polymers at pH 5, (d) PDMAEMA star polymers at pH 9, (e) diblock star polymers at pH 5, and (f) diblock star polymers at pH 9 adsorbed to the air/water interfaces. Polymer concentrations are (●) 0.1 (●) 0.05 (●) 0.01 (●) 0.005 (●) 0.001 (●) 0.0005 wt% 86

Figure 4.4. The magnitude of the complex dynamic dilatational moduli averaged over all frequencies for (●) PMEO₂MA, (▲) PDMAEMA and (■) diblock star polymers at the air/water interface at (a) pH 5 and (b) pH 9. Area strain amplitude is 5%. 88

Figure 4.5. Surface tension and droplet area oscillation for 0.01 wt% of (a) PMEO₂MA, (b) PDMAEMA, and (c) diblock star polymers at the air/water interface at pH 9. The surface area oscillation frequency is 0.1 Hz. (d) Fast Fourier transform analysis of surface tension response in the dynamic dilatational modulus experiments at the air/water interface: (○) PMEO₂MA, (Δ) PDMAEMA, and (□) diblock star polymers. A peak was detected at the forced oscillation frequency..... 90

Figure 4.6. Surface excess concentration for (●) PMEO₂MA, (▲) PDMAEMA and (■) diblock star polymers adsorption to the air/water interface at (a) pH 5 and (b) pH 9. 92

Figure 4.7. Apparent area fraction surface coverage calculated from the extent of adsorption and sizing data as $\theta = \pi R_h^2 \Gamma$ for (●) PMEO₂MA, (▲) PDMAEMA and (■) diblock star polymers adsorption to the air/water interface at (a) pH 5 and (b) pH 9..... 94

Figure 4.8. Surface pressure area isotherm for (a, b) PMEO₂MA, (c, d) PDMAEMA and (e, f) diblock star polymers adsorbed at air/water interface at pH 5 and pH 9. Ellipsometry provided the static surface excess concentration for each star concentration at which surface pressures were measured in independent experiments. Linear regression for the slope of π vs. $\ln(1/\Gamma)$ yields a static dilatational elasticity. 96

Figure 4.9. Effect of PMEO₂MA star polymer concentration on emulsion stability: (●) 0.1 (■) 0.05 (◆) 0.01 (▲) 0.005 (*) 0.001 wt%. Changes in height for (a) xylene-in-water and (b) cyclohexane-in-water emulsions at different concentrations of PMEO₂MA star polymers as a function of time. Lines serve to guide the eye. 101

Figure 4.10. Effect of PDMAEMA star polymer concentration on emulsion stability: (●) 0.1 (■) 0.05 (◆) 0.01 (▲) 0.005 (*) 0.001 wt%. Changes in height for (a) pH 5, xylene-in-water, (b) pH 9, xylene-in-water, (c) pH 5, cyclohexane-in-water and (d) pH 9, cyclohexane-in-water emulsions at different concentrations of PDMAEMA star polymers as a function of time. Lines serve to guide the eye..... 102

Figure 4.11. Effect of diblock star polymer concentration on emulsion stability: (●) 0.1 (■) 0.05 (◆) 0.01 (▲) 0.005 (*) 0.001 wt%. Changes in height for (a) pH 5, xylene-in-water, (b) pH 9, xylene-in-water, (c) pH 5, cyclohexane-in-water and (d) pH 9, cyclohexane-in-water emulsions at different concentrations of diblock star polymers as a function of time. Lines serve to guide the eye. 103

Figure 4.12. Interfacial pressure isotherm of (●) PMEO₂MA, (▲) PDMAEMA and (■) diblock star polymers adsorbed to the xylene/water interface at (a) pH 5 and (b) pH 9, and to the cyclohexane/water interface at (c) pH 5 and (d) pH 9. 104

Figure 4.13. Interfacial tension reduction as a function of time for (a) PMEO₂MA star polymers at pH 5, (b) PMEO₂MA star polymers at pH 9 (c) PDMAEMA star polymers at pH 5, (d)

PDMAEMA star polymers at pH 9, (e) diblock star polymers at pH 5, and (f) diblock star polymers at pH 9 adsorbed to the xylene/water interfaces. 107

Figure 4.14. Interfacial tension reduction as a function of time for (a) PMEO₂MA star polymers at pH 5, (b) PMEO₂MA star polymers at pH 9 (c) PDMAEMA star polymers at pH 5, (d) PDMAEMA star polymers at pH 9, (e) diblock star polymers at pH 5, and (f) diblock star polymers at pH 9 adsorbed to the cyclohexane/water interfaces. 108

Figure 4.15. The magnitude of the complex dynamic dilatational moduli averaged over all frequencies for (●) PMEO₂MA, (▲) PDMAEMA and (■) diblock star polymers adsorbed to the xylene/water interface at (a) pH 5 and (b) pH 9, and to the cyclohexane/water interface at (c) pH 5 and (d) pH 9. 110

Figure 4.16. Interfacial pressure as a function of interfacial area for three compression/expansion cycles of a xylene/water interface exposed to 0.001 wt% (a) PMEO₂MA star polymers and (c) diblock star polymers with 1 mM NaCl at pH 5. Dependence of calculated quasi-static moduli on interfacial pressure at the xylene/water interface for 0.001 wt% (b) PMEO₂MA star polymers and (d) diblock star polymers with 1 mM NaCl at pH 5. Symbols: (□) first, (Δ) second and (○) third cycles of large amplitude compression/expansion experiments. 114

Figure 4.17. Dynamic dilatational modulus as a function of interfacial pressure at the (a) xylene/water and (b) cyclohexane/water interface exposed to 0.001 wt% PMEO₂MA star polymer aqueous concentration. Experiments were repeated at least two times and the results were consistent. 127

Figure 4.18. Dynamic dilatational modulus as a function of interfacial of (□) 0.001 wt% and (Δ) 0.1 wt% PDMAEMA star polymer adsorbed to the xylene/water interface at (a) pH 5 and (b) pH 9, and to the cyclohexane/water interface at (c) pH 5 and (d) pH 9. 129

Figure 4.19. Dynamic dilatational modulus as a function of interfacial of (□) 0.001 wt%, (◇) 0.01 wt% and (Δ) 0.1 wt% diblock star polymer adsorbed to the xylene/water interface at (a) pH 5 and (b) pH 9, to the cyclohexane/water interface at (c) pH 5 and (d) pH 9. 131

Figure 4.20. Dilatational modulus as a function of interfacial pressure for PMEO₂MA star polymers at the (a) xylene/water and (b) cyclohexane/water interface obtained from (●) small amplitude oscillation after interface reached equilibrium, (□) large amplitude compression/expansion and (■,▲) small amplitude oscillation before the interface reached equilibrium. 132

Figure 4.21. Dilatational modulus as a function of interfacial pressure obtained from (●) small amplitude oscillation after interface reached equilibrium, (□, Δ) large amplitude compression/expansion and (■,▲) small amplitude oscillation before interface reached equilibrium for PDMAEMA star polymers adsorbed to the xylene/water interface at (a) pH 5 and (b) pH 9, and cyclohexane/water interface at (c) pH 5 and (d) pH 9. 134

Figure 4.22. Dilatational modulus as a function of interfacial pressure obtained from (●) small amplitude oscillation after interface reached equilibrium, (□, Δ) large amplitude compression/expansion and (■, ▲) small amplitude oscillation before interface reached equilibrium for diblock star polymers adsorbed to the xylene/water interface at (a) pH 5 and (b) pH 9, and cyclohexane/water interface at (c) pH 5 and (d) pH 9. 135

Figure 5.1. Stable xylene-in-water nanoemulsion were spontaneously produced with 0.1 wt% PMEO₂MA star polymers initially dispersed in aqueous phase (bottom phase) at time = (a) initial, (b) 1 hour, (c) 3 hours, (d) 24 hours, (e) 2 days, (f) 7 days and (g) 219 days after xylene and aqueous phase were brought into contact and left under quiescent conditions..... 142

Figure 5.2. Interfacial tension reduction as a function of time for 0.1 wt% of PMEO₂MA star polymers at xylene/water interface. Interfacial tension dropped to 6 mN/m within 15 mins..... 143

Figure 5.3. Droplet size distribution of xylene-in-water nanoemulsion at 8 days (○) and 308 days (□) after xylene and 0.1 wt% PMEO₂MA star polymer solution were brought into contact and left under quiescent conditions at room temperature..... 144

Figure 5.4. Effect of cooling to 4 °C and heating back to temperature on nanoemulsion droplet size distribution. Nanoemulsions was prepared by spontaneous emulsification using water fraction = 50% and PMEO₂MA star polymer concentration = 0.1 wt% at ambient temperature and left to rest for 35 days before cooled to 4 °C. After storing at 4 °C for 43 days, the nanoemulsion was brought back to room temperature. Size distribution was measured throughout the experiment to probe any temperature-induced effects..... 146

Figure 5.5. Effect of heating to 45 °C and cooling back to temperature on nanoemulsion droplet size distribution. Nanoemulsion was prepared by spontaneous emulsification using water fraction = 50% and PMEO₂MA star polymer concentration = 0.1 wt% at ambient temperature and left to rest for 15 days before cooling to 45 °C. After storing at 45 °C for 4 days, the nanoemulsion was brought back to room temperature. Size distribution was measured throughout the experiment to probe any temperature-induced effects..... 147

Figure 5.6. Effect of polymer concentration on droplet size distribution of nanoemulsions produced by spontaneous emulsification. Xylene-in-water nanoemulsions were prepared using 50% water volume fraction at ambient temperature and left under quiescent conditions for 6 days before size measurements. The concentrations of PMEO₂MA star polymer solutions: (○) 0.1 (◇) 0.05 (Δ) 0.025 (□) 0.01 wt%. 149

Figure 5.7. Interfacial tension isotherm of PMEO₂MA star polymers adsorbed to the xylene/water interface..... 149

Figure 5.8. Effect of water volume fraction (which changes the total amount of PMEO₂MA in nanoemulsion) on mean droplet diameter of nanoemulsions produced by spontaneous emulsification. Xylene-in-water nanoemulsions were prepared using various oil:water ratio at

ambient temperature and left under quiescent conditions for 6 days before size measurements. The concentrations of PMEO₂MA star polymer solutions: (○) 0.1 (◇) 0.05 (△) 0.025 (□) 0.01 wt%. 151

Figure 5.9. Nanoemulsion droplet size as a function of water volume fraction at room temperature (○), cooling down to 4 °C (◆) and heating back to room temperature (□). The concentration of PMEO₂MA star polymer was 0.1 wt%. The effects of cooling on the change in droplet size are more pronounced at higher water volume fraction. Upon heating back to the room temperature, the droplet size distributions became bimodal. 152

Figure 5.10. Photographs of macroemulsions produced by high shear homogenization using 0.1 wt% PMEO₂MA star polymer concentration at various water volume fractions at (a) the initial stage and (b) 10 days after sample preparation. Creaming occurred in macroemulsion samples due to the large size of droplets. (c) Mean droplet diameter as a function of water volume fraction of the new emulsion phase after the breakage of macroemulsions. 154

Figure 5.11. Droplet size distribution of the continuous phase of the macroemulsion produced using high shear homogenization with PMEO₂MA star polymer concentration 0.1 wt% and water volume fraction 0.9 after centrifugation at (◆) and after 6 days of resting (○). 156

Figure 5.12. Photographs of the macroemulsions produced by high shear homogenization with PMEO₂MA star polymer concentration 0.1 wt% and water volume fraction 0.9 (a) after centrifugation at 1800 rpm at 30 mins and (b) after 6 days of resting. The derived count rate measured by dynamic light scattering increased from (a) 72,000 kcps to (b) 105,000 kcps, suggesting that the free polymers in the continuous phase underwent spontaneous emulsification and formed nano-sized droplets after the macroemulsions was produced. 156

Figure 5.13. Xylene-in-water nanoemulsions produced (a) by spontaneous emulsification under quiescent conditions and (b) breakage of a macroemulsion. The concentration of Triton X-100 was 0.1 wt% and the water volume fraction was 0.5. (c) Size distribution of Triton X-100 stabilized emulsions produced by spontaneous emulsification (○) and by breakage of a macroemulsion (◆) 17 days after sample preparation. 158

Figure 5.14. Photographs of xylene-in-water nanoemulsions formed by spontaneous emulsification with (a) 0.1 wt% PMEO₂MA star polymer initially dispersed in water phase (bottom phase). (b) No spontaneous emulsification was observed when the PMEO₂MA stars were initially dispersed in xylene phase. (c) Xylene-in-water nanoemulsions spontaneously formed when same total amount of PMEO₂MA stars were initially dispersed both xylene and water phases (50/50 mass in each phase). Photographs were taken 106 days after the xylene and water phase came into contact. 160

1 Introduction

This dissertation presents star polymers as a novel class of efficient foaming agents and emulsifiers, and correlates the interfacial activity of star polymer adsorbed layer at fluid interfaces with corresponding foaming and emulsification performance.

1.1 Motivation

Foams and emulsions bear many similarities and are of interest for their widespread occurrence in processes related to the food, pharmaceutical, and cosmetics industries. Foams are dispersions of a large volume of gas in a small volume of liquid, whereas emulsions are mixtures of two immiscible liquids where one liquid is finely dispersed within the other liquid. Foams and emulsions are typically unstable due to their large interfacial area associated with the system. From a thermodynamic point of view, there is a tendency for foams and emulsions to phase separate in order to reduce their interfacial area and thus the interfacial energy. Stable foams and emulsions can be obtained by adding amphiphilic surfactants due to their affinity for the fluid interface and their ability to lower the interfacial energy. Yet, it has been found that foam and emulsion formation do not necessarily require amphiphilic surfactants but can also be efficiently promoted by colloidal particles.¹⁻⁶ Solid-stabilized emulsions, commonly referred to as Pickering emulsions,⁷ provide long term stability against coalescence, creaming and Ostwald ripening, and are able to maintain large discontinuous phase volume fractions for several months to over a year.^{8,9} One of the main contributions to the system stability is the extremely large adsorption energy of a colloidal particle to the interface.^{10,11} This creates an energy barrier against droplet coalescence which requires particles to desorb from the interface. Colloidal particles adsorbed at the air/water and oil/water interfaces retain the basic properties of surfactant-stabilized wet foams and emulsions. However, substitution of surfactants with colloidal particles is appealing in

several fields, such as personal care, pharmaceutical and food industries where surfactants may induce skin or other tissue irritation.¹²

Nanoparticulate polymer brushes, a novel class of surface active material that includes both polymer-grafted nanoparticles and multi-arm star polymers with a large number of chains emanating from a crosslinked core,^{13–16} are highly efficient emulsifiers.^{17–21} Their minimum concentration required to stabilize an emulsion is as low as 0.005 – 0.04 wt%,^{17,18,20,22} which is one to two orders of magnitude lower than commonly required for a particle-stabilized emulsion.^{9,23} Even at these low concentrations, emulsions stabilized by nanoparticulate polymer brushes retain the long-term stability commonly achieved with Pickering emulsions. The enhanced emulsifying efficiency is attributed to the interfacial activity of the polymer chains,^{19,20,24} but the detailed origins of their emulsifying efficiency have yet to be determined.

The nanoparticulate brush architecture that tethers multiple chains to a central core is key to their emulsifying performance – stable emulsions can be formed by nanoparticulate brushes whereas free polymers of the same type fail to stabilize emulsions.^{17,20} While preserving this basic architectural motif, changing the composition of the polymer chains is predicted to alter the conformation and location of adsorbed star polymers relative to a fluid interface.^{25,26} Chain composition can also dictate whether the preferred emulsion type is oil-in-water or water-in-oil.¹⁸ Furthermore, the interaction between the polymeric surfactants and therefore the dispersed phase can be tailored by introducing stimuli-responsive polymer chains into the nanoparticulate brush. This allows the formation of responsive foams or emulsions that can undergo reversible changes in response to external or internal stimuli, such as pH, temperature, and light.^{27–33}

The combination of thermodynamic, kinetic, and mechanical properties of an adsorbed nanoparticulate polymer brush layer that are responsible for efficient and effective emulsification, or of the related phenomenon of foaming, is not fully understood. A primary contributor to Pickering emulsion or foam stability is the very large adsorption energy of a particle that is partially wetted at a fluid interface.^{11,34} Considering the common tendency of polymer adsorption to be effectively irreversible, a high adsorption energy is also expected of nanoparticulate polymer brushes, but this would not be likely to distinguish them from simpler particulate or polymeric emulsifiers or foaming agents. Therefore, understanding the equilibrium and dynamic interfacial behaviors of these nanoparticulate polymer brushes at interfaces as well as the relationship between the structure of efficient nanoparticulate polymer brushes and fluid/fluid interfacial properties would be highly desirable for knowledge-based design of these particles.

Besides the interfacial properties determined by the structure and interparticle interaction of the adsorbed layer at the interface, emulsion stability and the droplet size can be affected by other factors such as the system composition, the fabrication method, and the environmental conditions after the emulsions are made.^{35–38} Nanoemulsions, defined as emulsions with droplet size on the order of 100 nm,^{39–44} are of particular interest due to their long term stability and high optical transparency, making them attractive for delivery systems in various applications. Previous investigations have shown that if both water and organic liquid are good solvents for a nanoparticulate brush emulsifier, the properties of the emulsion may depend on the phase in which the emulsifier was initially dispersed before emulsification. For example, the phase in which poly(2-dimethylamino)ethyl methacrylate (PDMAEMA)-grafted silica nanoparticles were dissolved did not dictate the preferred emulsion type but did dictate the droplet flocculation state

and the corresponding emulsion rheology.⁴⁵ The minimum concentration required for low grafting density PDMAEMA-grafted silica nanoparticles to stabilize an emulsion was larger when the particles were initially dispersed in xylene than in water.²¹ Hence, understanding the influence of preparation methods, emulsifier location, system composition and environmental change on the emulsion properties can improve the formation of emulsions and optimize storage conditions to extend shelf life.

1.2 Dissertation objectives

The overall objective of this work is to correlate the high efficiency of nanoparticulate polymer brush, as foaming agents and emulsifiers, with their architecture and the corresponding interfacial activity to provide the basis for the design of novel polymeric foam and emulsion stabilizers. Although several factors can be important for foaming and emulsification efficiency, this dissertation specifically addresses three interfacial characteristics: interfacial tension, dilatational modulus and extent of adsorption. To achieve this objective, a series of star polymers with well-controlled polymer brush structure and chemistry are prepared and used as a representative of nanoparticulate polymer brushes. The following approaches are applied to each star polymer.

1. Characterize star polymers to assess their molecular weight, composition, architecture, and aqueous solution properties.
2. Determine the foaming and emulsification abilities of star polymers in comparison to similar polymer grafted nanoparticles.
3. Investigate how star polymer composition and architecture affect their interfacial tension isotherm.

4. Identify how star polymer composition and architecture control dynamic dilatational modulus of star polymers adsorbed at fluid interfaces.
5. Determine how star polymer composition and architecture influence their adsorption behavior and affect their packing density at fluid interfaces.

To our knowledge, there has been no other work which has systematically investigated the effect of varying composition and architecture of star polymers on their interfacial activity at the air/water and oil/water interfaces. This dissertation attempts to provide the origins of high efficiency foaming and emulsification, give insight into the structure-function relationship for the star polymer adsorbed layer at the fluid interfaces, and confirm or refute the importance of corresponding interfacial properties for stabilizing foams and emulsions. This dissertation also addresses whether these fundamental adsorption characteristics depend on the phase in which star polymers are initially dispersed. Additionally, this dissertation investigates the effect of other factors including temperature, system composition and preparation method on the formation and stability of emulsions

1.3 Outline of dissertation

The dissertation is organized into six chapters and the summary of each chapters is presented below to provide the logical flow of this dissertation:

Chapter 1 gives a broad introduction, including an overview of the thesis problem, the background on the research questions, and key related interfacial properties: interfacial tension, dilatational modulus, and extent of adsorption.

Chapter 2 includes a description of the main materials and experimental methods used in this dissertation. The subsequent body chapters refer back to Chapter 2 for detailed experimental procedures.

Chapter 3 presents a detailed investigation of the interfacial activity of multi-arm poly(ethylene oxide) (PEO) star polymers and linear PEO polymers at air/water and oil/water interfaces. This chapter discusses the structure-function relationship of star polymers and identifies the correlation between the dynamic dilatational modulus with foaming and emulsification performance. Additionally, path-dependent adsorption behaviors at the xylene/water interface and the observation of spontaneous emulsification are reported. This work has been published under the title “Enhanced Interfacial Activity of Multi-Arm Poly(Ethylene Oxide) Star Polymers Relative to Linear Poly(Ethylene Oxide) at Fluid Interfaces.” Y. Huang, M. Lamson, K. Matyjaszewski, and R. D. Tilton. *Physical Chemistry Chemical Physics*, 2017, **19**, 23854 – 23868.⁴⁶

Chapter 4 presents detailed studies of the interfacial activity of various star polymers with the same structure but with polymer arms of different chemical compositions, including PMEO₂MA star polymers with homopolymer arms, PDMAEMA star polymers with weak polycation arms, and star polymers with block copolymer arms. The chapter investigates the effect of pH and chemical composition of the star polymers on interfacial behavior and identifies a possible relation between foaming and emulsification efficiency to the ability of adsorbed star polymers to resist ejection under interfacial compression. Additionally, the dependence of interfacial rheology on the history of the formation of adsorbed layers is examined. This work is part of a manuscript in preparation titled “Interfacial Activity of pH-Responsive Star polymers at

Fluid Interfaces and Correlation with the Corresponding Foam and Emulsion Properties” by the authors Y. Huang, K. Matyjaszewski, and R. D. Tilton.

Chapter 5 presents the formation of an extremely stable nanoemulsion produced by spontaneous emulsification with surface active PMEO₂MA star polymers. This chapter examines the effect of several factors including preparation method, temperature and composition on the droplet size and the stability of the nanoemulsions. This work is part of a manuscript in preparation titled “Nanoemulsion Formation by Spontaneous Emulsification with Surface Active Star Polymers” by the authors Y. Huang, K. Matyjaszewski, and R. D. Tilton.

Chapter 6 concludes the dissertation by providing a summary of major findings, original contributions, and future directions for the research project.

1.4 Background

1.4.1 Emulsion classification – Macro-, nano- and microemulsions

An emulsion is a mixture of two immiscible liquids with one liquid being finely dispersed in another liquid phase. According to the size of the droplets dispersed in the continuous phase and their thermodynamic properties, emulsions can be categorized as macroemulsions (classical emulsions), nanoemulsions and microemulsions. Macroemulsions are emulsions with droplets larger than 1 μm , whereas nanoemulsions and microemulsions have droplet size on the order of 100 nm. The confusion in nomenclature in the lower droplet size regime is due to the rapid rise of nanomaterials and nanotechnology research in the first decade of the 21st century; the term “microemulsions” was well-established before the term “nanoemulsions” was introduced. The major differences between these emulsions are summarized in **Table 1.1**. The physicochemical

properties of nanoemulsions and their preparation methods will be discussed in more detail in

Chapter 1.4.3.

Table 1.1. Comparison of macroemulsions, nanoemulsions (also referred to as miniemulsions) and microemulsions with respect to size, shape, stability, method of preparation, polydispersity, and appearance. Nanoemulsions and microemulsions have a larger surface area per unit volume than macroemulsions because of their size. In addition, due to a strong kinetic stability, nanoemulsions are less sensitive to physical and chemical changes. Table is adapted from *Soft Matter* (2011)³⁹ and *Soft Matter* (2016).⁴⁷

	Macroemulsions	Nanoemulsions	Microemulsions
Droplet size	1 – 100 μm	20 – 500 nm	10 – 100 nm
Shape	Spherical	Spherical	Spherical or lamellar
Stability	Weakly kinetically stable	Kinetically stable	Thermodynamically stable
Preparation method	High and low energy	High and low energy	Low energy
Polydispersity	Often high (> 40%)	Typically low (< 10 – 20%)	Typically low (< 10%)
Appearance	Turbid or opaque	Clear or turbid	Clear

Except for microemulsions, which are thermodynamically stable, emulsions are thermodynamically unstable, and therefore tend to phase separate over time through various physicochemical mechanisms, including coalescence, Ostwald ripening, flocculation, and creaming. Stabilizers such as emulsifiers, texture modifiers, ripening inhibitors, and weighting agents, are added to improve the long-term stability of emulsions.⁴⁸ Typically, amphiphilic molecules that have both hydrophilic and hydrophobic groups, i.e, surfactants, proteins, lipids and copolymers, are used as emulsifiers due to their ability to adsorb to the oil/water interface and lower the Gibbs free energy. Solid particles are found to be effective at stabilizing emulsions, known as Pickering emulsions,⁷ and will be discussed below in **Chapter 1.4.2.** Moreover, Janus particles,^{49,50} which resemble surfactant molecules in their amphiphilicity but

also exhibit unique properties that are not observed with surfactants adsorbed at fluid interfaces, have recently been developed as emulsifiers.

1.4.2 Pickering emulsions

Pickering emulsions are emulsions stabilized solely by solid particles. Particles with moderate wettability can strongly adsorb to oil/water interfaces. The adsorption energy (E_{ads}) of a particle to the interface is related to the oil/water interfacial tension (γ), the radius of the solid particles (R), and the contact angle of the particle measured through the aqueous phase (θ) by:^{5,10,11}

$$E_{ads} = -\pi R^2 \gamma (1 + \cos \theta)^2, \theta \geq 90^\circ \quad (1.1)$$

$$E_{ads} = -\pi R^2 \gamma (1 - \cos \theta)^2, \theta < 90^\circ \quad (1.2)$$

For a given particle with $R = 10$ nm, $\theta = 90^\circ$ and the interfacial tension of $\gamma = 36$ mN/m, the adsorption energy can be as large as ~ 2750 kT. This is much larger than the thermal fluctuation energy, suggesting that the particle is essentially irreversibly adsorbed.⁵¹ This large adsorption energy creates an energy barrier for particles to desorb from the fluid interface, which leads to extremely stable Pickering emulsions against coalescence.

According to the Bancroft rule, the phase where an emulsifier is more soluble becomes the continuous phase in the emulsion.⁵² The type of emulsion is dictated by the particle wettability, as shown in **Figure 1.1**.⁵¹ Particles with contact angle $\theta < 90^\circ$ stabilize oil-in-water (o/w) emulsions, whereas those with $\theta > 90^\circ$ stabilize water-in-oil (w/o) emulsions. However, some violations to the Bancroft rule have been observed.^{23,53-55} Previous work in our group also showed that the Bancroft rule does not hold for many of the systems studied; o/w emulsions

always formed regardless of the phase in which polymer grafted nanoparticles or star polymers were initially dispersed.^{17,45}

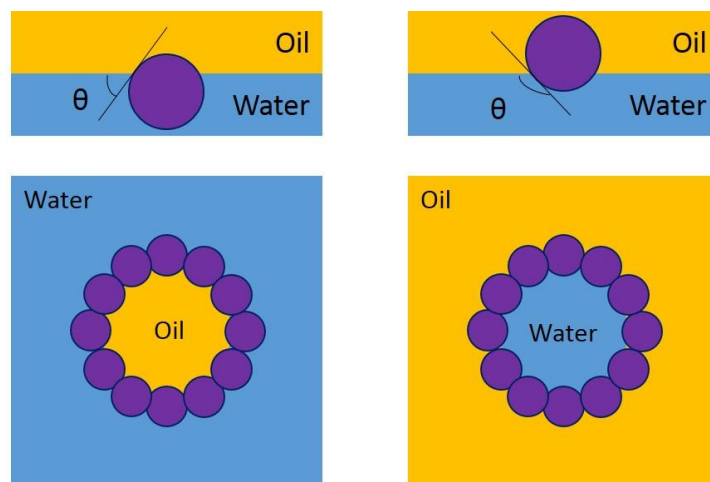


Figure 1.1. (upper) Position of a spherical particle at a planar oil/water interface for a contact angle $\theta < 90^\circ$ (left) and $\theta > 90^\circ$ (right). (lower) Corresponding type of emulsions based on particle wettability. For a particle with contact angle $\theta < 90^\circ$, the particle mostly resides in the aqueous phase and an oil-in-water emulsion forms (left). For a more hydrophobic particle $\theta > 90^\circ$, a water-in-oil emulsion (w/o) forms (right).

1.4.2.1 Particle wettability alteration via surface modification

The wettability of particles for Pickering emulsions can be tailored by functionalizing the surface. Two main strategies have been developed based on physical adsorption and chemical grafting of small molecules or polymers.^{5,56} For examples, the hydrophobicity of the negatively charged silica particles were modified by adsorbing trivalent La^{3+} cations, which enhanced the emulsion stability.⁵⁷ In addition, co-adsorption of surface active surfactants and nanoparticles formed surfactant-particle complexes at the fluid interface and synergistically improved the formation of the Pickering emulsions.^{21,58} Compared to small molecules, chemically grafting polymer arms onto nanoparticles by physical adsorption or chemical bonding makes the particles

extremely efficient emulsifiers.^{19,20,59–61} In this dissertation, emulsification efficiency refers to the minimum particle concentration needed to form a stable emulsion. The lower the minimum required polymer concentration is, the more efficient the emulsifier is. Previously our group has reported that silica particles grafted with sulfonated polystyrene brushes (PSS-SiO₂) stabilized trichloroethylene (TCE)-in-water emulsions for more than 6 months with particle concentration of 0.04 wt%.²⁰ Poly(2-(dimethylamino)ethyl methacrylate) grafted silica nanoparticles (PDMAEMA-SiO₂) were shown to reduce the oil/water interfacial tension and stabilize xylene-in-water and cyclohexane-in-water emulsions at particle concentration of 0.05 wt%.^{19,24} The desorption of a polymer grafted particle requires simultaneously detachment of many polymer arms from the interface at the same time, which creates an energy barrier even larger than removal of one bare particle. However, the mechanisms that are responsible for extremely efficient polymer-grafted particles emulsification are not well-understood.

1.4.2.2 Stimuli-responsive Pickering emulsions

Incorporating stimuli-responsive polymers into emulsifiers renders Pickering emulsions that are sensitive to pH and temperature changes,^{28,62} which can be particularly interesting for many applications, such as oil recovery,⁶³ emulsion polymerization,⁶⁴ and catalysis recycling.⁶⁵ The emulsions stabilized by poly(ethylene glycol) methacrylate-*co*-poly(2-(diethylamino)ethyl methacrylate) (PEGMA-PDEAEMA) latex particles can be demulsified at low pH and re-emulsified at high pH. A latex-to-microgel transition occurs when lowering the solution pH from 10 to 3, leading to interfacial desorption.³³ Studies have also shown that tertiary amine methacrylate-based block copolymers that adsorbed onto polystyrene latex nanoparticles were synthesized and employed as Pickering emulsifiers for stabilizing o/w emulsions. Acidification of the system causes desorption of the particles from the interface and droplet coalescence.^{66,67} While pH

adjustment typically requires addition of acid or base to an emulsion, temperature adjustment is easily applied without changing the chemical composition of the system. Polymers with a lower critical solution temperature (LCST) collapse when the temperature is raised above this critical temperature, allowing the use of temperature as a trigger to change material morphologies at the molecular scale and modulate Pickering emulsion stability. Temperature-induced emulsion phase inversion from o/w to w/o has been observed using polystyrene (PS) latex particles stabilized by a monodisperse diblock copolymer, poly(2-(dimethylamino)ethyl methacrylate-*block*-methyl methacrylate) (PDMAEMA-*b*-PMMA).⁵⁹ Emulsions stabilized with PDMAEMA-SiO₂ immediately broke at temperature above the critical flocculation temperature (CFT) of approximately 50 °C, as previously reported in our group.¹⁹ It has also been shown that poly(N-isopropylacrylamide) (PNIPAM) grafted polystyrene nanoparticles produced thermally responsive Pickering emulsions. When the emulsions were heated from room temperature to 40 °C, PNIPAM transitioned from a coil to a globule and caused emulsions to phase separate.⁶⁸ The mechanism by which emulsions destabilize in response to stimuli is not well studied but could be due to several factors. The change in solvent quality as a result of the change in temperature or pH could alter the particle adsorption energy to an unfavorable state which leads to particle desorption from the interface. The corresponding change in particle properties with the stimuli could also alter the structure of the adsorption layers at the interface, and therefore affect the mechanical properties of droplet stabilization.

1.4.3 Nanoemulsions

Nanoemulsions are oil-in-water or water-in-oil emulsions with droplet size on the order of 100 nm.³⁹⁻⁴⁴ The long-term stability of nanoemulsions makes them unique and desirable. In addition, nanoemulsions present advantages over conventional emulsions (macroemulsions with

droplet size around 3 – 10 μm) because of their small droplet sizes, which give a large surface area and free energy. Oil-in-water nanoemulsions are commonly used in drug delivery systems to encapsulate hydrophobic drugs,^{69–71} increase drug solubility⁷² and enhance the penetration rate of the materials into the human body.⁷³ The kinetic stabilization of nanoemulsions against flocculation, sedimentation and creaming leads to a more homogeneous structure, and has found numerous applications in the field of cosmetics and food industries.^{39,41,42} Nanoscale emulsion droplets also allow one to synthesize nanocomposites, nanoparticles and nanocapsules using nanoemulsions as templates.^{44,74,75} Therefore, understanding the change in nanoemulsion droplet size under different storage conditions may aid in the design of nanoemulsions for various applications.

There is often a confusion between nanoemulsions and microemulsions since these two types of colloidal dispersion bear numerous similarities but they also have important differences.^{43,76} Both nanoemulsions and microemulsions consist of oil (or water) droplets stabilized by surfactants and dispersed in continuous water (or oil) phase. They also possess similar physicochemical properties, such as long-term stability and high optical clarity due to their nanoscale droplet size. However, microemulsions are thermodynamically stable whereas nanoemulsions remain only kinetically stable.^{43,76} Therefore, the properties and structure of the nanoemulsions are affected by their preparation methods and their sample history. **Table 1.2** summarizes the major difference between two emulsion systems which can be used to distinguish nanoemulsions from microemulsions.

Table 1.2. Differences between nanoemulsions and microemulsions

	Nanoemulsions	Microemulsions
Long-term storage	Kinetically stable	Thermodynamically stable
Sample history	Path-dependent	Path-independent
Particle size distribution	Multiple peaks or single broad peak	Single narrow peak
Particle shape	Spherical	Spherical or non-spherical

Two main methods are typically used for preparing nanoemulsions: high-energy methods and low-energy methods.^{40,44,76} High-energy methods use mechanical devices to provide energy required to disrupt and mix the oil and water phases so that small droplets are formed. The most widely used high-energy methods include ultrasonic emulsification, high-pressure homogenization and microfluidic emulsification.⁷⁷⁻⁷⁹ Low-energy methods alter internal physical properties of the system such as temperature or composition to produce nanoemulsions and they are highly dependent on the nature of the system, such as solubility and geometry of the molecules. Low-energy methods are not frequently used in the industry compared to high-energy methods since the factors that affect the formation and stability of nanoemulsions are not fully understood. However, interest in low-energy methods has grown considerably in recent years due to its energy efficiency and ease of implementation. Different low-energy methods have been developed to form nanoemulsions, including spontaneous emulsification, phase inversion temperature and phase inversion composition methods.⁸⁰⁻⁸³

1.4.4 Spontaneous emulsification

Emulsions are typically prepared by intensive mechanical stirring to break up droplets until a desired size is obtained. However, spontaneous emulsification may occur when two immiscible liquids are brought into contact; an emulsion is instantly formed without the need of an external energy. This mixing energy originates from the difference in chemical potential

between the phases where the two bulk liquids are not initially at equilibrium, leading to a redistribution of matter across the liquid/liquid interface.^{84,85} Three principle mechanisms for spontaneous emulsification have been proposed based on interfacial turbulence, transient negative interfacial tension, and diffusion and stranding.^{85,86} (a) Interfacial turbulence is driven by an interfacial tension gradient. Although interfacial turbulence does increase the rate of emulsification, it may not be the dominant factor for spontaneous emulsification to occur. (b) Low (negative) interfacial tension results in the expansion of interfacial area and the formation of droplets. However, negative interfacial tension is not required for spontaneous emulsification to take place because the dispersion process itself increases entropy and thus decreases the free energy of the system. (c) Diffusion and stranding involves components diffusing between phases and emulsion droplets form due to the regions of supersaturation.^{84,87} New mechanisms for spontaneous emulsification have been proposed recently, such as explosion of a bilayer structure^{88,89}, inversion of a micellar solution,⁹⁰ and change in surfactant curvature.^{91,92} Although the mechanism responsible for spontaneous emulsification is not yet fully understood, these proposed mechanisms remain as an important reference for spontaneous emulsification studies.

1.4.5 Interfacial tension reduction

Interfacial tension results from the difference in energy between molecules at a fluid interface compared to their bulk counterparts. A molecule is in a lower energy state when in contact with a neighboring molecule of the same type than if it is alone. The interior molecules are surrounded on all sides by the same type of molecules whereas boundary molecules are missing neighbors and thus have a higher energy. The greater the dissimilarity between the two fluid phases, the larger the interfacial tension between them. Interfacial tension can be equally

described as the amount of energy required to create a unit area of interface between two immiscible liquids.

Surface active agents are compounds which tend to concentrate at the interface and reduce interfacial tension. Lowering interfacial tension facilitates the formation of foams and emulsions with considerably less energy input during homogenization and favors the formation of small droplets. For bare particles without polymers tethered to the surface, the interfacial tension is not significantly reduced upon particle adsorption.³ It has been shown that particles with polymer arms grafted from the core can effectively lower the interfacial tension. For example, poly(styrenesulfonate)-grafted silica reduced the trichloroethylene/water interfacial tension from 30 to 15 mN/m with 0.5 wt% of particles.²⁰ SiO₂-PDMAEMA brushes reduced the air/water surface tension to 45 mN/m at a concentration as low as 0.02 wt%.²⁴ The interfacial tension of dodecane/water was lowered by 33 mN/m with 0.003 wt% of poly(oligo(ethylene oxide) monomethyl ether methacrylate)-grafted iron oxide clusters.⁹³ The high efficiency for lowering the interfacial tension is attributed to the ability of these polymer-grafted particles to deliver a high concentration of polymer to the interface due to their compact structure.

1.4.6 Dilatational modulus

The dynamic mechanical properties of adsorbed layers, which relate the stresses in the interface to the deformation, are important in understanding of the stability of foams and emulsions. There are three basic deformation modes on a flat interface: shear, extension, and dilatation. (**Figure 1.2**) A fourth type of deformation mode, bending, can occur when the interface is curved. In a shearing deformation, a square area of interface is deformed into a parallelogram with base and height dimensions the same as the square. In an extensional

deformation, the same initial square is elongated to a rectangle with the total interfacial area kept constant. In a dilatational deformation, the area of the interface is increased or decreased, whereas the shape of the interface area remains the same. In bending, a deformation takes place normal to the interface, i.e., the curvature of the interface changes. Although there is much interest in measuring properties due to shear,^{94–96} extension,^{97–99} and bending^{100–102} at fluid interfaces, this dissertation focuses on dilatational deformations.

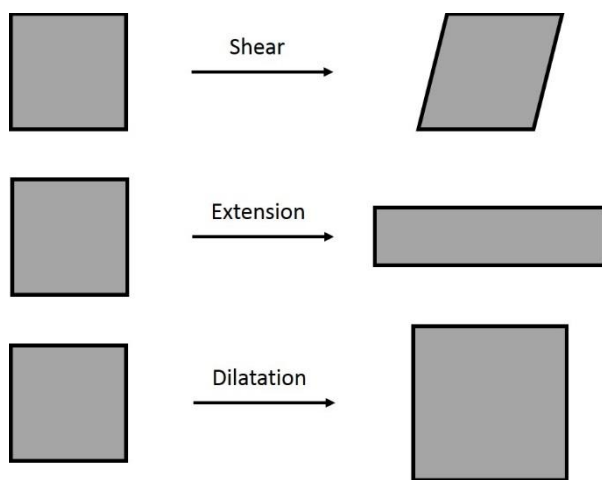


Figure 1.2. Types of interfacial deformation on a flat interface: shear, extension and dilatation.

The interfacial dilatational modulus measures the stiffness of the interface against a dilatational compression or expansion, which can contribute to the long-term stability of foams and emulsions. For two droplets to coalesce, they must get close enough to each other that the interface between them will be deformed in the dilatational (change of interfacial area) mode, and the ability of the adsorbed layer to induce a resistance to the dilatational deformation can enhance the stability of the system. Large dilatational modulus is related to slower

adsorption/desorption timescales of the stabilizers than the timescales on which the interface is perturbed, and a large dilatational modulus hinders the interdroplet film drainage.¹⁰³

The ability for polymers to deform or rearrange at the interface (i.e., structure of the adsorbed layer) can affect the interfacial dilatational modulus. For instance, globular proteins exhibit higher dilatational moduli than disordered proteins at the hexadecane/water interface, suggesting the elasticity of the interface increases with increasing rigidity of the adsorbed protein molecules.¹⁰⁴ A simulation has suggested that the structure of protein and polysaccharide adsorbed layers can be modulated by changing the electrostatic interactions, mixing ratio, ionic strength and order of adsorption to the interface, and therefore affects the surface dilatational modulus.¹⁰⁵ Studies have also shown that the foam stability is correlated to the dilatational rheology, which is influenced by the molar ratio of surfactants and oppositely charged polyelectrolytes in the solution resulting in different structure of adsorbed layer.^{106,107}

1.4.7 Polymer adsorption at fluid interfaces

The adsorption of polymers at a liquid/liquid interface has become increasingly important in recent years. For instance, many of the self-assembly processes involving macromolecules occur at such interfaces,^{108,109} and chemical reactions, such as polymerization or functionalization of macromolecules,¹¹⁰ can also be carried out at a liquid-liquid interface. Moreover, stability of emulsions is affected by an efficient migration of polymers (or surfactants) towards the boundaries between two fluids. When more polymer is adsorbed at the interface, a higher steric barrier is formed between droplets, which prevents coalescence and enhances the stability.^{111,112}

The driving force for polymer adsorption to an interface is balanced by (1) the enthalpy contribution in adsorption energy and (2) the entropy penalty upon polymer adsorption. The enthalpy contribution arises from the attractive polymer-interface interactions and the difference in polymer-solvent energy between the polymer in bulk solution and at the interface. The entropy penalty comes from the reduction in degree of freedom for polymers to explore more configurations when adsorbed from the bulk to the interface. The balance of these forces result in the conformation of polymers adsorbed at the interface like the one depicted in **Figure 1.3**. Linear polymers adsorb in a series of loops, tails and trains. Train segments correspond to those groups in the polymer that are in direct contact with the surface, while loops are segments that have no contact with the surface that connect trains and tails are the non-adsorbed chain ends. Adsorption of nanoparticulate polymer brushes at the interface is subject to the same balance of forces. Nanoparticulate polymer brushes adsorb with several arms contacting the interface and the rest of the chains extending to the bulk solution (**Figure 1.3b**).

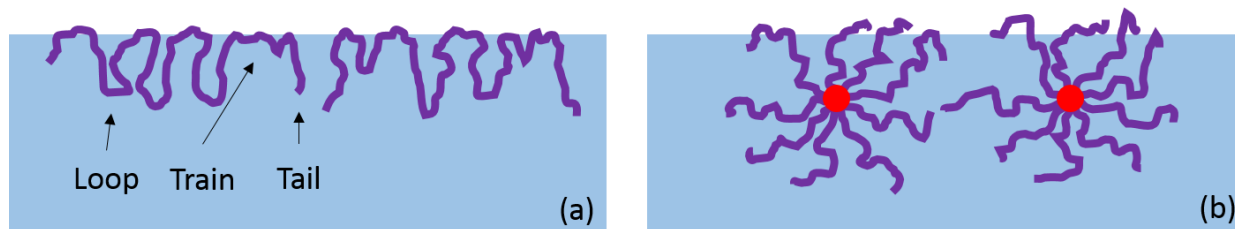


Figure 1.3. Structure of (a) linear polymers and (b) nanoparticulate polymer brushes adsorbed to a fluid/fluid interface.

Adsorption of polymers at a liquid/liquid interface is different from that at a solid/liquid interface. Polymers can have different degrees of segment penetration into both phases based on the solvent quality of each phases. Furthermore, if two liquids are immiscible, polymer

adsorption at the interface would screen the unfavorable interactions between two solvents and lower the interfacial tension.¹¹³ While the adsorption behavior of polymer chains at fluid interfaces has been extensively studied,¹¹³⁻¹¹⁷ the behavior of nanoparticulate polymer brushes at fluid interfaces has been less thoroughly investigated. Prior work as well as computer simulations have investigated the surface morphology and the conformation of nanoparticulate polymer brushes at fluid interfaces.^{60,118-122} The interactions between particle and hence the structure of the adsorbed layer are highly dependent on the length of the polymer chains and the solvent quality.^{118,121,122} Polymer brushes adapt more extended configuration with increasing chain lengths or when they reside in the better solvent. It has also been suggested that the star architecture favors the formation of highly curved interfaces; this surface morphology remains stable even at very high compression, unlike the linear diblock copolymers which tend to reconfigure at moderate compression.¹¹⁹

2 Materials and Methods

2.1 Polymer brush nanoparticles

All star polymers were synthesized by atom transfer radical polymerization (ATRP)^{123–127} in collaboration with the research group of Professor Krzysztof Matyjaszewski in the Department of Chemistry, Carnegie Mellon University. This section briefly summarized the synthesis of the materials. Detailed characterization of the star polymers used in this dissertation will be described in the associated major content chapters later on.

2.1.1 Multi-arm PEO star polymers

Poly(ethylene oxide) (PEO) star polymers are synthesized by atom transfer radical polymerization of PEO methacrylate macromonomers (PEO₄₅MA, molecular weight of 2000) with divinylbenzene (DVB) as a cross-linker. Detailed synthesis and characterization are published in previous work from our group.^{17,18} The resulting material has a densely cross-linked polymeric core surrounded by a hydrophilic corona of PEO₄₅MA arms. Gel permeation chromatography in tetrahydrofuran with multi-angle laser light scattering indicates the weight average molecular weight (M_w) is 1.76×10^5 . Factoring in the M_w , conversion of PEO₄₅MA and DVB indicates that each star polymer has 64 PEO arms on average.¹⁸ The PEO star polymers form limited aggregates in water, consisting of three or four PEO star polymers.¹²⁸

2.1.2 β -cyclodextrin core star polymers

Star polymers, consisting of a β -cyclodextrin core with 14 polymer arms, were synthesized using the “grafting from” atom transfer radical polymerization method.^{123–127} The functionalized β -cyclodextrin cores were first synthesized, followed by polymerization of di(ethylene glycol) methyl ether methacrylate (MEO₂MA) and 2-(dimethylamino)ethyl

methacrylate (DMAEMA) to generate PMEO₂MA and PDMAEMA star polymers, respectively. The full synthesis procedures for each star polymer were described in previously work from our group.¹²⁸ PMEO₂MA star polymer is a non-ionic polymer and exhibits a lower critical solution temperature (LCST) of 29 °C in water, whereas PDMAEMA star polymer is a weakly cationic polyelectrolyte whose degree of ionization depends on the pH and ionic strength of the aqueous solution. The LCST of PDMAEMA occurs in the range of 35 – 100 °C and is a function of pH.^{19,24,128–130} Diblock star polymers were synthesized by successive, chain extensive polymerization of DMAEMA from the PMEO₂MA star polymers, resulting in 14 block copolymer arms comprised of PMEO₂MA as an inner block and PDMAEMA as an outer block. The degree of polymerization and molecular weight of each star polymer were summarized in **Table 2.1**. The intensity-average hydrodynamic diameter of PMEO₂MA star polymers in water at 4, 25 and 45 °C, measured by dynamic light scattering with a Malvern Instruments Zetasizer Nano ZSP, are summarized in **Table 2.2**.

Table 2.1. Degree of polymerization and molecular weight of synthesized 14-arm star polymers

Name	Star polymer type	Degree of polymerization		MW
		MEO ₂ MA	DMAEMA	
PMEO₂MA stars	β-CD-(PMEO ₂ MA) ₁₄	50	N/A	135,000
PDMAEMA stars	β-CD-(PDMAEMA) ₁₄	N/A	62	140,000
Diblock stars	β-CD-(PMEO ₂ MA-b-PDMAEMA) ₁₄	50	35	212,000

Table 2.2. Temperature effect on the hydrodynamic diameter of PMEO₂MA star polymers in water

Temperature (°C)	Hydrodynamic diameter (nm)
4	8.1 ± 0.45
25	7.8 ± 0.42
45	160 ± 11

2.2 Linear polymers, surfactants and solvents

Linear PEO polymers with molecular weights of 2×10^5 and 1×10^6 (denoted as PEO 200k and PEO 1000k) were purchased from Sigma-Aldrich, and linear PEO with a molecular weight of 6000 (PEO 6k) was purchased from Fluka. The linear PEO samples were used as received. Triton X-100 was purchased from J. T. Baker Chemical Co. and used as received. Water was deionized and purified to a resistivity of $18.2 \text{ M}\Omega \cdot \text{cm}$ using a Barnstead Nanopure Diamond system. Xylene (98.5%) was purchased from Spectrum Chemicals and used as received. Cyclohexane (99+%) purchased from Alfa Aesar was further purified by passage through a basic alumina column to remove trace surface active impurities. Interfacial tensions of clean oil/water interfaces were measured to ensure the absence of surface active contaminants. Sodium chloride (NaCl, VWR Life Science AMRESCO) was used to tune ionic strength of aqueous solutions, and pH adjustments were made using 0.1 M solutions of HCl (BDH Chemicals) or NaOH (Fisher Chemical). Unless otherwise specified, the salt concentration in β -cyclodextrin core star polymer solutions was 1 mM NaCl. All experiments were conducted at room temperature, approximately 22°C .

2.3 Experimental methods and techniques

This section details the primary experimental methods used to study the foaming/emulsification efficiencies and stability, and the interfacial properties of star polymers adsorbed at fluid interfaces. Foam and emulsions were generated using a high shear homogenizer. The interfacial properties were characterized using a number of surface sensitive measurement techniques. Pendant drop tensiometry was used to determine interfacial tension and dilatational modulus from the shape of a pendant liquid drop. Ellipsometry was used to evaluate

the extent of adsorption of star polymers at fluid interface. The dynamic light scattering methods were used to probe size and charge of the star polymers.

2.3.1 Foaming and emulsification

2.3.1.1 Foaming

Foaming was carried out using a sawtooth homogenizer (Biospec Tissue Tearor 985370-395) at 1.65 Watts for one minute with a 10 mL polymer solution in water. The solutions were contained in 2.4 cm diameter glass vials. After foaming, the foam height was recorded as a function of time to characterize its stability. Foams were stored in sealed glass vials at room temperature.

2.3.1.2 High shear emulsification

Emulsions were made using the sawtooth homogenizer at the same power output (1.65 W) for one minute. The 1:1 volume ratio of oil:water is defined to be the preferred emulsion type condition,^{11,131} which was determined by drop test measurements. Unless otherwise specified, polymers were dispersed in water before emulsification. Emulsion stability was measured by monitoring the height change of each phase (oil, emulsion, and/or water phase) over time. Emulsions were stored in sealed glass vials at room temperature.

2.3.2 Pendant drop tensiometry

2.3.2.1 Interfacial tension measurements

Equilibrium air/water and oil/water interfacial tensions were measured as a function of bulk polymer concentration using pendant drop tensiometry¹³² (Biolin Scientific Optical Tensiometer). An aqueous drop of polymer solution was created at the end of a needle and

suspended in air or oil. The drop shape was recorded and the interfacial tension was determined by analysis according to:

$$\gamma = \Delta\rho g \frac{R_0^2}{\beta} \quad (2.1)$$

where γ is interfacial tension, $\Delta\rho$ is density difference between the fluids, g is gravitational constant, R_0 is radius of drop curvature at apex, and β is Bond number. The Bond number can be determined through the Young-Laplace equation expressed as three first order equations:

$$\frac{dx}{ds} = \cos \varphi \quad (2.2)$$

$$\frac{dz}{ds} = \sin \varphi \quad (2.3)$$

$$\frac{d\varphi}{ds} = 2 - \beta z - \frac{\sin \varphi}{x} \quad (2.4)$$

where x is the horizontal coordinate, z is the vertical coordinate, φ is the angle of rotation measured from the apex, and s is the arc length, as depicted in **Figure 2.1**.

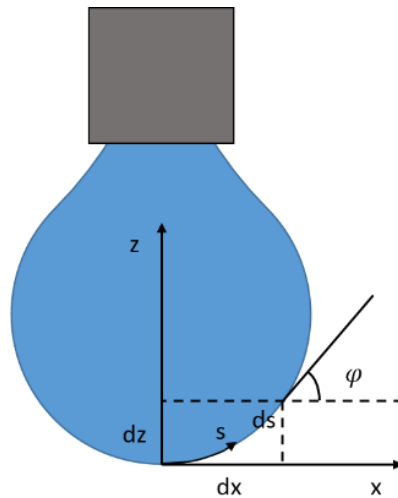


Figure 2.1. The pendant drop geometry. An aqueous drop of polymer solution was created at the end of a needle and suspended in air or oil. The drop shape was recorded and the interfacial tension was determined by analysis according to the Young-Laplace equation.

For each measurement, the time-dependent interfacial tension was monitored to ensure the interfacial tension had reached equilibrium. Interfacial tensions of clean air/water and oil/water interfaces were measured with both the pendant drop tensiometer and a du Noüy ring tensiometer, and the values were consistent. All interfacial tension reduction results are reported as interfacial pressures (Π), which is defined as the difference between the interfacial tension of polymer-free interface (γ_0) and polymer-adsorbed interface (γ).

$$\Pi = \gamma_0 - \gamma \quad (2.5)$$

2.3.2.2 Dynamic dilatational modulus measurements

The dynamic dilatational modulus was determined using the pendant drop tensiometer with a controlled sinusoidal oscillation of the drop volume. The drop surface area and the interfacial tension were simultaneously recorded. Before any dilatational modulus measurement, the drop was maintained at a constant volume to reach equilibrium as indicated by a constant interfacial tension. Dilatational experiments were conducted for varying bulk polymer concentration and oscillation frequency at a fixed areal strain amplitude of 3 – 5%.

The dynamic dilatational modulus (E_d) is defined as¹⁰⁴

$$E_d = \frac{d\gamma}{d \ln A} \approx A_0 \frac{\Delta\gamma}{\Delta A} \quad (2.6)$$

where γ is the total interfacial tension, A_0 is the initial interfacial area, and ΔA is the amplitude of the interfacial area oscillation. In a dynamic experiment, the total interfacial tension may have both equilibrium and non-equilibrium contributions related to rate-dependent dissipation or elastic deformations in the interface. When a small amplitude oscillation at frequency ω is applied to the system, the complex interfacial dilatational modulus (E^*) is determined by

$$\gamma(t)e^{i(\omega t + \delta)} = E^* \frac{\Delta A}{A_0} e^{i\omega t} \quad (2.7)$$

$$E^* = E' + iE'' \quad (2.8)$$

where δ is the phase angle between the forced area oscillation and the interfacial tension response, and E' and E'' are the elastic (storage) and viscous (loss) moduli, respectively.¹⁰⁴ The elastic part accounts for the recoverable energy stored in the interface whereas the viscous part accounts for energy lost through relaxation processes. The viscous modulus may be influenced by the adsorption/desorption dynamics of polymers or by viscous dissipation in the deforming interface. The dynamic dilatational modulus can differ from the equilibrium, or “Gibbs”, dilatational elasticity when viscous losses, non-equilibrium deformations or dynamic adsorption and desorption processes accompany the forced area oscillation of an adsorbed layer.

It should be noted here that the modulus measured with this method is not pure dilatational modulus but the combination of the dilatational and bending modulus. When measuring properties of curved interfaces, bending modulus can be important and its magnitude depends on the curvature of the interface.^{133–135} However, the star polymer adsorbed layers generally exhibit very small bending moduli compared to the dilatational moduli. This is evident in the results shown in **Figure 2.2**, where the measured modulus is independent of the droplet volume used in the pendant drop tensiometry. **Table 2.3** summarizes the corresponding interfacial pressures, the radii and bond numbers for PEO stars and diblock stars at different droplet volumes during small amplitude oscillation.

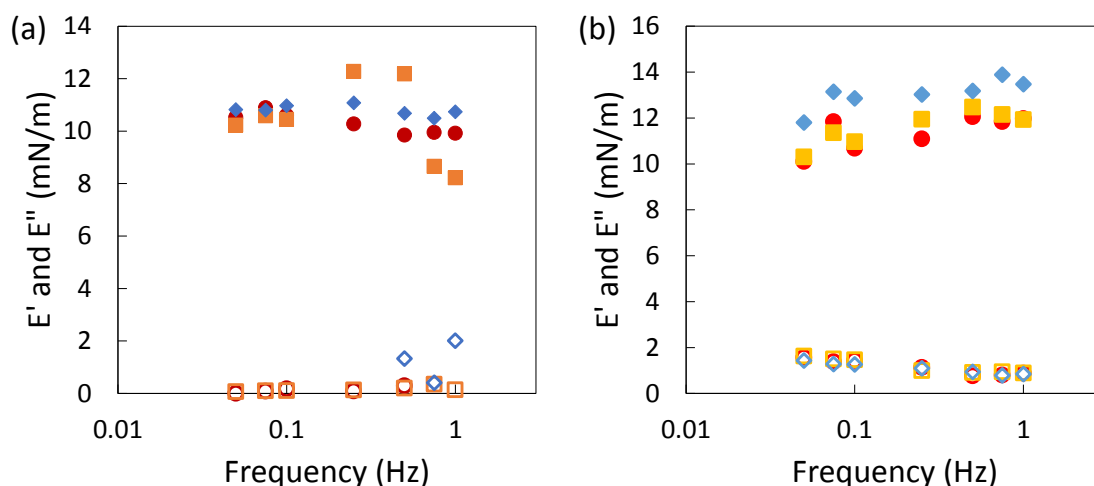


Figure 2.2. The storage (filled symbols) and loss (empty symbols) dynamic dilatational modulus of 0.01 wt% (a) multi-arm PEO star polymers and (b) diblock star polymers adsorbed at cyclohexane/water interface as a function of frequency with different volume droplet. (a) Droplet volume: (●, ○) 15 μL (■, □) 5 μL and (◆, ◇) 3 μL . The measured interfacial tensions before the dilatational experiments were 25.7 ± 0.05 , 25.1 ± 0.5 , and 25.6 ± 0.8 mN/m for droplet volume 15, 5, and 3 μL , respectively. (b) Droplet volume: (●, ○) 8 μL (■, □) 6 μL and (◆, ◇) 4 μL . The measured interfacial tensions before the dilatational experiments were 10.6 ± 0.02 , 10.9 ± 0.03 , and 11.7 ± 0.09 mN/m for droplet volume 8, 6, and 4 μL , respectively.

Table 2.3. Drop volume and the corresponding drop radius, measured interfacial tension and calculated Bond number for 0.01 wt% PEO star polymers and 0.01 wt% diblock star polymers adsorbed at cyclohexane/water interface during small amplitude oscillation

Star polymer	Drop volume (μL)	Drop radius (mm)	Interfacial tension (mN/m)	Bond number
PEO stars	15	1.5	25.6 ± 0.0005	0.2 ± 0.005
	5	1.0	24.5 ± 0.004	0.1 ± 0.01
	3	0.9	25.4 ± 0.004	0.07 ± 0.01
Diblock stars	8	1.2	10.5 ± 0.0006	0.31 ± 0.006
	6	1.1	11.2 ± 0.0008	0.25 ± 0.005
	4	1.0	11.8 ± 0.001	0.18 ± 0.006

2.3.2.3 Large amplitude, interfacial compression and expansion

The oil/water interfacial mechanics were also probed through large amplitude compressions and expansions to measure the dilatational modulus using pendant drop tensiometry. Before each measurements, the drop was maintained at a constant volume until the interfacial tension showed little change with time. The drop volume was then decreased or increased at a constant rate of 0.05 $\mu\text{L/s}$, which corresponds to the rate of interfacial area change of 0.07 – 0.1 mm^2/s . The change in interfacial tension and interfacial area was recorded for three interfacial compression and expansion cycles. The dilatational modulus was calculated using equation (2.6).

2.3.3 **du Noüy ring tensiometry**

The du Noüy ring method involves slowly lifting a ring, often made of platinum, from the surface of a liquid. The force (F) required to raise the ring from the liquid surface is measured and related to the interfacial tension (γ) of the liquid:

$$F = W_{ring} + 2\pi(R_i + R_o)\gamma \quad (2.9)$$

where R_i and R_o is the inner and outer radius of the ring, and W_{ring} is difference between the weight of the ring and the buoyant force.

Comparison of interfacial tension lowering when dispersing polymers in xylene or in water was done with a du Noüy ring tensiometer using the method for liquid/liquid interfaces.^{136,137} This was done to ensure a large volume of both the oil and water phases, in order to eliminate possible artifacts due to polymer depletion from dilute solutions in the small pendant drop when comparing adsorption from xylene or from water. Between each reading, the ring was rinsed by ethanol, acetone, and deionized water. For each measurement, the clean

xylene/water interfacial tension (γ_0) was measured before an aliquot of concentrated polymer stock solution was injected into either the xylene or water phase. The sample was gently stirred for five minutes with a magnetic stir bar in the aqueous phase and then allowed to equilibrate for a minimum of 12 hours before measuring the interfacial tension (γ). A second measurement was recorded 24 hours after the first measurement. Samples were covered between measurements to minimize evaporation. The two measured values were within experimental error, indicating the interfacial tension had equilibrated.

2.3.4 Ellipsometry

Adsorption at air/water and oil/water interfaces was measured using a phase-modulated ellipsometer (Beaglehole Instruments Picometer) with a polarized 632.8 nm laser beam.¹³⁸ Angles of incidence were set near the Brewster angle, and the measured ellipticity ρ was interpreted using parameters defined by Beaglehole:¹³⁸

$$x = \text{Re}(\rho) \frac{2}{1 + \text{Re}(\rho)^2 + \text{Im}(\rho)^2} \quad (2.10)$$

$$y = \text{Im}(\rho) \frac{2}{1 + \text{Re}(\rho)^2 + \text{Im}(\rho)^2} \quad (2.11)$$

For interfacial films much thinner than the incident light wavelength, the x parameter depends primarily on the refractive indices of the bulk phases while the y parameter is sensitive to the local variation of refractive index caused by the adsorbed layer.

Adsorption measurements were carried out in a glass Petri dish (diameter = 10 cm) containing 40 mL of water. For oil/water systems 40 mL of xylene or cyclohexane (depth of each phase = 0.5 cm) were carefully poured onto the water. Optical light guides similar to those described by Benjamins and co-workers¹³⁹ were used to pass the incident and reflected beams

through the oil layer to measure the oil/water interface. As a check on instrument alignment and the absence of surface-active impurities, the x and y parameters of a clean interface were recorded for 600 s to make sure they were stable and matched the theoretically expected values at the beginning of each experiment.

Adsorption isotherms were measured by adding a concentrated polymer stock solution to either the aqueous phase or the organic phase as appropriate to obtain the desired concentration. The solution was gently stirred for one minute with a glass rod and then allowed to rest for at least 12 h to reach a steady signal. The Δx and Δy ellipsometry signals (change compared to the clean interface) were recorded and averaged over 600 s at each incident angle afterwards.

For the air/water interface, the final Δx and Δy values were analyzed as a function of incident angle to determine the optical average refractive index and thickness of the adsorbed film using the single homogeneous film striated medium optical model¹⁴⁰ (air of refractive index 1.00, adsorbed film of refractive index n_f and thickness d_f , and bulk aqueous phase of refractive index n_0). The surface excess concentration (Γ) was then determined *via* the de Feijter relation¹⁴¹

$$\Gamma = \frac{d_f(n_f - n_0)}{dn/dc} \quad (2.12)$$

where dn/dc is the refractive index increment of the polymer solution, previously reported to be 0.13 cm³/g for both linear PEO and PEO star polymers in aqueous solution.¹³ The refractive index of the bulk aqueous solution, n_0 , was determined from the refractive index of pure water, 1.333, corrected for the polymer concentration and refractive index increment. TF Companion software (Semicon Software Inc.) was used to determine the optical average thickness of the adsorbed layer, for an assumed refractive index of the adsorbed layer. For the air/water interface, uncertainties in the refractive index and the corresponding thickness of the adsorbed film were

mutually off-setting, such that the surface excess concentration determined from equation (2.12) was independent of the assumed refractive index to within 10%. As will be discussed in **Chapter 3.7**, this was not the case for the oil/water interfacial systems, where the more limited optical contrast between the two liquids and the polymers prevented an unambiguous determination of surface excess concentrations.

2.3.5 Light scattering

2.3.5.1 Dynamic light scattering

Dynamic light scattering (DLS) measurements are performed on a Malvern ZetaSizer ZSP equipped with a He-Ne 633 nm laser. DLS is used to determine the hydrodynamic size distribution of star polymers and is appropriate for particle size range $\sim 1 \text{ nm} - 1 \text{ }\mu\text{m}$. DLS measures the fluctuations of the scattered light intensity from the suspended particles or polymers induced by Brownian motions as a function of time. These fluctuations can ultimately be related to the diffusion coefficients of the scattering species by analyzing the autocorrelation functions from the intensity data. The diffusion coefficient is proportional to the lifetime of the exponential decay and multiple exponential functions were employed to provide a distribution of diffusion coefficients. The corresponding hydrodynamic radius of the particles is then determined by the Stokes-Einstein relation.

The intensity size distributions favor larger particles due to the fact that the scattered light intensity is proportional to the radius of the particle raised to the sixth power.¹⁴² Therefore, to more accurately represent the particle size population, intensity-weighted distributions can be converted to number-weighted distribution which requires input of the refractive index of the scattering particles and solvent quality. The refractive index used for multi-arm PEO star

polymers, linear PEO and PMEO₂MA star polymers was 1.465. The refractive index of PDMAEMA stars and diblock stars was assumed to be similar to pure PDMAEMA (n = 1.44). Number distributions were only weakly sensitive to adjustments in refractive index.

2.3.5.2 Electrophoretic light scattering

Electrophoretic mobility of star polymers was measured with a Malvern ZetaSizer ZSP in a disposable folded capillary cell containing two gold electrodes. A voltage drop is applied across the capillary cell while collecting scattering intensity from the suspended species. The frequency of incident light is then compared to the frequency of scattered light in the presence of an oscillating applied electric field. Particles or polymers that have a net charge or a net zeta potential will travel towards the oppositely charged electrode with a velocity, which results in a phase shift between the frequencies of incident light and scattered light. The electrophoretic mobility of the scattering species can then be extracted from the measured phase shift. The electrophoretic mobility (μ_E) is defined as

$$\mu_E = \frac{v}{E} \quad (2.13)$$

where v is the particle velocity and E is the strength of the applied electric field. The zeta potential of the particle is calculated from the electrophoretic mobility using the generalized von Smoluchowski equation and Henry function, $f(\kappa a)$:

$$\mu_E = \frac{\varepsilon \varepsilon_0 \zeta}{\eta} f(\kappa a) \quad (2.14)$$

$$f(\kappa a) = \frac{2}{3} \left[1 + \frac{1}{2 \left(1 + \frac{2.5}{\kappa a (1 + 2e^{-\kappa a})} \right)^3} \right] \quad (2.15)$$

where ε is the fluid dielectric constant, ε_0 is the permittivity of free space, ζ is the zeta potential, η is the fluid viscosity, κ is the Debye length, and a is the radius of the particle.

3 Interfacial activity of PEO star polymers at fluid interfaces

Reprinted (adapted) with permission from Y. Huang, M. Lamson, K. Matyjaszewski, and R. D. Tilton. Enhanced Interfacial Activity of Multi-Arm Poly(Ethylene Oxide) Star Polymers Relative to Linear Poly(Ethylene Oxide) at Fluid Interfaces. *Physical Chemistry Chemical Physics*, 2017, **19**, 23854 – 23868

3.1 Introduction

This chapter compares the interfacial activity of multi-arm poly(ethylene oxide) (PEO) star polymers and linear PEO chains at both air/water and oil/water interfaces. In order to understand how polymer structure controls interfacial behaviors, we determine the interfacial tension reduction (interfacial pressure), dynamic dilatational modulus and extent of adsorption of multi-arm PEO star polymers. They were prepared by atom transfer radical polymerization^{123–127} using PEO macromonomers. Each star possesses approximately 64 arms that have a molecular weight of 2000. The results are compared with linear PEO chains having molecular weights of 6000, 2×10^5 , or 1×10^6 . These were chosen to be comparable to a single arm of the star polymer, to an entire star polymer, and to the limited aggregates consisting of three or four PEO star polymers that form when they are dispersed in water.¹²⁸ Air/water, cyclohexane/water and xylene/water interfaces were investigated. The last two interfaces offer the opportunity to investigate adsorption to an interface with a poor solvent (cyclohexane) or with a good solvent (xylene) for PEO, where significant differences in organic phase penetration should be expected.

To motivate the interfacial studies we first report on the effectiveness of PEO stars and linear PEO as foam stabilizers and then report their interfacial activity at the air/water interface. This is followed by a brief comparison of PEO stars and linear PEO as emulsifiers, followed in

turn by reporting their interfacial activity at xylene/water and cyclohexane/water interfaces. Finally, path-dependent adsorption behaviors at the xylene/water interface are reported.

The results show that PEO star polymers produce larger interfacial tension reduction and dynamic dilatational moduli than linear PEO of any of the considered molecular weights, at each interface type. Adsorption isotherms measured by ellipsometry indicate that star polymers achieve higher surface excess concentration than the linear polymers at each interface. Star polymer adsorption characteristics are found to be path dependent, yielding significantly different interfacial tension reduction and interfacial films when initially dispersed in the xylene or aqueous phase, while none of the linear PEO samples display a path dependence. PEO star polymers in xylene drive spontaneous emulsification of quiescent xylene/water samples. This happens only when PEO stars are dispersed in xylene, not when dispersed in water, and it does not occur with linear PEO. This is consistent with the observations of path-dependent adsorption behavior.

3.2 Linear PEO and PEO star polymers characterization

PEO star polymers were synthesized by atom transfer radical polymerization^{123–127} of PEO methacrylate macromonomers (PEO₄₅MA, molecular weight of 2000) with divinylbenzene (DVB) as a cross-linker, as previously reported.¹⁸ The weight average molecular weight (M_w) was determined to be 1.76×10^5 by gel permeation chromatography in tetrahydrofuran with multi-angle laser light scattering. Factoring in the M_w , conversion of PEOMA, and DVB indicates that each star polymer has 64 PEO arms on average.¹⁸ Linear PEO polymers with molecular weights of 6000, 2×10^5 and 1×10^6 (denoted as PEO 6k, PEO 200k and PEO 1000k) were chosen to be comparable with to a single arm of the star polymer, to an entire star polymer, and to the limited

aggregates consisting of three or four PEO star polymers that form when they are dispersed in water.¹²⁸ The number-average hydrodynamic radii for PEO stars and linear polymers in water, measured by dynamic light scattering with a Malvern Instruments Zetasizer Nano instrument, are summarized in **Table 3.1**.

Table 3.1. Number-average hydrodynamic radii for PEO stars and linear polymers

Polymer	PEO 6k	PEO 200k	PEO 1000k	Stars
R_h (nm)	1.81 ± 0.02	4.6 ± 0.3	5.1 ± 1.2	6.6 ± 0.3

3.3 Interfacial behavior at air/water interface

3.3.1 Foaming efficiency and stability

Aqueous foaming results for PEO star concentrations varying from 0.001 to 0.1 wt% are summarized in **Figure 3.1**. Higher PEO star concentrations yielded greater initial foam volumes with smaller bubble sizes (**Figure 3.1a**). For concentrations of 0.005 to 0.1 wt%, significant fractions of the initial foam were retained after two hours of aging (**Figure 3.1b**). As the foam started to destabilize through the mechanisms of disproportionation and bubble coalescence, the bubbles started to grow and the foam height decreased. The apparent increase in foam height for the 0.005 wt% concentration resulted from the uncertainty of localizing the interface between the foam and the aqueous phase, as the interface was distorted by large bubbles. The foam was completely lost within 24 hours. No stable foam was produced with any of the linear PEO polymers for similar concentrations. The foams collapsed completely within 5 minutes after preparation. Just as the association of multiple arms with a dense polymer core makes PEO stars efficient emulsifiers,¹⁷ the nanoparticulate brush character of PEO star polymers renders them more effective foaming agents than linear PEO. This greater foaming effectiveness of PEO stars compared to linear PEO motivates a comparison of their fundamental interfacial behaviors at the

air/water interface, just as their superior emulsifying performance motivates a study of interfacial behavior at oil/water interfaces.

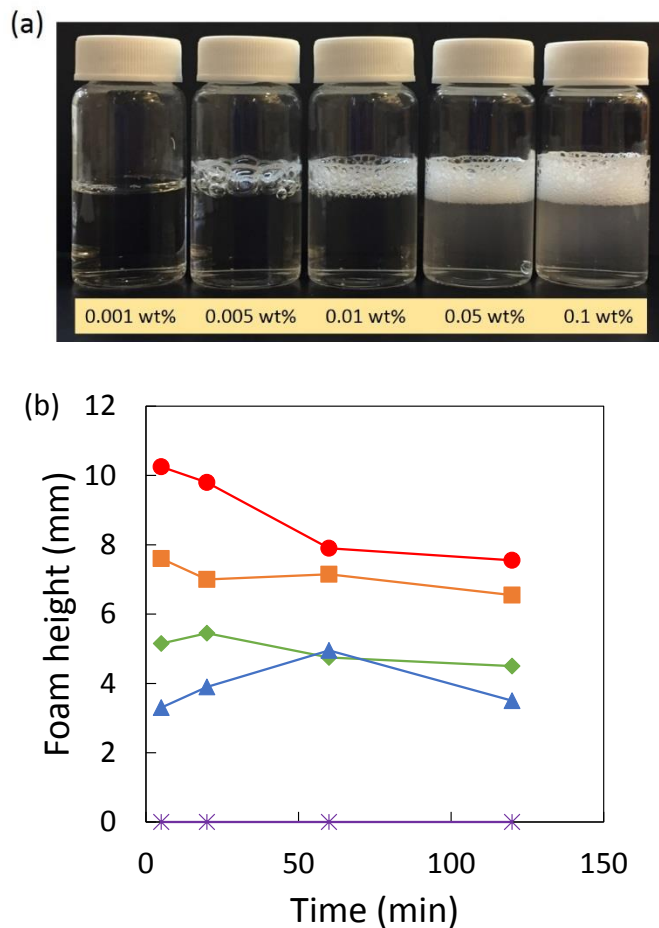


Figure 3.1. (a) Photographs of foams for varying concentrations of PEO stars 5 minutes after preparation. (b) Changes in foam height for different concentrations of PEO stars as a function of time: (●) 0.1 (■) 0.05 (◆) 0.01 (▲) 0.005 (*) 0.001 wt%. Lines serve to guide the eye.

3.3.2 Interfacial tension reduction

Figure 3.2 shows the surface pressure isotherms for PEO star polymers and linear PEO adsorbed at the air/water interface. The linear PEO 6k produced the lowest surface pressure, suggesting the smallest density of PEO segments penetrating the interface and/or the weakest

inter-chain interactions among all the polymers sampled. PEO 200k and PEO 1000k surface pressure isotherms were similar to each other and showed little dependence on bulk concentration. This has been observed previously¹⁴³ for high molecular weight PEO and is consistent with high affinity adsorption and a constant degree of polymer segment penetration of the interface. PEO star polymers produced the highest surface pressures (10 – 13 mN/m) and showed the greatest dependence on bulk concentration. These surface pressures are smaller than those achieved by PDMAEMA-grafted silica nanoparticles with high PDMAEMA chain grafting density and similar to those achieved by moderate grafting density PDMAEMA-grafted silica nanoparticles at the air/water interface.²⁴

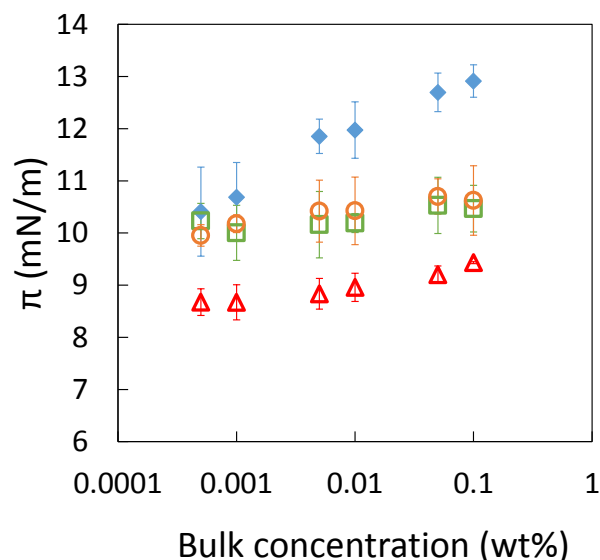


Figure 3.2. Surface pressure isotherm of (♦) PEO stars and linear (□) PEO 1000k, (○) PEO 200k, and (Δ) PEO 6k adsorbed to the air/water interface.

The larger surface pressure achieved by PEO stars than by linear PEO is consistent with more extensive segment penetration of the interface for PEO stars. Whereas linear PEO chains distribute segments among adsorbed trains and non-adsorbed loops and tails to balance the

entropic and enthalpic contributors to the overall adsorption energy,¹⁴⁴ the highly constrained PEO chains in the multi-arm star polymers perhaps hinder the formation of non-adsorbed loops.

Dynamic surface tension data indicate (**Figure 3.3**) that linear PEO reached its saturation conditions at the air/water interface more rapidly than PEO stars. The surface tensions of the linear PEO solutions dropped rapidly to their final value as the droplets were generated, while the surface tension relaxed over the course of approximately an hour to the final value for PEO stars. Despite their rapid adsorption relative to PEO stars, linear PEO chains were not effective foaming agents as PEO stars were.

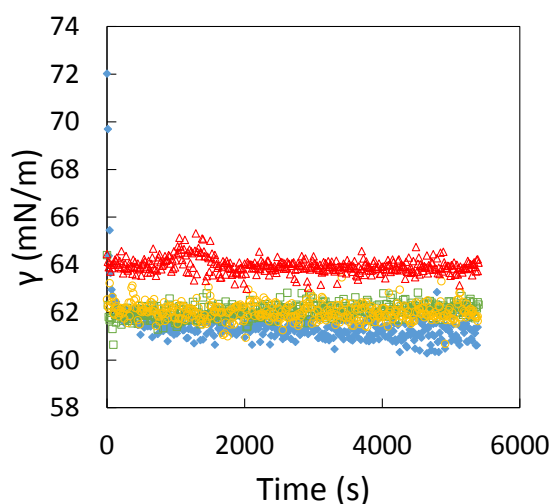


Figure 3.3. Interfacial tension reduction for 0.05 wt% of PEO stars and linear PEO at air/water interface: (♦) PEO stars and linear (□) PEO 1000k, (○) PEO 200k, and (Δ) PEO 6k.

3.3.3 Dynamic dilatational elasticity

Figure 3.4 reports the magnitude of the complex dynamic dilatational modulus of PEO star polymers adsorbed at the air/water interface as a function of oscillation frequency with a constant 3% area strain amplitude at different bulk concentrations. PEO stars produced moduli

between approximately 6 and 9 mN/m and showed no significant dependence on frequency ranging from 0.05 – 1 Hz (**Figure 3.4a**). These moduli are small compared to moduli observed to be on the order of several tens to over 100 mN/m for gel-forming protein layers at the air/water interface,¹⁴⁵ or moduli well over 100 mN/m for dense monolayers of insoluble surfactants.¹⁴⁶ The PEO star dilatational moduli are more similar to those measured for PDMAEMA-grafted silica nanoparticles²⁴ and spread monolayers of moderately hydrophobic particles at the air/water interface¹⁴⁷ or for either spread or adsorbed monolayers of low molecular weight poly(propylene glycol),¹⁴⁸ a more hydrophobic polymer than PEO.

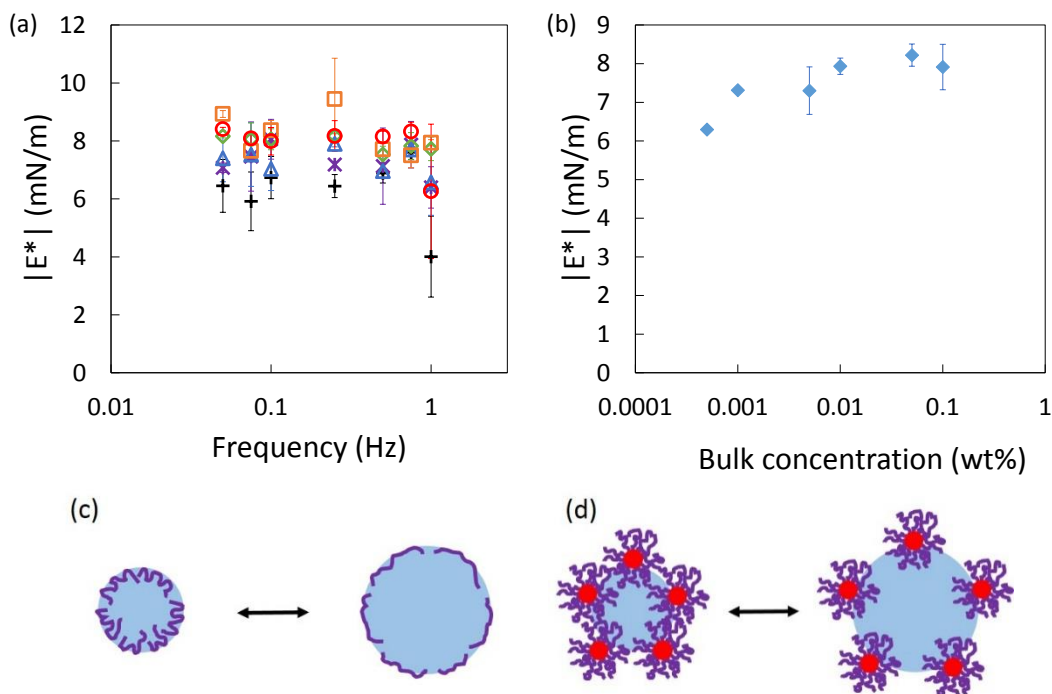


Figure 3.4. (a) The magnitude of the complex dynamic dilatational modulus of PEO stars adsorbed at the air/water interface as a function of frequency with 3% strain amplitude at different bulk concentrations: (○) 0.1 (□) 0.05 (◇) 0.01 (△) 0.005 (*) 0.001 (+) 0.0005 wt%. (b) The magnitude of the complex dynamic dilatational moduli averaged over all frequencies for PEO stars at the air/water interface. Schematic illustration showing how adsorbed (c) linear and (d) star polymers at the air/water interface differ in their response to the perturbation of surface area. (The illustrated area change is exaggerated relative to the 3% strain amplitude imposed in the experiments.)

The lack of a frequency dependence in the measured range suggests that any adsorption/desorption processes that could occur, would do so on longer timescales than those sampled here. Furthermore, the dynamic dilatational modulus averaged over all frequencies showed a modest increase with increasing bulk concentration (**Figure 3.4b**). Both the modulus and the surface pressure achieved by PEO star adsorption increased approximately 30% with increasing bulk concentration (**Figure 3.2**). In each experiment with PEO stars at the air/water interface, the dilatational storage modulus (E') accounted for 94 to 99% of the magnitude of the complex modulus. The insignificance of the loss modulus (E'') indicates that the PEO star layer is primarily elastic in the ~ 0.1 to 1 Hz frequency range. This is evident in the sample data shown in **Figure 3.5a**, where there is no significant phase angle between the sinusoidal interfacial tension and area oscillations. The dynamic dilatational elastic modulus will be compared to the static dilatational modulus below, after ellipsometry results are presented for PEO star surface excess concentrations.

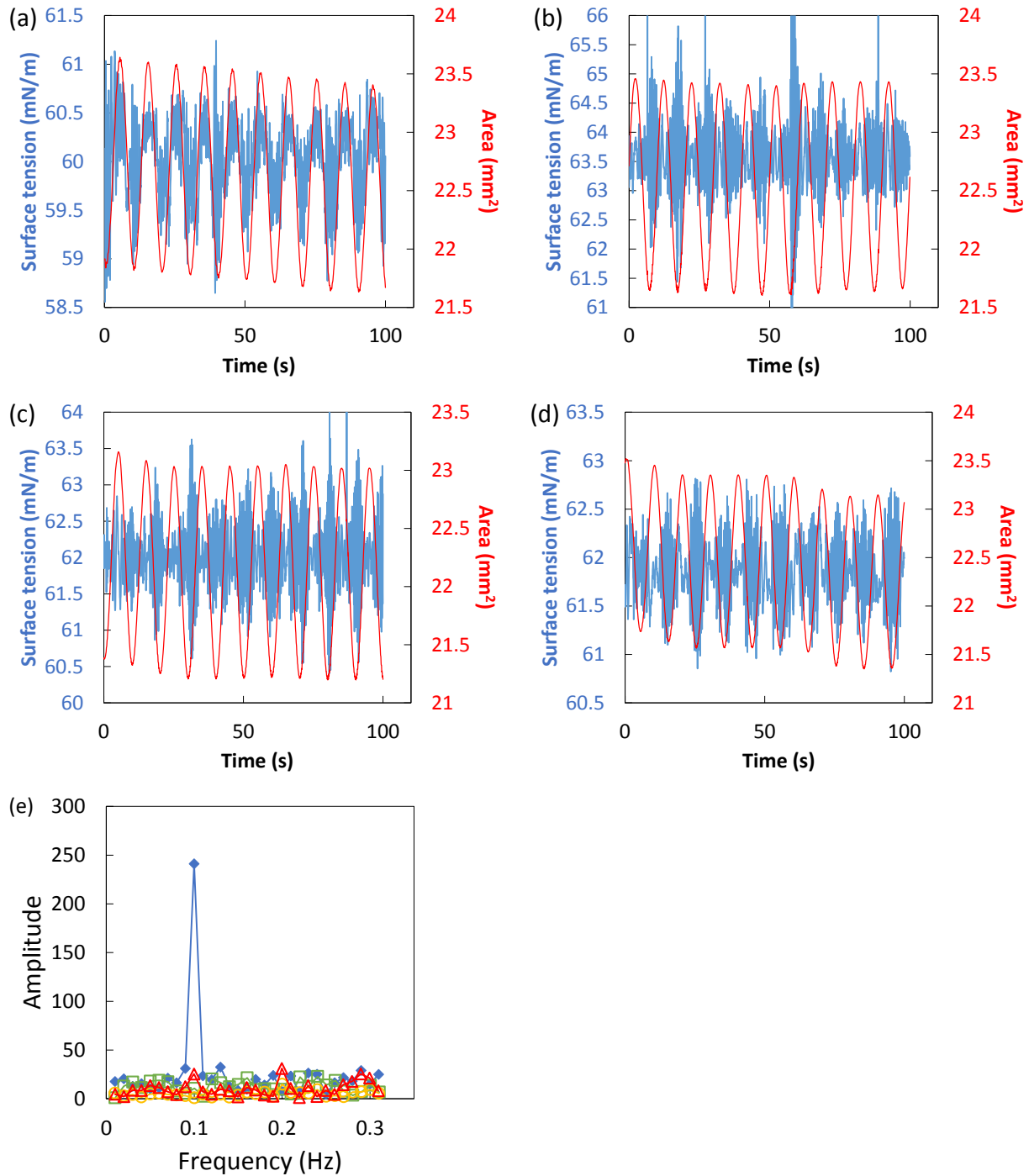


Figure 3.5. Surface tension and droplet area oscillation for 0.05 wt% of (a) PEO stars, linear (b) PEO 6k, (c) PEO 200k and (d) PEO 1000k at the air/water interface. The surface area oscillation frequency is 0.1 Hz. (e) Fast Fourier transform analysis of the surface tension data during forced surface area oscillations at the air/water interface confirms the lack of a dilatational elastic response for linear PEO, while PEO stars demonstrate a strong peak at the frequency of the forced area oscillation: (◆) PEO stars and linear (□) PEO 1000k, (○) PEO 200k, and (△) PEO 6k.

Whereas PEO stars produced finite dilatational moduli, none of the adsorbed linear PEO samples produced a detectable dilatational modulus. As seen in the representative data in **Figure 3.5, b – d**, the surface tension response for adsorbed linear PEO was not sinusoidal but instead merely fluctuated around the equilibrium tension with a similar signal:noise ratio as observed in a stationary drop. To check the absence of a forced interfacial tension change, the raw data was fast Fourier transformed. No peak was detectable at the forced oscillation frequency for linear PEO (**Figure 3.5e**). These measurements are made for frequencies between 0.1 and 1 Hz and differ from a previous surface light scattering analysis of capillary waves which indicated significant elasticity at high frequencies for linear PEO monolayers at the air/water interface.¹⁴⁹ The difference illustrates the important dependence of the dynamic dilatational modulus on the relative time scales of polymer conformational relaxations and interface deformation.

The absence of dilatational elasticity for linear PEO is attributed to its highly flexible structure which allows facile reconfiguration of polymer loops and tails at the interface when the area is perturbed at low frequency. During the surface area oscillation, the chains may freely shift segments between non-adsorbed loops and tails and adsorbed trains and thereby maintain a constant degree of interfacial penetration and constant surface pressure (see schematic illustration in **Figure 3.4c**). On the other hand, the PEO star adsorbed layer does exhibit dilatational elasticity. Conformational changes in the star polymer arms are restricted owing to the strong lateral constraints placed on them by neighboring chains in the same star polymer. These multi-arm PEO stars lack the configurational freedom to readily adjust the degree of interfacial penetration in response to a forced surface area change. Thus, the star polymers retain their configuration to a large extent and experience a surface dilution, decreasing surface pressure, upon area expansion and a surface densification, increasing surface pressure, upon area

reduction, as depicted schematically in **Figure 3.4d**. As the data in next section will show, the PEO stars are tightly packed at the air/water interface. In that case, lateral elastic compression of PEO chains on the closely packed PEO stars could contribute significantly to the dilatational elasticity. Then, the interfacial dilatational elasticity may reflect the compressional elasticity of the star polymers themselves. The compressional elastic character of nanoparticulate polymer brushes has been noted previously.¹⁵⁰

3.3.4 Large amplitude surface compression and expansion

To further investigate the structure of the PEO star adsorbed layer at the air/water interface, the surface pressure versus area isotherms were obtained from slow, large amplitude interfacial compression and expansion using the pendant drop tensiometer (**Figure 3.6**). Adsorbed layer compression significantly increased its surface pressure. There was no hysteresis between interfacial compression and expansion, and data from three compression/expansion cycles collapsed onto a single curve, suggesting that PEO stars are irreversibly adsorbed to the air/water interface. The isotherms showed no evidence of abrupt transitions in the adsorbed layer, and the quasi-static dilatational modulus $-d\Pi/d\ln A$ determined from the slow compression and expansion cycles increased smoothly to ~ 25 mN/m with increasing surface pressure. The moduli were $\sim 6 - 10$ mN/m at surface pressures below 15 mN/m, consistent with the dynamic dilatational moduli measured from the small amplitude oscillations (**Figure 3.4b**). Highly compressed monolayers had a modulus of ~ 30 mN/m at $\Pi = 25$ mN/m (**Figure 3.6b**).

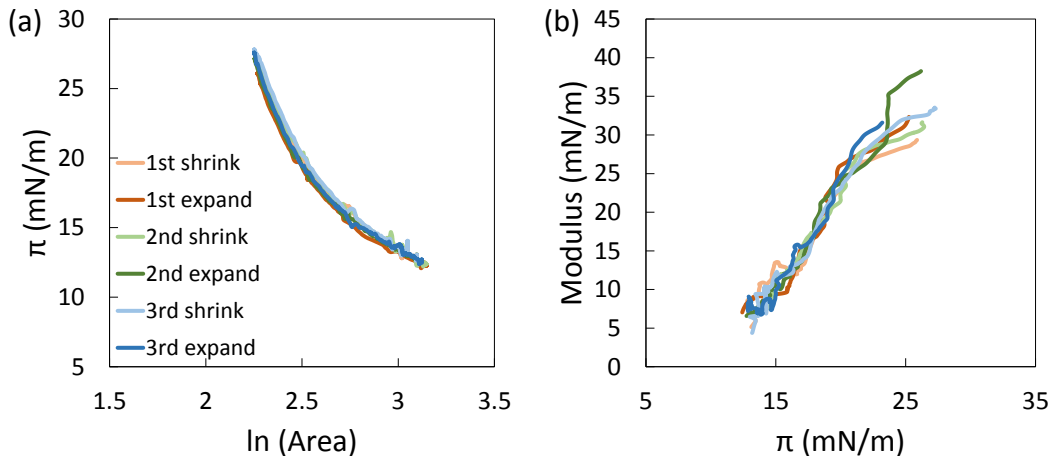


Figure 3.6. (a) Surface pressure versus area (mm^2) isotherm for PEO stars at air/water interface. The bulk concentration of PEO stars is 0.001 wt%. The surface area compression and expansion rate was kept in the range of $0.07 - 0.1 \text{ mm}^2/\text{s}$. Three cycles of surface compression and expansion were recorded. (b) Compression and expansion modulus for PEO stars at air/water interface as a function of surface pressure deduced from the surface pressure versus area isotherm. Three cycles of surface compression and expansion were recorded.

3.3.5 Extent of adsorption

Surface excess concentrations were measured using ellipsometry over a concentration range corresponding to the surface pressure measurements. As depicted in **Figure 3.7a**, the linear PEO 200k and PEO 1000k polymers produced a surface excess concentration, Γ , of approximately $0.5 \text{ mg}/\text{m}^2$ (and $\sim 0.3 \text{ mg}/\text{m}^2$ for PEO 6k) that does not vary with bulk concentration, which is consistent with the constant surface pressure (**Figure 3.2**). This surface excess concentration is similar to high molecular weight PEO adsorption measurements on solid hydrophobic surfaces and on hydrophilic silica surfaces.^{13,151–154} Adsorption of PEO star polymers increased from $\Gamma = 1.32 \pm 0.05 \text{ mg}/\text{m}^2$ at 0.0005 wt% bulk concentration to $\Gamma = 2.28 \pm 0.06 \text{ mg}/\text{m}^2$ at 0.1 wt%. The significantly higher surface excess concentration for star polymers is consistent with the efficient packing of mass in the compact star polymer architecture. The strong constraints on chain rearrangement at the interface inhibit the spreading of individual

stars, confining all of the mass to a small interfacial area. The additional mass is contained in the direction perpendicular to the interface. These experimental findings support the conclusions of molecular simulations that predict weak conformational perturbation of highly constrained multi-arm star polymers upon adsorption.¹⁵⁵ The present results for the air/water interface are consistent with the greater surface excess concentrations observed for star polymers than for linear polymers on solid surfaces.¹³ The mobility of the fluid interface relative to the immobile solid/liquid interface does not change the qualitative comparison of linear and star polymer adsorption.

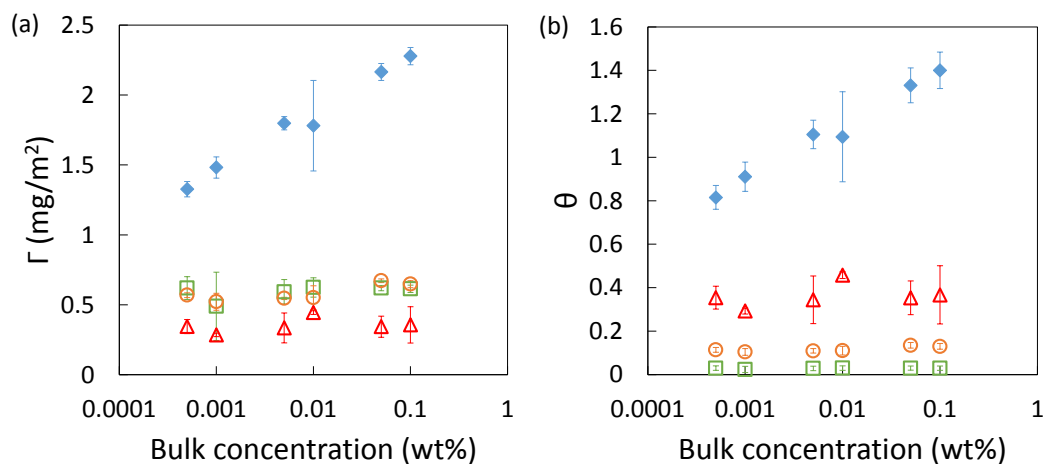


Figure 3.7. (a) Surface excess concentration and (b) apparent area fraction surface coverage for (◆) PEO stars and linear (□) PEO 1000k, (○) PEO 200k, and (△) PEO 6k adsorption to the air/water interface.

It is noted that attempting to deduce the surface excess concentration from the slope of the surface pressure isotherm (**Figure 3.2**) using the Gibbs adsorption equation would suggest $\Gamma = \sim 0$ mg/m² for linear PEO and an anomalously high value of $\Gamma = \sim 25$ mg/m² for PEO stars. Previous research has also shown that PEO adsorption produces a constant surface pressure over a wide concentration range.¹⁴³ The large discrepancy between the surface excess concentration

deduced from the Gibbs equation and that measured by ellipsometry indicates that simple application of the Gibbs adsorption equation without additional considerations of the thermodynamics of adsorbed polymer layers is inappropriate. The surface pressure is controlled by the density of polymer segments penetrating the interface and the polymer conformation adopted at the interface.

In order to estimate the degree of crowding at the interface, the area fraction surface coverage (θ) corresponding to each surface excess concentration was estimated by assuming that the projected area of a particular adsorbed species is equal to the cross-sectional area defined by its hydrodynamic radius R_h measured in bulk solution (*i.e.*, assuming minimal perturbation upon adsorption):¹⁴

$$\theta = \pi R_h^2 \Gamma \frac{N_A}{M} \quad (3.1)$$

where M is the molar mass and N_A is Avogadro's number. These area fraction estimates are plotted in **Figure 3.7b**. The low area fraction surface coverage for all linear PEO polymers (< 0.5) is expected for adsorbed homopolymers. The PEO star polymers are evidently densely packed on the surface. Their estimated area fraction coverage exceeds unity as the bulk concentration increases. This need not be interpreted as the formation of multilayers. It is more likely that the closely packed stars do experience some lateral compression (their projected area is decreased) upon adsorption. There is also evidence based on light scattering and atomic force microscopy¹³ that these PEO stars form small, slightly anisotropic aggregates in water. A crowding-induced re-orientation to place the long axis of the aggregates normal to the interface would be consistent with area fractions exceeding unity. Furthermore, there is likely size-dependent selective adsorption from the disperse sample. In any case, the evidence suggests

close-packing of elastic PEO stars, which is consistent with the existence of a significant dynamic dilatational modulus that is almost entirely elastic in origin. The formation of a dense, elastic adsorbed layer at even the most dilute PEO star concentrations examined here may be responsible for the better foaming performance of PEO stars compared with linear PEO.

3.3.5.1 Gibbs elasticity

The long-time (static) surface pressure (**Figure 3.2**) and the surface excess concentration (**Figure 3.7**) are both available for each bulk PEO star polymer concentration. Analysis of the static data according to equation (2.6), where A scales as $1/\Gamma$, yields the static dilatational elastic modulus as:

$$E_d = \frac{d\gamma}{d \ln A} = -\frac{d\pi}{d \ln A} = \frac{d\pi}{d \ln \Gamma} = -\frac{d\pi}{d \ln 1/\Gamma} \quad (3.2)$$

which would be the equilibrium or Gibbs elasticity for a thermodynamically equilibrated, fully insoluble monolayer. This analysis indicates a constant static dilatational elastic modulus of 5.1 mN/m over the concentration range examined here (**Figure 3.8**). Dynamic dilatational moduli ranged from 6 to 9 mN/m, indicating that static effects account for the majority of the dynamic modulus, with the remainder likely reflecting non-equilibrium reconfigurations during the 0.1 to 1 Hz forced oscillation.

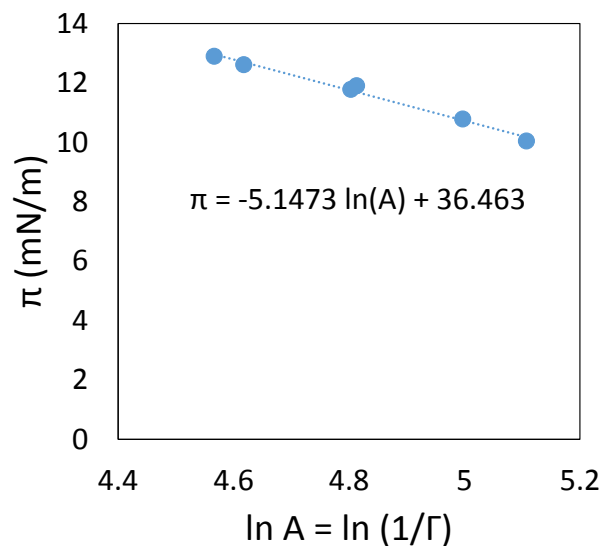


Figure 3.8. Surface pressure area isotherm for PEO stars adsorbed at air/water interface. Ellipsometry provided the static surface excess concentration for each PEO star concentration at which surface pressures were measured in independent experiments. Linear regression for the slope of π vs. $\ln(1/\Gamma)$ yields a static dilatational elasticity $E_d = 5.1$ mN/m.

3.3.5.2 Solution depletion upon polymer adsorption

The kinetics of polymer adsorption is influenced by the diffusion of polymer from the bulk to the surface. Polymer depletion from the bulk solution upon polymer adsorption is more pronounced in the pendant drop experiments than in the ellipsometry experiments due to the small volume of a pendant drop. **Table 3.2** summarizes the estimated change in the bulk concentration upon polymer adsorption for PEO stars and linear PEO in pendant drop experiments. The analysis is based on the assumptions that the pendant drop is spherical and a closed system, meaning that no polymers are added to the system after the drop is generated despite the fact that the pendant drop is connected to the bulk reservoir. Depletion from the bulk decreases the total polymer flux to the interface, which leads to slower transport dynamic to surfaces and lower surface excess concentration. As shown in **Table 3.2**, polymer depletion

becomes more pronounced at low bulk concentrations. Nearly 60% of PEO stars and ~ 15 – 30% of linear PEO are depleted from the bulk solution with concentration of 0.0005 wt%, which is consistent with their slower dynamic surface tension reduction at low bulk polymer concentrations.

Table 3.2. Estimated change in the bulk concentrations upon polymer adsorption for PEO stars and linear PEO with a 10 μ L pendant drop at different bulk concentrations. The analysis is based on the assumptions of a spherical pendant drop and no polymer diffusion from the bulk reservoir to the pendant drop. The surface excess concentrations are obtained *via* ellipsometry using large glass petri dishes.

Polymer	Conc. (wt%)	Total polymer (mg)	Γ (mg/m ²)	Polymer at interface (mg)	Polymer at interface /Initial in bulk (%)
PEO stars	0.1	0.01	2.28	0.0000511	0.51
	0.05	0.005	2.17	0.0000486	0.97
	0.01	0.001	1.78	0.0000400	4.00
	0.005	0.0005	1.80	0.0000404	8.07
	0.001	0.0001	1.48	0.0000333	33.26
	0.0005	0.00005	1.33	0.0000298	59.55
PEO 1000k	0.1	0.01	0.61	0.0000138	0.14
	0.05	0.005	0.62	0.0000139	0.28
	0.01	0.001	0.62	0.0000140	1.40
	0.005	0.0005	0.59	0.0000133	2.66
	0.001	0.0001	0.49	0.0000110	10.98
	0.0005	0.00005	0.62	0.0000139	27.80
PEO 200k	0.1	0.01	0.65	0.0000145	0.15
	0.05	0.005	0.67	0.0000151	0.30
	0.01	0.001	0.55	0.0000124	1.24
	0.005	0.0005	0.55	0.0000122	2.45
	0.001	0.0001	0.52	0.0000117	11.71
	0.0005	0.00005	0.57	0.0000128	25.54
PEO 6k	0.1	0.01	0.36	0.0000080	0.08
	0.05	0.005	0.34	0.0000077	0.15
	0.01	0.001	0.44	0.0000100	1.00
	0.005	0.0005	0.33	0.0000075	1.50
	0.001	0.0001	0.28	0.0000064	6.38
	0.0005	0.00005	0.34	0.0000077	15.46

3.4 Interfacial behavior at oil/water interfaces

3.4.1 Emulsification efficiency and stability

Stable emulsions were formed with 0.005 wt% and higher concentrations of PEO stars for both xylene/water and cyclohexane/water systems (**Figure 3.9**), consistent with prior findings.^{17,18} All emulsions were oil-in-water with dispersed oil droplet volume fractions exceeding 70 vol%. No stable emulsions were formed using any of the linear PEO samples; those emulsion droplets coalesced immediately after homogenization. This motivates the comparison of star and linear PEO behaviors at these liquid/liquid interfaces.

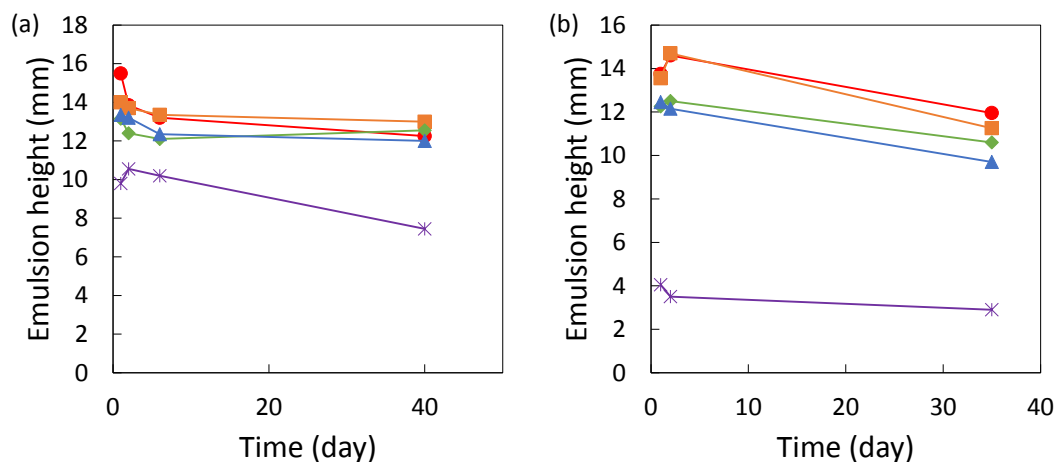


Figure 3.9. Effect of PEO star concentration on emulsion stability: (●) 0.1 (■) 0.05 (◆) 0.01 (▲) 0.005 (*) 0.001 wt%. Changes in height for (a) xylene-in-water and (b) cyclohexane-in-water emulsions at different concentrations of PEO stars as a function of time. Lines serve to guide the eye.

3.4.2 Interfacial tension reduction

Interfacial pressure isotherms measured by pendant drop tensiometry for PEO stars and linear PEO adsorbed at xylene/water and cyclohexane/water interfaces are plotted in **Figure 3.10**. The polymers were initially dispersed in water for these experiments. Interfacial tensions

for clean xylene/water and cyclohexane/water interfaces were measured to be 37.0 ± 0.2 and 49.9 ± 0.4 mN/m, respectively, which agree with values reported in the literature.^{24,156–158}

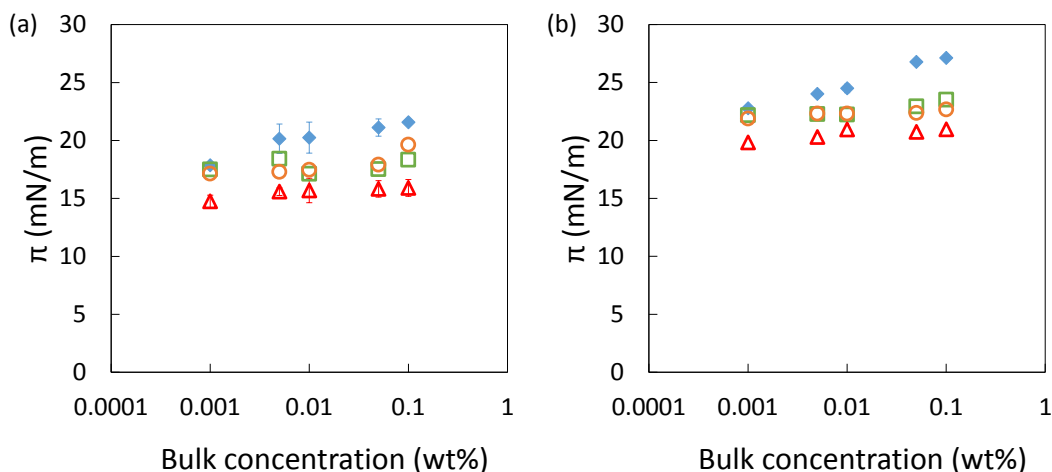


Figure 3.10. Interfacial pressure isotherm of (♦) PEO stars and linear (□) PEO 1000k, (○) PEO 200k, and (△) PEO 6k adsorbed from water to (a) xylene/water and (b) cyclohexane/water interfaces.

We hypothesize that the solvent quality of the organic phase for the polymers can alter the interfacial tension and polymer adsorption energy, with enthalpic factors deriving from segmental contacts with one or the other solvent, and entropic factors deriving from the associated conformational differences when one solvent is more readily penetrated by polymer segments than the other. There would be minimal segmental penetration into a poor solvent, but possibly substantial penetration into a good solvent. Xylene and cyclohexane were used to represent a good and a poor solvent, respectively, for PEO. Comparing **Figure 3.10a and b** indicates that these two interfaces showed the same trends, but the interfacial pressure measured at the cyclohexane/water interface was consistently several mN/m higher than at the xylene/water interface. This may be associated with greater compaction of polymer chains at the

poor solvent interface associated with the difference in adsorption enthalpy compared to the good solvent interface.¹²¹

The interfacial pressure isotherms for these oil/water interfaces showed similar trends to the air/water interface (**Figure 3.2**). PEO star interfacial pressures increased with the bulk concentration (although not as strongly as at the air/water interface) and were consistently greater than the linear PEO interfacial pressures (but again, not as much as at the air/water interface). The surface pressures produced by PEO stars are comparable to those produced by PDMAEMA-grafted silica nanoparticles at the xylene/water interface.²⁴ The PEO star surface pressures are smaller compared to poly(oligo(ethylene oxide) monomethyl ether methacrylate) functionalized iron oxide nanoparticles at the dodecane/water interface⁹³ but are larger than those measured at the trichloroethylene/water interface for silica particles modified with a strong polyelectrolyte, poly(styrenesulfonate).²⁰ Also similar to the air/water interface, linear PEO 6k produced the lowest interfacial pressure, and the interfacial pressure of linear polymers did not depend significantly on their bulk concentration. These observations indicate that the compact star polymer structure favors more extensive interfacial penetration than linear PEO at these liquid/liquid interfaces, as was observed at the air/water interface.

3.4.3 Dynamic dilatational elasticity

The magnitudes of the complex dynamic dilatational modulus of PEO stars adsorbed at xylene/water and cyclohexane/water interfaces are presented in **Figure 3.11**. These were on the order of 10 mN/m, just slightly larger than moduli at the air/water interface and similar to those measured for PDMAEMA-grafted silica nanoparticles at the xylene/water interface.²⁴ As with the air/water interface, the storage modulus E' accounted for more than 95% of the magnitude of

the complex modulus for adsorbed PEO stars at xylene/water and cyclohexane/water for frequencies between 0.1 and 1 Hz. Similar to observations at the air/water interface, the PEO star modulus showed little dependence on oscillation frequency. The concentration dependence was somewhat more pronounced than it was at the air/water interface (**Figure 3.11c and d**). As with the air/water interface, linear PEO did not produce a significant dynamic dilatational modulus at either the xylene/water or cyclohexane/water interface. Similar to the air/water interface, forced oscillation of the xylene/water or cyclohexane/water interfacial area yielded no response in the interfacial tension for linear PEO. The response to the forced area oscillation was within the experimental noise (**Figure 3.12 – Figure 3.13**). The lack of a dilatational response for linear PEO is again attributed to facile redistribution of segments between non-adsorbed loops and tails and adsorbed trains, whereas the finite dilatational modulus for the adsorbed PEO stars is attributed to hindered chain reconfiguration and/or elastic compression of closely packed star polymers at the interface.

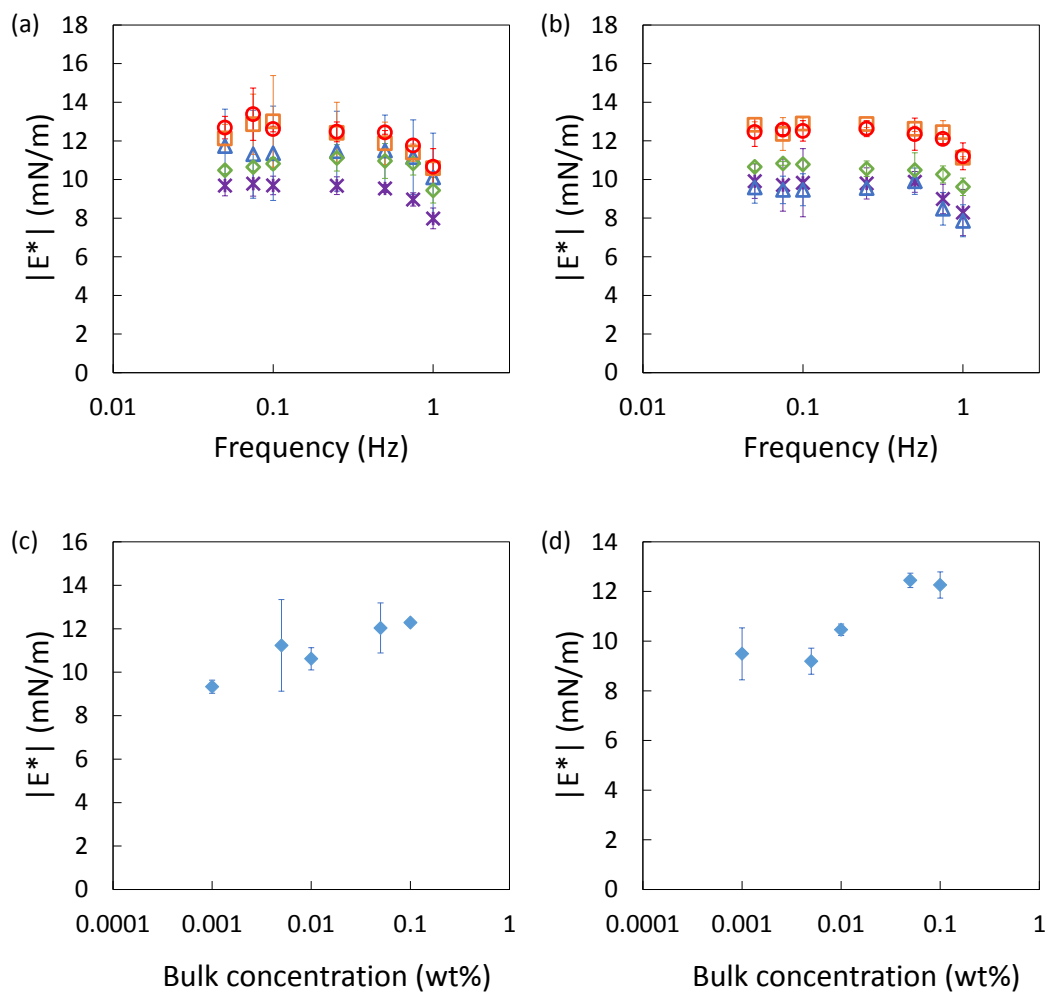


Figure 3.11. The magnitude of the complex dynamic dilatational modulus of PEO stars adsorbed at the (a) xylene/water interface and (b) cyclohexane/water interface as a function of frequency with 3% strain amplitude at different bulk concentrations: (\circ) 0.1 (\square) 0.05 (\diamond) 0.01 (\triangle) 0.005 ($*$) 0.001 wt%. Concentration dependence of the magnitude of the complex dynamic dilatational moduli, averaged over all tested frequencies, of PEO stars at the (c) xylene/water and (d) cyclohexane/water interface.

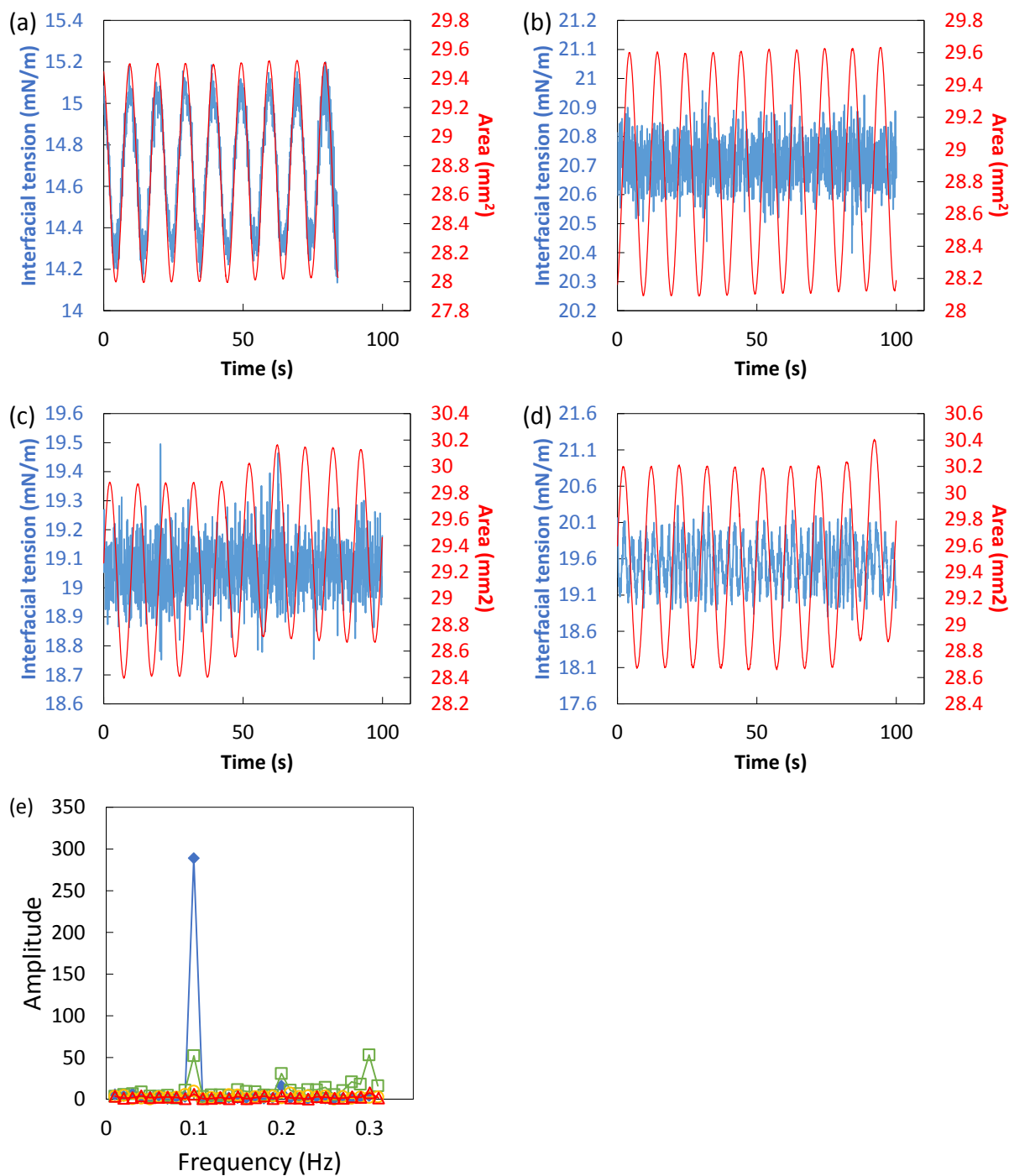


Figure 3.12. Interfacial tension and droplet area oscillation for 0.05 wt% of (a) PEO stars, linear (b) PEO 6k, (c) PEO 200k and (d) PEO 1000k at the xylene/water interface. The oscillation frequency is 0.1 Hz. (e) Fast Fourier transform analysis of interfacial tension response in the dynamic dilatational modulus experiments at the xylene/water interface: (◆) PEO stars and linear (◻) PEO 1000k, (○) PEO 200k, and (△) PEO 6k. No peak was detected for linear PEO at the forced oscillation frequency.

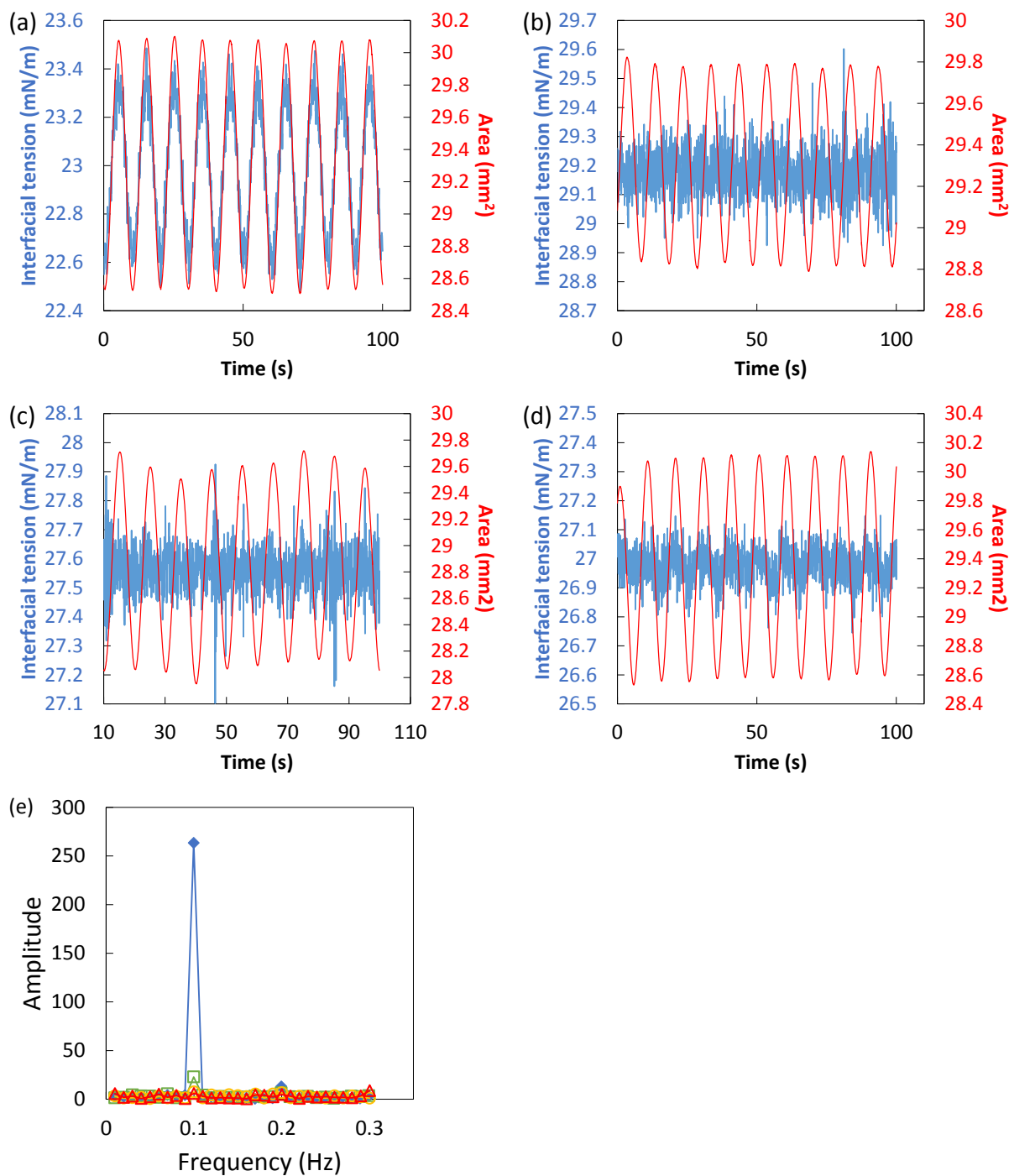


Figure 3.13. Interfacial tension and droplet area oscillation for 0.05 wt% of (a) PEO stars, linear (b) PEO 6k, (c) PEO 200k and (d) PEO 1000k at the cyclohexane/water interface. The oscillation frequency is 0.1 Hz. (e) Fast Fourier analysis of interfacial tension response in the dynamic dilatational modulus experiments at the cyclohexane/water interface: (\blacklozenge) PEO stars and linear (\square) PEO 1000k, (\circ) PEO 200k, and (\triangle) PEO 6k. No peak was detected for linear PEO at the forced oscillation frequency.

This behavior may be important for the high emulsifying efficiency of PEO stars. Adsorbed layers that form at low bulk concentrations produced significant interfacial pressure and dilatational elasticity. Prior investigations have shown that a significant dilatational modulus hinders thin film drainage and enables the adsorbed layer to resist interfacial deformation,^{103,106,107} processes that precede emulsion droplet coalescence. Although caution must be observed when extrapolating from experiments with relatively large drops probed over a limited range of frequencies to emulsions and foams with dynamic processes that occur over widely separated timescales, the observed dilatational elasticity of adsorbed PEO star polymer layers may be a key factor that distinguishes their good emulsifying and foaming performance from the poor performance of linear PEO.

3.4.4 Large amplitude interfacial compression and expansion

Slow compression and expansion experiments of the oil/water interface were also performed to further investigate the behavior of the PEO star adsorbed layers (**Figure 3.14**). Unlike the air/water interface, there was significant hysteresis between compression and expansion of the xylene/water interface. It was strongest during the first compression/expansion cycle. There was very little hysteresis for the cyclohexane/water interface. The data therefore suggests that some of the PEO stars desorbed into the xylene phase during the first compression. Similar to the air/water interface, the quasi-static moduli increase with increasing interfacial pressures and are consistent with dynamic dilatational moduli obtained from small amplitude oscillations at low surface pressures. However, unlike the air/water interface, the compression modulus reached a maximum at high degrees of compression. This indicates a structural change of the adsorbed layer. A decrease in modulus at Π above ~ 30 mN/m or ~ 40 mN/m for xylene/water or cyclohexane/water, respectively, may suggest a monolayer collapse.

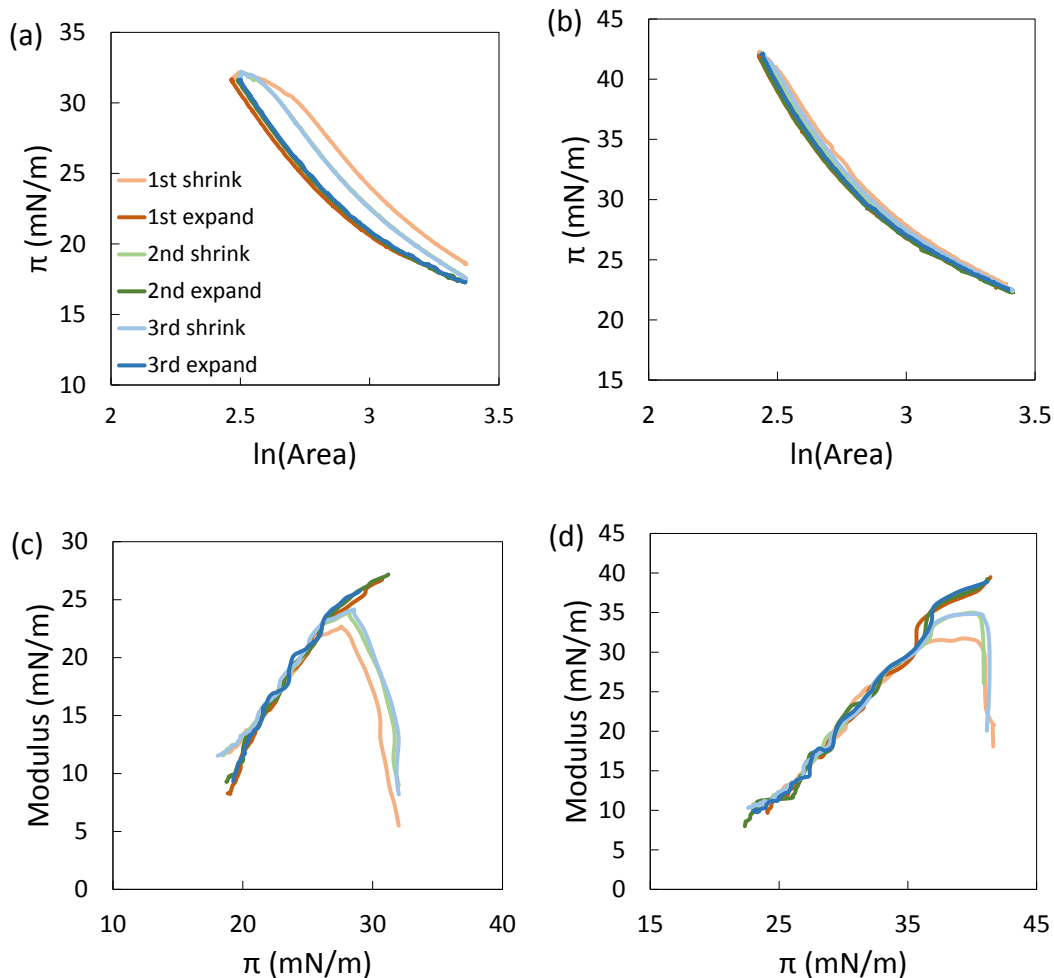


Figure 3.14. Interfacial pressure versus area (mm^2) isotherm for PEO stars at (a) xylene/water and (b) cyclohexane/water interface. The concentration of PEO stars in water is 0.001 wt%. The interfacial compression and expansion rate was kept in the range of $0.07 - 0.1 \text{ mm}^2/\text{s}$. In (a), the second and third cycles are overlapping. Compression and expansion modulus for PEO stars at (c) xylene/water and (d) cyclohexane/water interface as a function of interfacial pressure deduced from the interfacial pressure versus area isotherm. Three cycles of interfacial compression and expansion were recorded.

3.4.5 Extent of adsorption

Adsorption of PEO stars and linear PEO at the xylene/water interface was measured by ellipsometry. Unambiguous conversion of the ellipsometry signals to the surface excess concentration at the xylene/water interface is much more difficult because the refractive index contrast between xylene and water is relatively small ($n_{water} = 1.333$ and $n_{xylene} = 1.500$) compared to the air/water interface ($n_{water} = 1.333$ and $n_{air} = 1.000$). In such a system that has small optical contrast, the value of $d_f (n_f - n_0)$ is highly dependent on the assumed optical properties of the adsorbed layer (see **Chapter 3.7** for detailed analysis), and thus the surface excess concentration cannot be uniquely determined *via* equation ((2.12). The adsorbed layers are too thin for ellipsometry to directly resolve their thickness and index, even with multi-angle scanning, so one is forced to assume an index (or thickness) and extract the thickness (or index) from fitting the ellipsometric data. Whereas the surface excess concentration calculated from the index and thickness was robust and insensitive to the assumed parameter value for the air/water interface, the surface excess concentration was highly sensitive to the assumed value for the xylene/water interface.

Nevertheless, the measured ellipsometric parameters still provide insight into the relative adsorbed amounts of the different polymers at the interface. **Figure 3.15a** shows Δy , the change in the ellipsometric y parameter (see equation (2.11)) relative to the initially clean interface, measured at the xylene/water interface as a function of bulk concentration. The measured Δy decreased with increasing bulk concentration for linear PEO 6k and the PEO stars, which is an indication of increasing adsorption. This is based on the theoretically predicted dependence of the y parameter on the adsorbed layer thickness, for an assumed value of the layer refractive index (**Figure 3.15b**). Increasing thickness at constant index equates to increasing surface excess

concentration. For linear PEO 200k and 1000k, the measured Δy became independent of the bulk concentration, indicating the interface had reached saturation. The observation of more negative Δy for PEO stars than for any of the linear polymers suggests that the extent of PEO star adsorption is greater than for linear PEO, consistent with trends at the air/water interface (**Figure 3.7**). It is noted that measuring PEO adsorption at the cyclohexane/water interface using ellipsometry is extremely difficult since the optical contrast between the water and the cyclohexane is extremely small ($n_{\text{water}} = 1.333$ and $n_{\text{cyclohexane}} = 1.425$), making it hard to distinguish Δy from the noise.

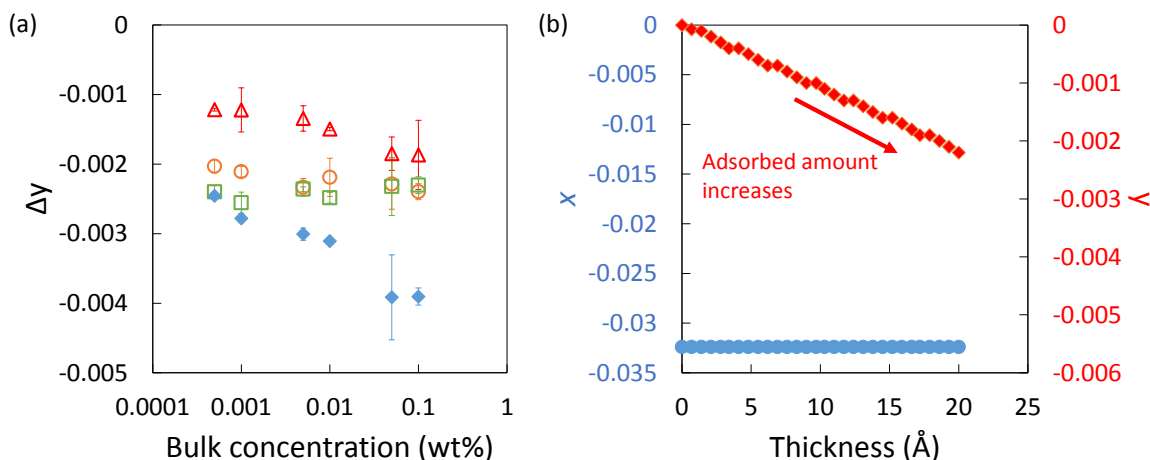


Figure 3.15. (a) Measured ellipsometric Δy as a function of bulk polymer concentration adsorbed from water to the xylene/water interface: (\blacklozenge) PEO stars (\square) PEO 1000k (\circ) PEO 200k (\triangle) PEO 6k. (b) Theoretically predicted dependence of (\bullet) x and (\blacklozenge) y on the thickness of a homogeneous adsorbed layer with $n_f = 1.44$ at 42° angle of incidence.

3.4.6 Path-dependent adsorption

3.4.6.1 Interfacial pressure when dispersing polymers in different phases

Xylene is a good solvent for PEO, providing the opportunity to compare adsorption to the xylene/water interface when the polymers access the interface from either the oil or the water

side of the interface. **Figure 3.16** compares equilibrium interfacial pressures for different PEO forms adsorbed from either xylene or water as a function of the bulk concentration. For any of the linear PEO samples, the interfacial pressure isotherms were independent of the phase from which the polymers adsorbed. This suggests that linear PEO chains readily equilibrate and adopt similar conformations with similar degrees of interfacial penetration regardless of their route to the interface.

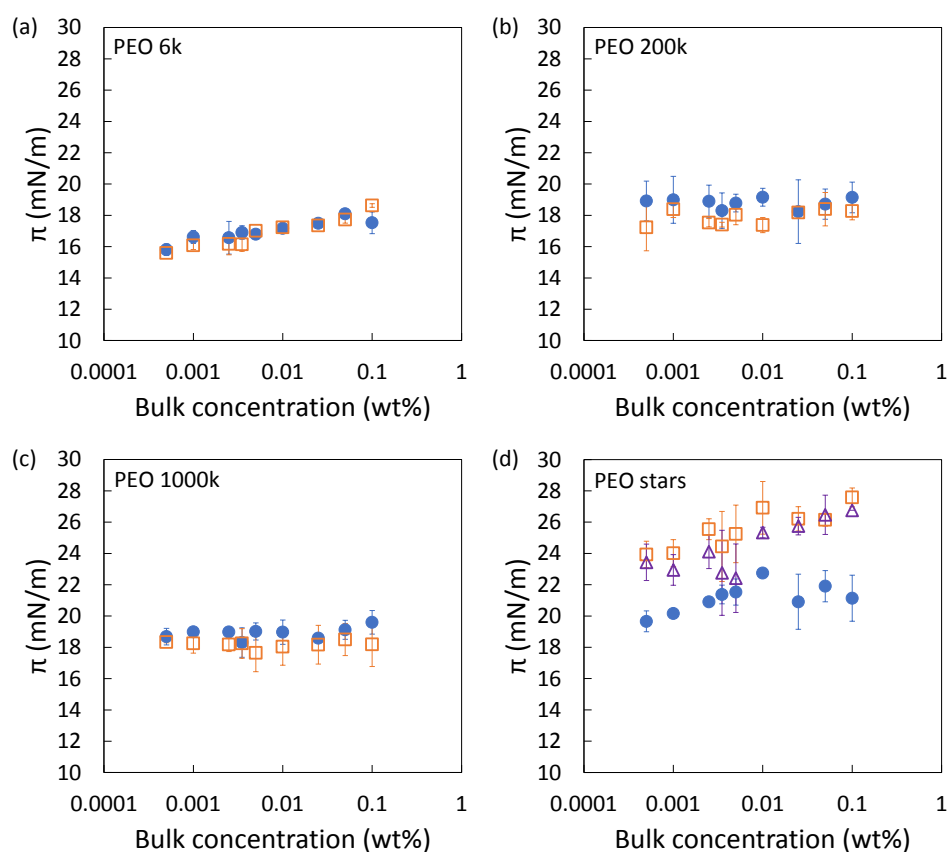


Figure 3.16. Comparison of xylene/water interfacial pressure isotherms for linear (a) PEO 6k, (b) PEO 200k, (c) PEO 1000k and (d) PEO stars adsorbed from xylene (\square), from water (\bullet) or from both xylene and water phases with half the total mass of PEO stars dispersed in each phase (Δ).

In contrast, PEO star polymers displayed significantly greater (by ~ 20 to 25%) interfacial pressures when adsorbing from the xylene phase than from the aqueous phase (**Figure 3.16d**). Greater interfacial pressures were also achieved by dispersing PEO stars simultaneously in both xylene and water phases. In the latter case, half of the PEO stars were dispersed in each phase. This discrepancy, which persisted even after two days of equilibration, indicates that PEO star polymer layers adopt different structures that persist for long times, depending on their initial environment. The star polymers are accessing different states separated by a significant energy barrier depending on their path to the interface. Additional insights into the structure of the interfacial film are obtained from ellipsometry.

3.4.6.2 Ellipsometry when dispersing polymers in different phases

Ellipsometry of the xylene/water interface indicates that the interfacial structures that produce significant differences in interfacial pressure (**Figure 3.16**) are dramatically different when PEO stars adsorb from xylene or from water, as shown in **Figure 3.17**. The observation of large changes in both ellipsometric signals, Δx and Δy , when the PEO stars were initially dispersed in the xylene phase indicates that an extremely thick layer was formed at the interface. The measured Δy for PEO stars adsorbing from xylene was much larger in magnitude than the value produced when they adsorbed from water. The large Δx is remarkable. Recall that for thin films, x is nearly insensitive to the film refractive index and is dominated by the bulk indices.

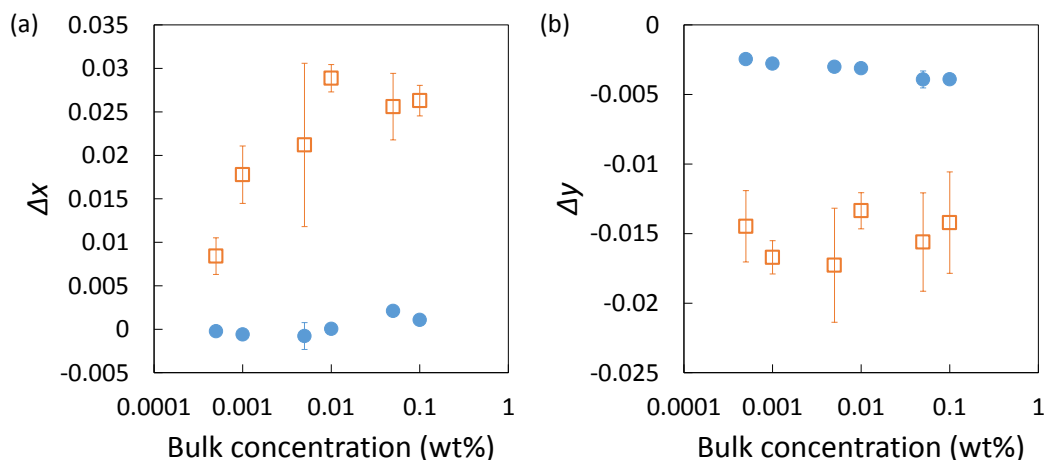


Figure 3.17. Change in ellipsometric parameters (a) Δx and (b) Δy for PEO star adsorption to the xylene/water interface from xylene (□) or from water (●).

This suggests that the adsorbed layer is much thicker than a monolayer. Calculations with the striated interface optical model, assuming several possible indices for the adsorbed film ($n_f = 1.38, 1.40, 1.44$ or 1.48), indicate that the adsorbed layer must have been at least 200 nm thick to produce such changes in both x and y . Furthermore, the measured dependence of the ellipsometric parameters on incident angle showed significant systematic discrepancies from the homogeneous film optical model, indicating a complex film structure exists. Although the exact value of Δx was not reproduced in replicate experiments, the production of a large Δx value was reproducible. Furthermore, the large changes in Δx and Δy persisted even after 10 days of sample equilibration. This pronounced difference in the interfacial structure depending on the path taken by PEO stars to the interface is consistent with the differences in interfacial pressure. Visual and microscopic inspection of the xylene/water system, presented in [Chapter 3.5](#), suggest that the interfacial film produced when PEO stars are initially in xylene is a water-in-oil emulsion.

3.5 Spontaneous emulsification with multi-arm PEO star polymers

We observed that when PEO stars were initially dispersed in xylene and brought into contact with pure water with minimal disturbance, the xylene phase became turbid after one hour, whereas initially both phases were transparent (**Figure 3.18**). A turbid region formed in the less dense xylene top phase above the xylene/water interface and gradually expanded upward until it reached the top of the xylene phase. In addition, the xylene phase turbidity was more pronounced for higher PEO star concentrations (**Figure 3.19**). This phenomenon was also observed when PEO stars were initially dispersed simultaneously in both xylene and water phases (**Table 3.3**). However, this phenomenon did not occur when PEO stars were initially dispersed in water before contacting xylene, nor for any linear PEO initially dispersed in either phase. The turbidity production observed here is not the result of a polymer phase separation. PEO star dispersions in xylene that were not in contact with water remained transparent indefinitely, and pre-saturation of xylene with water did not lead to a PEO star dispersion becoming turbid.

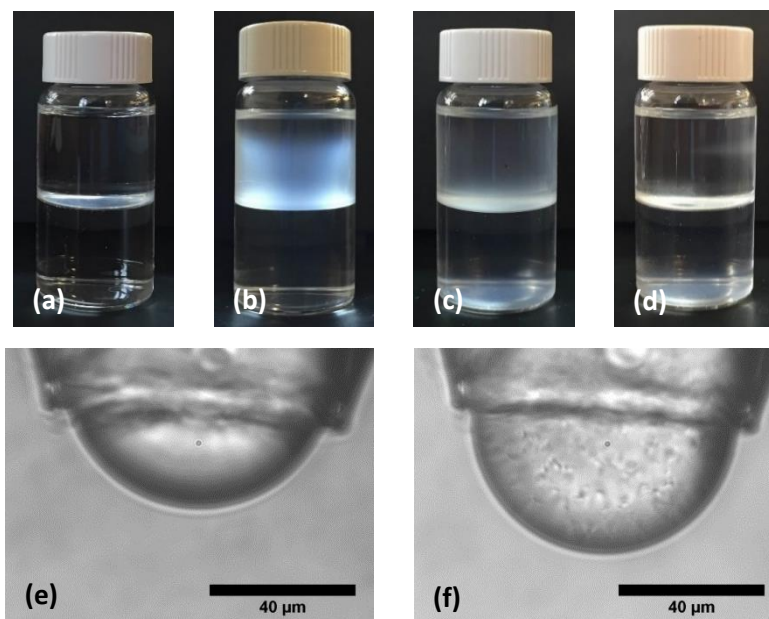


Figure 3.18. Photographs of xylene/water with 0.1 wt% PEO stars initially dispersed in xylene (top phase) at time = 0, 3, 24, and 96 h after sample preparation, (a) – (d), respectively. Microscope images of spontaneous emulsification commencing at the interface between a xylene droplet of 0.1 wt% PEO stars surrounded by water at (e) the initial stage and (f) 20 seconds after the two liquids were brought into contact. The microscope images were taken using a microtensiometer apparatus.^{24,159}

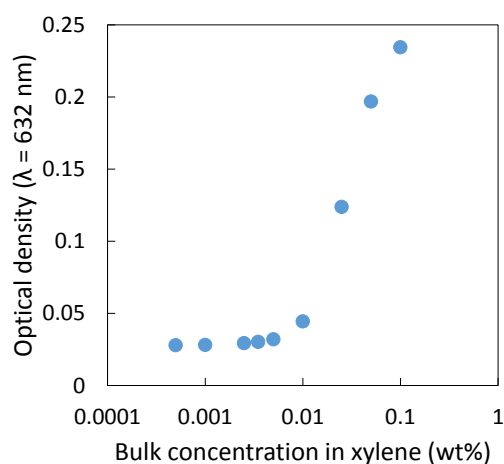


Figure 3.19. Optical density of the xylene phase of the xylene/water system 3.5 hours after sample preparation. PEO stars were initially dispersed in xylene. Turbidity increased with the bulk concentration of PEO stars initially dispersed in xylene, indicating increasing spontaneous emulsification of water into xylene.

Table 3.3. Photographs of xylene/water with 0.1 wt% PEO stars initially dispersed in water (bottom phase), initially dispersed in xylene, and initially dispersed in both xylene and water phases with the same total amount of PEO stars (50/50 mass in each phase)

	Initial	1 h	2 h	3 h	4 h	17 h	24 h
PEO stars in water							
PEO stars in xylene							
PEO stars in water and xylene							

At longer times on the order of 24 to 96 hours, the turbidity was observed to settle back toward the interface. This suggests that the turbidity results from spontaneous emulsification of water into the xylene phase. The emulsion sedimentation at longer times likely reflects water droplet coarsening. Such a sedimented emulsion layer would explain the thick interfacial film detected by ellipsometry (**Figure 3.17**). Microscopic inspection of a microscale xylene drop confirmed the spontaneous emulsification. **Figure 3.18e and f** show microscope images of a xylene droplet immersed in water. The xylene droplet contains 0.1 wt% PEO stars. Within 20 s

of contacting the xylene droplet with water, microscopic droplets of water were observed to form at the xylene/water interface and to be convected upwards (against gravity) inside the xylene drop. Visible observation in the microscope showed considerable fluid shear at the interface, presumably due to Marangoni flow induced by PEO star adsorption generating localized interfacial tension gradients.¹⁶⁰ These microscopic observations are consistent with the observations in macroscopic vials (**Figure 3.18a – d**). Note that the time scales for the spontaneous emulsification process are much shorter in the microscopic drop (**Figure 3.18e and f**) than in the macroscopic samples because of the decreased length scales over which mass transfer must occur.

We finish by proposing a mechanism based on the difference in PEO star solubility between the two liquids to explain the occurrence of spontaneous emulsification only when PEO stars are initially dispersed in the xylene phase, and not when they are in the aqueous phase. Because the two liquids are not initially in equilibrium, there is a driving force for PEO stars to redistribute between the xylene and aqueous phases. The following hypothesized description refers to each stage of the schematic illustration in **Figure 3.20**. (a) When the xylene phase containing PEO stars first contacts the water phase, some of the PEO stars adsorb to the interface and some start to diffuse into the aqueous phase due to the greater solubility of PEO in water than in xylene⁸⁴ (see **Chapter 3.6** for detail analysis). (b) Adsorption reduces interfacial tension and increases interfacial fluctuations. (c) Any non-uniformity in the local interfacial tension depression drives a localized Marangoni flow that draws water into the budding droplets. Since PEO stars have entered the aqueous phase, PEO stars may access all sides of the budding droplet now, from both the xylene and water sides, to help seal off a droplet. Marangoni interfacial shear may help dislodge water droplets from the interface. The occurrence of spontaneous

emulsification when dispersing PEO stars simultaneously in both xylene and water phases (**Table 3.3**) is consistent with the proposed mechanism whereby the opportunity for PEO stars to access the interface from either phase facilitates droplet formation in the xylene phase. The lack of spontaneous emulsification when PEO stars are initially dispersed only in the aqueous phase may reflect the significantly weaker driving force for them to diffuse into the weaker xylene solvent, hindering the ability of PEO stars to access the budding droplet from both sides.

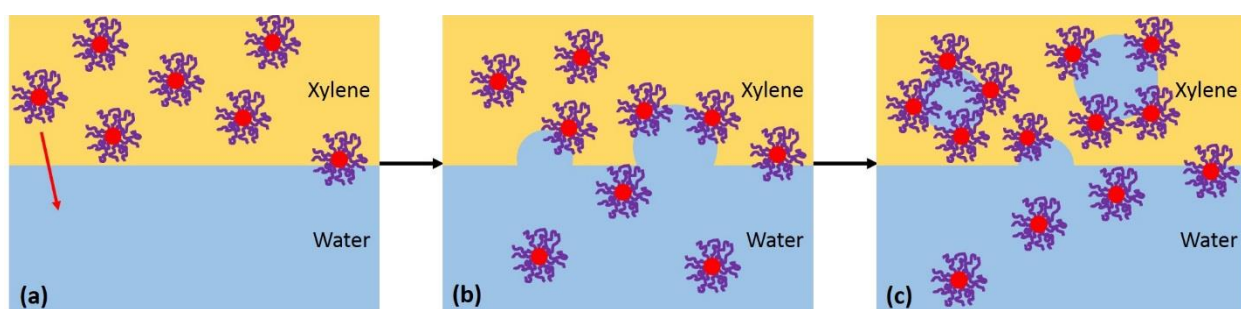


Figure 3.20. Proposed hypothetical mechanism for the spontaneous emulsification occurring at the interface between a PEO star-rich xylene phase and a water phase. Each stage is explained in the text.

3.6 Partition coefficient for PEO between xylene and water

To calculate the partition coefficient for PEO between xylene and water, a sample was made at a 1:1 xylene/water volume ratio with high concentration of linear PEO 6k in the water phase (33 wt%) and no PEO in the xylene phase. The refractive indices of both xylene and water phases were measured immediately after sample preparation and a week after the preparation. As shown in **Table 3.4**, we observed no change in refractive index, indicating that almost all PEO stayed in the water phase instead of diffusing into the xylene phase.

Table 3.4. Change in refractive index of xylene and water phases in xylene/PEO-water system

Refractive index	Xylene	PEO-water (33 wt%)
At initial time	1.4946	1.3801
After a week	1.4947	1.3808

Another sample with 1:1 xylene/water volume ratio with high concentration of linear PEO 6k (0.10035 g/mL of PEO 6k in xylene) initially in the xylene phase was prepared, with no PEO in the water. The partitioning of PEO 6k between xylene and water phases was examined by measuring the refractive index, as shown in **Table 3.5**. The increase in refractive index of the water phase indicates that some of PEO 6k in the xylene phase diffused into the water phase. The redistribution of PEO 6k is due to the greater solubility of PEO in water than in xylene phase.

Table 3.5. Change in refractive index of xylene and water phases in PEO-xylene/water system

Refractive index	PEO-xylene (10 wt%)	Water
At initial time	1.4958	1.3326
After a day	1.4954	1.3445

The refractive index of water phase, 1.3445, indicates that the final concentration of water phase was 0.091 g/mL. Thus, the partition coefficient for PEO 6k between water and xylene can be calculated:

$$P_{water/xylene} = \frac{0.091}{0.10035 - 0.091} = 9.73 \quad (3.3)$$

3.7 Analysis for ellipsometric determination of surface excess concentration

As previously mentioned in **Chapter 2.3.4**, the surface excess concentration can be calculated from ellipsometrically determined optical properties of an adsorbed layer using the de Feijter relation:¹⁴¹

$$\Gamma = \frac{d_f(n_f - n_0)}{dn/dc} \quad (2.12)$$

where n_0 is the refractive index of the bulk polymer solution, and d_f and n_f are the optical average thickness and refractive index of the adsorbed layer, respectively, and dn/dc is the refractive index increment of the polymer solution, previously reported to be 0.13 cm³/g for both PEO linear and star polymers.¹³

Here we model the dependence of the calculated surface excess concentration on the assumed refractive index of a PEO adsorbed used when analyzing ellipsometry data. We first generate the ellipsometric parameters for a “true” PEO adsorbed layer using a refractive index of 1.44 and a thickness of 20 Å. These “true” optical properties give a y parameter (see **Chapter 2.3.4**, equation (2.11)) according to the homogeneous film striated media optical model that one would obtain experimentally. Then, to mimic the data fitting process, we take an initial guess for the refractive index of the thin adsorbed layer (n_f), fit for the thickness of the adsorbed layer (d_f) which gives the same y parameter, and calculate the surface excess concentration using de Feijter relation.

3.7.1.1 Air/water

Figure 3.21 shows the calculated surface excess concentration (Γ) of a PEO adsorbed at the air/water interface ($n_{water} = 1.333$ and $n_{air} = 1.000$). Varying the initial guess for the refractive index of the adsorbed layer from 1.40 to 1.46 (the latter upper limit corresponding to the

refractive index of pure PEO) only changes the surface excess concentration by 10%. This indicates that the errors of assumed and fitted optical properties (n_f and d_f) are mutually compensating. Therefore, the value of $d_f(n_f - n_0)$ is nearly invariant (to within $\sim 10\%$), meaning the surface excess concentration calculated by de Feijter relation is nearly independent of the optical properties of the adsorbed layer at the air/water interface, and quantitative comparisons can be made with $\sim 10\%$ tolerance for uncertainty.

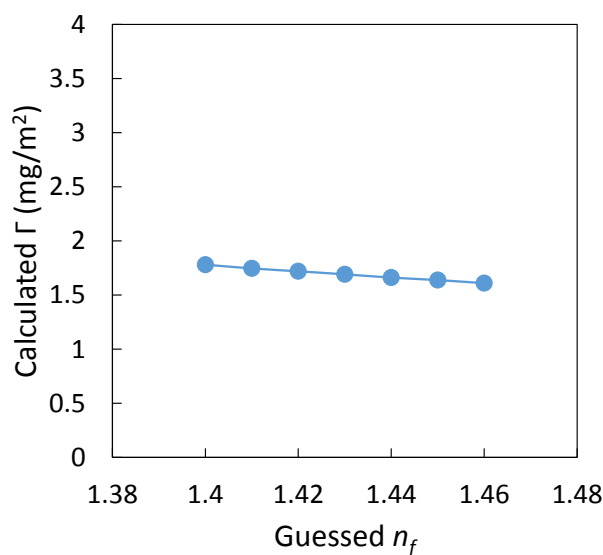


Figure 3.21. Calculated surface excess concentration as a function of the guessed refractive index of the adsorbed PEO layer at the air/water interface, based on analysis of the ellipsometric y parameter for the “true” adsorbed layer that has refractive index of 1.44 and thickness of 20 Å. The angle of incidence is 53°.

3.7.1.2 Xylene/water

For PEO adsorption at the xylene/water interface, we follow the same modeling procedure as in the air/water system by assuming the “true” adsorbed layer has refractive index of 1.44 and thickness of 20 Å. As illustrated in **Figure 3.22**, the modeling results show that the surface excess concentration of PEO at the xylene/water interface is highly dependent on the

value of the guessed refractive index used when analyzing ellipsometric data. The difficulty of obtaining the accurate value of the surface excess concentration results from the weaker optical contrast between the xylene and water phases ($n_{water} = 1.333$ and $n_{xylene} = 1.500$), making the ellipsometric signals less sensitive to the local variation of refractive index caused by the adsorbed layer. In other words, the uncertainty of fitting the experimental data for the optical properties of the adsorbed thin film is large, making it impossible to unambiguously determine the surface excess concentration.

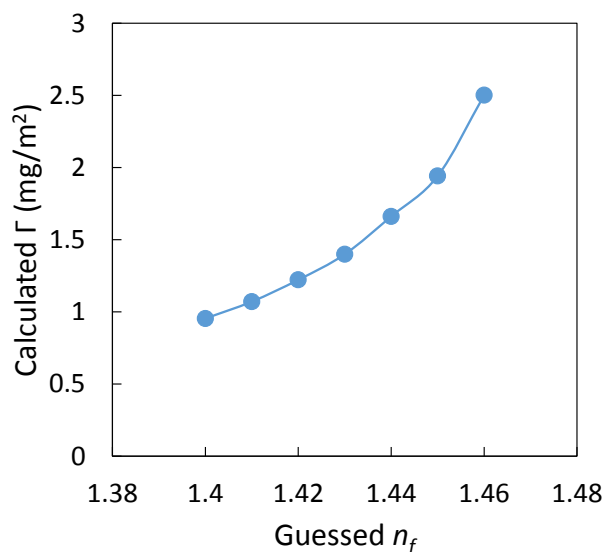


Figure 3.22. Calculated surface excess concentration as a function of the guessed refractive index of the adsorbed PEO layer at the xylene/water interface, based on analysis of the ellipsometric ψ parameter for the “true” adsorbed layer that has refractive index of 1.44 and thickness of 20 Å. The angle of incidence is 43°.

3.7.1.3 Measuring from both xylene and aqueous phase

An approach has been proposed in the literature, which allows the determination of both film thickness and refractive index by making ellipsometry measurements from both organic phase and aqueous phase.¹⁶¹ To test the method of measuring from both organic and aqueous

phases, we followed the same modeling procedure mentioned above and estimated the surface excess concentration based on different “guessed” refractive index of the thin film by assuming the “true” adsorbed layer has refractive index of 1.44 and thickness of 20 Å. As illustrated in **Figure 3.23**, the modeled surface excess concentration obtained from both sides shows the same trend, indicating that making measurements from both sides is, unfortunately, not able to solve the uncertainty of the optical properties of the adsorbed layer in the xylene/water system.

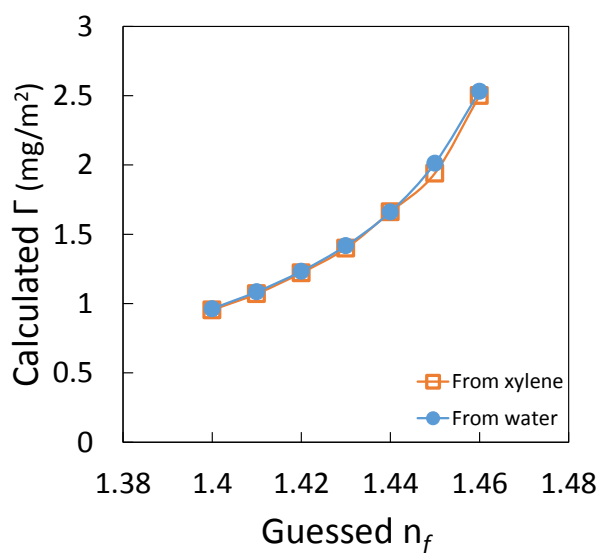


Figure 3.23. Calculated surface excess concentration measured from both xylene and water phases as a function of the guessed refractive index of the adsorbed PEO layer at the xylene/water interface, based on analysis of the ellipsometric γ parameter for the “true” adsorbed layer that has refractive index of 1.44 and thickness of 20 Å. The angle of incidence measuring from xylene and water is 43° and 47°, respectively.

3.8 Conclusions

Several fundamental interfacial activity characteristics have been compared for multi-arm star polymers and linear polymers with the same chemical composition as the star polymer arms. Interfacial tensiometry, dynamic dilatational elasticity, and ellipsometry demonstrate that multi-

arm PEO star polymers exhibit significantly different fundamental adsorption characteristics from those exhibited by linear PEO chains that have molecular weights that approximate either the molecular weight of individual star polymer arms, of an entire star polymer, or of star polymer aggregates in water. Similar differences in interfacial behavior are manifested at the air/water interface, the cyclohexane/water interface that represents an immiscible poor solvent/good solvent interface, and the xylene/water interface that represents an immiscible good solvent/good solvent interface.

The compact star polymers generate significantly larger interfacial pressures than linear polymers. PEO star polymers produce significant dynamic dilatational elastic moduli that are nearly purely elastic in nature with little or no dilatational viscous character, at each of these interfaces, whereas linear PEO layers produce no detectable dilatational elasticity in the 0.1 to 1 Hz frequency range. The lack of an elastic response of adsorbed linear PEO to forced interfacial area oscillations is attributed to facile redistribution of segments among non-adsorbed loops and tails and adsorbed trains that maintains a constant interfacial pressure throughout the forced area oscillations at these frequencies. The highly constrained chains of the PEO stars are proposed to be less able to reconfigure during area oscillations, leading to an increase in interfacial tension upon area dilation.

PEO stars adsorb to significantly greater extents than linear PEO, producing two- to three-fold greater surface excess concentrations and achieving area fraction coverages that indicate densely packed adsorbed layers. More extensive PEO star adsorption is verified quantitatively by ellipsometry at the air/water interface and demonstrated qualitatively by ellipsometry at the xylene/water interface. The determination that PEO star layers are densely

packed suggests that elastic deformation of closely packed PEO stars during forced interfacial area oscillations may also contribute to the measured dilatational elastic modulus of their adsorbed layers. The greater surface excess concentrations produced by PEO star adsorption are due to the compact star polymer structure. Not able to spread along the interface as a linear polymer can, star polymers present all of their mass in a relatively small projected area at the interface.

Unlike linear PEO, multi-arm PEO star polymers are effective emulsifiers and foaming agents. Since both linear PEO and PEO star polymers reduce interfacial tension, this alone is an unlikely factor to differentiate their emulsifying and foaming performance. The differentiation may arise primarily from the significant dynamic dilatational elasticity produced by PEO star adsorption, and its absence from adsorbed linear PEO layers. Dense, elastic PEO star layers may better resist drop or bubble coalescence.

PEO stars exhibit a pronounced sensitivity to the adsorption path. When adsorbed to the xylene/water interface from xylene, they produce significantly larger interfacial pressures, spontaneous emulsification and persistent thick interfacial films, that may consist of a dense sedimented emulsion phase, compared to interfacial layers produced by adsorption from the aqueous phase. Linear PEO experiences no such path dependence.

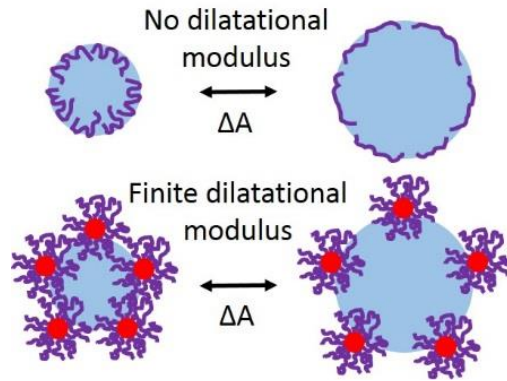


Figure 3.24. The observed dilatational elasticity of adsorbed PEO star polymer layers may be a key factor that distinguishes their good emulsifying and foaming performance from the poor performance of linear PEO.

4 Interfacial activity of β -cyclodextrin core star polymers at fluid interfaces

4.1 Introduction

This chapter compares the interfacial activity of 14-arm poly(di(ethylene glycol) methyl ether methacrylate) (PMEO₂MA) star polymers, poly(2-(dimethylamino)ethyl methacrylate) (PDMAEMA) star polymers, and star polymers with block copolymer arms (PMEO₂MA-PDMAEMA) at both air/water and oil/water interfaces. In order to understand how polymer chemistry controls interfacial behaviors at different conditions, we determine the interfacial tension reduction, dynamic dilatational modulus and extent of adsorption of star polymers. Similar to **Chapter 3**, air/water, cyclohexane/water and xylene/water interfaces were investigated. The last two interfaces again offer the opportunity to investigate adsorption to an interface with a poor solvent (cyclohexane) or with a good solvent (xylene) for all the star polymers studied in this chapter.

The incorporation of PDMAEMA into the polymer chains imparts pH-responsiveness into the star polymers. PDMAEMA is a weak polyelectrolyte and has a pK_a around 7.0 – 7.5 in aqueous solution.^{162,163} The dimethylamine groups in the polymer are protonated at low pH and the polymer becomes more positively charged. At high pH, the polymer arms collapse due to the lack of electrostatic repulsion. Studies have reported the hydrodynamic radius of PDMAEMA-grafted silica particles was dependent on pH and temperature as a result of the conformational response of the grafted layers to different solvent conditions.^{14,162,164} It was also shown that PDMAEMA brushes grafted from gold surfaces displayed pH-triggered protein uptake and release behaviors.¹⁶⁵ The degree of ionization plays an important part on stabilizing thin films and emulsions. Additionally, since the polymer adsorption rate, the adsorbed layer conformation and the polymer interactions between polyelectrolytes depend strongly on the pH,¹⁶⁶ choosing

appropriate polymer chains or analogous star polymers allows the creation of pH-responsive foams and emulsions.^{31–33}

In the following, we first report the effects of pH on the size and charge characteristics of the star polymers. These factors dictate polymer interactions and affect star polymer packing on air/water and oil/water interfaces. Next, the effectiveness of various stars as foaming agents is presented to motivate the interfacial studies, and the comparison of their interfacial activity at the air/water interface is reported. Then, emulsification performance with these star polymers is presented, followed by reporting their interfacial activity at xylene/water and cyclohexane/water interfaces.

4.2 β -cyclodextrin core star polymers characterization

Table 4.1 reports the number-average hydrodynamic diameters of various star polymers in aqueous solution at pH 5 and pH 9 measured by dynamic light scattering. PMEO₂MA star polymer has a hydrodynamic diameter of 7.3 ± 0.3 nm, which is independent of pH. The size of the PDMAEMA star polymer decreased when pH increased from 5 to 9. The collapse of a star polymer is due to reduced segment-segment electrostatic repulsions, resulting in de-swelling of the star polymer. In contrast, the diblock star polymer has a hydrodynamic diameter of 12 nm and showed no change in size when pH increased. This is attributed to the lower degree of polymerization of the PDMAEMA block (DP ~ 35) per polymer chain than the homo-block PDMAEMA star polymers (DP ~ 62), which makes the size change induced by electrostatic repulsion less pronounced. Intensity-average hydrodynamic diameters and the polydispersity of star polymers is summarized in **Table 4.2**, which shows that both PDMAEMA and diblock star polymers reduced their sizes at high pH due to the lack of electrostatic repulsion. This is also

evident in the zeta potential measurements shown in **Table 4.3**. The electrophoretic mobility decreased with increasing pH for both PDMAEMA and diblock star polymers because of the deprotonation of PDMAEMA brush. PMEO₂MA stars displayed a zeta potential around zero, indicating that they are neutrally charged and do not gain translational velocity in response to an applied electric field. It is worth mentioning that the hydrodynamic diameters presented here are derived from the Stoke-Einstein equation, which relates the measured diffusion coefficient to the size of an equivalent hard sphere. Therefore, the reported hydrodynamic diameters for the permeable stars should be interpreted as qualitative changes with respect to pH instead of the actual size of the star polymers.

Table 4.1. Number-average hydrodynamic diameters for various 14-arm star polymers in 1 mM NaCl aqueous solution at pH 5 and pH 9. Dynamic light scattering measurements were made at 20 °C with 0.1 wt% star polymer concentration

Star polymer	Hydrodynamic diameter (nm)	
	pH 5	pH 9
PMEO ₂ MA stars	7.0 ± 0.3	7.0 ± 0.3
PDMAEMA stars	9.0 ± 0.03	7.8 ± 0.7
Diblock stars	12.2 ± 0.5	12.7 ± 2.1

Table 4.2. Z-average hydrodynamic diameters and the polydispersity for various 14-arm star polymers in 1 mM NaCl aqueous solution at pH 5 and pH 9. Dynamic light scattering measurements were made at 20 °C with 0.1 wt% star polymer concentration

Star polymer	Hydrodynamic diameter (nm)		PDI	
	pH 5	pH 9	pH 5	pH 9
PMEO ₂ MA stars	9.3 ± 0.2	9.3 ± 0.2	0.104	0.104
PDMAEMA stars	19.3 ± 0.4	14.7 ± 0.3	0.261	0.259
Diblock stars	39.4 ± 0.3	28.2 ± 0.7	0.380	0.210

Table 4.3. Zeta potentials for various 14-arm star polymers in 1 mM NaCl aqueous solution at pH 5 and pH 9. Dynamic light scattering measurements were made at 20 °C with 0.1 wt% star polymer concentration

Star polymer	Zeta potential (mV)	
	pH 5	pH 9
PMEO ₂ MA stars	2.36 ± 1.24	2.36 ± 1.24
PDMAEMA stars	19.3 ± 2.5	7.1 ± 1.3
Diblock stars	37.2 ± 0.9	10.0 ± 0.4

4.3 Interfacial behavior at air/water interface

4.3.1 Foaming efficiency and stability

Aqueous foaming results for star polymers at pH 5 and pH 9, and the time for foams to completely collapse are summarized in **Table 4.4**. PMEO₂MA star polymers are the most effective at stabilizing foams among these three star polymers. For concentrations of 0.05 and 0.1 wt%, the foam destabilized through bubble coalescence and completely collapsed after 105 and 140 minutes, respectively. No stable foams were produced with PDMAEMA and diblock star polymers at pH 5 when the star polymers are swollen and positively charged. The foams collapsed immediately after ceasing the mechanical agitation. At pH 9, the PDMAEMA and diblock star polymers were able to stabilize foams but the foams only lasted for 10 – 15 minutes. The foaming performance of these cyclodextrin-core star polymers was not as efficient as multi-arm PEO stars, which can stabilize foams at 0.005 – 0.1 wt% for more than 2 hours, as reported previously.⁴⁶ The difference in formability at various conditions motivates a comparison of their interfacial behavior at the air/water interface.

Table 4.4. Concentrations of star polymers to stabilize foams and the corresponding foam stability

Star polymers	pH	Concentration (wt%)	Foam stability (min)
PMEO ₂ MA stars	5 & 9	0.1	140
		0.05	105
PDMAEMA stars	5	No foam	N/A
	9	0.1	11
		0.05	7
Diblock stars	5	No foam	N/A
	9	0.1	15
		0.05	15

4.3.2 Surface tension reduction

Figure 4.1 shows the surface pressure isotherms at pH 5 and pH 9 for star polymers adsorbed at the air/water interface. PMEO₂MA star polymers (circle symbols) showed high affinity to the air/water interface and produced the highest surface pressures (15 – 30 mN/m). In addition, the surface pressures showed no dependence on the pH due to the non-ionic property of PMEO₂MA. These surface pressures are similar to those achieved by copolymer of MEO₂MA and oligo(ethylene glycol) methacrylate (OEGMA), and MEO₂MA-co-OEGMA-grafted iron oxide particles.¹⁶⁷ PDMAEMA star polymers (triangle symbols) achieved surface pressures < 5 mN/m at pH 5. These low surface pressures are attributed to the strong electrostatic repulsion between positively charged PDMAEMA star polymers at low pH, which prevents them from adsorption to the air/water interface. At pH 9, PDMAEMA star polymers are neutralized and collapsed. The absence of electrostatic forces resulted in the increase in surface pressure from 1 to 28 mN/m when bulk concentration increased from 0.0005 wt% to 0.1 wt%. The surface pressures produced with PDMAEMA star polymer concentrations greater than 0.05 wt% are similar to those achieved by PDMAEMA-grafted silica nanoparticles with high grafting density

and linear PDMAEMA at pH 7.5.²⁴ The surface pressures produced by diblock star polymers reached values between those achieved by PMEO₂MA and PDMAEMA stars at both pH 5 and pH 9. This is possibly attributed to the fact that the inner block polymers (PMEO₂MA) have high affinity to the interface and therefore enhance the adsorption compared to homopolymer PDMAEMA stars.

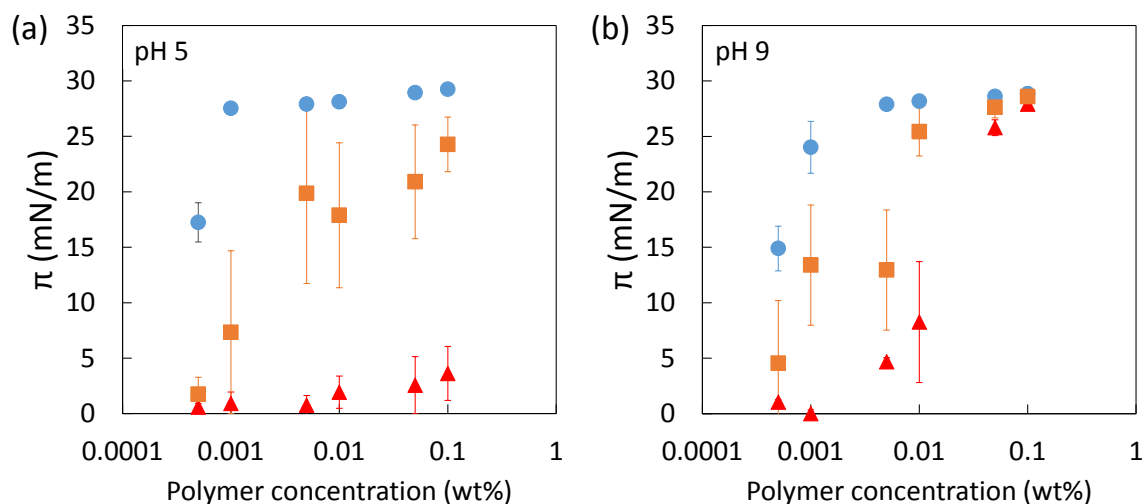


Figure 4.1. Surface pressure isotherm of (●) PMEO₂MA, (▲) PDMAEMA and (■) diblock star polymers adsorbed to the air/water interface at (a) pH 5 and (b) pH 9.

A comparison of dynamic surface tension for 0.1 wt% diblock star polymers adsorbed to the air/water interface at pH 5 and pH 9 is shown in **Figure 4.2**. The surface tensions at pH 5 and pH 9 both reached ~ 45 mN/m. However, the surface dynamic was very different. At pH 9, the surface tension dropped rapidly to their final value as the droplet was generated, while at pH 5 the surface tension slowly relaxed. For more diluted polymer concentrations, a steady value was not yet reached even after 16 hours at low pH (**Figure 4.3e**). The difference in the dynamic surface tension lowering suggests the importance of degree of ionization in the PDMAEMA

polymer adsorption to the air/water interface. Charged polymer chains approaching the surface will experience a repulsive force which increases as the adsorbed polymers accumulate at the surface, resulting in the slower adsorption rate. It is possible that the slow adsorption of PDMAEMA and diblock stars to the interface at low pH results in a low surface coverage, leading to the instant rupture of the foam films.

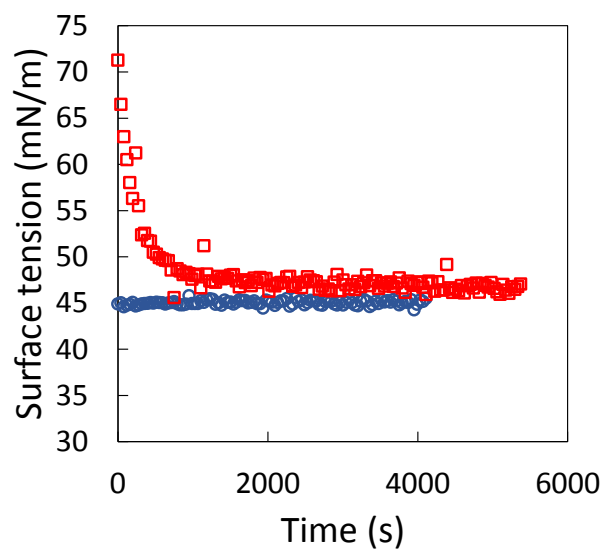


Figure 4.2. Surface tension as a function of time for 0.1 wt% diblock star polymers at the air/water interface at (□) pH 5 and (○) pH 9.

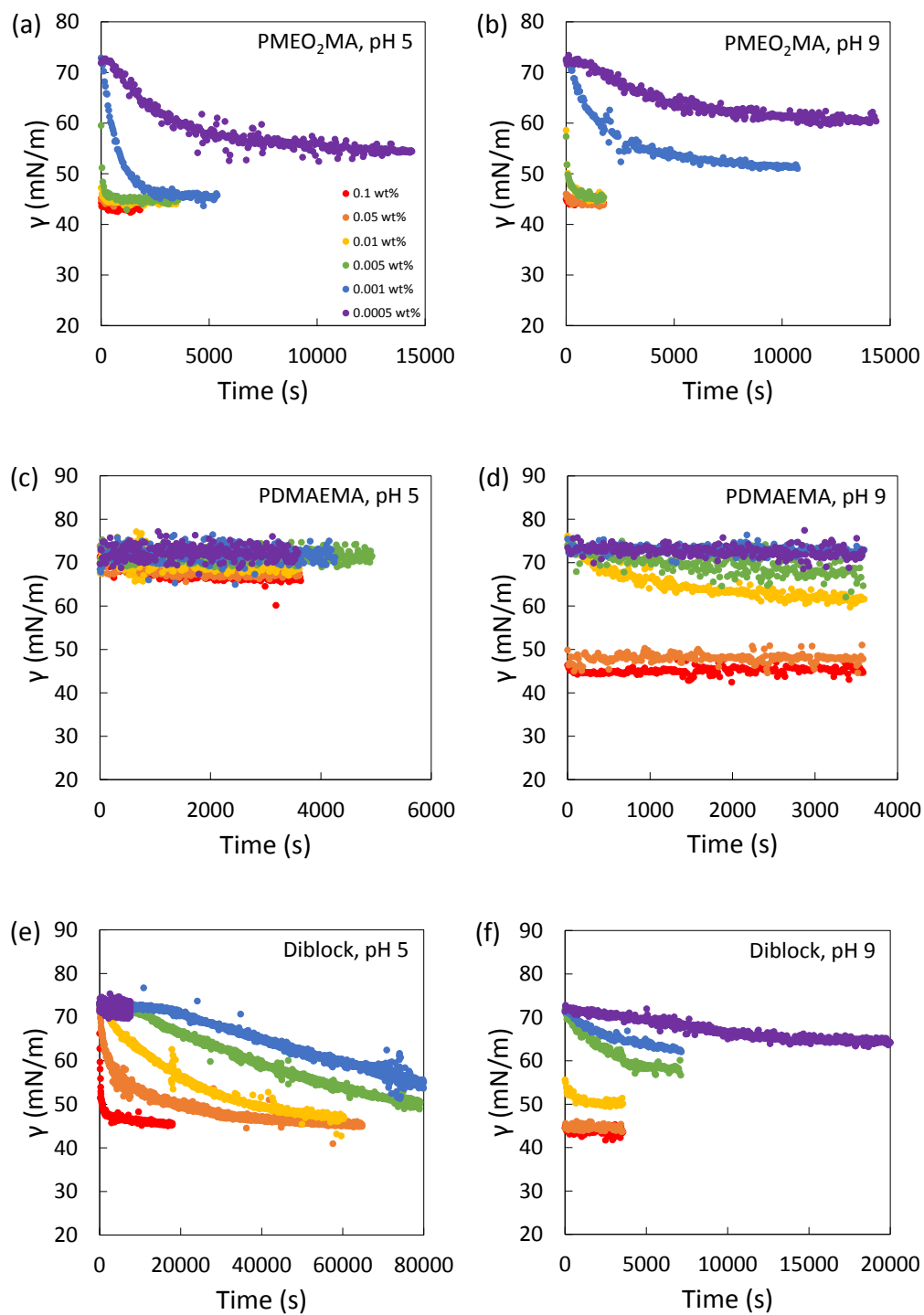


Figure 4.3. Surface tension reduction as a function of time for (a) PMEO₂MA star polymers at pH 5, (b) PMEO₂MA star polymers at pH 9 (c) PDMAEMA star polymers at pH 5, (d) PDMAEMA star polymers at pH 9, (e) diblock star polymers at pH 5, and (f) diblock star polymers at pH 9 adsorbed to the air/water interfaces. Polymer concentrations are (●) 0.1 (●) 0.05 (●) 0.01 (●) 0.005 (●) 0.001 (●) 0.0005 wt%

4.3.3 Dynamic dilatational elasticity

Figure 4.4 reports the magnitude of the complex dynamic dilatational modulus of star polymers adsorbed at the air/water interface at pH 5 and pH 9 with a 5% area strain amplitude. PMEO₂MA star polymers showed a decrease in dilatational modulus as the star polymer concentration continuously increased at both pH 5 and pH 9. This is attributed to the high affinity adsorption of PMEO₂MA stars to the air/water interface (**Figure 4.1**). When the interface expands, the PMEO₂MA stars adsorb to the surface and rapidly adjust the surface tension, resulting in low dynamic dilatational modulus. The dynamic surface tension (**Figure 4.3**) indicates that the surface tension reached the final value as soon as the droplet was generated for higher star polymer concentrations. PDMAEMA star polymers produced very small dilatational modulus (< 7 mN/m). This is consistent with low surface pressure (**Figure 4.1a**) and again suggests that very little amount of positively charged PDMAEMA adsorbed to the interface. The diblock produced relatively high dilatational modulus compared to PMEO₂MA and PDMAEMA star polymers at pH 5 despite being positively charged. This is possibly associated to the moderate surface pressures that diblock stars achieved (**Figure 4.1**) and the slow polymer adsorption rate to the interface (**Figure 4.3**), which restrains the adsorbed layers from reaching equilibrium during area perturbation. At pH 9, both PDMAEMA and diblock star polymers approached electrostatically neutral, and showed an increase followed by a decrease in dilatational modulus with increasing polymer concentration (**Figure 4.4b**). The increase in dilatational modulus at low polymer concentration is due to more polymer segments adsorbed to the interface when the bulk polymer concentration increases. However, further increases in the polymer concentration enhance the flux of polymer chains toward the interface, which rapidly adjusts the degree of interfacial penetration in response to a forced surface area change. It has

also been reported that the dilatational modulus ran through a maximum with increasing bulk concentrations with two nonionic surfactants *n*-dodecyl- β -D-maltoside (β -C₁₂G₂) and tetraethyleneglycol-monodecyl ether (C₁₀E₄) at air/water interface.¹⁶⁸ Increase of the bulk concentration has two different effects on the surface elasticity. First, the amount of polymers adsorbed at the interface increases, which leads to a higher surface tension change (and thus the surface elasticity) during area oscillation. Second, the polymer exchange between bulk and adsorbed species is increased with increasing bulk concentration; the degree of interfacial penetration is readily adjusted in response to a forced surface area change. In general, the trends that we observed from the dynamic surface tension and the dilatational modulus show: (1) low dilatational modulus is achieved when there is only small amount of polymer adsorbed to the interface, and (2) fast polymer adsorption rate tends to decrease the dilatational modulus.

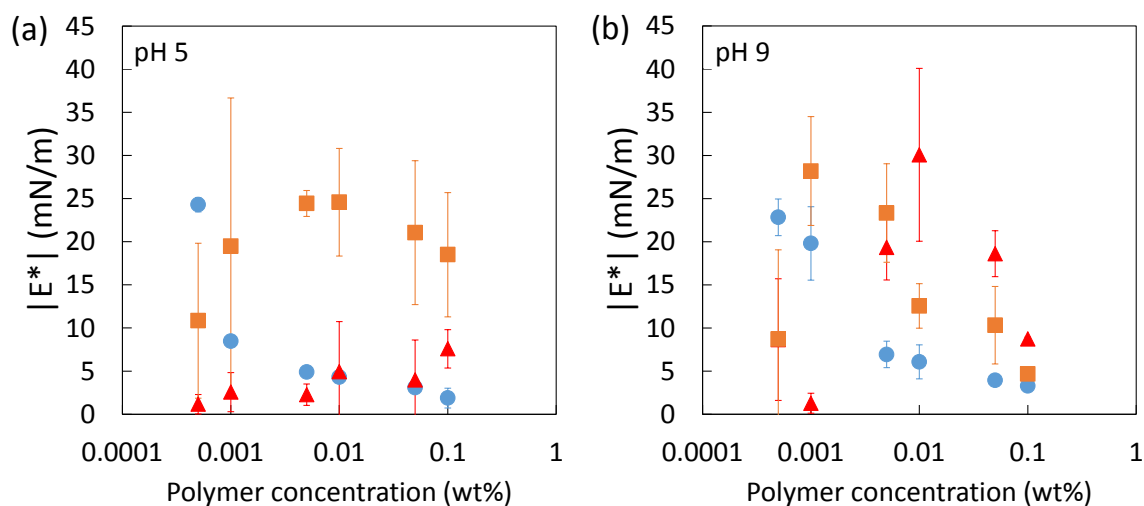


Figure 4.4. The magnitude of the complex dynamic dilatational moduli averaged over all frequencies for (●) PMEO₂MA, (▲) PDMAEMA and (■) diblock star polymers at the air/water interface at (a) pH 5 and (b) pH 9. Area strain amplitude is 5%.

For all star polymers at the air/water interface, the magnitude of dilatational loss modulus (E'') is negligible, indicating that the star polymer adsorbed layers are primarily elastic in the 0.05 – 0.1 Hz frequency range. This is evident in the sample data shown in **Figure 4.5** that the sinusoidal interfacial tension and area oscillations are in phase and no significant phase angle is detected. The nearly purely elastic adsorbed star polymer layers have also been noted previously.⁴⁶ It is worth mentioning that results for star polymers at air/water interface show no frequency dependence on the dilatational modulus, suggesting that the polymer adsorption/desorption time scale is not being probed in the range of tested frequencies.

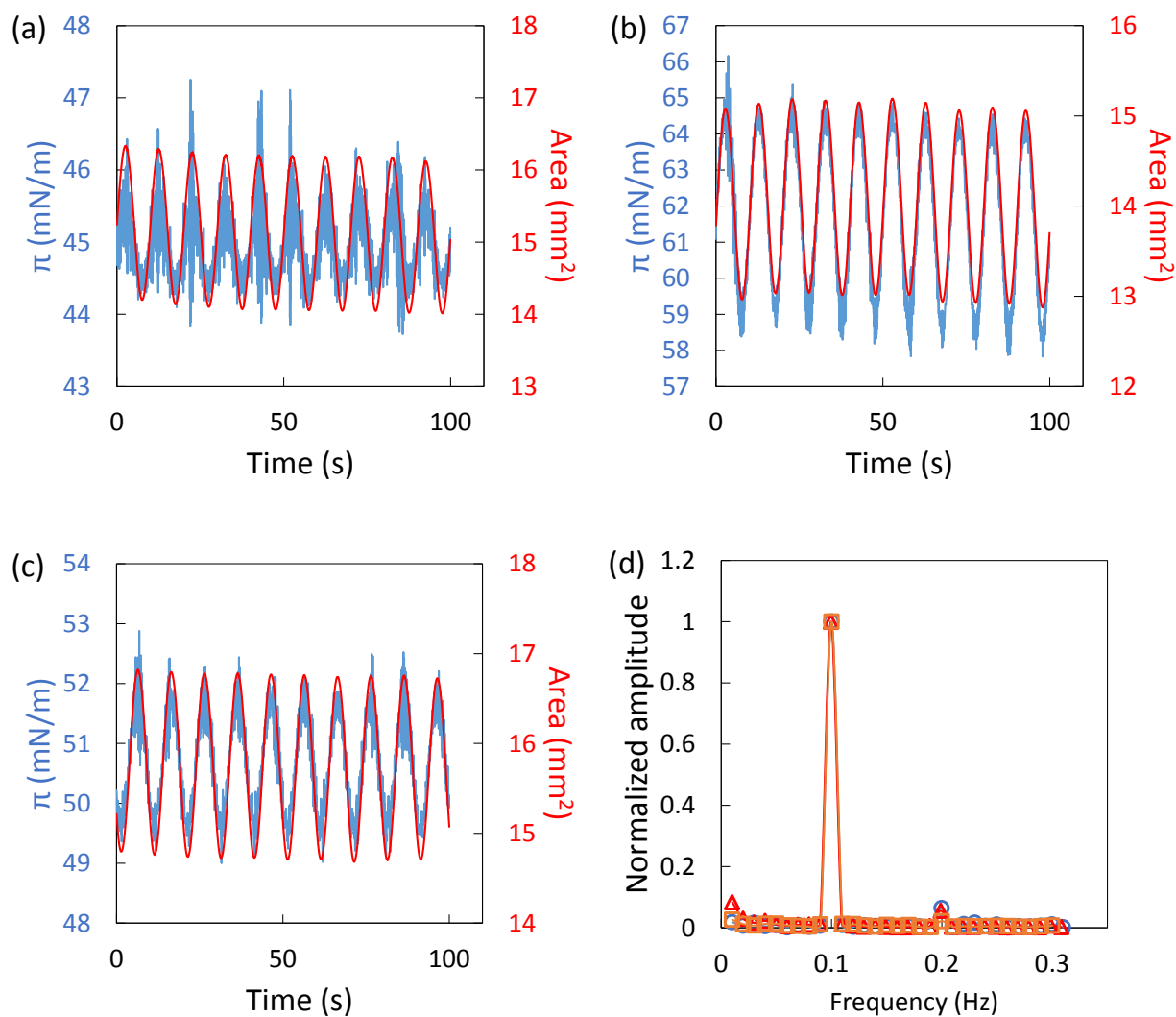


Figure 4.5. Surface tension and droplet area oscillation for 0.01 wt% of (a) PMEO₂MA, (b) PDMAEMA, and (c) diblock star polymers at the air/water interface at pH 9. The surface area oscillation frequency is 0.1 Hz. (d) Fast Fourier transform analysis of surface tension response in the dynamic dilatational modulus experiments at the air/water interface: (○) PMEO₂MA, (Δ) PDMAEMA, and (□) diblock star polymers. A peak was detected at the forced oscillation frequency.

It has been demonstrated that the surface dilatational properties of the adsorbed layer are important factors for foam stability.^{107,169,170} Prior investigation has also shown that the observed dilatational elasticity of adsorbed PEO star polymer layers may be responsible for their good

foaming performance, and distinguishes PEO stars from linear PEO being poor foaming agents that produced no detectable dilatational modulus.⁴⁶ However, despite the fact that star polymers studied here produce non-zero dynamic dilatational modulus, little correlation is found between their ability to stabilize foams and the magnitude of dilatational modulus. This suggests that dilatational modulus is sensitive to the structural change in the adsorbed layer during area perturbation but is not necessarily a predictor of the foam stability.

4.3.4 Extent of adsorption

Adsorption of star polymers to the air/water interface was measured using ellipsometry over a concentration range corresponding to the surface pressure measurements. As presented in **Figure 4.6**, the PMEO₂MA star polymer produced surface excess concentrations (Γ) from 1.97 ± 0.47 to 3.05 ± 0.51 mg/m² when the polymer concentration increased from 0.0005 to 0.1 wt%. The significantly higher surface excess concentration for PMEO₂MA star polymers than the other two stars studied here is consistent with the high surface pressure (**Figure 4.1**). The high surface affinity and small size allow the efficient packing of PMEO₂MA star polymers at the interface and result in greater adsorption. PDMAEMA star polymers adsorbed to the air/water interface with relatively low extent of adsorption ($\Gamma < 0.4$ mg/m²) at pH 5, which is again attributed to the strong electrostatic repulsion interactions between positively charged star polymers which inhibit closer packing. This surface excess concentration is slightly smaller than the linear PDMAEMA adsorbed to air/water and silica interfaces.^{14,24} Adsorption of diblock star polymers at pH 5 increased from $\Gamma = 0.28 \pm 0.21$ mg/m² at 0.0005 wt% bulk concentration to 1.58 ± 0.16 mg/m² at 0.1 wt%. The measured surface excess concentrations are between those of PMEO₂MA stars and PDMAEMA stars, which again confirms that the extent of adsorption is

enhanced by the high surface activity of inner PMEO₂MA polymer block but compromised by the intra- and interchain repulsion of outer PDMAEMA polymer block.

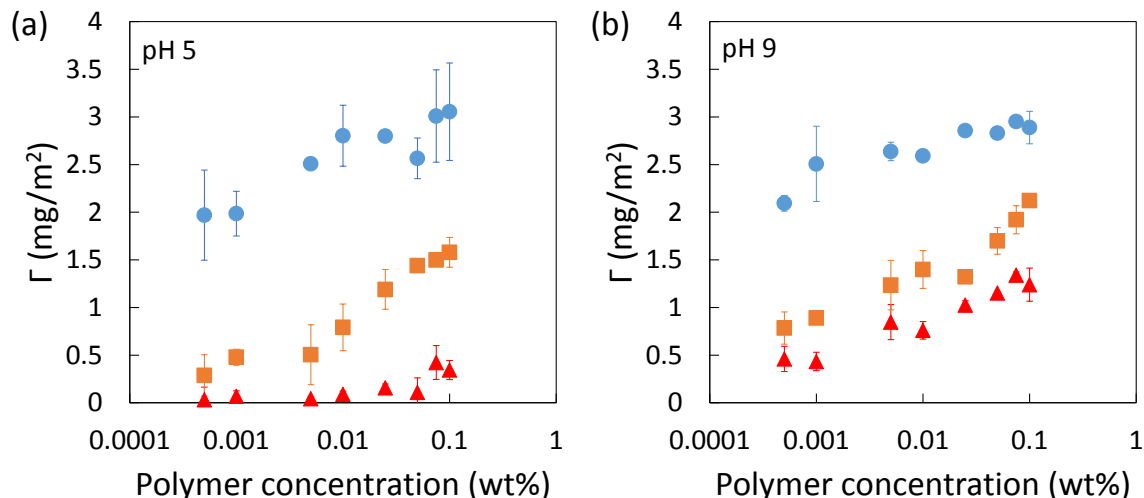


Figure 4.6. Surface excess concentration for (●) PMEO₂MA, (▲) PDMAEMA and (■) diblock star polymers adsorption to the air/water interface at (a) pH 5 and (b) pH 9.

As pH increased and the PDMAEMA and diblock became deprotonated, the surface excess concentration increased for both star polymers. As depicted in **Figure 4.6b**, the PDMAEMA stars produced $\Gamma = 0.5 - 1.2 \text{ mg/m}^2$ while the diblock stars produced $\Gamma = 0.8 - 2.1 \text{ mg/m}^2$ at bulk concentration from 0.0005 – 0.1 wt%. At high pH, the decreased charge weakens the lateral electrostatic repulsion at the air/water interface and allows more star polymers adsorption. Furthermore, the smaller size of star polymers due to the collapsed brush chains favor closer packing at the interface. The increase in extent of adsorption at reduced charge density is consistent with the trend in surface pressures and has been observed for linear polyelectrolyte¹⁷¹ and PDMAEMA-grafted silica particles.¹⁴ It is noted that the extent of adsorption at pH 9 for PDMAEMA and diblock stars is consistently higher ($\sim 0.6 \text{ mg/m}^2$) than

those at pH 5. However, the effect of pH on the dynamic of adsorption was not probed here since each interface was given at least 12 hours to relax before measurements were taken.

The area fraction surface coverage (θ) was calculated from the surface excess concentration (Γ) and hydrodynamic radius (R_h) to estimate the degree of crowding at the interface using the relation discussed in **Chapter 3.3.5**:

$$\theta = \pi R_h^2 \Gamma \frac{N_A}{M} \quad (3.1)$$

where M is the molar mass and N_A is Avogadro's number. Assuming that the projected area of an adsorbed star polymer is equal to the cross-sectional area defined by its hydrodynamic radius measured in bulk solution, these calculated area fractions are plotted in **Figure 4.7**. Despite their high surface excess concentration, PMEO₂MA star polymers produced a surface coverage of 0.3 – 0.5. At pH 5 where the PDMAEMA polymer chains are highly swollen, the surface coverage was < 0.1 for all polymer concentrations, which is consistent with the low surface pressure (**Figure 4.1**). Surface coverage increased from ~ 0.1 to ~ 0.3 with increasing bulk concentration at pH 9 where more PDMAEMA star polymers adsorbed with polymer brushes collapsed. It has been observed previously that the dilute adsorption layer of anionic surfactant sodium dodecyl sulfate (SDS) was sufficient to stabilize foams despite low surface pressure and low surface coverage achieved,¹⁷² which was attributed to a significant electrostatic repulsion between the foam film surfaces. Nevertheless, no foam was produced for PDMAEMA star polymers at pH 5 even though a high electrostatic repulsion between the film surfaces would be expected. Diblock star polymer achieved a surface coverage of 0.1 – 0.4 at pH 5. A significant increase in surface coverage when the brushes collapsed at pH 9 due to the absence of electrostatic repulsion between diblock star polymers, which allows them to pack densely on the surface. It should be

noted that the area fraction surface coverage calculated using equation (3.1)) is in fact very sensitive to the size of the star polymers. Since the star polymers are not monodisperse (see **Table 4.2** for polydispersity) and the equation is based on the simple assumption that star polymers exhibit minimal changes in polymer conformation upon adsorption to the interface, the value reported here should not be overinterpreted. Yet, the observed qualitative trend suggests that the adsorption of the star polymers with weakly polycation blocks are dependent on pH. Higher surface coverage is achieved at high pH because of the lack of lateral electrostatic repulsion.

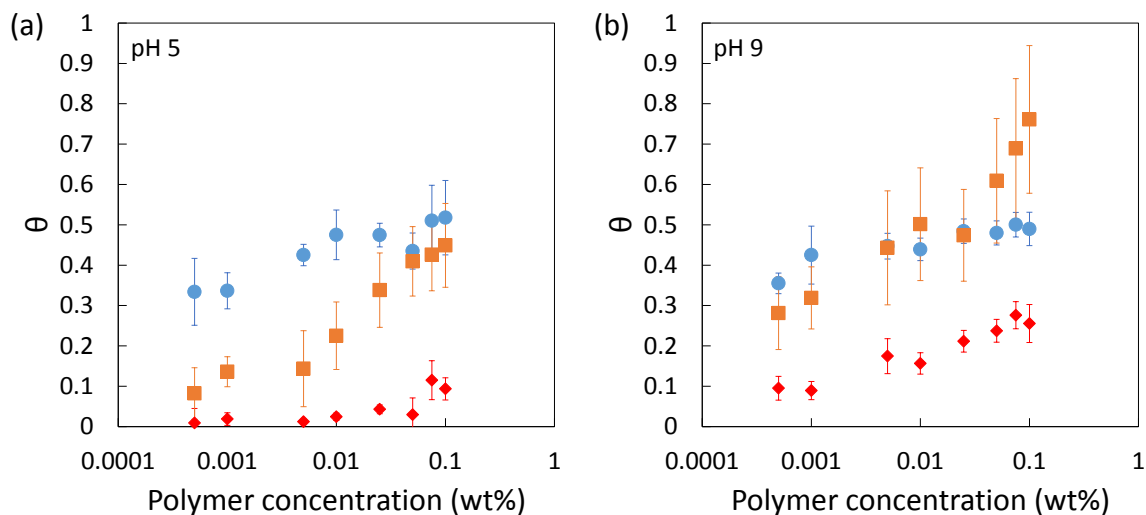


Figure 4.7. Apparent area fraction surface coverage calculated from the extent of adsorption and sizing data as $\theta = \pi R_h^2 \Gamma$ for (●) PMEO₂MA, (▲) PDMAEMA and (■) diblock star polymers adsorption to the air/water interface at (a) pH 5 and (b) pH 9.

4.3.4.1 Gibbs elasticity

The static dilatational elasticity for star polymers is evaluated using the static surface pressure (**Figure 4.1**) and the surface excess concentration (**Figure 4.6**) by equation (3.2):

$$E_d = \frac{d\gamma}{d \ln A} = -\frac{d\pi}{d \ln A} = \frac{d\pi}{d \ln \Gamma} = -\frac{d\pi}{d \ln 1/\Gamma} \quad (3.2)$$

which gives the equilibrium or Gibbs elasticity for a thermodynamically equilibrated, fully insoluble monolayer. **Figure 4.8** shows the static surface pressure area isotherm for PMEO₂MA, PDMAEMA and diblock stars adsorbed at air/water interface at pH 5 and pH 9. The static dilatational elasticity is obtained by linear regression of surface pressure area isotherm over the concentration range examined here. The analysis indicates a static dilatational modulus of ~ 20 mN/m for PMEO₂MA stars, which is higher than those obtained through small amplitude oscillation at higher bulk concentrations (**Figure 4.4**). The difference in static dilatational modulus and dynamic dilatational modulus is probably due to the diffusional interchange of star polymers between bulk solution and polymer reconfiguration following the area perturbation. Since static dilatational modulus measures the sensitivity of the surface pressure to changes in the surface concentration, dynamic dilatational modulus accounts for the polymer relaxation. Similar phenomena are observed for PDMAEMA and diblock stars at pH 9 where the static dilatational modulus is higher than the measured dynamic dilatational modulus. In contrast, PDMAEMA and diblock stars at pH 5 produced static dilatational modulus that is comparable to dynamic dilatational modulus. It should be noted that in **Figure 4.8** the static dilatational modulus is determined by fitting the surface pressure area isotherm with one straight line. However, more data points are needed to perform a piecewise calculation of the slope for the Gibbs modulus.

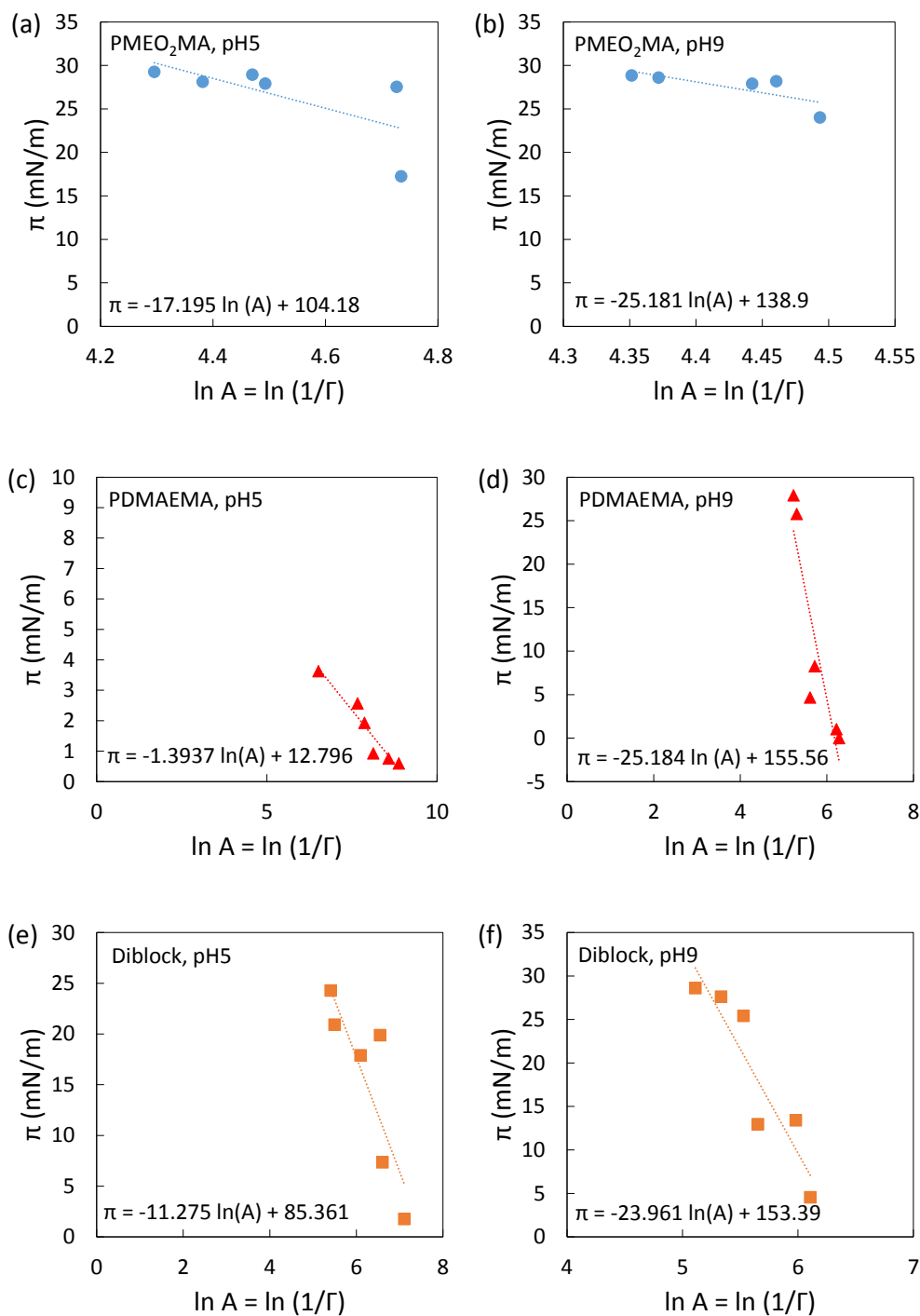


Figure 4.8. Surface pressure area isotherm for (a, b) PMEO₂MA, (c, d) PDMAEMA and (e, f) diblock star polymers adsorbed at air/water interface at pH 5 and pH 9. Ellipsometry provided the static surface excess concentration for each star concentration at which surface pressures were measured in independent experiments. Linear regression for the slope of π vs. $\ln(1/\Gamma)$ yields a static dilatational elasticity.

4.3.4.2 Solution depletion upon polymer adsorption

Polymer adsorption will result in the polymer depletion from the bulk solution and therefore affect the kinetics of polymer adsorption. Similar to the discussion in **Chapter 3.3.5.2**, **Table 4.5** and **Table 4.6** summarize the depletion effect from the bulk solution upon polymer adsorption for star polymers in pendant drop experiments at pH 5 and pH 9, respectively. The analysis assumes that the pendant drop is spherical and no polymers are added to the system after the drop is generated despite the fact that the pendant drop is connected to the bulk reservoir. As shown in **Table 4.5** and **Table 4.6**, nearly all of the available PMEO₂MA stars are depleted at the bulk concentration of 0.0005 wt%. The decrease of bulk concentration leads to a decrease in polymer flux to the surface, which is consistent with the slower dynamic surface tension reduction at air/water interface (**Figure 4.3**). At pH 5, almost no PDMAEMA star polymers are depleted in the pendant drop. The PDMAEMA star polymer adsorption is inhibited because of the strong electrostatic repulsion interactions between the positively charged star polymers. At pH 9, the PDMAEMA arms in the stars are neutralized and the lack of electrostatic repulsion allows more polymers adsorbed to the interface. Therefore, the depletion effect at pH 9 for PDMAEMA stars is more pronounced. Similar to the trend observed for PDMAEMA star polymers, more diblock star polymers are depleted at pH 9 than at pH 5 due to higher extent of adsorption.

Table 4.5. Estimated change in the bulk concentrations upon polymer adsorption for star polymers with an 8 μ L pendant drop at different bulk concentrations at pH 5. The analysis is based on the assumptions of a spherical pendant drop and no polymer diffusion from the bulk reservoir to the pendant drop. The surface excess concentrations are obtained *via* ellipsometry using large glass petri dishes.

Polymer	Conc. (wt%)	Total polymer (mg)	Γ (mg/m²)	Polymer at interface (mg)	Polymer at interface /Initial in bulk (%)
PMEO₂MA stars	0.1	0.008	3.05	0.0000591	0.74
	0.05	0.004	2.57	0.0000496	1.24
	0.01	0.0008	2.80	0.0000542	6.78
	0.005	0.0004	2.51	0.0000485	12.13
	0.001	0.00008	1.99	0.0000384	48.01
	0.0005	0.00004	1.97	0.0000381	95.25
PDMAEMA stars	0.1	0.008	0.34	0.0000067	0.08
	0.05	0.004	0.11	0.0000021	0.05
	0.01	0.0008	0.09	0.0000017	0.22
	0.005	0.0004	0.04	0.0000008	0.21
	0.001	0.00008	0.07	0.0000013	1.66
	0.0005	0.00004	0.03	0.0000006	1.57
Diblock stars	0.1	0.008	1.58	0.0000305	0.38
	0.05	0.004	1.44	0.0000279	0.70
	0.01	0.0008	0.79	0.0000153	1.91
	0.005	0.0004	0.50	0.0000098	2.44
	0.001	0.00008	0.48	0.0000093	11.57
	0.0005	0.00004	0.29	0.0000056	13.94

Table 4.6. Estimated change in the bulk concentrations upon polymer adsorption for star polymers with a 6 μL pendant drop at different bulk concentrations at pH 9. The analysis is based on the assumptions of a spherical pendant drop and no polymer diffusion from the bulk reservoir to the pendant drop. The surface excess concentrations are obtained *via* ellipsometry using large glass petri dishes.

Polymer	Conc. (wt%)	Total polymer (mg)	Γ (mg/m^2)	Polymer at interface (mg)	Polymer at interface /Initial in bulk (%)
PMEO₂MA stars	0.1	0.006	2.89	0.0000461	0.77
	0.05	0.003	2.83	0.0000452	1.51
	0.01	0.0006	2.59	0.0000414	6.89
	0.005	0.0003	2.64	0.0000421	14.04
	0.001	0.00006	2.51	0.0000400	66.72
	0.0005	0.00003	2.09	0.0000334	111.45
PDMAEMA stars	0.1	0.006	1.24	0.0000198	0.33
	0.05	0.003	1.15	0.0000184	0.61
	0.01	0.0006	0.76	0.0000121	2.02
	0.005	0.0003	0.85	0.0000135	4.51
	0.001	0.00006	0.43	0.0000069	11.54
	0.0005	0.00003	0.46	0.0000074	24.54
Diblock stars	0.1	0.006	2.12	0.0000339	0.56
	0.05	0.003	1.70	0.0000271	0.90
	0.01	0.0006	1.40	0.0000223	3.72
	0.005	0.0003	1.24	0.0000197	6.57
	0.001	0.00006	0.89	0.0000142	23.67
	0.0005	0.00003	0.78	0.0000125	41.75

4.4 Interfacial behavior at oil/water interface

4.4.1 Emulsification efficiency and stability

Table 4.7 summarizes the minimum concentration required for star polymers to stabilize xylene/water and cyclohexane/water emulsions at pH 5 and pH 9 using a 1:1 oil:water volume ratio. These concentrations refer to the star concentrations initially dispersed in the aqueous phase. All emulsions were oil-in-water and showed no sign of droplet coalescence for at least a week. Some emulsions were stable for more than 2 months and their change in emulsion height

is reported in **Figure 4.9 – Figure 4.11**. The discontinuous oil volume fraction in the emulsion was typically ~ 70% and no neat oil phase was observed when the emulsions were first created, indicating that 100% of the available oil was dispersed in the emulsion phase. **Table 4.7** shows that the diblock star polymers are the most efficient emulsifiers among the three stars studied here. The concentration required for diblock stars to stabilize an emulsion is the lowest. Stable xylene/water and cyclohexane/water emulsions were formed with ~ 0.005 – 0.05 wt% of diblock stars, which is comparable to those using multi-arm PEO stars (0.005 wt%)⁴⁶ and low grafting density PDMAEMA-grafted silica nanoparticles (0.05 wt%).¹⁹ Surprisingly, the PDMAEMA and diblock star polymers became more efficient at stabilizing emulsions at pH 5 than at pH 9. This trend is completely opposite from the foaming results (**Table 4.4**) where no foams was made at low pH. It is also observed that lower star polymer concentrations were required to stabilize cyclohexane/water emulsions than xylene/water emulsions except for diblock stars at pH 9. Similar results were reported previously where an emulsion was created with cyclohexane but not with xylene using PDMAEMA-grafted silica nanoparticles at 70 °C with 10 mM NaCl.¹⁹ This is attributed to different polymer conformation when stars adsorbed at the interface with different solvent quality of the organic phase. Polymer chains can adopt an extended configuration into a good solvent but not into a poor solvent. Xylene and cyclohexane were used to represent a good and a poor solvent, respectively, for each of the star polymers studied in this work. The difference in emulsifying performance motivates the comparison of different star polymers behaviors at xylene/water and cyclohexane/water interfaces.

Table 4.7. Minimum concentrations of star polymers to stabilize oil-in-water emulsions

System	pH	PMEO ₂ MA stars (wt%)	PDMAEMA stars (wt%)	Diblock stars (wt%)
Xylene/water	5	0.05	0.01	0.001 – 0.005
	9	0.05	0.1	0.005 – 0.01
Cyclohexane/water	5	0.01	0.005	0.005
	9	0.01	0.1	0.01 – 0.05

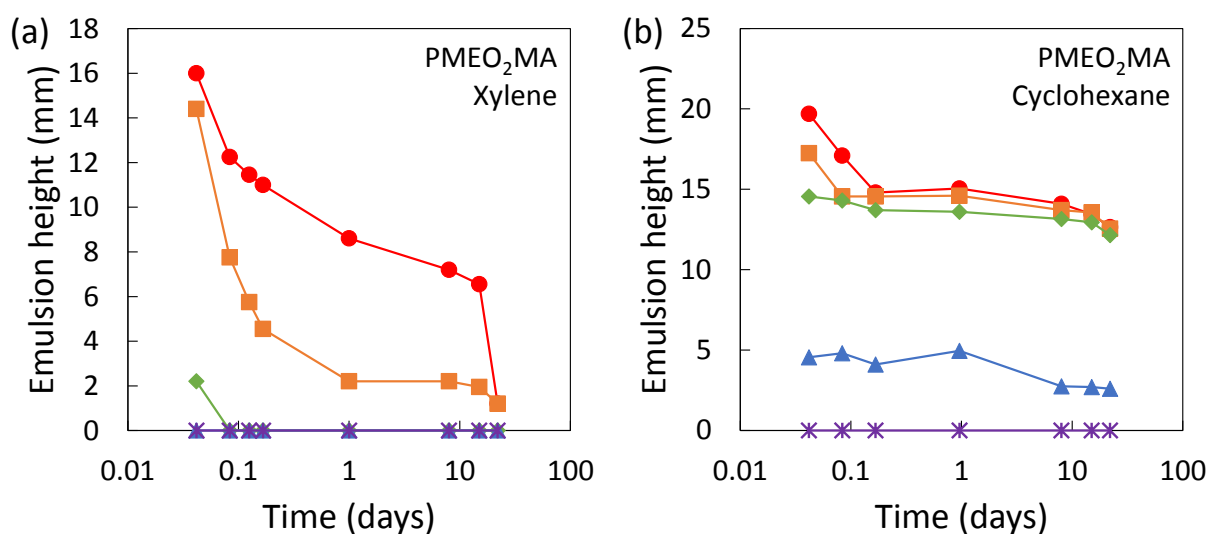


Figure 4.9. Effect of PME₂MA star polymer concentration on emulsion stability: (●) 0.1 (■) 0.05 (◆) 0.01 (▲) 0.005 (*) 0.001 wt%. Changes in height for (a) xylene-in-water and (b) cyclohexane-in-water emulsions at different concentrations of PME₂MA star polymers as a function of time. Lines serve to guide the eye.

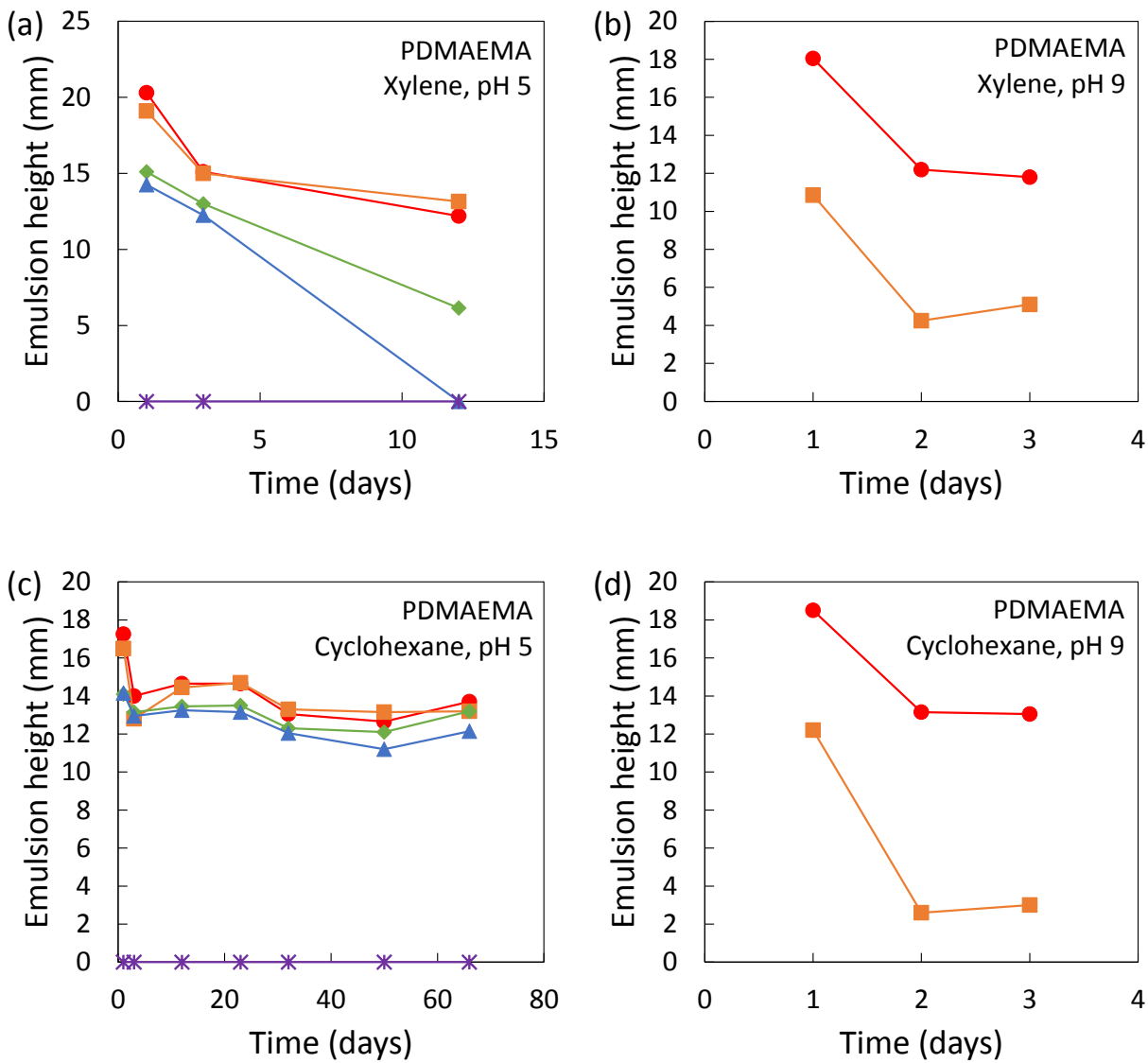


Figure 4.10. Effect of PDMAEMA star polymer concentration on emulsion stability: (●) 0.1 (■) 0.05 (◆) 0.01 (▲) 0.005 (*) 0.001 wt%. Changes in height for (a) pH 5, xylene-in-water, (b) pH 9, xylene-in-water, (c) pH 5, cyclohexane-in-water and (d) pH 9, cyclohexane-in-water emulsions at different concentrations of PDMAEMA star polymers as a function of time. Lines serve to guide the eye.

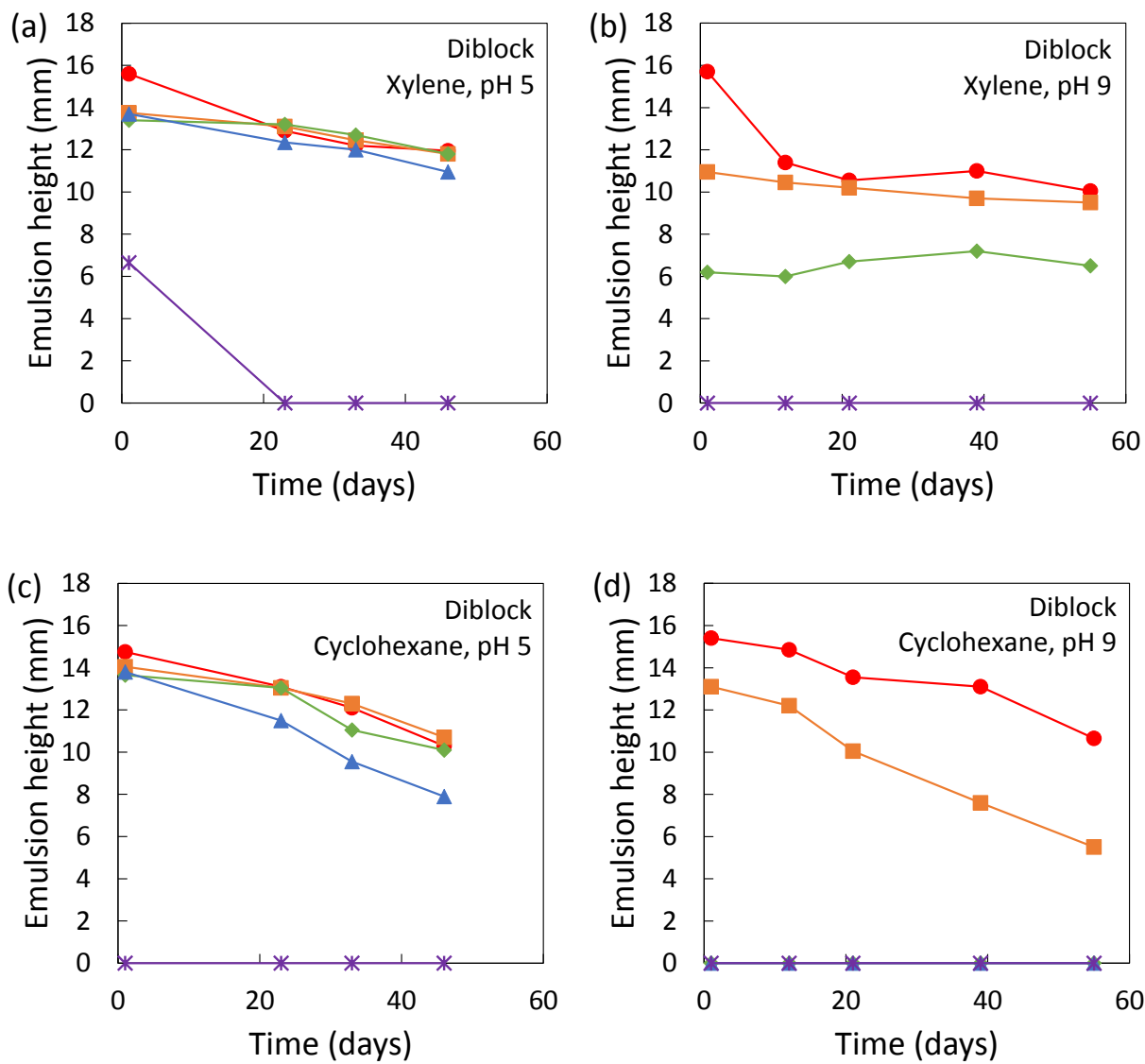


Figure 4.11. Effect of diblock star polymer concentration on emulsion stability: (●) 0.1 (■) 0.05 (◆) 0.01 (▲) 0.005 (*) 0.001 wt%. Changes in height for (a) pH 5, xylene-in-water, (b) pH 9, xylene-in-water, (c) pH 5, cyclohexane-in-water and (d) pH 9, cyclohexane-in-water emulsions at different concentrations of diblock star polymers as a function of time. Lines serve to guide the eye.

4.4.2 Interfacial tension reduction

Figure 4.12 shows interfacial pressure isotherms measured by pendant drop tensiometry for PMEO₂MA stars, PDMAEMA stars and diblock stars adsorbed at xylene/water and cyclohexane/water interfaces. The polymers were initially dispersed in water. Interfacial tensions for clean xylene/water and cyclohexane/water interfaces were measured to be 37.0 ± 0.2 and 49.9 ± 0.4 mN/m, respectively, which agree with values reported in the literature.^{24,156–158}

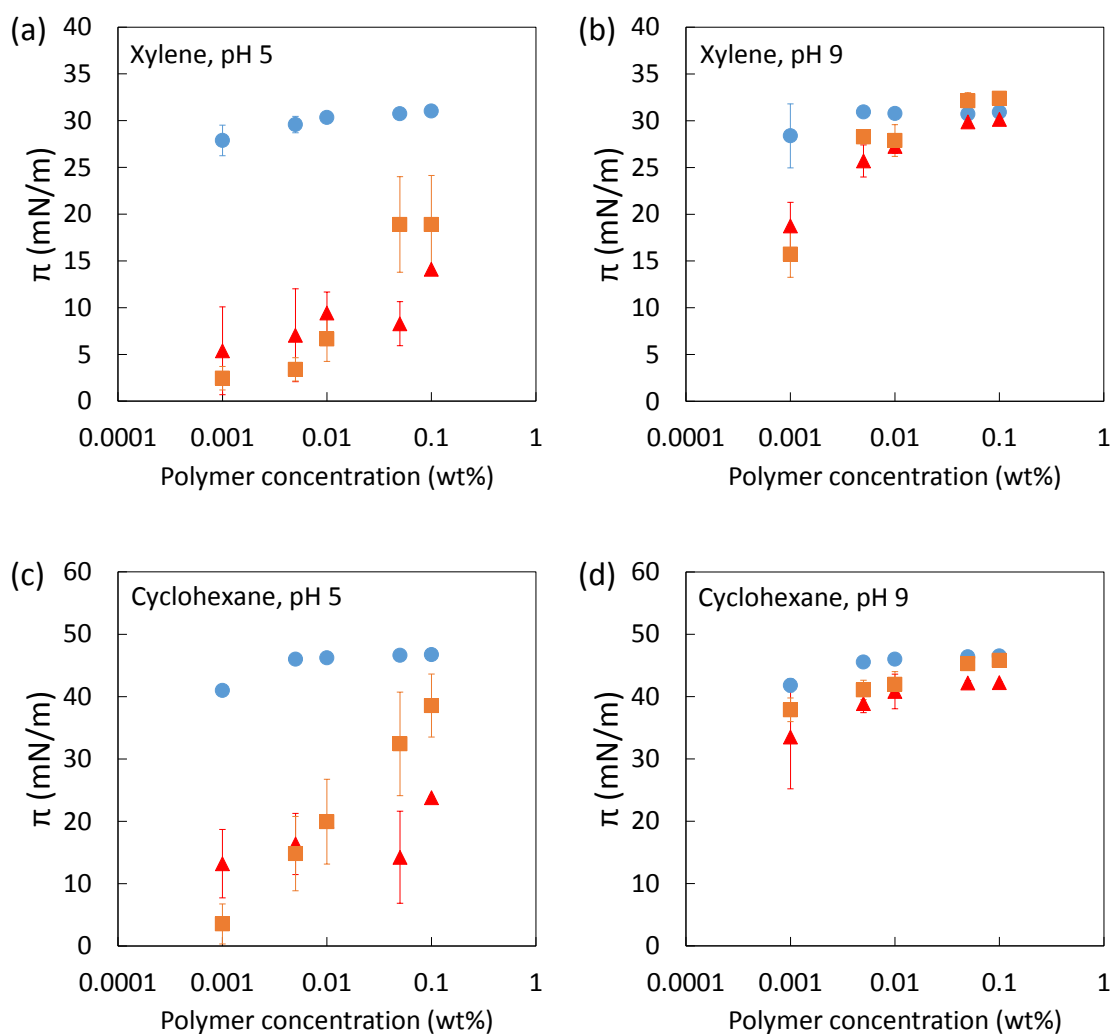


Figure 4.12. Interfacial pressure isotherm of (●) PMEO₂MA, (▲) PDMAEMA and (■) diblock star polymers adsorbed to the xylene/water interface at (a) pH 5 and (b) pH 9, and to the cyclohexane/water interface at (c) pH 5 and (d) pH 9.

As seen in **Figure 4.12**, two interfaces show similar trends, but the measured interfacial pressure at the cyclohexane/water interface was consistently several mN/m higher than at the xylene/water interfaces. As discussed earlier, different adsorbed polymer conformation is expected as the polymer-solvent interactions can affect the chain topology and the polymer adsorption energy. Polymer chains can penetrate into the good solvent (xylene) but not the poor solvent (cyclohexane). Thus, the difference in interfacial pressure may be associated with the difference in adsorption enthalpy with more extended polymer chain configuration reaching to the good solvent interface compared to the poor solvent interface.

Similar to the trend at the air/water interface, PMEO₂MA stars exhibited high affinity adsorption to the interface and achieved the greatest interfacial pressures at both xylene/water and cyclohexane/water interfaces. The interfacial pressures produced by PMEO₂MA stars are larger than those reported with multi-arm PEO stars⁴⁶ and PDMAEMA-grafted silica nanoparticles²⁴ at the xylene/water and cyclohexane/water interfaces. Different from the observations at the air/water interface that PDMAEMA stars barely lowered the surface tension and achieved a low surface coverage at pH 5, PDMAEMA stars produced interfacial pressure of 5 – 15 mN/m at the xylene/water and 13 – 23 mN/m at the cyclohexane/water interface. This reduction in interfacial tension at low pH suggests that PDMAEMA stars were able to adsorb to the interface despite being strongly positively charged. At pH 5, interfacial pressure of PDMAEMA and diblock stars increased with the bulk concentration and produced comparable interfacial pressures except at high bulk concentrations where diblock stars achieved greater interfacial pressures than PDMAEMA stars (**Figure 4.12a** and **Figure 4.12c**). Again, similar to the air/water interface, PDMAEMA and diblock star polymers produced higher interfacial pressure at pH 9 than at pH 5. Moreover, these three star polymers reached comparable

interfacial pressures at the cyclohexane/water interface at pH 9 (**Figure 4.12d**). The increase in interfacial pressure at high pH is associated with the lack of electrostatic repulsion and the collapse of the PDMAEMA chains at high pH, leading to the compact star polymer structure that favors more polymer segments penetrating the interface. The effect of electrostatic repulsion between swollen polymer chains at low pH on interfacial tension reduction can be seen in the dynamic interfacial tension measurements (**Figure 4.13 – Figure 4.14**) The interfacial tension reduced more rapidly at pH 9 than at pH 5 for both PDMAEMA and diblock star polymers, indicating that increasing the charge density of the polyelectrolytes reduces its rate of adsorption to an uncharged interface.

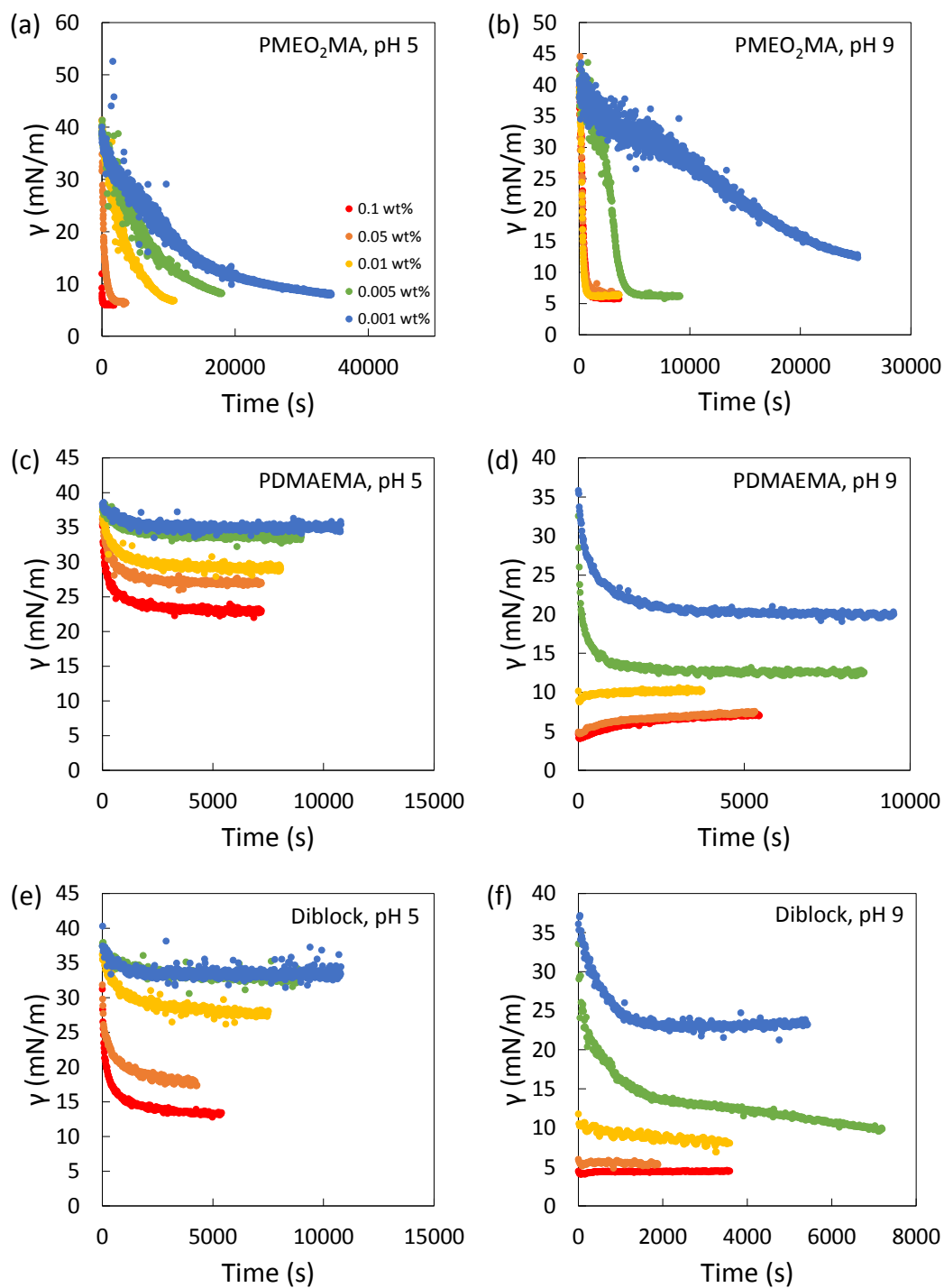


Figure 4.13. Interfacial tension reduction as a function of time for (a) PMEO₂MA star polymers at pH 5, (b) PMEO₂MA star polymers at pH 9 (c) PDMAEMA star polymers at pH 5, (d) PDMAEMA star polymers at pH 9, (e) diblock star polymers at pH 5, and (f) diblock star polymers at pH 9 adsorbed to the xylene/water interfaces.

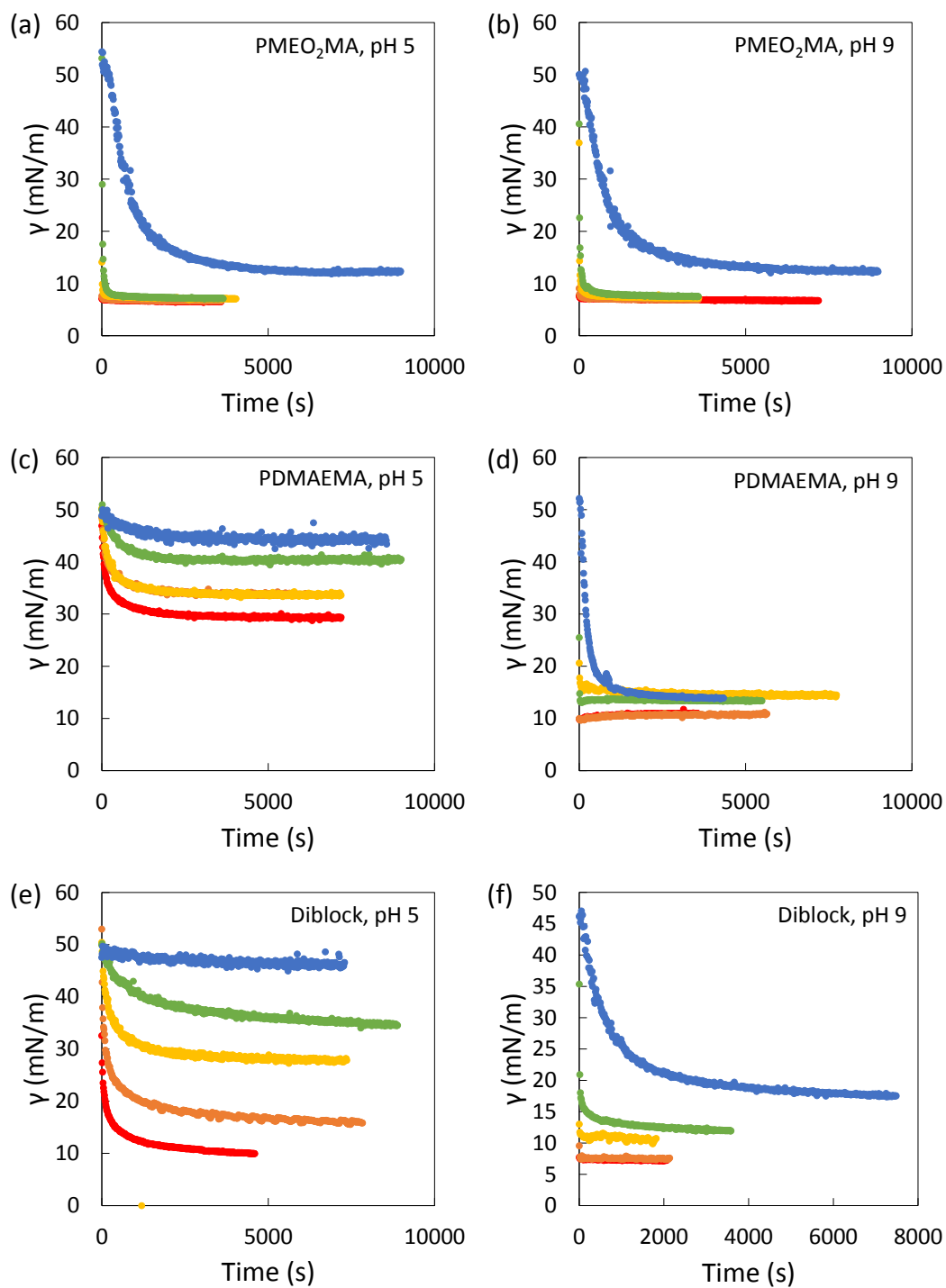


Figure 4.14. Interfacial tension reduction as a function of time for (a) PMEO₂MA star polymers at pH 5, (b) PMEO₂MA star polymers at pH 9 (c) PDMAEMA star polymers at pH 5, (d) PDMAEMA star polymers at pH 9, (e) diblock star polymers at pH 5, and (f) diblock star polymers at pH 9 adsorbed to the cyclohexane/water interfaces.

4.4.3 Dynamic dilatational elasticity

The mechanical properties of the oil/water interface were probed by measuring interfacial dilatational modulus through three approaches, which are small amplitude oscillation after interface relaxation, large amplitude compression after interface relaxation, and small amplitude oscillation before interface relaxation.

4.4.3.1 Small amplitude oscillation after interface relaxation

Figure 4.15 presents the magnitude of the complex dynamic dilatational modulus ($|E^*|$) of star polymers adsorbed at xylene/water and cyclohexane/water interfaces at pH 5 and pH 9. The dilatational modulus was measured after the interface was given enough time to relax and the interfacial tension reached a steady value. Similar to air/water interface, the dynamic dilatational modulus of PMEO₂MA star polymers (circle symbols) decreased with increasing bulk concentration. This is again attributed to the high adsorption rate and fast polymer exchange rate between the adsorbed and dissolved PMEO₂MA star polymers, which allows the interface to produce only a small change in degree of interfacial penetration during area oscillation. PDMAEMA and diblock star polymers showed complex interfacial behavior at oil/water interfaces. At pH 5, positively charged PDMAEMA stars showed a small increase in modulus when polymer concentration increased at xylene/water interface but had little dependence on polymer concentration at cyclohexane/water interface. The modulus of diblock stars increased from $|E^*| = 6.0 \pm 3.2$ mN/m at 0.001 wt% to $|E^*| = 22.6 \pm 5.3$ mN/m at 0.1 wt% at xylene/water interface, whereas the modulus at cyclohexane/water initially increased with polymer concentration, reached a maximum $|E^*| = 35.8 \pm 9.3$ mN/m at 0.01 wt% and then decreased as the concentration increased. This interfacial phenomenon is the result of the combination of electrostatic repulsion and the diffusion relaxation. In addition, the concentration at which the

maximum occurs depends on the diffusion coefficient and thus the static and dynamic adsorption properties of the star polymers.¹⁶⁸ At pH 9, the modulus of PDMAEMA stars (triangle symbols) first increased and then decreased with polymer concentration, whereas the modulus of diblock stars (square symbols) monotonically decreased with polymer concentration at both oil/water interfaces. The decrease in modulus at higher star polymer concentration is again attributed to the fast diffusion relaxation, which reduces the excess interfacial tension ($d\gamma$) after perturbation of the interfacial area.

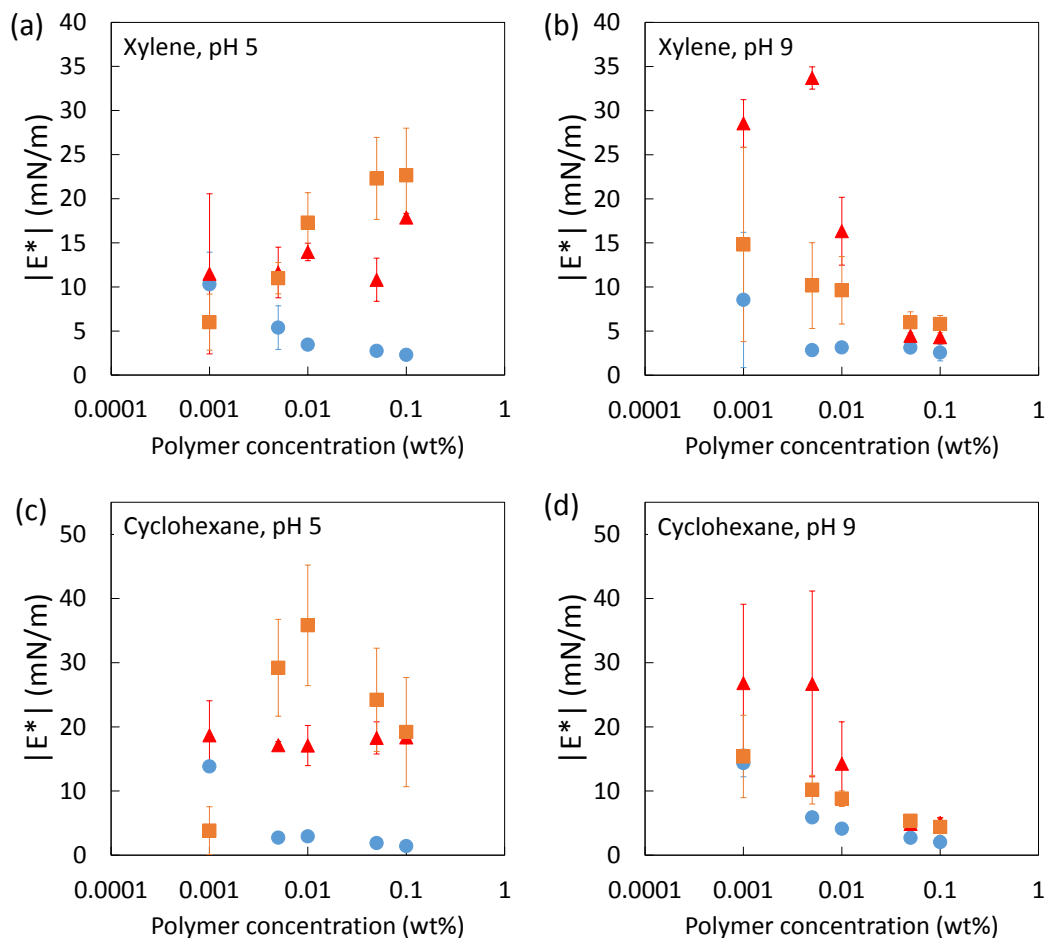


Figure 4.15. The magnitude of the complex dynamic dilatational moduli averaged over all frequencies for (●) PMEO₂MA, (▲) PDMAEMA and (■) diblock star polymers adsorbed to the xylene/water interface at (a) pH 5 and (b) pH 9, and to the cyclohexane/water interface at (c) pH 5 and (d) pH 9.

All star polymer adsorbed layers were nearly purely elastic in the 0.05 to 1 Hz frequency range. The storage modulus E' accounted for more than 90% of the magnitude of the complex modulus for adsorbed stars at xylene/water and cyclohexane/water interfaces. Similar to the observations at the air/water interface, the modulus showed little dependence on the oscillation frequency.

Considering that emulsion droplet generation and coalescence involve interfacial deformations, the interfacial dilatational response is particularly relevant to emulsifying performance. Finite dynamic dilatational modulus has been reported to be the key factor to distinguish high emulsifying efficiency of PEO stars from the poor emulsifying performance of linear PEO which produced no detectable modulus.⁴⁶ Prior investigations also correlated the dilatational modulus with the ability for adsorbed layer to resist interfacial deformation and hinder the thin film drainage,^{103,107} which retards the rate of droplet coalescence. The results show that these three star polymers all produce non-zero moduli at oil/water interface, which possibly accounts for their effectiveness at stabilizing emulsions (i.e., the ability to produce emulsions). However, no qualitative relationships between dilatational modulus and their emulsification performance can be addressed at this point. As presented in **Figure 4.15**, the measured magnitude of the dynamic dilatational modulus for star polymers does not necessarily correlate with their emulsifying efficiency (**Table 4.7**). It has been reported previously that PDMAEMA homopolymers achieved a greater dilatational modulus of 14.2 ± 0.5 mN/m than the modulus measured for PDMAEMA-grafted silica nanoparticles (10.6 ± 1.0 mN/m) at the xylene/water interface,²⁴ yet the linear PDMAEMA was unable to stabilize emulsions with the polymer concentration as low as reported with PDMAEMA-grated silica nanoparticles (0.05 wt% at pH 7.5).¹⁹ Additionally, conflicting results were found on the interfacial rheology with

the corresponding emulsion properties. Some researchers have reported that the overall emulsion lifetime is dominated by the ripening and correlated with the low-frequency surface elasticity,¹⁷³ whereas others have shown a correlation between emulsion stability and dilatational elasticity at high frequencies but not at low frequencies for moderate surfactant concentrations.¹⁷⁴ It is noted that dynamic dilatational modulus only probes the corresponding extra stresses of the adsorbed layer upon area dilation. If the emulsification efficiency and stability is not solely governed by the dilatational stresses, then the measured dilatational modulus is not necessarily a predictor for the emulsifying performance.

4.4.3.2 Large amplitude, slow compression and expansion after interface relaxation

To further investigate the behavior of the star polymer adsorbed layer and the effect of changing interfacial area on the interfacial mechanics, slow compression and expansion experiments of the oil/water interface were performed. Interfacial pressure-area (Π -A) isotherms were obtained from large amplitude compression and expansion of star adsorbed layers using pendant drop tensiometry. Different from the dynamic dilatational modulus measurements where the strain amplitude was typically around 5%, the area change in these compression/expansion experiments was $> 40\%$. This allows probing of the interparticle interactions between adsorbed species, the compressibility and the adsorption/desorption exchange kinetics in equilibrated adsorbed layers.

Two distinctive trends of interfacial behavior were observed. **Figure 4.16a** shows one representative data of the interfacial pressure as a function of interfacial area for three compression/expansion cycles of a xylene/water interface exposed to 0.001 wt% PMEO₂MA star polymers at pH 5. Significant hysteresis was observed between the first compression/expansion

cycle of the interface followed by two consecutive compression/expansion cycles that traced the same interface pressure-interfacial area curve, suggesting that some of the PMEO₂MA stars either desorbed from the interface or the interparticle interaction was changed (i.e., star polymer re-orientation) during the first compression. The quasi-static modulus ($d\Pi/d\ln A$) was calculated as a function of interfacial pressure and plotted in **Figure 4.16b**. The monotonic decrease in modulus with increasing interfacial pressure (compression of polymer adsorbed layer) suggests that the PMEO₂MA star polymers were more vulnerable to forced desorption during compression. The fact that PMEO₂MA star polymer exhibited a small but finite modulus during compression shows that they did retain some ability to resist ejection, or else the modulus would have been zero during compression if ejection held the interfacial pressure constant. Another representative interfacial pressure-area behavior is observed at xylene/water interface with 0.001 wt% diblock star polymers at pH 5. **Figure 4.16c** shows that as the interface was compressed, the interfacial area decreased and the interfacial pressure slightly increased, until a critical area was reached, below which the interface pressure increased rapidly. Again, the strongest hysteresis was observed between the first compression/compression cycle, indicating that the timescales for star polymer re-adsorption or relaxation after the first compression is greater than the timescale of the interfacial dilation. As **Figure 4.16d** illustrated, diblock star polymers at the xylene/water interface at pH 5 shows the trend of increasing modulus with increasing interfacial pressure. This suggests that the diblock star polymers were resistant to being ejected from the interface during compression. The increasing modulus has been noted previously for multi-arm PEO star polymers⁴⁶ (**Figure 3.14**) and is attributed to the compressibility of the polymer brushes¹⁵⁰ to the neighboring stars during polymer crowding.

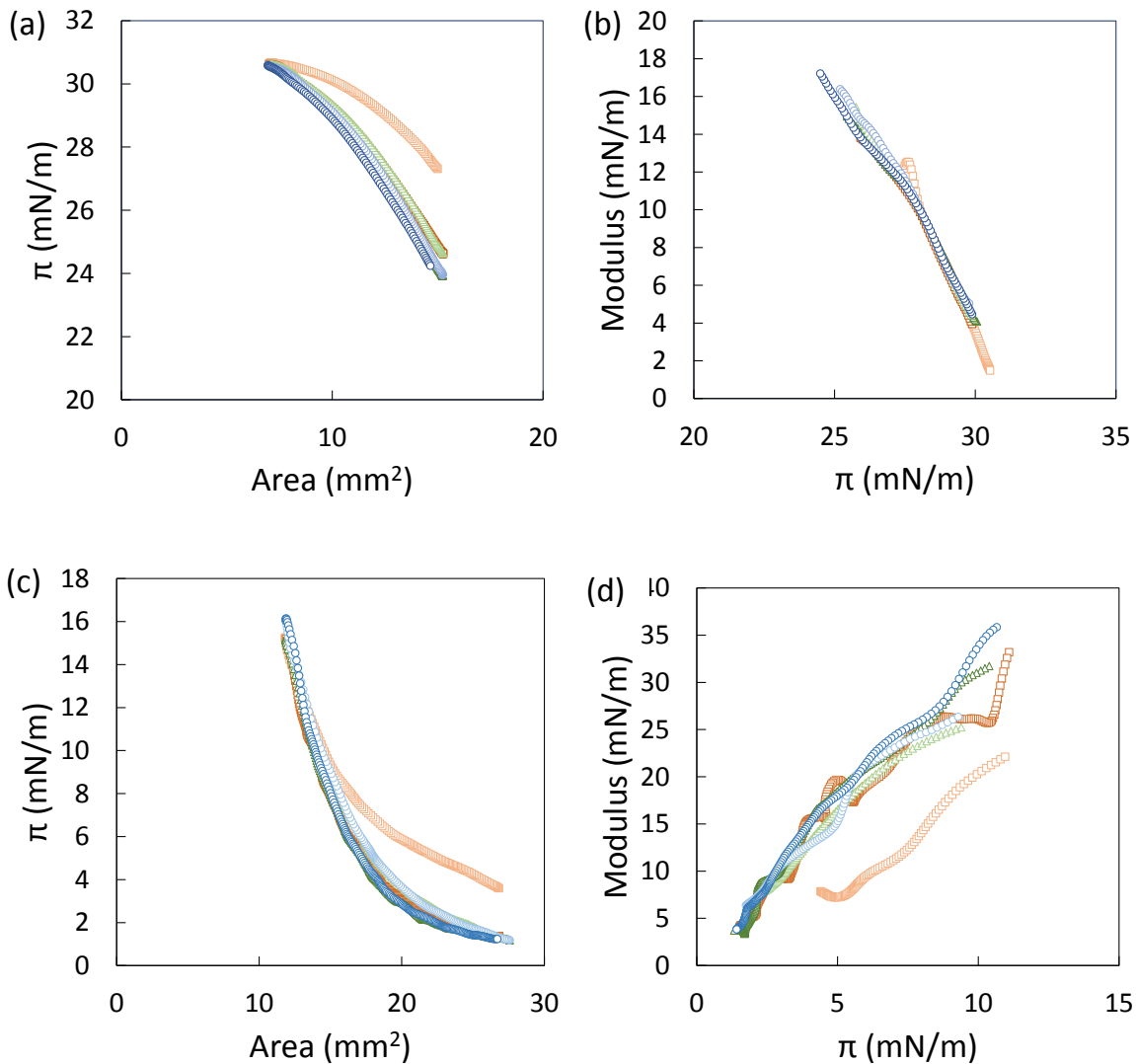


Figure 4.16. Interfacial pressure as a function of interfacial area for three compression/expansion cycles of a xylene/water interface exposed to 0.001 wt% (a) PMEO₂MA star polymers and (c) diblock star polymers with 1 mM NaCl at pH 5. Dependence of calculated quasi-static moduli on interfacial pressure at the xylene/water interface for 0.001 wt% (b) PMEO₂MA star polymers and (d) diblock star polymers with 1 mM NaCl at pH 5. Symbols: (\square) first, (Δ) second and (\circ) third cycles of large amplitude compression/expansion experiments.

The interfacial behavior of all the star polymers at different conditions is plotted in **Table 4.8 – Table 4.11** and the trends of the quasi-static modulus, with increasing interfacial pressure during compression, are summarized in **Table 4.12**. PMEO₂MA star polymers showed a

decreasing modulus with increasing interfacial pressure at the xylene/water and cyclohexane/water interface, indicating that polymers are more vulnerable to desorption during interfacial compression. PDMAEMA and diblock star polymers showed a trend of increasing dilatational modulus with increasing interfacial pressure at pH 5, suggesting that these two star polymers remained pinned at the interface and had a higher resistance to ejection during interfacial compression. In contrast, the modulus decreased with increasing interfacial pressure for both PDMAEMA and diblock star polymers at high pH, indicating star polymers exhibit a transition from irreversible adsorption to partially reversible adsorption at the oil/water interface when pH increases from 5 to 9. It is noted that the quasi-static moduli increase with increasing interfacial pressures and are consistent with dynamic dilatational moduli obtained from small amplitude oscillations at low surface pressures. Moreover, the observed trend of quasi-static moduli is correlated with their emulsifying performance (**Table 4.7**). That is, star polymers that are irreversibly adsorbed at the interface and are able to resist ejection upon forced adsorbed layer compression show better emulsifying efficiency, whereas star polymers that are more vulnerable to forced desorption have less emulsifying efficiency (i.e., they require higher concentrations to stabilize emulsions). This qualitatively distinctive behavior between the star polymers with various structures may be important for distinguishing the emulsifying performance of emulsifiers and related to the emulsion stability. Ostwald ripening and coalescence of emulsion droplets involve decreasing of the interfacial area that leads to compression of the interface. Therefore, ejection of adsorbed emulsifiers under compression might be a mechanism for emulsion failure.

Table 4.8. Interfacial pressure – interfacial area isotherms for various star polymer at the xylene/water interface with 0.001 wt% aqueous concentration

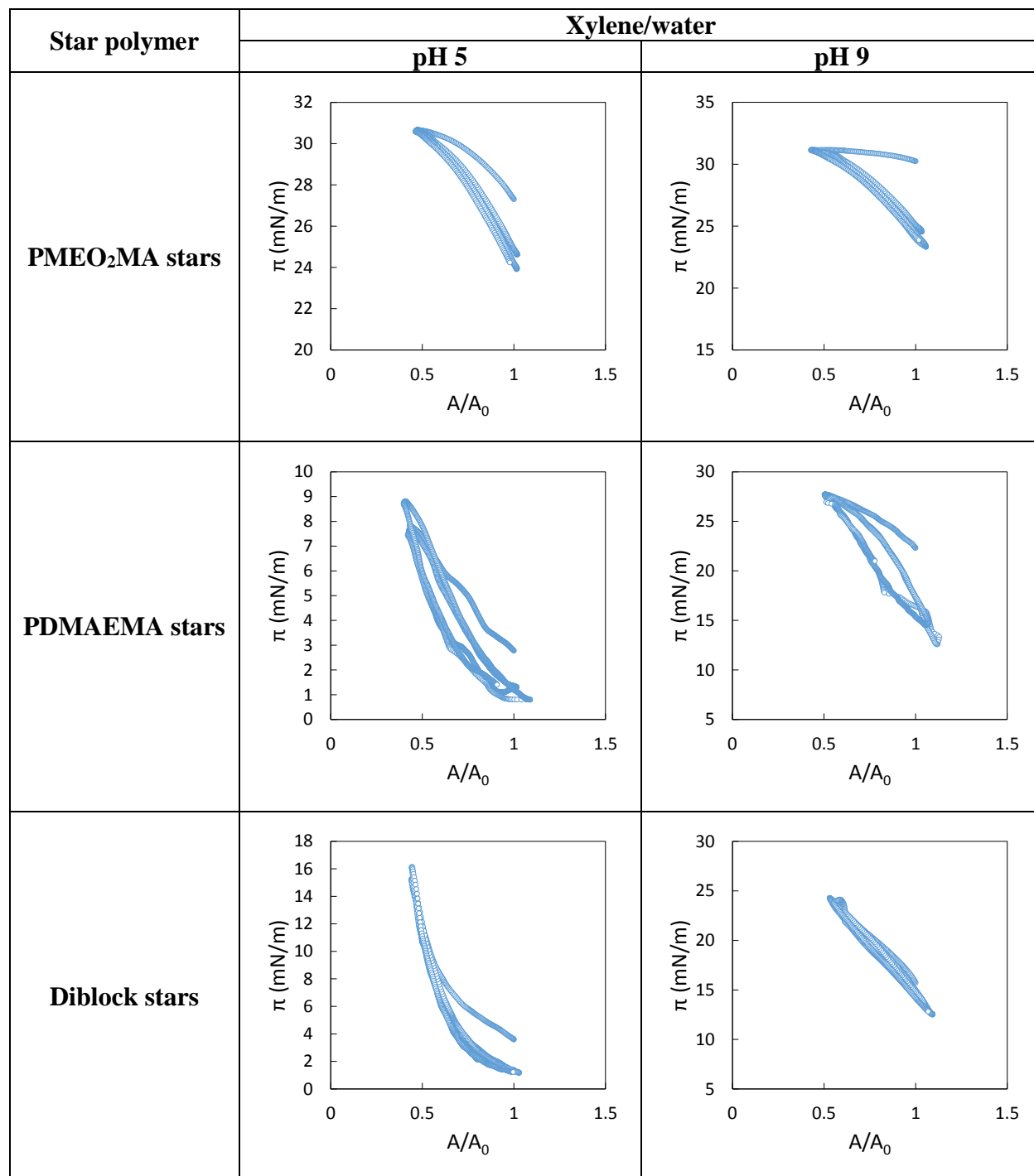


Table 4.9. Interfacial pressure – interfacial area isotherms for various star polymer at the cyclohexane/water interface with 0.001 wt% aqueous concentration

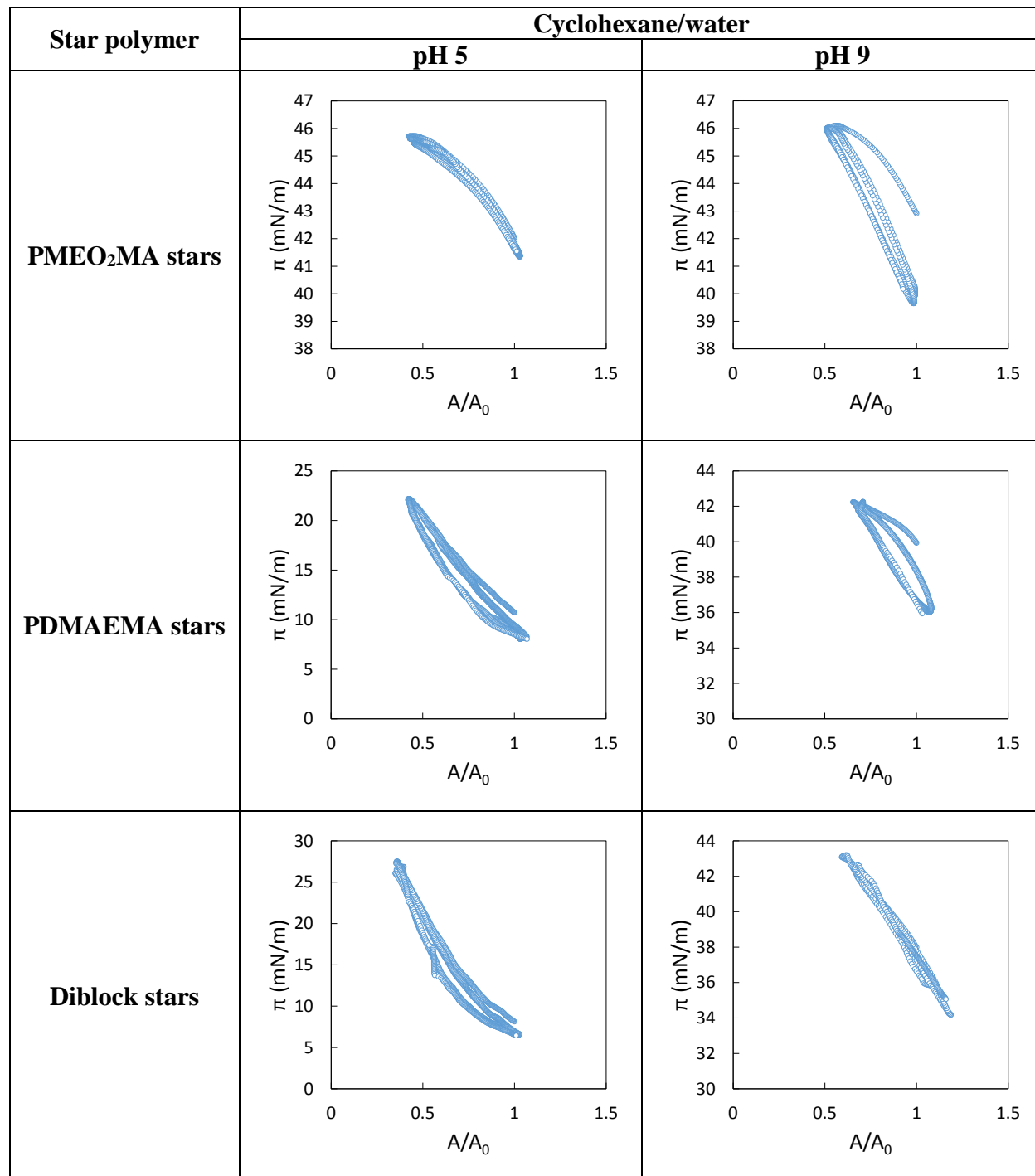


Table 4.10. Dependence of calculated quasi-static moduli on interfacial pressure for 0.001 wt% star polymers with 1 mM NaCl at the xylene/water interface

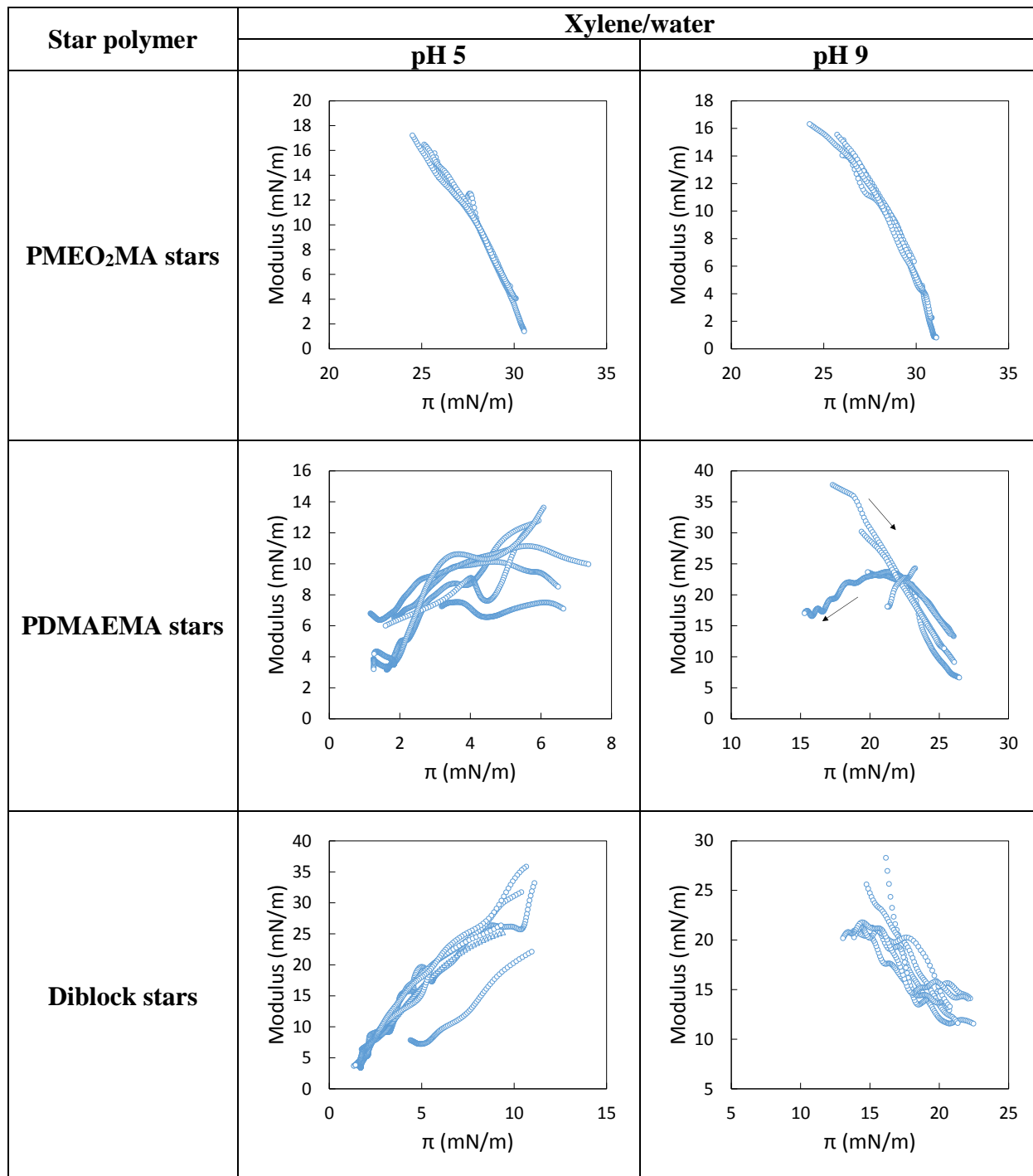


Table 4.11. Dependence of calculated quasi-static moduli on interfacial pressure for 0.001 wt% star polymers with 1 mM NaCl at the cyclohexane/water interface

Star polymer	Cyclohexane/water	
	pH 5	pH 9
PMEO₂MA stars		
PDMAEMA stars		
Diblock stars		

Table 4.12. The trends of quasi-static modulus with increasing interfacial pressure during compression of the adsorbed layer for all three star polymers at xylene/water and cyclohexane/water interface with 0.001 wt% aqueous concentration at pH 5 and pH 9, 1 mM NaCl

System	pH	PMEO ₂ MA stars	PDMAEMA stars	Diblock stars
Xylene/water	5	Decreasing	Increasing	Increasing
	9	Decreasing	Decreasing	Decreasing
Cyclohexane/water	5	Decreasing	Slightly Increasing	Increasing
	9	Decreasing	Decreasing	Decreasing

The large amplitude compression results presented thus far were obtained for star polymer concentration of 0.001 wt%. To study the concentration effect on the structure of the adsorbed layer and the interparticle interactions, we performed large amplitude, slow compression and expansion at oil/water interface with 0.1 wt% star polymer concentrations. From the dynamic interfacial tension reduction results, further increasing the bulk concentration results in faster adsorption of star polymer to the interface, which may change the polymer packing and thus influence the interfacial behavior. The interfacial pressure – interfacial area (Π -A) isotherms and the calculated quasi-static moduli with respect to interfacial pressure are plotted in **Table 4.13** – **Table 4.16** and summarized in **Table 4.17**. Two trends were observed: (1) a decreasing modulus with increasing interfacial pressure, and (2) the interfacial pressure barely changes during interfacial compression and expansion and the modulus remains small (denoted as N/A in **Table 4.17**). At pH 5, the modulus of the PDMAEMA and diblock stars showed a decrease with increasing interfacial pressure at star concentration of 0.1 wt%, whereas the modulus showed an increase with interfacial pressure at a low bulk concentration of 0.001 wt% (**Table 4.12**). This suggests that the increase of the bulk concentration crowded the interface and part of star polymers were ejected from the interface during compression. At pH 9,

all three star polymers produced small moduli and the interfacial pressure only slightly increased during compression. This indicates that the interface was nearly saturated with star polymers. During area perturbation, the degree of interfacial penetration was quickly adjusted by the exchange of adsorbed and dissolved star polymers, and the re-orientation of adsorbed star polymers. This renders the interface with a nearly constant interfacial tension and therefore a small modulus. Combining the results in **Table 4.12** and **Table 4.17**, it was suggested that increasing the bulk concentration leads to a higher amount of star polymer adsorption at the interface, and the high degree of crowding at the interface forced star polymer to desorb from the interface upon area oscillation. Furthermore, a prior investigation has shown that a correlation exists between the foam stability and the “effective” surface elasticity, which takes into account of the actual surface concentration, diffusion coefficient, and the frequency of the external disturbances which initiate the rupture of the foam films.¹⁷⁰ We hypothesize that the similar correlation can be made for emulsion stability. That is, emulsification efficiency and stability is not only related to the ability of emulsifiers to resist the ejection during interfacial compression but also to the packing of emulsifiers at the interface.

Table 4.13. Interfacial pressure – interfacial area isotherms for various star polymer at the xylene/water interface with 0.1 wt% aqueous concentration

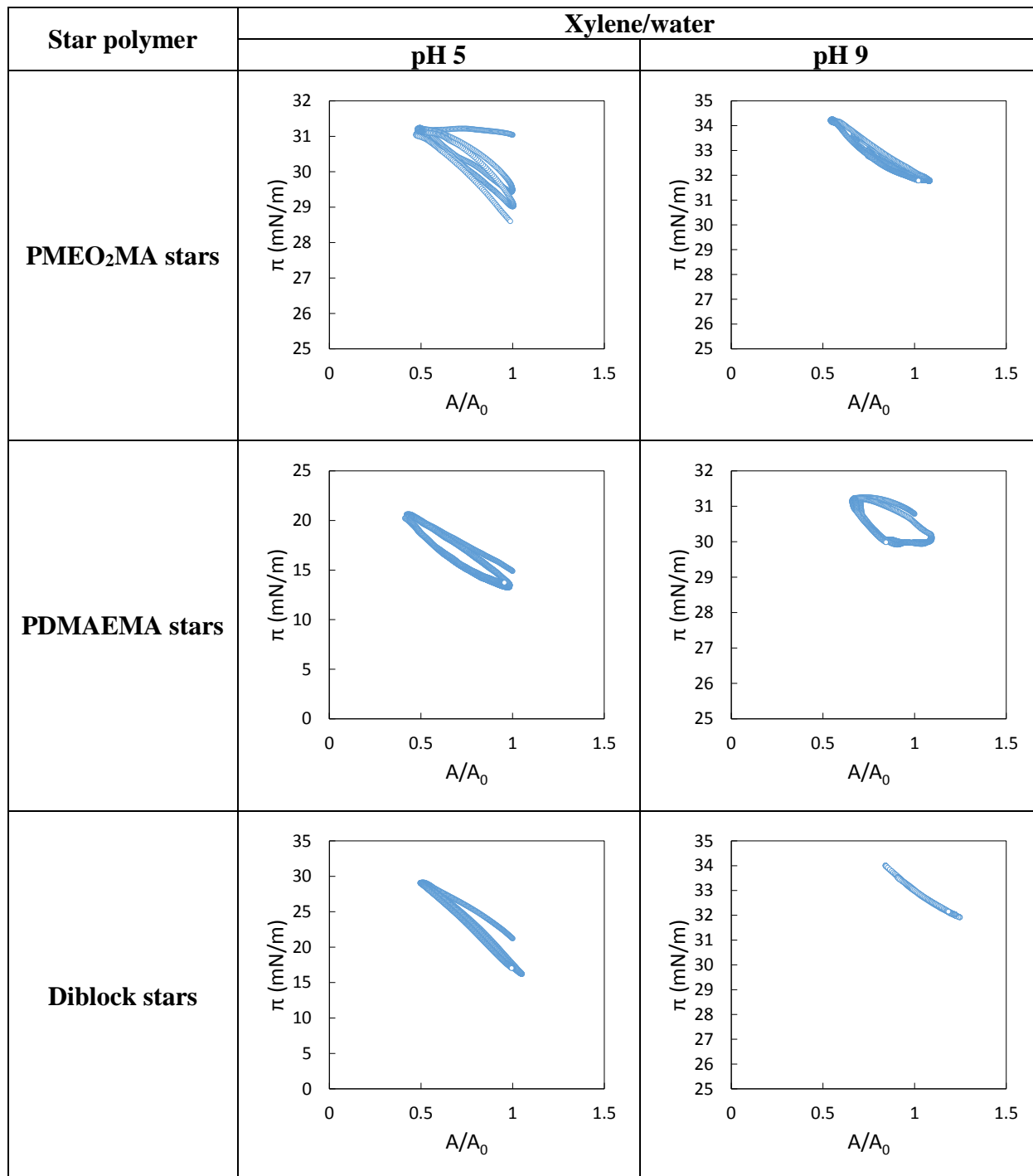


Table 4.14. Interfacial pressure – interfacial area isotherms for various star polymer at the cyclohexane/water interface with 0.1 wt% aqueous concentration

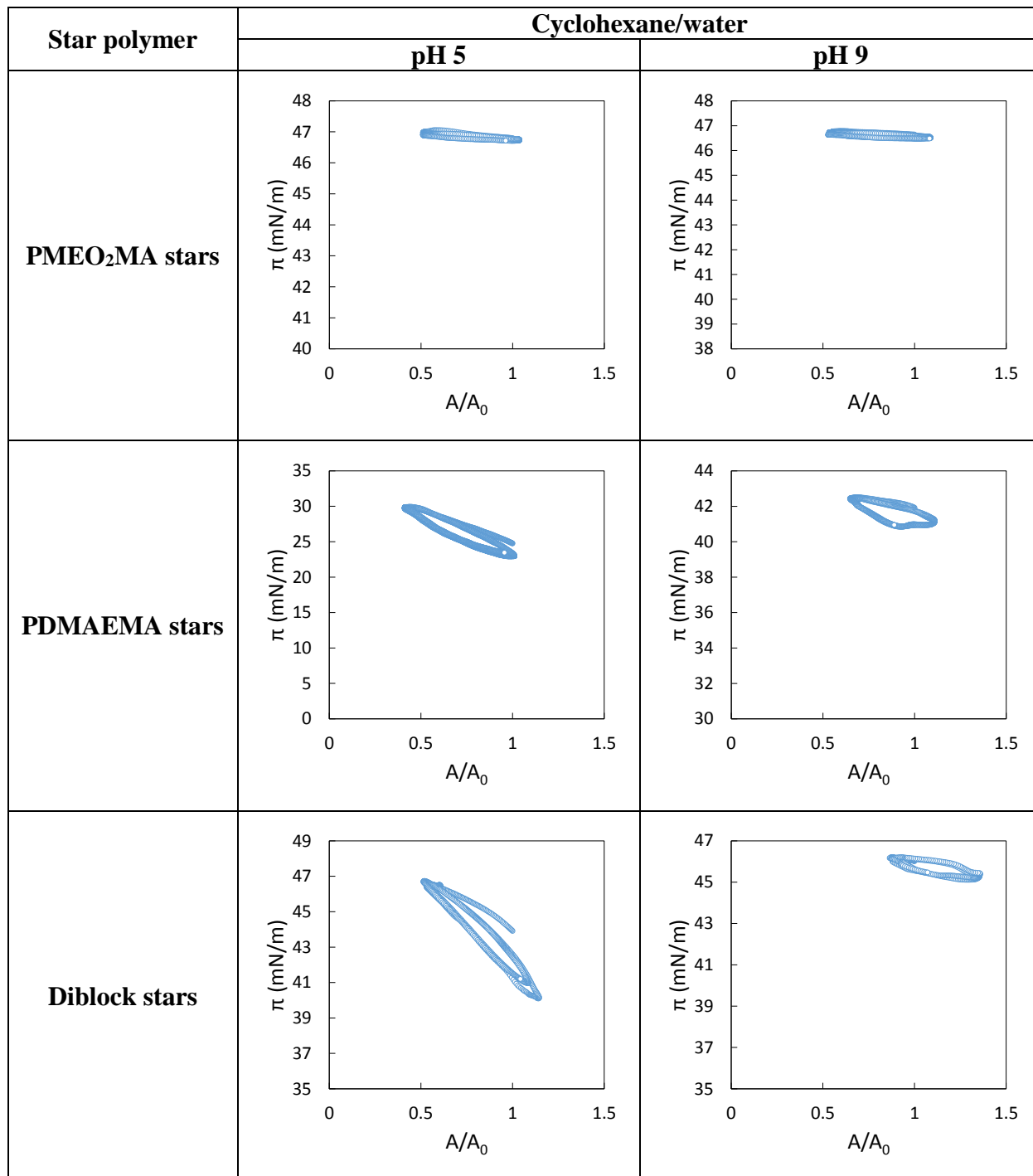


Table 4.15. Dependence of calculated quasi-static moduli on interfacial pressure for 0.1 wt% star polymers with 1 mM NaCl at the xylene/water interface

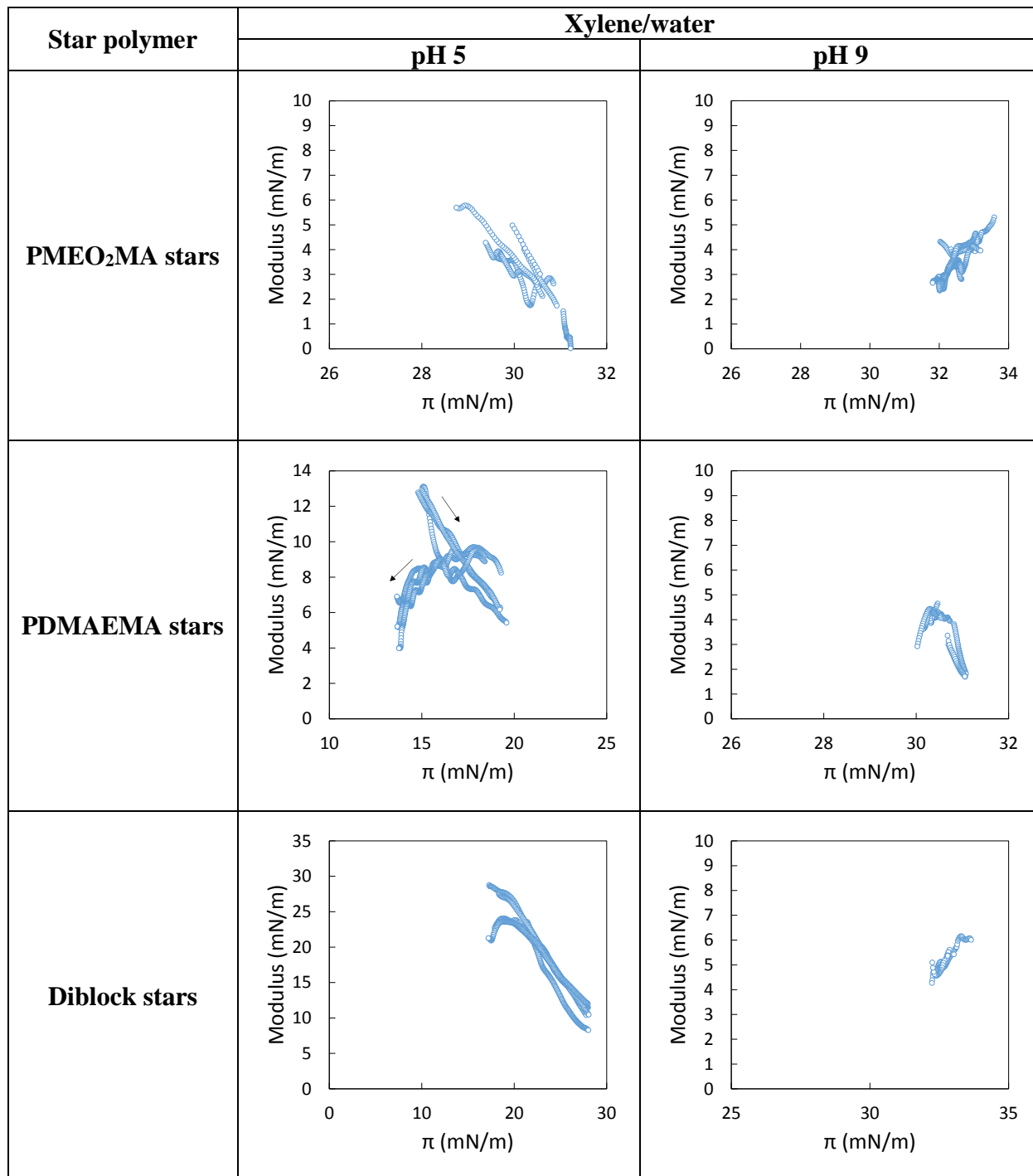


Table 4.16. Dependence of calculated quasi-static moduli on interfacial pressure for 0.1 wt% star polymers with 1 mM NaCl at the cyclohexane/water interface

Star polymer	Cyclohexane/water	
	pH 5	pH 9
PMEO₂MA stars		
PDMAEMA stars		
Diblock stars		

Table 4.17. The trends of quasi-static modulus with increasing interfacial pressure during compression of the adsorbed layer for all three star polymers at xylene/water and cyclohexane/water interface with 0.1 wt% aqueous concentration at pH 5 and pH 9, 1 mM NaCl

System	pH	PMEO ₂ MA stars	PDMAEMA stars	Diblock stars
Xylene/water	5	Decreasing	Decreasing	Decreasing
	9	N/A	N/A	N/A
Cyclohexane/water	5	N/A	Decreasing	Decreasing
	9	N/A	N/A	N/A

4.4.3.3 Dilatational modulus versus interfacial pressure

It could be supposed the interfacial pressure and dilatational elasticity depends on the history of the formation of adsorbed layers. If the characteristic timescale for adsorbed layer to relax and establish a local equilibrium is comparable to the timescale of the interfacial perturbation, all the interfacial properties can be well described by the dependence on the interfacial pressure. The mechanics of a star polymer adsorbed layer at shorter time were probed using pendant drop tensiometry through applying small amplitude oscillations to the drop as soon as it was generated, and the corresponding dilatational modulus was measured over time before the relaxation of the adsorbed layer. Once the interfacial tension reached an “equilibrium” value during oscillation, the drop was slightly compressed to increase the interfacial pressure and the corresponding dilatational modulus at smaller volume was measured through small amplitude oscillations.

Figure 4.17 shows the measured dynamic dilatational modulus as a function of interfacial pressure at the xylene/water and cyclohexane/water interface exposed to 0.001 wt% PMEO₂MA star polymer aqueous concentration during adsorption. At very short times when the interfacial pressure was less than 10 mN/m, the dilatational modulus (ϵ) at xylene/water interface

(Figure 4.17a) steadily increased with increasing interfacial pressure (Π) and followed the $\varepsilon = 2$ Π relation, which has also been observed previously.^{175,176} The modulus kept increasing as more star polymers adsorbed to the interface and achieved a maximum of 26 mN/m at $\pi \sim 17$ mN/m and then decreased with further increases of interfacial pressure, which is attributed to the fast diffusional relaxation.¹⁷⁵ The dependence of dilatational modulus on interfacial pressure at cyclohexane/water showed a similar trend to the xylene/water interface. The modulus increased as more PMEO₂MA star polymers adsorbed at the interface until a critical interfacial pressure was reached, above which the modulus decreased with increasing interfacial pressure. It is worth mentioning that the interface was primarily elastic and the loss modulus (E'') was insignificant.

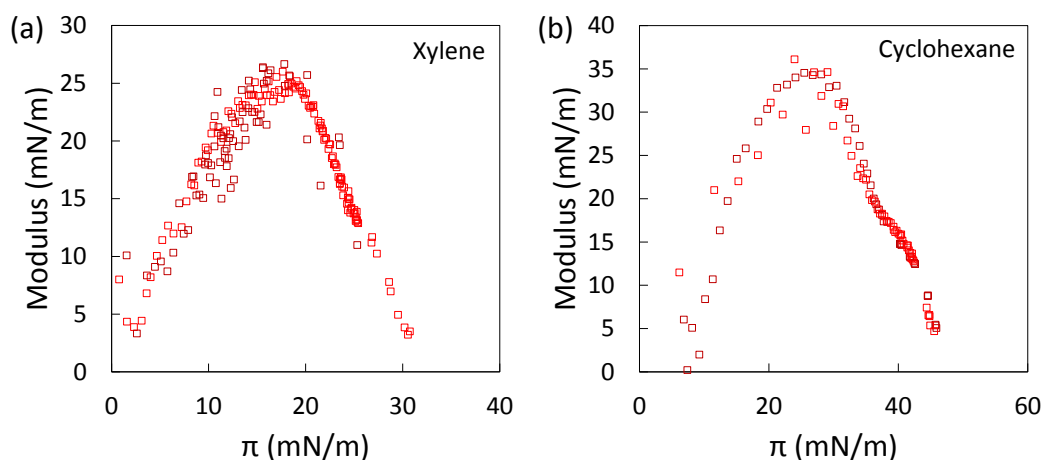


Figure 4.17. Dynamic dilatational modulus as a function of interfacial pressure at the (a) xylene/water and (b) cyclohexane/water interface exposed to 0.001 wt% PMEO₂MA star polymer aqueous concentration. Experiments were repeated at least two times and the results were consistent.

Figure 4.18 shows the measured dynamic dilatational modulus as a function of interfacial pressure at the xylene/water and cyclohexane/water interface during PDMAEMA star polymer adsorption. At pH 5, the modulus increased with increasing interfacial pressure and

achieved a modulus ~ 20 mN/m at interfacial pressure $\Pi = 20$ mN/m for 0.001 wt% PDMAEMA star polymer concentration (square symbols) at both xylene/water and cyclohexane/water interface. Further compression of the interface only slightly increased the interfacial pressure and dilatational modulus. The concentration of PDMAEMA star polymers was then increased to 0.1 wt% (triangle symbols) to probe the concentration effects on the interfacial behavior. At the xylene/water interface, the moduli measured at 0.1 wt% and 0.001 wt% star polymers were found to approximately coincide with a single curve. Furthermore, the fact that we did not observe a modulus that reached a maximum and decreased with increasing interfacial pressure at the xylene/water interface is possibly attributed to the low adsorption of PDMAEMA star polymers to the interface at low pH due to their strong electrostatic repulsions. The modulus obtained at cyclohexane/water interface with 0.1 wt% PDMAEMA star polymer at pH 5 shows a different behavior from the low concentration. The curves overlapped at low interfacial pressures but diverged into separate branches at high interfacial pressures. The modulus of 0.1 wt% PDMAEMA star polymers (triangle symbols) achieved ~ 40 mN/m at interfacial pressure of 38 mN/m. In contrast, the modulus of PDMAEMA star polymers at high pH show a qualitatively similar behavior as observed with PMEO₂MA star polymers (**Figure 4.17**). The parabolic shape of the modulus with respect to interfacial pressure suggests that an increase in surface concentration (and therefore the interfacial tension) has two different effects on dilatational modulus. First, an increase in surface concentration leads to a higher interfacial gradient corresponding to the same degree of interfacial deformation, resulting in higher dilatational modulus. Second, as more star polymers adsorbed to the interface, further increases in the surface concentration enhanced the polymer exchange between bulk and interface. The layer of adsorbed star polymers becomes more soluble at higher interfacial pressures and faster diffusion

relaxation leads to a decrease in dilatational modulus. The different interfacial behavior with increasing pH is also consistent with a greater extent of PDMAEMA star polymer adsorption due to the lack of electrostatic repulsions.

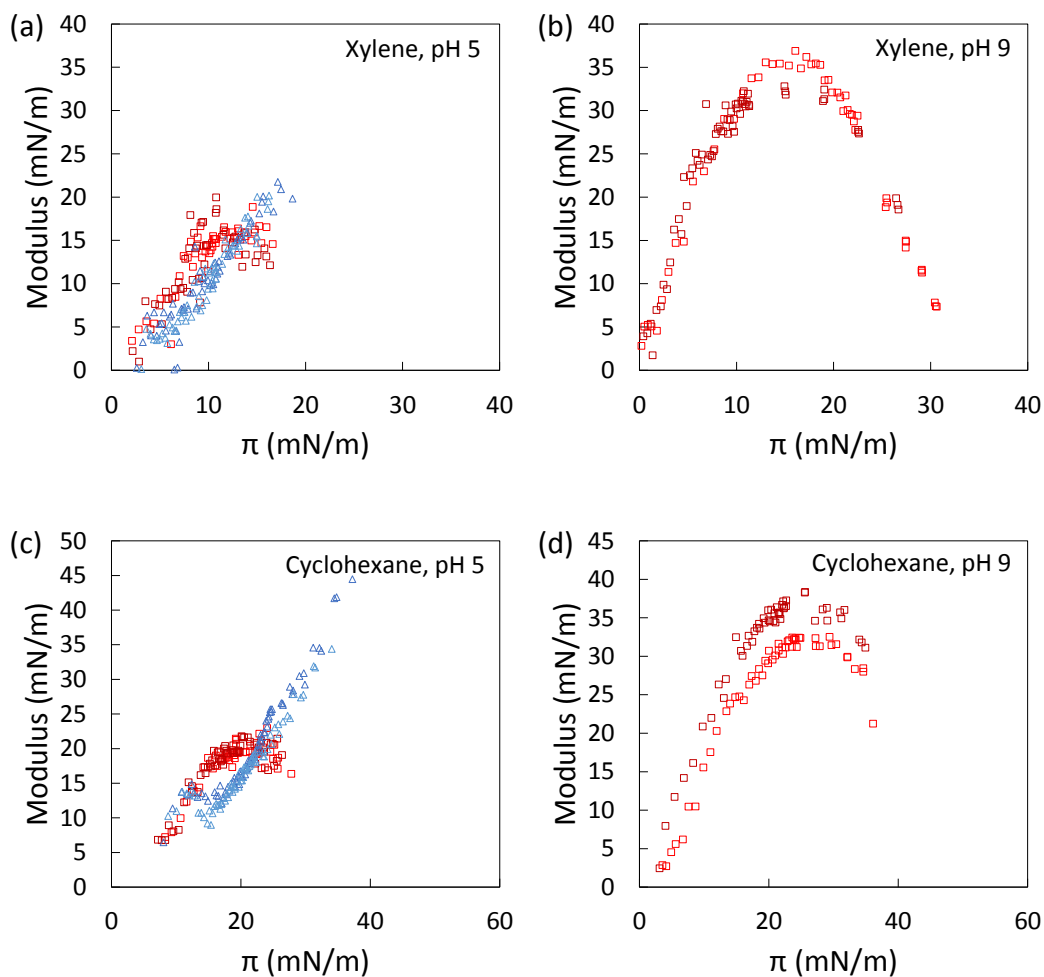


Figure 4.18. Dynamic dilatational modulus as a function of interfacial of (\square) 0.001 wt% and (Δ) 0.1 wt% PDMAEMA star polymer adsorbed to the xylene/water interface at (a) pH 5 and (b) pH 9, and to the cyclohexane/water interface at (c) pH 5 and (d) pH 9.

Figure 4.19 shows the measured dynamic dilatational modulus as a function of interfacial pressure at the xylene/water and cyclohexane/water interface during diblock star polymer adsorption. Similar trends were observed for both xylene/water and cyclohexane/water

interfaces. Increase the bulk star polymer concentration from 0.01 wt% (diamond symbols) to 0.1 wt% (triangle symbols) at pH 5 further increased the dilatational modulus at low and intermediate interfacial pressures. The modulus reached a maximum of 24 mN/m at xylene/water and 29 mN/m at cyclohexane/water interface and then decreased with increasing interfacial pressure. This suggests that interfacial properties depend on the formation history of the diblock star polymer adsorbed layer and cannot be solely described by interfacial pressure. At higher bulk concentrations, the faster diffusion of star polymers from the bulk to the interface can result in different packing density at the interface, which leads to different interparticle interactions and thus a different modulus. This is evident in **Figure 4.19**, where at pH 5, a higher modulus was obtained at a higher concentration at a fixed interfacial pressure. At pH 9, the modulus increased with increasing interfacial pressure at 0.001 wt% diblock star polymers (square symbols). Further compression of the interface only slightly increased the interfacial pressure and dilatational modulus. However, the modulus decreased with increasing interfacial pressure at 0.01 wt% diblock star polymers (diamond symbols). This is again consistent with a higher surface concentration of star polymers which allows fast interface relaxation during area perturbation.

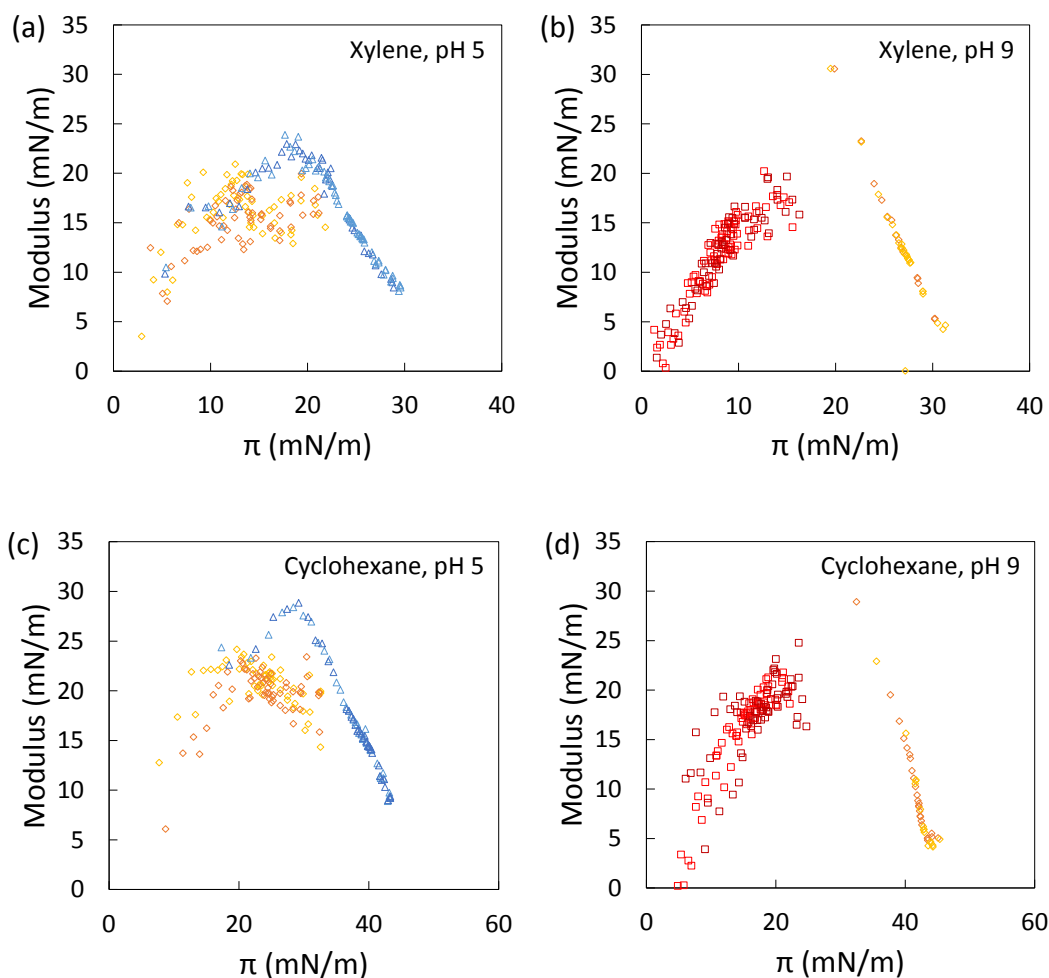


Figure 4.19. Dynamic dilatational modulus as a function of interfacial of (\square) 0.001 wt%, (\diamond) 0.01 wt% and (\triangle) 0.1 wt% diblock star polymer adsorbed to the xylene/water interface at (a) pH 5 and (b) pH 9, to the cyclohexane/water interface at (c) pH 5 and (d) pH 9.

4.4.3.4 Comparison of dilatational modulus obtained by different methods

To probe the effect of sample history on the interfacial behavior, the moduli obtained through small amplitude oscillation and large amplitude, slow compression and expansion for various bulk concentrations were compared. **Figure 4.20** illustrates the dilatational modulus obtained from different methods as a function of interfacial pressure for PMEO₂MA star polymers at xylene/water and cyclohexane/water interfaces. Interestingly, all measurements fell

onto a parabolic master curve for both systems, indicating that the interface properties of the adsorbed layer are mainly described by the interfacial pressures. If there is no exchange between adsorbed and bulk species or, moreover, the interfacial tension adjusts instantaneously to the equilibrium value within the timescale of perturbation, the interface is purely elastic and the dilatational modulus can be determined by the dependence of interfacial pressure.¹⁷⁷ This dependence of modulus on the interfacial pressure is possibly attributed to the high exchange of PMEO₂MA star polymers between interface and bulk solution, and fast configuration rearrangement of adsorbed star polymers to an equilibrium state. The observation that dilatational modulus depends only on the interfacial pressure regardless of the adsorption times or bulk concentrations has been reported previously with synthetic surfactants adsorbed at air/water interface.¹⁷⁸

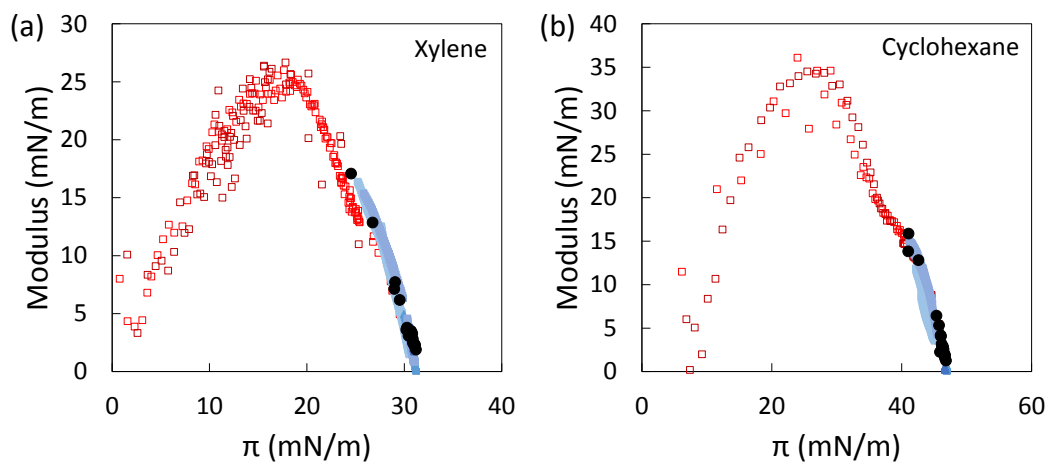


Figure 4.20. Dilatational modulus as a function of interfacial pressure for PMEO₂MA star polymers at the (a) xylene/water and (b) cyclohexane/water interface obtained from (●) small amplitude oscillation after interface reached equilibrium, (□) large amplitude compression/expansion and (■, ▲) small amplitude oscillation before the interface reached equilibrium.

The dilatational moduli obtained from different methods for PDMAEMA and diblock star polymers at different conditions as a function of interfacial pressure are plotted in **Figure 4.21** and **Figure 4.22**, respectively. Different from the observations with PMEO₂MA star polymers, the measured dilatational modulus depends on the route to form the adsorbed layer. The modulus obtained from different methods does not converge to a single curve and the discrepancy is more pronounced at low pH when the star polymers are positively charged. This behavior indicates that the modulus is not solely described by the interfacial pressure but highly depends on the structure of the adsorbed layer, which is affected by the interactions between polymers, bulk concentrations, and the relaxation of polymer in the interfacial layer. Studies have shown that increasing the bulk concentration decreased the dilatational modulus at higher interfacial tension but had no effect at lower interfacial tension. This was attributed to the faster diffusion relaxation of polymer at higher bulk concentrations.¹⁷⁸ We hypothesize that the scattered behavior measured at pH 5 for PDMAEMA and diblock star polymers is due to the highly charged nature of the polymer. The formation of the adsorbed layer that experiences electrostatic repulsions is sensitive to the adsorption time and the bulk concentration. The interactions and relaxation process of polymer can also be affected by the way the interface is perturbed, which leads to a complex interfacial behavior. At pH 9 when the polymer arms are collapsed, the dilatational moduli obtained from different methods are less scattered and almost coincide at cyclohexane/water interface (**Figure 4.21d** and **Figure 4.22d**). This could be attributed to the lack of electrostatic repulsion between adsorbed and bulk star polymers, which enhances the diffusion exchange upon interface perturbation and enables interfacial tension to quickly adjust to equilibrium value.

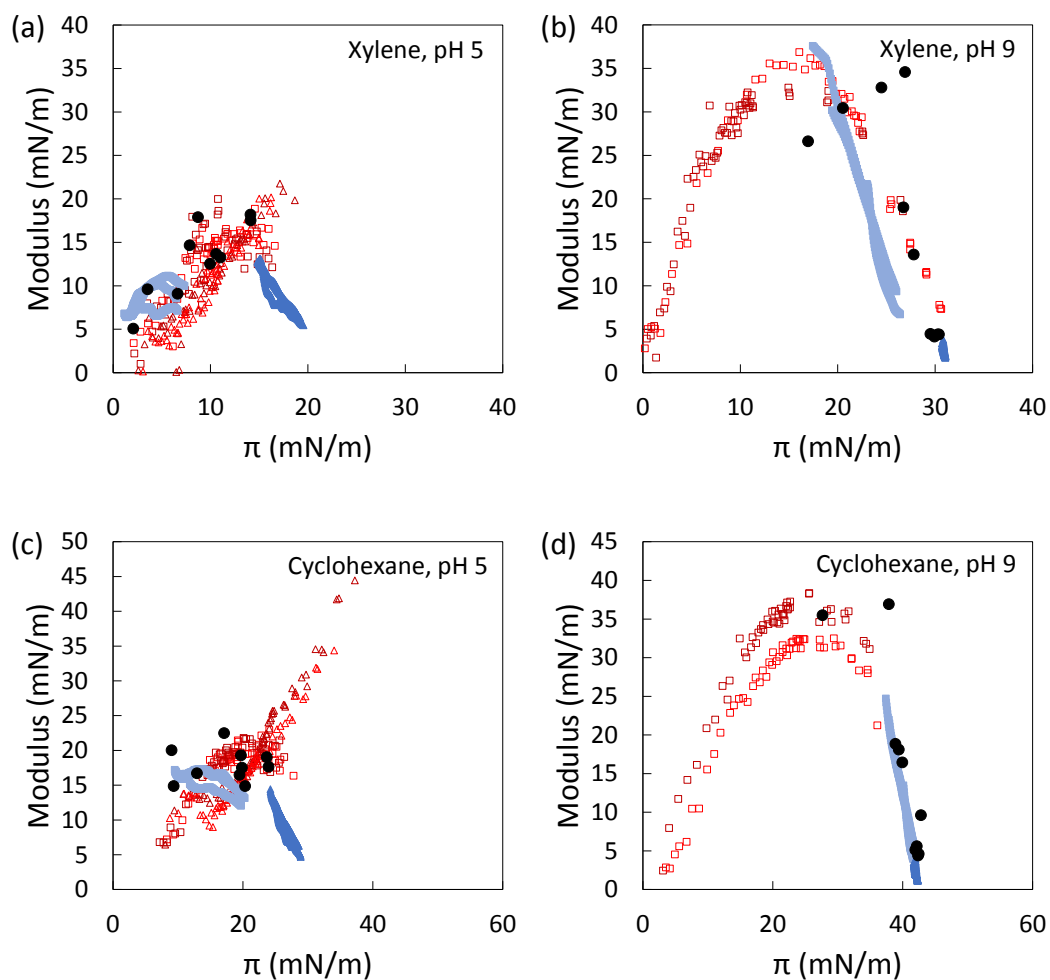


Figure 4.21. Dilatational modulus as a function of interfacial pressure obtained from (●) small amplitude oscillation after interface reached equilibrium, (□, Δ) large amplitude compression/expansion and (■, ▲) small amplitude oscillation before interface reached equilibrium for PDMAEMA star polymers adsorbed to the xylene/water interface at (a) pH 5 and (b) pH 9, and cyclohexane/water interface at (c) pH 5 and (d) pH 9.

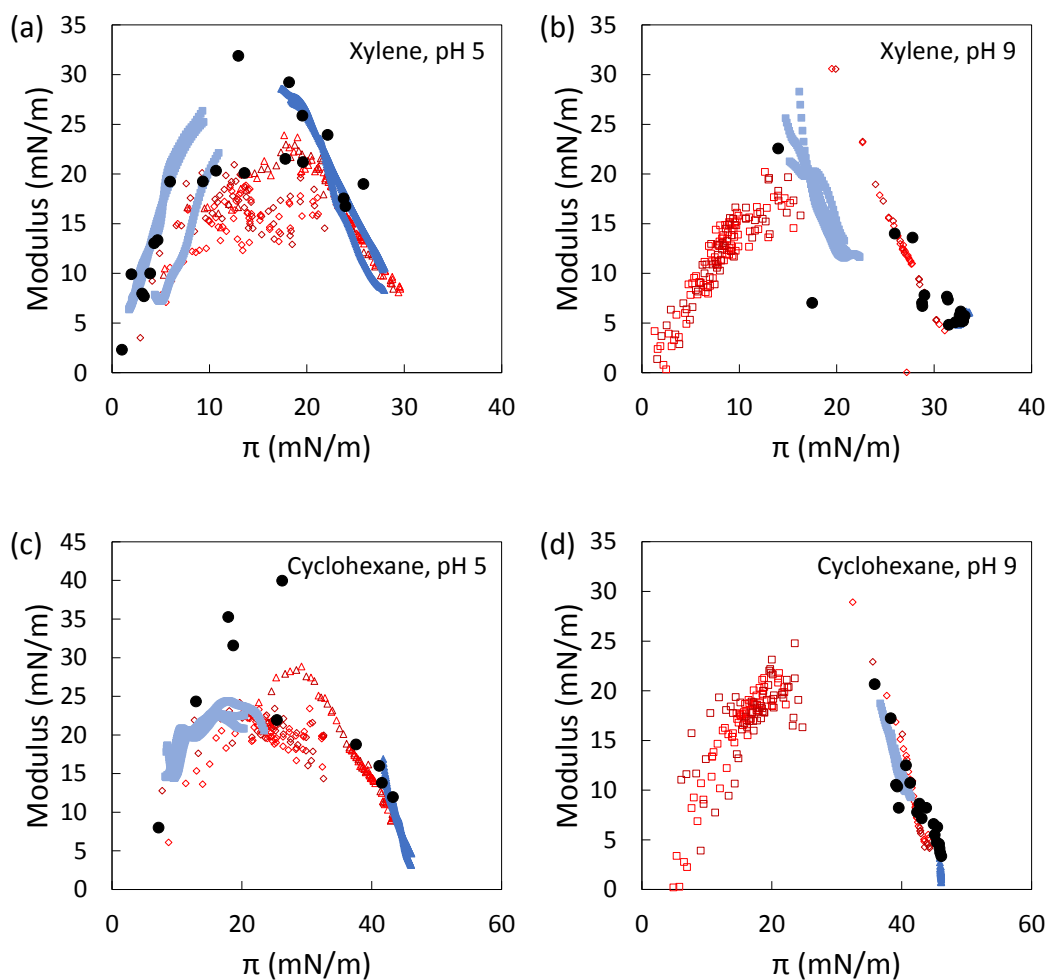


Figure 4.22. Dilatational modulus as a function of interfacial pressure obtained from (●) small amplitude oscillation after interface reached equilibrium, (□, Δ) large amplitude compression/expansion and (■, ▲) small amplitude oscillation before interface reached equilibrium for diblock star polymers adsorbed to the xylene/water interface at (a) pH 5 and (b) pH 9, and cyclohexane/water interface at (c) pH 5 and (d) pH 9.

Our results indicates that the dilatational modulus for star polymers is complex and sensitive to the structure of the adsorbed layer and the interactions of the star polymers, which also depends on the interface aging, bulk concentration and polymer relaxation. We have shown that diblock star polymers are the most efficient emulsifiers among the three β -cyclodextrin core star polymers studied, and PDMAEMA and diblock star polymers can stabilize emulsions at lower bulk concentrations at pH 5 than at pH 9 (**Table 4.7**). Although the ability of star polymers

to resist ejection from the interface during forced interfacial compression could be important, no obvious trend was observed in the dilatational modulus with the emulsification performance of star polymers. This suggests that the dynamic dilatational modulus may not solely be a predictor for the emulsification performance. The mechanisms governing the emulsifying efficiency and stability are still not clearly understood, and further research is needed in this area.

4.5 Conclusions

Several fundamental interfacial activity characteristics have been investigated for three β -cyclodextrin core star polymers with the same architecture but with polymer arms of different chemical compositions. Non-ionic PMEO₂MA star polymers have an average size of 7 nm, whereas PDMAEMA and diblock star polymers demonstrate size and charge that are responsive to pH change. Interfacial tensiometry, dynamic dilatational elasticity and ellipsometry measurements indicate that adsorption characteristics of star polymers are affected by the degree of ionization, the chemical position of the polymer chains, and the interactions between star polymers. Similar differences in the interfacial behavior are observed at the air/water interface, the xylene/water interface that represents a good solvent/good solvent interface, and the cyclohexane/water interface that represents a poor solvent/good solvent interface.

The high affinity of PMEO₂MA star polymers for the interface leads to significantly larger interfacial pressures and greater extent of adsorption than PDMAEMA and diblock star polymers. Qualitative differences in electrostatic adsorption behavior exist for PDMAEMA and diblock star polymers at different pHs. Whereas adsorption of PDMAEMA and diblock star polymers is inhibited at low pH when the star polymers are positively charged and experience strong electrostatic repulsion, a significant amount of PDMAEMA and diblock star polymers can

adsorb at high pH due to the collapse of polymers arms which allows more polymer segment penetration. The adsorption and surface coverage of star polymers adsorbed at air/water interface are quantitatively characterized by ellipsometry. More extensive adsorption of PDMAEMA and diblock star polymers at high pH rather than at low pH suggests that the lack of lateral electrostatic repulsion favors denser packing on the interface.

Dynamic dilatational modulus is affected by the concentration, the exchange dynamic between adsorbed and bulk species, and the interactions between star polymers. At lower concentrations, the dilatational modulus is dominated by the intermolecular interactions at the interface, which results in the increasing dilatational modulus with increasing bulk concentration. At higher concentrations, the dilatational modulus is controlled by diffusion, which leads to the decrease in dilatational modulus with increasing bulk concentration. The measured dilatational modulus ran through a maximum with increasing interfacial pressure which strongly support the mechanism described above. The dilatational modulus obtained from large amplitude interface compression and expansion probed the vulnerability of star polymers to ejection during compression. The results suggest that at low bulk concentration, PDMAEMA and diblock star polymers are able to resist forced desorption at low pH more than at high pH, whereas PMEO₂MA star polymers desorb from the oil/water interface upon compression. At high bulk concentrations, star polymers are ejected from the interface upon area perturbation induced by polymer crowding at the interface. Furthermore, the mechanical properties of interfaces depend on the formation and deformation history of the star polymer adsorbed layer, and thus cannot be independently described by interfacial pressures.

PMEO₂MA star polymers were more effective at stabilizing foams compared to the other two star polymers at various conditions. Diblock star polymers were shown to be the most efficient emulsifiers at pH 5; they are able to stabilize emulsions at a concentration of 0.005 wt%. We have not observed a linear correlation between interfacial characteristics with the foaming and emulsifying efficiency of star polymers. Our results suggest that the stability of an emulsion is sensitive to the trend of the dilatational modulus with increasing interfacial pressures. However, dynamic dilatational modulus may not solely be a predictor for the foaming and emulsifying performance. Further research is needed to clarify the mechanism of emulsification (and foaming).

5 Nanoemulsion formation by spontaneous emulsification with star polymers

5.1 Introduction

The emulsifier plays an important part in the formation and stability of a nanoemulsion. Previous studies have shown that the properties of nanoemulsions produced by spontaneous emulsification depends on the types of emulsifiers.^{37,179,180} The choice of emulsifiers is often limited by commercial availability. Using synthetic polymers as emulsifiers can be advantageous and has more flexibility with size, responsiveness to stimuli and topology. In addition, the viscoelastic properties of nanoemulsions can be varied by changing the composition and structure of the polymeric surfactants,¹⁸¹ which could be used to engineer new applications.

Stable xylene-in-water nanoemulsions were produced by spontaneous emulsification with the presence of 14-arm poly(di(ethylene glycol) methyl ether methacrylate) (PMEO₂MA) star polymers in water. These nanoemulsions are extremely stable against flocculation, creaming and Ostwald ripening. The enhanced long term stability and high optical transparency of nanoemulsions, consisting of droplets with size on the order of 100 nm, are beneficial for applications such as drug delivery, food and cosmetic industries. Therefore, understanding the factors that determine the droplet size when well-defined emulsion properties are needed is desired. This chapter investigates the effect of temperature and composition on the size of nanoemulsion droplets. Cooling increases the nanoemulsion droplet size whereas heating has no effect on the droplet size. Dynamic light scattering measurements indicate that increasing the water volume fraction and the polymer concentration increases the droplet size. PMEO₂MA star polymers are also able to stabilize macroemulsions produced by high shear homogenization. These macroemulsions are allowed to break, yielding a new emulsion phase that is similar to

nanoemulsion produced by quiescent emulsification. Spontaneously formed nanoemulsions are found to be path dependent that the initial location of the star polymers is important.

Spontaneous emulsification happens only when PMEO₂MA are initially dispersed in water, not when dispersed in xylene.

5.2 Emulsion preparation methods

5.2.1 Nanoemulsions prepared by quiescent conditions

Nanoemulsions were prepared in 2.4 cm diameter scintillation glass vials. Xylene was gently poured onto the PMEO₂MA star polymer solutions and the Triton X-100 solutions with minimal disturbance. Unless otherwise specified, PMEO₂MA star polymers and Triton X-100 were dispersed in water. Samples were then left under quiescent conditions for visual inspections. Spontaneous emulsification of xylene-in-water droplets was observed with a translucent region diffusing from the xylene/water interface towards the bottom of the glass vial, leading to a stable nanoemulsion as shown in **Figure 5.1**. The concentration of Triton X-100 was 0.1 wt% and the concentration of PMEO₂MA star polymers was varied from 0.01 to 0.01 wt% with the water volume fraction from 0.1 to 0.9. Note the concentrations described in this work only consider the concentration of the water phase unless stated otherwise. The nanoemulsion droplet size distribution was measured by dynamic light scattering with a Zetasizer Nano ZSP (Malvern Instruments). Light scattering was monitored at an angle of 173° using a laser beam with a wavelength at 633 nm.

The samples were subjected to temperature excursions after the nanoemulsions were spontaneously formed. One set of nanoemulsion samples were first cooled to 4 °C by placing them in a temperature-controlled room for a long period of time to ensure the samples had

reached stable states. The samples were then taken out of the cold room and stored at room temperature. Another set of nanoemulsion samples were first heated to 45 °C in an oven and brought back to room temperature. The effect of cooling, heating and returning to room temperature on nanoemulsion stability was investigated by measuring the variation of droplet size distribution with time of storage at different temperatures. All size measurements were done in duplicates and the average results were reported.

5.2.2 Macroemulsions prepared by high shear homogenization

Macroemulsions with varied water volume fractions were made using a sawtooth homogenizer (Biospec Tissue Tearor 985370-395) at 1.65 Watts for one minute. Unless otherwise specified, polymers were dispersed in water before emulsification. These macroemulsions were then left to rest and allowed micron-sized emulsion droplets to break at room temperature with minimal perturbation. Breakage did not produce macroscopic phase separation into two bulk phases; instead it yielded a new emulsion phase that was translucent. Droplet size distributions were measured using dynamic light scattering for the new emulsion phase after macroemulsion breakage.

5.3 PMEO₂MA star-stabilized nanoemulsions

Stable xylene-in-water nanoemulsions were formed *via* spontaneous emulsification when PMEO₂MA star polymers were initially dispersed in water and brought into contact with pure xylene with minimal disturbance, as shown in **Figure 5.1**. The aqueous phase (bottom phase) became translucent after 3 hours, whereas initially both phases were transparent. The first sign of spontaneous emulsification appeared about an hour after contact with the xylene phase in the form of a translucent region with a boundary at a distance of 1 to 2 mm below the interface. The

boundary became more evident and a milky white layer of emulsion began to expand downwards until it reached the bottom of the aqueous phase. The emulsification continued for at least one or two days as the turbidity of the bottom phase increased until the emulsion phase was opaque. The opaque production observed here is not the result of polymer phase separation. PMEO₂MA star dispersions in water that were not in contact with xylene remained transparent, and pre-saturation of water with xylene did not lead to a PMEO₂MA star dispersion becoming opaque. In addition, the bottom phase turned back to transparent if the top phase (xylene phase) completely evaporated. Spontaneous water-in-xylene emulsification when multi-arm poly(ethylene oxide) (PEO) star polymers are initially dispersed in xylene was previously reported.⁴⁶ Unlike the unstable emulsion that the PEO star polymer produced,⁴⁶ the PMEO₂MA star-stabilized xylene-in-water emulsions were highly stable for over 10 months. We note that these emulsions were still stable at the time of this writing. PMEO₂MA star polymers was varied from 0.01 to 0.1 wt% and the turbidity is more pronounced for higher star concentration. The water volume fraction was varied from 0.1 to 0.9 and no phase inversion composition has yet been identified.

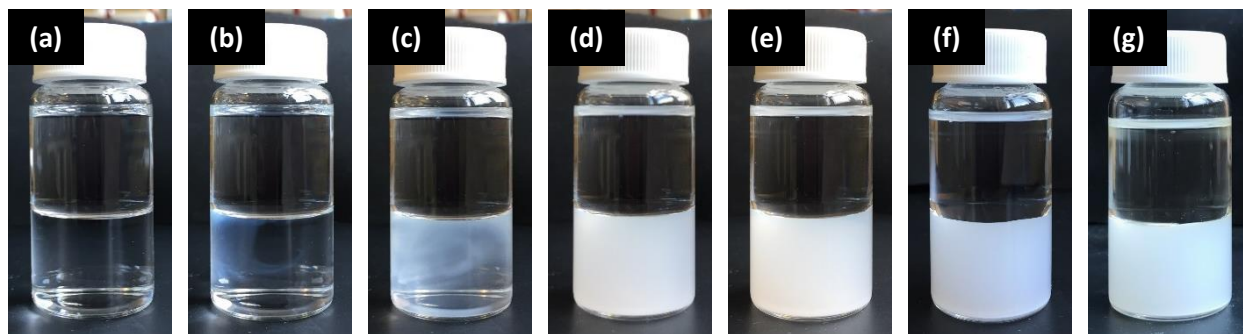


Figure 5.1. Stable xylene-in-water nanoemulsion were spontaneously produced with 0.1 wt% PMEO₂MA star polymers initially dispersed in aqueous phase (bottom phase) at time = (a) initial, (b) 1 hour, (c) 3 hours, (d) 24 hours, (e) 2 days, (f) 7 days and (g) 219 days after xylene and aqueous phase were brought into contact and left under quiescent conditions.

The presence of PMEO₂MA star polymers at xylene/water interface is critical in spontaneous emulsification. The polymer adsorption reduces the interfacial tension and causes interfacial fluctuations. The interfacial tension of xylene and 0.1 wt% PMEO₂MA star polymers solution reached 6 mN/m within 15 mins (**Figure 5.2**). Local interfacial tension gradient drives a Marangoni flow that draws the xylene downward into budding droplets, which are stabilized by PMEO₂MA star polymers. **Figure 5.3** shows the droplet size distribution of the emulsion phase produced under quiescent method at room temperature. The intensity mean droplet size was bimodal with two peaks around 36 ± 2.8 nm (7.5%) and 233 ± 14 nm (92.5%) at 8 days after sample preparation. At 308 days, the mean droplet size increased to a single peak at 350 ± 26 nm. Because of the small size of nanoemulsions, Ostwald ripening is the main destabilization mechanism.^{44,182} As shown in **Figure 5.3**, the disappearance of the smaller droplet size and the slightly increase of the larger droplet size over the course of 10 months indicates that the nanoemulsions underwent Ostwald ripening at an extremely slow rate.

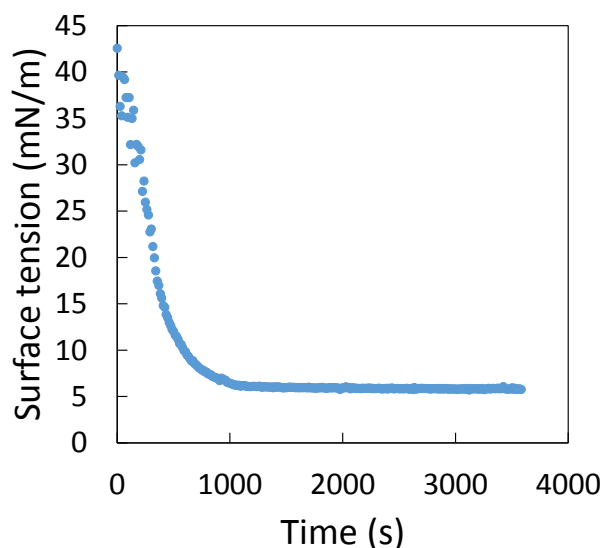


Figure 5.2. Interfacial tension reduction as a function of time for 0.1 wt% of PMEO₂MA star polymers at xylene/water interface. Interfacial tension dropped to 6 mN/m within 15 mins.

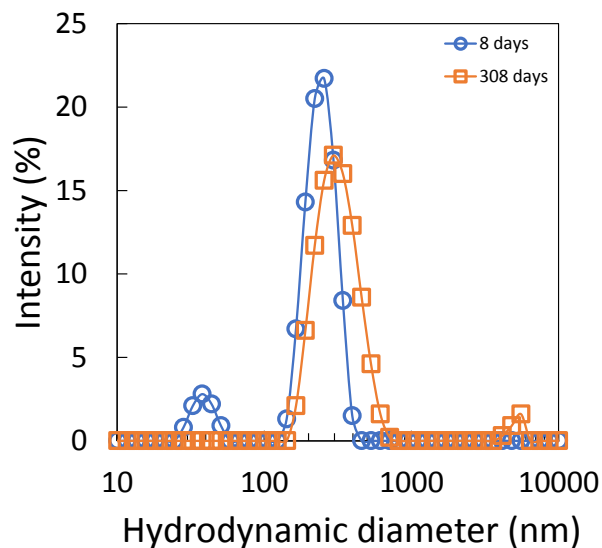


Figure 5.3. Droplet size distribution of xylene-in-water nanoemulsion at 8 days (○) and 308 days (□) after xylene and 0.1 wt% PMEO₂MA star polymer solution were brought into contact and left under quiescent conditions at room temperature.

5.4 Factors affecting nanoemulsion droplet size

5.4.1 Effect of temperature on nanoemulsion droplet size

One parameter that could influence the droplet size distribution is temperature since PMEO₂MA star polymers exhibit a lower critical solution temperature (LCST) at 29 °C in water. To study the influence of temperature on the size of existing nanoemulsion droplets, the nanoemulsion samples were subjected to temperature excursions. Two sets of nanoemulsion samples with concentration varied from 0.01 wt% to 0.1 wt% and water fraction from 0.1 to 0.9 were prepared *via* spontaneous emulsification under quiescent conditions. The first set of samples were cooled to 4 °C followed by slowly increasing the temperature back to room temperature. The second set of samples were heated to 45 °C and then were brought back to the room temperature. Droplet size measurements were made to probe any thermally-induced effects.

5.4.1.1 Cooling

Figure 5.4 shows that spontaneously formed xylene-in-water nanoemulsions using 0.1 wt% PMEO₂MA star polymer and 50% water volume fraction had a mean droplet hydrodynamic diameter at ~ 150 nm. The mean droplet diameter remain unchanged for 35 days, indicating that the nanoemulsion was extremely stable. After storing the nanoemulsion sample at 4 °C for 22 days, the mean droplet size increased to ~ 500 nm with a peak at smaller droplet size (~ 95 nm). This suggests that the increase in temperature induces the coalescence and coarsening of the droplets. Interestingly, upon heating the nanoemulsion back to room temperature, the droplet size decreased and the size distributions became bimodal, with a population of droplets with diameters ~ 50 nm and a population ~ 300 nm. The re-formation of the smaller droplets indicates evidence of partial conversion of large droplets to small droplets, which shows the opposite direction of Ostwald ripening. The nanoemulsion was then allowed to relax at room temperature and the droplet size distribution barely changed and remained bimodal even after 3 months.

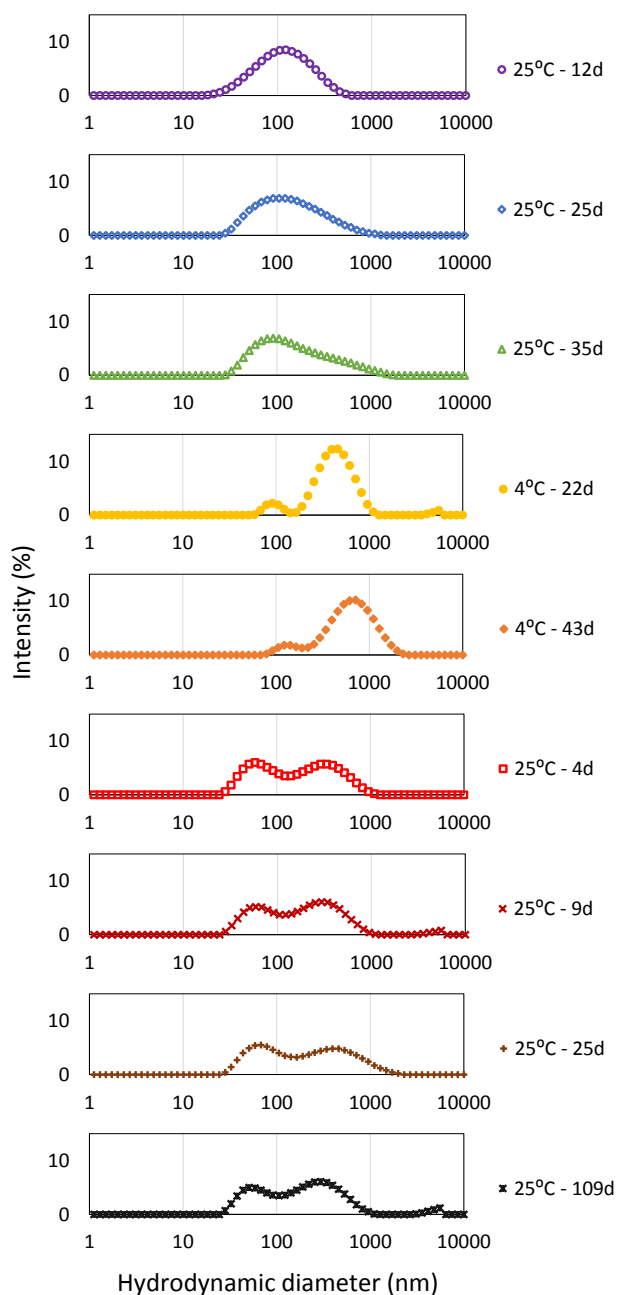


Figure 5.4. Effect of cooling to 4 °C and heating back to temperature on nanoemulsion droplet size distribution. Nanoemulsions was prepared by spontaneous emulsification using water fraction = 50% and PMEO₂MA star polymer concentration = 0.1 wt% at ambient temperature and left to rest for 35 days before cooled to 4 °C. After storing at 4 °C for 43 days, the nanoemulsion was brought back to room temperature. Size distribution was measured throughout the experiment to probe any temperature-induced effects.

5.4.1.2 Heating

Figure 5.5 shows that heating has little effect on the droplet size distributions of nanoemulsions with 0.1 wt% PMEO₂MA star polymer and 50% water volume fraction. The mean droplet size remained unchanged when temperature was elevated to 45 °C, which is above the LCST of PMEO₂MA star polymer (29 °C). Furthermore, the nanoemulsion phase showed no change in visual appearance as temperature increased. This suggests that the collapse of polymers which already adsorbed at the droplet interface impede droplet flocculation and coalescence. Upon cooling back to room temperature, the droplet size distribution stayed almost the same and no appearance change was observed.

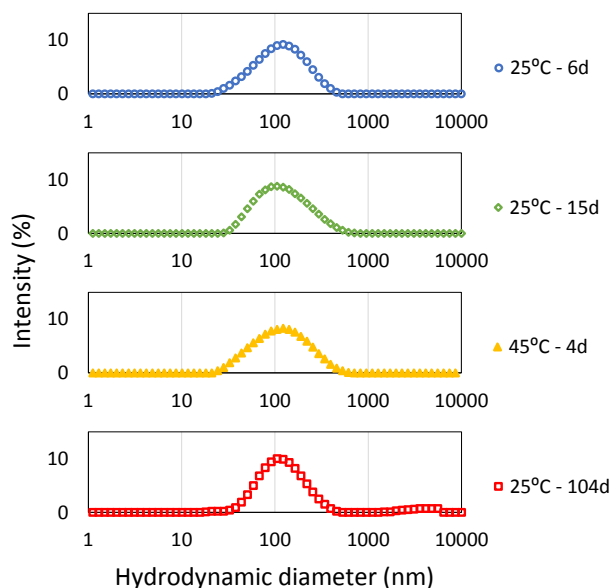


Figure 5.5. Effect of heating to 45 °C and cooling back to temperature on nanoemulsion droplet size distribution. Nanoemulsion was prepared by spontaneous emulsification using water fraction = 50% and PMEO₂MA star polymer concentration = 0.1 wt% at ambient temperature and left to rest for 15 days before cooling to 45 °C. After storing at 45 °C for 4 days, the nanoemulsion was brought back to room temperature. Size distribution was measured throughout the experiment to probe any temperature-induced effects.

5.4.2 Effect of polymer concentration on nanoemulsion droplet size

We examined the influence of PMEO₂MA star polymer concentration on the size of the droplets formed in nanoemulsions produced by spontaneous emulsification. The water volume fraction was fixed at 50% and the polymer concentration was varied from 0.01 wt% to 0.1 wt%. The emulsion with 0.01 wt% star polymer concentration produced a mean droplet diameter around 100 nm indicates that nanoemulsions can be formed by spontaneous emulsification at extremely low star polymer concentration, which could potentially be useful in some commercial applications. Interestingly, the mean droplet diameter slightly increases (from 100 to 130 nm) when we increase the star polymer concentration from 0.01 wt% to 0.1 wt% (**Figure 5.6**). This trend is opposite to some of the previous studies where they have reported an increase in the amount of surfactants adsorbed at the oil/water interface decreased the interfacial tension and allowed them to stabilize larger interfacial area created during emulsification, which facilitate the formation of smaller droplets.^{183,184} However, the fact that the interfacial tension reached the same and fairly low value at the star polymer concentrations from 0.01 wt% to 0.1 wt% (**Figure 5.7**) suggests that the droplet size is dominated by other factors when spontaneous emulsification occurs. A few studies have also observed the same trend as the mean droplet diameter increased with the surfactant concentration when a certain surfactant concentration was exceeded.^{37,185–188} The formation of a viscous liquid crystalline phase limits the breakup of the interface and more energy is required to generate smaller droplets. In addition, the scattering intensity of nanoemulsion phase was more pronounced at higher star polymer concentrations (**Table 5.1**).

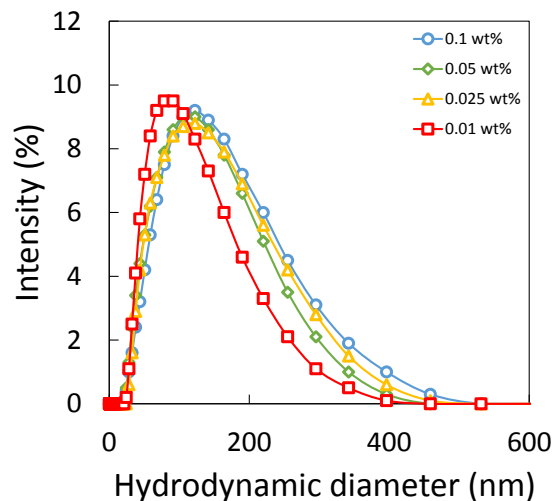


Figure 5.6. Effect of polymer concentration on droplet size distribution of nanoemulsions produced by spontaneous emulsification. Xylene-in-water nanoemulsions were prepared using 50% water volume fraction at ambient temperature and left under quiescent conditions for 6 days before size measurements. The concentrations of PMEO₂MA star polymer solutions: (○) 0.1 (◇) 0.05 (△) 0.025 (□) 0.01 wt%.

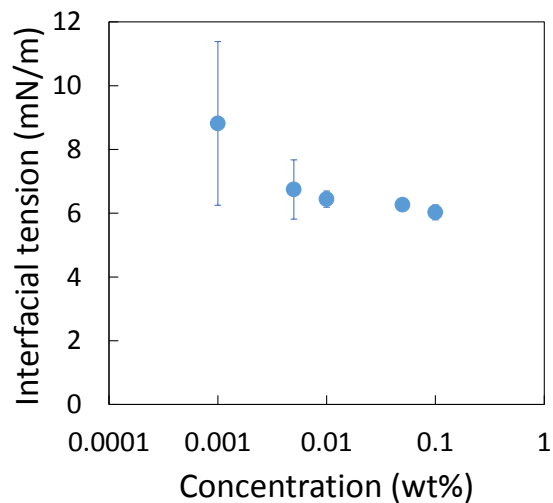


Figure 5.7. Interfacial tension isotherm of PMEO₂MA star polymers adsorbed to the xylene/water interface.

Table 5.1. Derived count rate of nanoemulsions at different star polymer concentrations measured by dynamic light scattering. Xylene-in-water nanoemulsions were prepared using 50% water volume fraction at ambient temperature and left under quiescent conditions for 6 days before measurements. Higher derived count rate usually indicates higher concentration or larger droplets.

Star polymer concentration (wt%)	Derived count rate (kcps)
0.1	203,000 ± 673
0.05	123,000 ± 244
0.025	73,000 ± 268
0.01	18,000 ± 127

5.4.3 Effect of water volume fraction on nanoemulsion droplet size

The effect of water volume fraction on the nanoemulsion droplet size was investigated by preparing a series of emulsions by spontaneous emulsification with various oil:water ratio. At a fixed PMEO₂MA star polymer concentration, increasing the water volume fraction increases the total amount of PMEO₂MA stars presented in the nanoemulsions. The results show that the mean droplet size increases with the water volume fraction (**Figure 5.8**) except for the lowest star polymer concentration at 0.01 wt%, where the droplet size slightly decreases for water volume fractions over 80%. As for star polymer concentration at 0.1 wt%, the smallest droplets with the narrowest distribution were formed at 10% water volume fraction (d ~ 69 nm and PDI ~ 0.19) whereas the largest droplets with the broadest distribution were formed at 90% water volume fraction (d ~ 207 nm and PDI ~ 0.28). Similar trends were observed for star polymer concentration at 0.025 and 0.5 wt%. This is consistent with what we have observed when varying star polymer concentration (**Figure 5.6**). When increasing the water volume fraction at a fixed star polymer concentration in water, the total amount of PMEO₂MA star polymer increases and larger size of nanoemulsion droplet was obtained. We hypothesize that this could potentially attribute to the difference in diffusion rates of polymer relocating from aqueous phase to xylene phase. However, the mechanism controlling the size of spontaneous formed droplet is not yet

understood and needs further investigation. It is worth mentioning that at higher water volume fraction, the effects of cooling on the change in droplet size are more pronounced (**Figure 5.9**). That is, larger droplets were formed when the nanoemulsion was cooled to 4 °C at higher water volume fraction.

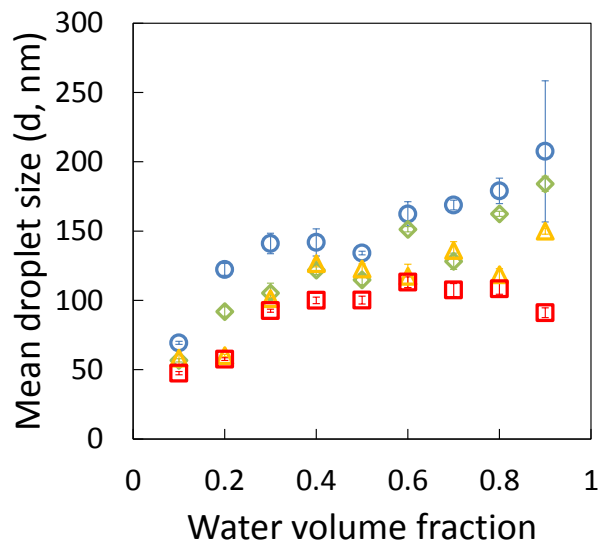


Figure 5.8. Effect of water volume fraction (which changes the total amount of PMEO₂MA in nanoemulsion) on mean droplet diameter of nanoemulsions produced by spontaneous emulsification. Xylene-in-water nanoemulsions were prepared using various oil:water ratio at ambient temperature and left under quiescent conditions for 6 days before size measurements. The concentrations of PMEO₂MA star polymer solutions: (○) 0.1 (◇) 0.05 (△) 0.025 (□) 0.01 wt%.

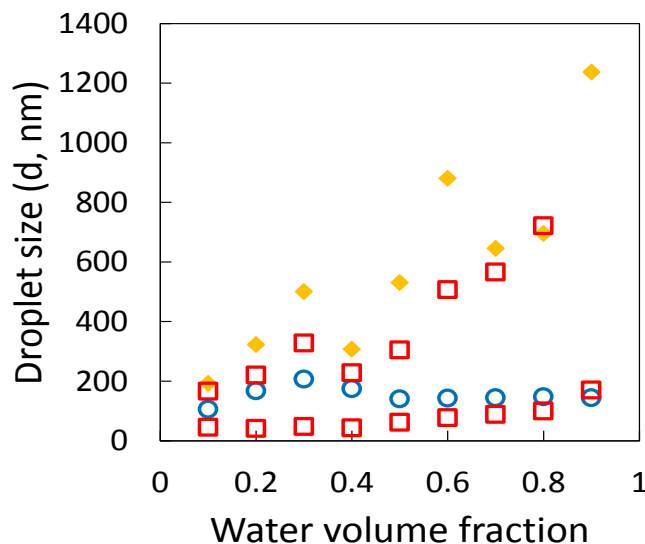


Figure 5.9. Nanoemulsion droplet size as a function of water volume fraction at room temperature (\circ), cooling down to 4 °C (\blacklozenge) and heating back to room temperature (\square). The concentration of PMEO₂MA star polymer was 0.1 wt%. The effects of cooling on the change in droplet size are more pronounced at higher water volume fraction. Upon heating back to the room temperature, the droplet size distributions became bimodal.

5.5 Macroemulsions “break” into nanoemulsions

5.5.1 PMEO₂MA star polymers as emulsifiers

Since a nanoemulsion is only kinetically stable, the stability and properties of nanoemulsions may depend on the preparation methods. Here a series of macroemulsions at different water volume fractions were prepared using a sawtooth homogenizer and stability of macroemulsions was monitored. The macroemulsions were left to rest and allowed the micron-sized droplets to break. **Figure 5.10a** shows the initial stage of macroemulsions stabilized by PMEO₂MA star polymer with various water volume fractions. When the water volume fraction is less than 20%, no macroemulsion was formed. For water volume fraction greater than 30%, stable xylene-in-water macroemulsions were formed and no phase inversion composition was

observed. **Figure 5.10b** shows the photographs of macroemulsions 10 days after preparation and the occurrence of emulsion creaming at longer times is due to the large size of droplets.

Interestingly, we found that the phase under the macroemulsion phase was translucent instead of transparent, which suggests that it was not a neat water phase. Even if after the breakage of macroemulsion, it did not produce macroscopic phase separation into two bulk phases; instead it yields a new emulsion phase with the appearance and the droplet size distribution that are similar to that produced under quiescent conditions. Dynamic light scattering measurements of the new emulsion phase gave a mean droplet size around 100 nm for various water volume fractions, as shown in **Figure 5.10c**.

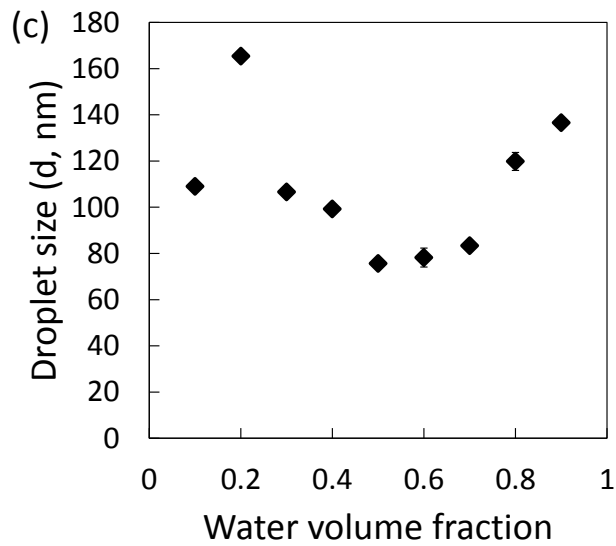
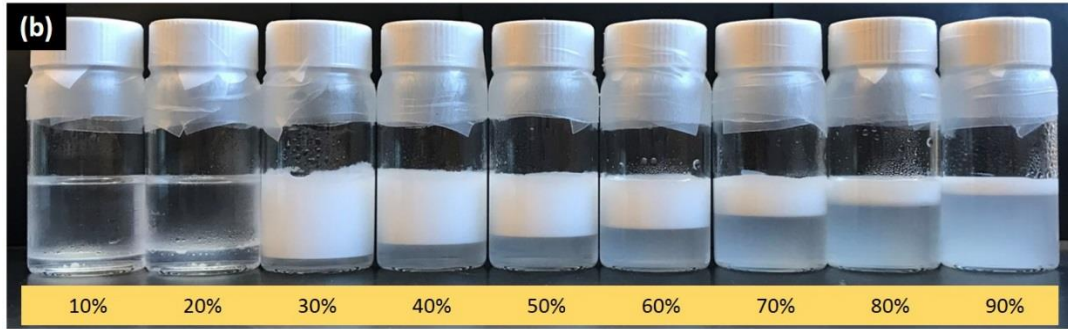
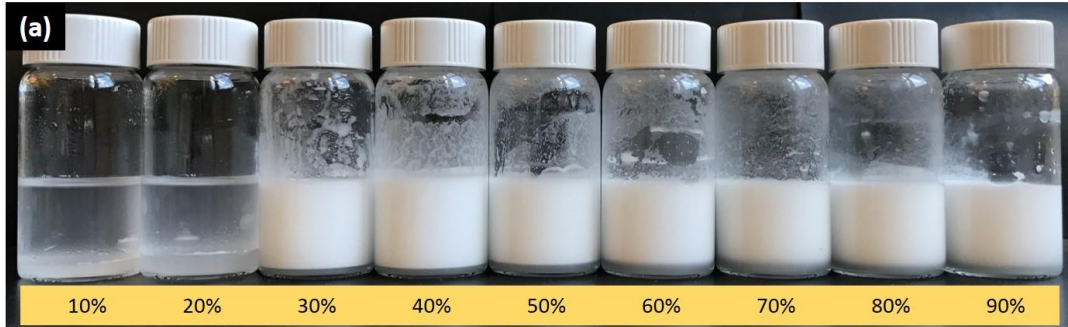


Figure 5.10. Photographs of macroemulsions produced by high shear homogenization using 0.1 wt% PMEO₂MA star polymer concentration at various water volume fractions at (a) the initial stage and (b) 10 days after sample preparation. Creaming occurred in macroemulsion samples due to the large size of droplets. (c) Mean droplet diameter as a function of water volume fraction of the new emulsion phase after the breakage of macroemulsions.

In order to understand whether the new nanoemulsion phase was formed by high shear homogenization or by spontaneous emulsification with the presence of micron-sized droplets. We first prepared a PMEO₂MA star-stabilized macroemulsion using a homogenizer with polymer concentration = 0.1 wt% and water volume fraction = 0.9. The sample was then centrifuged at 1800 rpm for 30 mins to separate the micron-sized droplets and the continuous phase. After centrifugation, the bottom phase (continuous phase) was not as opaque as the one after creaming occurred (**Figure 5.10b**). The dynamic light scattering measurement shows that the sample was very polydisperse (PDI ~ 0.7) with three peaks at around 20 nm, 190 nm and 4.8 μm (**Figure 5.11**). The largest size is likely due to the small amount of macroemulsion droplets being accidentally transferred when taking the bottom liquid out of the vial. The peaks at small (20 nm) and medium size (190 nm) suggest that the continuous phase contained both free star polymers and nanoemulsions. The existence of free star polymers in the continuous phase allows the spontaneous emulsification to occur after the macroemulsion was produced, resulting in the growing of the nano-sized droplets while micron-sized droplets break. This is evident in the photographs shown in **Figure 5.12**, where there is an increase in the scattering intensity of the nanoemulsion phase, and the disappearance of the small size peak after 6 days of sample preparation (**Figure 5.11**). In other words, instead of macroscopic phase separation into two bulk phases, destabilization of a macroemulsion leads to the spontaneous formation of a nanoemulsion phase.

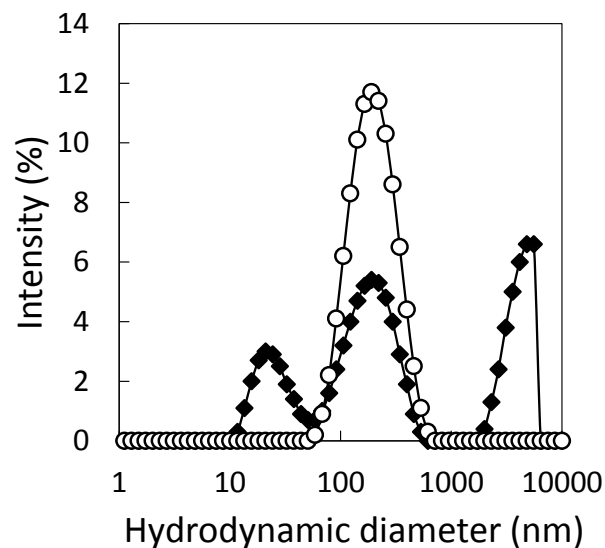


Figure 5.11. Droplet size distribution of the continuous phase of the macroemulsion produced using high shear homogenization with PMEO₂MA star polymer concentration 0.1 wt% and water volume fraction 0.9 after centrifugation at (♦) and after 6 days of resting (○).

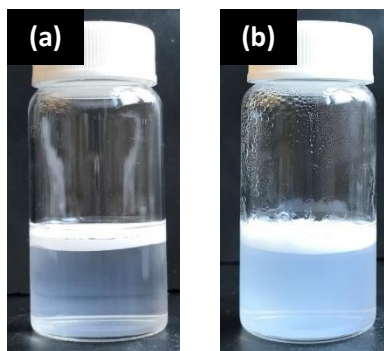


Figure 5.12. Photographs of the macroemulsions produced by high shear homogenization with PMEO₂MA star polymer concentration 0.1 wt% and water volume fraction 0.9 (a) after centrifugation at 1800 rpm at 30 mins and (b) after 6 days of resting. The derived count rate measured by dynamic light scattering increased from (a) 72,000 kcps to (b) 105,000 kcps, suggesting that the free polymers in the continuous phase underwent spontaneous emulsification and formed nano-sized droplets after the macroemulsions was produced.

5.5.2 Triton X-100 as emulsifiers

To investigate if the ability to produce a nanoemulsion using both quiescent emulsification and breakage of a high shear homogenized macroemulsion is a unique property of PMEO₂MA star polymer, we prepared two xylene/water emulsions using Triton X-100 as surfactants. One sample was left under quiescent condition without stirring and the other was emulsified using a sawtooth homogenizer. Spontaneous emulsification was observed when xylene and 0.1 wt% Triton X-100 solution were put in contact (**Figure 5.13a**) with minimal perturbation, which has also been previously reported.¹⁸⁹ The sample that has been homogenized was allowed to rest and the droplet size distribution of the bottom phase was measured after the macroemulsion broke. As shown in **Figure 5.13c**, the emulsion formed under quiescent condition has a mean droplet size at 500 nm whereas the emulsion formed after micron-sized droplets breakage has a mean droplet size around 300 nm. This indicates that after the large droplets in the macroemulsion broke, a nanoemulsion formed, which is consistent with what we observed with PMEO₂MA star polymers. However, the scattering intensity of the quiescent emulsification sample (derived count rate ~ 100,000 kcps) was much higher than that of macroemulsion breakage sample (derived count rate ~ 10,000 kcps). The difference in droplet size and scattering intensity may attribute to the redistribution of materials during high shear homogenization, resulting in different final structure. As will be discussed below, the location of the surfactants can be important for spontaneous emulsification.

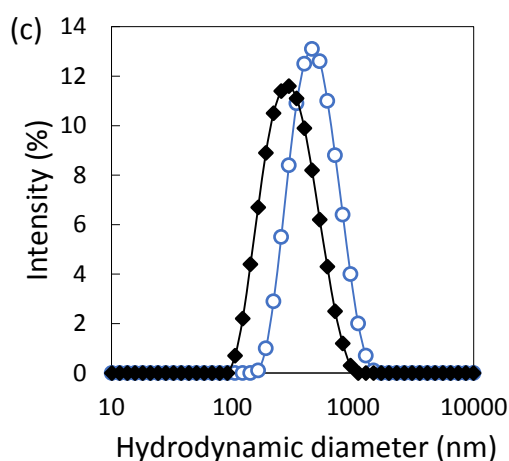
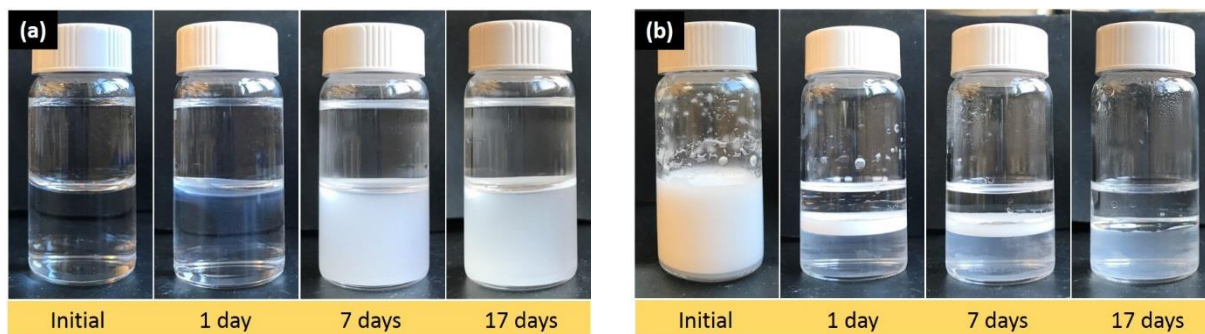


Figure 5.13. Xylene-in-water nanoemulsions produced (a) by spontaneous emulsification under quiescent conditions and (b) breakage of a macroemulsion. The concentration of Triton X-100 was 0.1 wt% and the water volume fraction was 0.5. (c) Size distribution of Triton X-100 stabilized emulsions produced by spontaneous emulsification (○) and by breakage of a macroemulsion (◆) 17 days after sample preparation.

5.6 Path-dependent PMEO₂MA star-stabilized nanoemulsions

Previously proposed mechanism for the occurrence of spontaneous emulsification only when multi-arm poly(ethylene oxide) (PEO) stars are initially dispersed in the xylene phase, and not when they are in the aqueous phase is based on the diffusion of multi-arm PEO stars from the xylene phase into the aqueous phase.⁴⁶ The difference in solubility of PEO stars in two phases drives PEO stars to redistribute themselves across interface and provides the energy required for

spontaneous emulsification. Similarly, we investigate the effect of initial location of PMEO₂MA star polymers on the phenomenon of spontaneous emulsification. The results show that when PMEO₂MA stars were initially dispersed in xylene phase, no spontaneous emulsification was observed (**Figure 5.14b**). Both xylene and water phases remained transparent even with a gentle stir (**Table 5.2**). We note that this phenomenon is mirrored with spontaneously formed water-in-xylene emulsion with multi-arm PEO stars dispersed in xylene.⁴⁶ This opposite trend is possibly attributed to PMEO₂MA stars being more hydrophobic than PEO stars. PMEO₂MA stars exhibit a lower critical solution temperature (LCST) of 29 °C in water and PEO stars has a LCST of 95 °C,¹⁷ suggesting PMEO₂MA stars are less soluble in water than PEO stars. PMEO₂MA stars are fully dispersed in xylene as soon as they are added to xylene phase. However, because of the limited amount of materials, the partition coefficient for PMEO₂MA stars between xylene and water cannot be determined. Similar to the proposed mechanism in **Chapter 3.5**, we hypothesize that the difference in PMEO₂MA star solubility between two liquid phases drives PMEO₂MA stars to redistribute themselves from water to xylene phase and provides energy to spontaneously form xylene-in-water nanoemulsions. The path-dependent property of PMEO₂MA stars also confirms that oil-in-water nanoemulsions were formed instead of microemulsions since microemulsion is thermodynamically stable and the properties and structure should not depend on the preparation methods. In addition, the PMEO₂MA stars were initially dispersed in both xylene and water phase with the same total amount of star polymers (50/50 mass in each phase) and the sample also formed nanoemulsion spontaneously (**Figure 5.14c**). However, the dynamic of spontaneous emulsification was slower than that when the stars were initially located in water phase (**Table 5.2**). Previous studies have shown that the size of nanoemulsion droplets depends on the initial location of surfactant^{180,190} It is the redistribution of the materials across the

boundary that drives spontaneous emulsification and facilitates the small droplets formation, rather than the final composition of the system.⁸¹

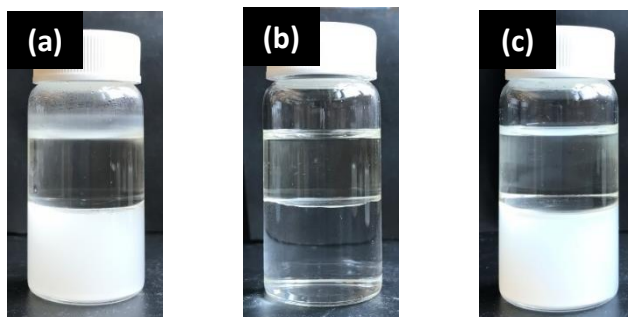
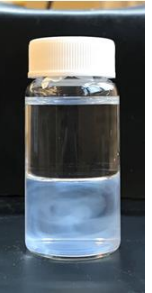


Figure 5.14. Photographs of xylene-in-water nanoemulsions formed by spontaneous emulsification with (a) 0.1 wt% PMEO₂MA star polymer initially dispersed in water phase (bottom phase). (b) No spontaneous emulsification was observed when the PMEO₂MA stars were initially dispersed in xylene phase. (c) Xylene-in-water nanoemulsions spontaneously formed when same total amount of PMEO₂MA stars were initially dispersed both xylene and water phases (50/50 mass in each phase). Photographs were taken 106 days after the xylene and water phase came into contact.

Table 5.2. Photographs of xylene/water with 0.1 wt% PMEO₂MA stars initially dispersed in water (bottom phase), initially dispersed in xylene, and initially dispersed in both xylene and water phases with the same total amount of PMEO₂MA stars (50/50 mass in each phase)

	Initial	1 h	3 h	5 h	18 h	48 h
PMEO ₂ MA stars in water						
PMEO ₂ MA stars in xylene						
PMEO ₂ MA stars in xylene with gentle stir						
PMEO ₂ MA stars in water and xylene						

5.7 Conclusions

Stable xylene-in-water nanoemulsions were produced by spontaneous emulsification with PMEO₂MA star polymer initially dispersed in water phase. The nanoemulsions were proven to be extremely stable for over 10 months with small increase in droplet size. We examined several factors that affect the properties of PMEO₂MA star-stabilized nanoemulsions. Cooling had a major impact on the size of the nanoemulsion droplets. The droplet size increased when the temperature decreased from room temperature to 4 °C. A portion of large droplets converted back to small droplets upon heating back to the room temperature, resulting in a bimodal size distribution. On the other hand, heating the nanoemulsions to 45 °C, which is above the LCST of PMEO₂MA star polymer, had little effect on the droplet size. We also showed that the mean droplet size increased with increasing polymer concentration and water volume fraction. Although the physicochemical properties that determine the droplet size still need to be established, these results suggest that the spontaneous emulsification method can be used for producing nanoemulsions at a wide range of conditions.

Macroemulsions that made by high shear homogenization were allowed to rest and break. Breakage of a macroemulsion yielded a new nanoemulsion phase with the appearance and the droplet size distribution that were similar to that produced under quiescent emulsification. Dynamic light scattering measurement of the continuous phase in the macroemulsion suggests that the spontaneous emulsification occurs during the breakage of big droplets, leading to the formation of nanoemulsions. Similar results were observed for emulsions stabilized with Triton X-100, indicating that macroemulsions breaking into nanoemulsions may be applied to various systems.

Nanoemulsions produced by spontaneous emulsification exhibit a sensitivity to initial location of the PMEO₂MA star polymers. Spontaneous emulsification occurs only when PMEO₂MA stars are initially dispersed in the water phase. No spontaneously formed nanoemulsion is observed when star polymers are dispersed in the xylene phase even with a gentle stir.

6 Conclusions and future work

6.1 Summary of observations

Star polymers with well-defined composition and architecture have been synthesized by atom transfer radical polymerization. This dissertation has confirmed that star polymers are effective and efficient foam and emulsion stabilizers. This work was the first systematic study of the effect of star polymer structure and chemistry on their interfacial activity at fluid interfaces. Three important interfacial characteristics have been investigated: interfacial tension reduction, dynamic dilatational modulus, and extent of adsorption of star polymers at air/water and oil/water interfaces. The contributions of these interfacial activity to high foaming and emulsifying efficiency of star polymers have been determined.

Non-ionic multi-arm PEO star polymers were able to stabilize foams and emulsions at a concentration of 0.005 wt%. PEO star polymers achieved significantly higher interfacial pressures and extent of adsorption than linear PEO due to their compact star polymer structure. Tethering a large number of polymer arms to a core inhibits star polymers from spreading along the interface, and confines all their mass in a relatively small projected area, which results in a densely packed adsorbed layer at the interface. No dynamic dilatational modulus was detected with linear PEO adsorbed layers. This is attributed to their highly flexible structure which allows fast conformation change in response to area oscillation. In contrast, the finite dynamic dilatational modulus produced by PEO star polymers adsorbed layers is caused by the highly constrained arms that are less able to reconfigure during area perturbation. This distinctive interfacial feature may be related to the high efficiency of star polymers as foaming agents and emulsifiers. Additionally, adsorption of star polymers were found to be path-dependent.

The interfacial properties of three β -cyclodextrin core star polymers with the same architecture but different chemistries were also studied. Diblock star polymers were able to stabilize xylene-in-water and cyclohexane-in-water emulsions at pH 5 at an extremely low concentration that are comparable to multi-arm PEO star polymers (0.005 wt%). PDMAEMA and diblock star polymers display pH dependent size and charge properties. Increases in interfacial pressure and extent of adsorption for PDMAEMA and diblock star polymers were observed when the pH increased from 5 to 9. At high pH, PDMAEMA and diblock star polymers adsorbed to the interface in a relatively collapsed state due to charge neutralization and formed a densely packed layer. We have observed that the dilatational modulus of the star polymer adsorbed layer runs through a maximum with increasing interfacial pressure. This is attributed to the balance of intraparticle interactions, which increases the modulus with increasing concentration, and the exchange dynamic between adsorbed and bulk species, which reduces the modulus with increasing concentration. The ability of star polymers to resist desorption under interfacial compression and produce interfaces with significant dilatational elastic moduli may be correlated with their high emulsifying efficiency and favors emulsion stability. However, further study is required to gain a better understanding of foam and emulsion formation mechanism.

A final study demonstrated that extremely stable xylene-in-water nanoemulsions were formed at a wide range of conditions *via* spontaneous emulsification with PMEO₂MA star polymers. Temperature and system composition were varied to examine their effects on nanoemulsion droplet size. While heating did not affect the droplet size, cooling increased the droplet size. Moreover, when nanoemulsions were brought back to room temperature, a portion of large droplets decomposed into small droplets, resulting in a bimodal size distribution. When given sufficient time, macroemulsions that were created by high shear homogenization were

found to break into a new nanoemulsion phase, with the appearance and the droplet size distribution similar to that produced under quiescent emulsification. Similar results were observed with Triton X-100, suggesting that macroemulsions breaking into nanoemulsions may be a universal phenomenon for spontaneously formed nanoemulsions. In addition, the initial location of PMEO₂MA star polymers are important for spontaneous emulsification to occur.

6.2 Original contributions

The research findings in this dissertation provide fundamental understanding of interfacial behavior of surface active star polymers underlying their strong emulsifying and foaming efficiency. The investigation of star polymers adsorbed at fluid interfaces in this dissertation complements the previous work performed in our group that developed nanoparticulate polymer brushes as efficient emulsifiers.⁴⁵ The following is a list of notable contributions resulting from this work.

- Proved that star polymers are effective and efficient foam stabilizers. Stable foams were created with 0.005 wt% of multi-arm PEO star polymers and significant fractions of initial foam were retained after two hours of aging.
- Confirmed that incorporating a weakly polycation into the star polymer arms imports responsive interfacial behavior to pH changes.
- Identified the significant dynamic dilatational elasticity produced by star polymers may be a key factor that distinguishes their good emulsifying and foaming performance from the poor performance of linear PEO.

- Identified that dynamic dilatational modulus does not linearly correlate with foaming and emulsifying performance. The packing density and the exchange dynamics of emulsifiers need to be taken into account.
- Identified the ability of star polymers to resist ejection under interfacial compression may correlate with high emulsifying efficiency and stability.
- Identified that interfacial properties of star polymer adsorbed layers does not solely depend on their interfacial pressure, but also depends on the structure of the adsorbed layer and the interactions of the star polymers.
- Proposed a mechanism based on the difference in multi-arm PEO star polymer solubility between two liquids to explain the occurrence of spontaneous emulsification only when PEO stars polymer are initially dispersed in the xylene phase, and not when they are in the aqueous phase.
- First to demonstrate the spontaneous formation of extremely stable nanoemulsions with surface active star polymers.
- First to demonstrate that macroemulsions breaking into spontaneously produced nanoemulsions can be observed to various systems.

6.3 Future work

6.3.1 Neutron scattering characterization of emulsions stabilized by star polymers

This dissertation assessed the importance of specific interfacial properties of star polymers adsorbed at fluid interfaces under a variety of conditions. While much is understood about the properties of star polymers adsorbed at a relatively planar oil/water interface of a large total area through interfacial tension and rheology measurements, and extent of adsorption (qualitatively at oil/water interface), the emulsification ability of a star polymer with complex

molecular architecture and composition is ultimately tied to its microstructure and interactions both in solution and at the droplet fluid/fluid interface.

Small angle neutron scattering has been used as a characterization tool for interfacial self-assembly and has already been applied to emulsion and emulsion-like systems, including vesicles,^{191,192} liposomes,¹⁹²⁻¹⁹⁴ intrabilayer polymerization,¹⁹⁵ and surfactant-stabilized emulsions.¹⁹⁶⁻¹⁹⁸ A direct extension of the work in this dissertation would involve utilizing neutron scattering to study star polymer-stabilized emulsions. For emulsion systems, in-situ neutron scattering experiments offer the ability to probe droplets in their native geometric conformation and are capable of quantifying the surface coverage of emulsifiers, resolving changes in structure and the interactions of star polymers upon adsorption to the oil/water interface of emulsion droplets. In addition, neutron scattering allows us to determine the structural composition of the interface by contrast-matching solvents to obtain the scattering signal from the interface. Small angle neutron scattering (SANS) will be used to resolve scattering from the adsorbed star polymers and ultra-small angle neutron scattering (USANS) will be used to resolve scattering from the micron-sized droplets. To quantify surface coverage of star polymer, the scattering data will be fitted by an analytical scattering model for Pickering emulsions.¹⁹⁹ Insights from such experiments will shed-light on the microstructural origin of high-efficiency emulsifying properties and help guide the design of future star polymer surfactants.

6.3.2 Interfacial exchange dynamics

This dissertation investigated the adsorption behavior of star polymers at oil/water interfaces and correlated emulsifiers having resistance against forced desorption with high

emulsifying efficiency. To further understand adsorption/desorption behavior of star polymer at the interface, the exchange dynamics between the bulk and adsorbed species could be explored *via* total internal reflection – fluorescence recovery after photobleaching (TIR-FRAP) without perturbing the interface or the bulk suspension.²⁰⁰ The interfacial exchange dynamic can be probed by first adsorption of fluorescently tagged star polymers to the interface, followed by selectively photobleaching a small area of the interface. Subsequent exchange between adsorbed photobleached species and fluorescent bulk species will produce a recovery in the fluorescence intensity. Combined with the dynamic interfacial tension measurements, these experiments will provide information on adsorption/desorption mechanisms and lateral diffusion of star polymers within the adsorbed layer.

References

- (1) Gonzenbach, U. T.; Studart, A. R.; Tervoort, E.; Gauckler, L. J. Stabilization of Foams with Inorganic Colloidal Particles. *Langmuir* **2006**, *22* (26), 10983–10988.
- (2) Dickinson, E. Food Emulsions and Foams: Stabilization by Particles. *Curr. Opin. Colloid Interface Sci.* **2010**, *15* (1–2), 40–49.
- (3) Vignati, E.; Piazza, R.; Lockhart, T. P. Pickering Emulsions: Interfacial Tension, Colloidal Layer Morphology, and Trapped-Particle Motion. *Langmuir* **2003**, *19* (17), 6650–6656.
- (4) Binks, B. P.; Lumsdon, S. O. Stability of Oil-in-Water Emulsions Stabilised by Silica Particles. *Phys. Chem. Chem. Phys.* **1999**, *1* (12), 3007–3016.
- (5) Chevalier, Y.; Bolzinger, M. A. Emulsions Stabilized with Solid Nanoparticles: Pickering Emulsions. *Colloids Surfaces A Physicochem. Eng. Asp.* **2013**, *439*, 23–34.
- (6) Hunter, T. N.; Pugh, R. J.; Franks, G. V.; Jameson, G. J. The Role of Particles in Stabilising Foams and Emulsions. *Adv. Colloid Interface Sci.* **2008**, *137* (2), 57–81.
- (7) Pickering, S. U. Emulsions. *J. Chem. Soc. Trans.* **1907**, *91*, 2001–2021.
- (8) Midmore, B. R. Preparation of a Novel Silica-Stabilized Oil/Water Emulsion. *Colloids Surfaces A Physicochem. Eng. Asp.* **1998**, *132* (2–3), 257–265.
- (9) Ashby, N. P.; Binks, B. P. Pickering Emulsions Stabilised by Laponite Clay Particles. *Physical Chemistry Chemical Physics*. 2000, pp 5640–5646.
- (10) Pieranski, P. Two-Dimensional Interfacial Colloidal Crystals. *Phys. Rev. Lett.* **1980**, *45* (7), 569–572.
- (11) Binks, B. P.; Lumsdon, S. O. Pickering Emulsions Stabilized by Monodisperse Latex Particles: Effects of Particle Size. *Langmuir* **2001**, *17* (15), 4540–4547.
- (12) Bárány, E.; Lindberg, M.; Lodén, M. Unexpected Skin Barrier Influence from Nonionic Emulsifiers. *Int. J. Pharm.* **2000**, *195* (1–2), 189–195.
- (13) Saigal, T.; Riley, J. K.; Golas, P. L.; Bodvik, R.; Claesson, P. M.; Matyjaszewski, K.; Tilton, R. D. Poly(Ethylene Oxide) Star Polymer Adsorption at the Silica/Aqueous Interface and Displacement by Linear Poly(Ethylene Oxide). *Langmuir* **2013**, *29*, 3999–4007.

- (14) Riley, J. K.; Matyjaszewski, K.; Tilton, R. D. Electrostatically Controlled Swelling and Adsorption of Polyelectrolyte Brush-Grafted Nanoparticles to the Solid/Liquid Interface. *Langmuir* **2014**, *30*, 4056–4065.
- (15) Riley, J. K.; Tilton, R. D. Sequential Adsorption of Nanoparticulate Polymer Brushes as a Strategy to Control Adhesion and Friction. *Langmuir* **2016**, *32* (44), 11440–11447.
- (16) Lamson, M.; Chen, L.; Zhong, M.; Wu, D.; Matyjaszewski, K. Nitrogen-Doped Nanocarbons Derived from Tetrazine Cross-Linked Poly(4-Cyanostyrene)-Silica Hybrids. *Macromol. Chem. Phys.* **2017**, *218* (18), 1600524.
- (17) Saigal, T.; Yoshikawa, A.; Kloss, D.; Kato, M.; Golas, P. L.; Matyjaszewski, K.; Tilton, R. D. Stable Emulsions with Thermally Responsive Microstructure and Rheology Using Poly(Ethylene Oxide) Star Polymers as Emulsifiers. *J. Colloid Interface Sci.* **2013**, *394*, 284–292.
- (18) Li, W.; Yu, Y.; Lamson, M.; Silverstein, M. S.; Tilton, R. D.; Matyjaszewski, K. PEO-Based Star Copolymers as Stabilizers for Water-in-Oil or Oil-in-Water Emulsions. *Macromolecules* **2012**, *45*, 9419–9426.
- (19) Saigal, T.; Dong, H.; Matyjaszewski, K.; Tilton, R. D. Pickering Emulsions Stabilized by Nanoparticles with Thermally Responsive Grafted Polymer Brushes. *Langmuir* **2010**, *26* (18), 15200–15209.
- (20) Saleh, N.; Sarbu, T.; Sirk, K.; Lowry, G. V.; Matyjaszewski, K.; Tilton, R. D. Oil-in-Water Emulsions Stabilized by Highly Charged Polyelectrolyte-Grafted Silica Nanoparticles. *Langmuir* **2005**, *21* (11), 9873–9878.
- (21) Saigal, T.; Xu, J.; Matyjaszewski, K.; Tilton, R. D. Emulsification Synergism in Mixtures of Polyelectrolyte Brush-Grafted Nanoparticles and Surfactants. *J. Colloid Interface Sci.* **2015**, *449*, 152–159.
- (22) Xie, G.; Kryszewski, P.; Tilton, R. D.; Matyjaszewski, K. Heterografted Molecular Brushes as Stabilizers for Water-in-Oil Emulsions. *Macromolecules* **2017**, *50* (7), 2942–2950.
- (23) Golemanov, K.; Tcholakova, S.; Kralchevsky, P. A.; Ananthapadmanabhan, K. P.; Lips, A. Latex-Particle-Stabilized Emulsions of Anti-Bancroft Type. *Langmuir* **2006**, *22* (11), 4968–4977.
- (24) Alvarez, N. J.; Anna, S. L.; Saigal, T.; Tilton, R. D.; Walker, L. M. Interfacial Dynamics and Rheology of Polymer-Grafted Nanoparticles at Air-Water and Xylene-Water Interfaces. *Langmuir* **2012**, *28* (21), 8052–8063.

- (25) Almusallam, A. S.; Sholl, D. S. Brownian Dynamics Simulations of Copolymer-Stabilized Nanoparticles in the Presence of an Oil-Water Interface. *J. Colloid Interface Sci.* **2007**, *313* (1), 345–352.
- (26) Yong, X. Modeling the Assembly of Polymer-Grafted Nanoparticles at Oil-Water Interfaces. *Langmuir* **2015**, *31* (42), 11458–11469.
- (27) Wei, Z.; Yang, Y.; Yang, R.; Wang, C. Alkaline Lignin Extracted from Furfural Residues for PH-Responsive Pickering Emulsions and Their Recyclable Polymerization. *Green Chem.* **2012**, *14* (11), 3230–3236.
- (28) Tang, J.; Quinlan, P. J.; Tam, K. C. Stimuli-Responsive Pickering Emulsions: Recent Advances and Potential Applications. *Soft Matter* **2015**, *11* (18), 3512–3529.
- (29) Takahashi, Y.; Fukuyasu, K.; Horiuchi, T.; Kondo, Y.; Stroeve, P. Photoinduced Demulsification of Emulsions Using a Photoresponsive Gemini Surfactant. *Langmuir* **2014**, *30* (1), 41–47.
- (30) Zhu, Y.; Wang, J.; Li, X.; Zhao, D.; Sun, J.; Liu, X. Self-Assembly and Emulsification of Dopamine-Modified Hyaluronan. *Carbohydr. Polym.* **2015**, *123*, 72–79.
- (31) Shu, X.; Meng, Y.; Wan, L.; Li, G.; Yang, M.; Jin, W. PH-Responsive Aqueous Foams of Oleic Acid/Oleate Solution. *J. Dispers. Sci. Technol.* **2014**, *35* (2), 293–300.
- (32) Binks, B. P.; Murakami, R.; Armes, S. P.; Fujii, S.; Schmid, A. PH-Responsive Aqueous Foams Stabilized by Ionizable Latex Particles. *Langmuir* **2007**, *23* (17), 8691–8694.
- (33) Morse, A. J.; Armes, S. P.; Thompson, K. L.; Dupin, D.; Fielding, L. A.; Mills, P.; Swart, R. Novel Pickering Emulsions Based on PH-Responsive Poly(2-(Diethylamino)Ethyl Methacrylate) Latexes. *Langmuir* **2013**, *29*, 5446–5475.
- (34) Gonzalez-Ochoa, H.; Arauz-Lara, J. L. Spontaneous Two-Dimensional Spherical Colloidal Structures. *Langmuir* **2007**, *23* (10), 5289–5291.
- (35) Bengoechea, C.; Romero, A.; Aguilar, J. M.; Cordobés, F.; Guerrero, A. Temperature and PH as Factors Influencing Droplet Size Distribution and Linear Viscoelasticity of O/W Emulsions Stabilised by Soy and Gluten Proteins. *Food Hydrocoll.* **2010**, *24* (8), 783–791.
- (36) Pérez, M. P.; Wagner, J. R.; Márquez, A. L. Influence of Different Factors on the Particle Size Distribution and Solid Fat Content of Water-in-Oil Emulsions. *J. Am. Oil Chem. Soc.* **2016**, *93* (6), 793–801.
- (37) Saberi, A. H.; Fang, Y.; McClements, D. J. Fabrication of Vitamin E-Enriched

- Nanoemulsions: Factors Affecting Particle Size Using Spontaneous Emulsification. *J. Colloid Interface Sci.* **2013**, *391* (1), 95–102.
- (38) Silva, H. D.; Cerqueira, M. A.; Vicente, A. A. Influence of Surfactant and Processing Conditions in the Stability of Oil-in-Water Nanoemulsions. *J. Food Eng.* **2015**, *167*, 89–98.
- (39) McClements, D. J. Edible Nanoemulsions: Fabrication, Properties, and Functional Performance. *Soft Matter* **2011**, *7* (6), 2297–2316.
- (40) Koroleva, M. Y.; Yurtov, E. V. Nanoemulsions: The Properties, Methods of Preparation and Promising Applications. *Russ. Chem. Rev.* **2012**, *81* (1), 21–43.
- (41) Sonneville-Aubrun, O.; Simonnet, J. T.; L'Alloret, F. Nanoemulsions: A New Vehicle for Skincare Products. *Adv. Colloid Interface Sci.* **2004**, *108–109* (03), 145–149.
- (42) Rao, J.; McClements, D. J. Food-Grade Microemulsions, Nanoemulsions and Emulsions: Fabrication from Sucrose Monopalmitate & Lemon Oil. *Food Hydrocoll.* **2011**, *25* (6), 1413–1423.
- (43) Anton, N.; Vandamme, T. F. Nano-Emulsions and Micro-Emulsions: Clarifications of the Critical Differences. *Pharm. Res.* **2011**, *28* (5), 978–985.
- (44) Anton, N.; Benoit, J. P.; Saulnier, P. Design and Production of Nanoparticles Formulated from Nano-Emulsion Templates-A Review. *J. Control. Release* **2008**, *128* (3), 185–199.
- (45) Saigal, T. Development of Novel Pickering Emulsifiers Using Polymer Grafted Nanoparticles, Carnegie Mellon University, 2011.
- (46) Huang, Y.-R.; Lamson, M.; Matyjaszewski, K.; Tilton, R. D. Enhanced Interfacial Activity of Multi-Arm Poly(Ethylene Oxide) Star Polymers Relative to Linear Poly(Ethylene Oxide) at Fluid Interfaces. *Phys. Chem. Chem. Phys.* **2017**, *19* (35), 23854–23868.
- (47) Gupta, A.; Eral, H. B.; Hatton, T. A.; Doyle, P. S. Nanoemulsions: Formation, Properties and Applications. *Soft Matter* **2016**, *12* (11), 2826–2841.
- (48) McClements, D. J.; Jafari, S. M. Improving Emulsion Formation, Stability and Performance Using Mixed Emulsifiers: A Review. *Adv. Colloid Interface Sci.* **2018**, *251*, 55–79.
- (49) Jiang, S.; Granick, S. Controlling the Geometry (Janus Balance) of Amphiphilic Colloidal Particles. *Langmuir* **2008**, *24* (6), 2438–2445.

- (50) Tu, F.; Lee, D. Shape-Changing and Amphiphilicity-Reversing Janus Particles with PH-Responsive Surfactant Properties. *J. Am. Chem. Soc.* **2014**, *136* (28), 9999–10006.
- (51) Aveyard, R.; Binks, B. P.; Clint, J. H. Emulsions Stabilised Solely by Colloidal Particles. *Adv. Colloid Interface Sci.* **2003**, *100–102* (SUPPL.), 503–546.
- (52) Bancroft, W. D. The Theory of Emulsification, I. *J. Phys. Chem.* **1912**, *16* (3), 177–233.
- (53) Binks, B. P. Relationship between Microemulsion Phase Behavior and Macroemulsion Type in Systems Containing Nonionic Surfactant. *Langmuir* **1993**, *9* (1), 25–28.
- (54) Smith, D. H.; Lim, K. H. Morphology and Inversion of Dispersions of Two Fluids in Systems of Three and Four Thermodynamic Dimensions. *J. Phys. Chem.* **1990**, *94* (9), 3746–3752.
- (55) Besnard, L.; Protat, M.; Malloggi, F.; Daillant, J.; Cousin, F.; Pantoustier, N.; Guenoun, P.; Perrin, P. Breaking of the Bancroft Rule for Multiple Emulsions Stabilized by a Single Stimulable Polymer. *Soft Matter* **2014**, *10* (36), 7073–7087.
- (56) Xiao, M.; Xu, A.; Zhang, T.; Hong, L. Tailoring the Wettability of Colloidal Particles for Pickering Emulsions via Surface Modification and Roughness. *Front. Chem.* **2018**, *6*, 1–14.
- (57) Frith, W. J.; Pichot, R.; Kirkland, M.; Wolf, B. Formation, Stability, and Rheology of Particle Stabilized Emulsions: Influence of Multivalent Cations. *Ind. Eng. Chem. Res.* **2008**, *47* (17), 6434–6444.
- (58) Yuan, Q.; Williams, R. A. CO-Stabilisation Mechanisms of Nanoparticles and Surfactants in Pickering Emulsions Produced by Membrane Emulsification. *J. Memb. Sci.* **2016**, *497*, 221–228.
- (59) Binks, B. P.; Murakami, R.; Armes, S. P.; Fujii, S. Temperature-Induced Inversion of Nanoparticle-Stabilized Emulsions. *Angew. Chemie - Int. Ed.* **2005**, *44* (30), 4795–4798.
- (60) Isa, L.; Amstad, E.; Schwenke, K.; Del Gado, E.; Ilg, P.; Kröger, M.; Reimhult, E. Adsorption of Core-Shell Nanoparticles at Liquid-Liquid Interfaces. *Soft Matter* **2011**, *7* (17), 7663–7675.
- (61) Saleh, N.; Phenrat, T.; Sirk, K.; Dufour, B.; Ok, J.; Sarbu, T.; Matyjaszewski, K.; Tilton, R. D.; Lowry, G. V. Adsorbed Triblock Copolymers Deliver Reactive Iron Nanoparticles to the Oil/Water Interface. *Nano Lett.* **2005**, *5* (12), 2489–2494.
- (62) Galaev, I. Y.; Mattiasson, B. “Smart” Polymers and What They Could Do in

Biotechnology and Medicine. *Trends Biotechnol.* **1999**, *17* (8), 335–340.

- (63) Masliyah, J.; Zhou, Z. J.; Xu, Z.; Czarnecki, J.; Hamza, H. Understanding Water-Based Bitumen Extraction from Athabasca Oil Sands. *Can. J. Chem. Eng.* **2008**, *82* (4), 628–654.
- (64) Liu, Y.; Jessop, P. G.; Cunningham, M.; Eckert, C. A.; Liotta, C. L. Switchable Surfactants. *Science*. **2006**, *313* (5789), 958–960.
- (65) Wiese, S.; Spiess, A. C.; Richtering, W. Microgel-Stabilized Smart Emulsions for Biocatalysis. *Angew. Chemie - Int. Ed.* **2013**, *52* (2), 576–579.
- (66) Amalvy, J. I.; Unali, G. F.; Li, Y.; Granger-Bevan, S.; Armes, S. P.; Binks, B. P.; Rodrigues, J. A.; Whitby, C. P. Synthesis of Sterically Stabilized Polystyrene Latex Particles Using Cationic Block Copolymers and Macromonomers and Their Application as Stimulus-Responsive Particulate Emulsifiers for Oil-in-Water Emulsions. *Langmuir* **2004**, *20* (11), 4345–4354.
- (67) Read, E. S.; Fujii, S.; Amalvy, J. I.; Randall, D. P.; Armes, S. P. Effect of Varying the Oil Phase on the Behavior of PH-Responsive Latex-Based Emulsifiers: Demulsification versus Transitional Phase Inversion. *Langmuir* **2004**, *20* (18), 7422–7429.
- (68) Tsuji, S.; Kawaguchi, H. Thermosensitive Pickering Emulsion Stabilized by Poly(N-Isopropylacrylamide)-Carrying Particles. *Langmuir* **2008**, *24* (7), 3300–3305.
- (69) Kumar, M.; Misra, A.; Babbar, A. K.; Mishra, A. K.; Mishra, P.; Pathak, K. Intranasal Nanoemulsion Based Brain Targeting Drug Delivery System of Risperidone. *Int. J. Pharm.* **2008**, *358* (1–2), 285–291.
- (70) Lovelyn, C.; Attama, A. A. Current State of Nanoemulsions in Drug Delivery. *J. Biomater. Nanobiotechnol.* **2011**, *2* (5), 626–639.
- (71) Shakeel, F.; Baboota, S.; Ahuja, A.; Ali, J.; Aqil, M.; Shafiq, S. Nanoemulsions as Vehicles For Transdermal Delivery Of aceclofenac. *AAPS Pharm. Sci. Tech* **2007**, *8* (4), 104.
- (72) Zhang, Y.; Shang, Z.; Gao, C.; Du, M.; Xu, S.; Song, H.; Liu, T. Nanoemulsion for Solubilization, Stabilization, and In Vitro Release of Pterostilbene for Oral Delivery. *AAPS PharmSciTech* **2014**, *15* (4), 1000–1008.
- (73) Kim, J. H.; Ko, J. A.; Kim, J. T.; Cha, D. S.; Cho, J. H.; Park, H. J.; Shin, G. H. Preparation of a Capsaicin-Loaded Nanoemulsion for Improving Skin Penetration. *J. Agric. Food Chem.* **2014**, *62* (3), 725–732.

- (74) Landfester, K. Miniemulsion Polymerization and the Structure of Polymer and Hybrid Nanoparticles. *Angew. Chemie - Int. Ed.* **2009**, *48* (25), 4488–4508.
- (75) Alvarado, A. G.; Nolla, J.; Rabelero, M.; Pérez-Carrillo, L. A.; Arellano, M.; Mendizábal, E.; Solans, C.; Puig, J. E. Poly(Hexyl Methacrylate) Nanoparticles Templating in Nanoemulsions-Made by Phase Inversion Temperature. *J. Macromol. Sci. Part A Pure Appl. Chem.* **2013**, *50* (4), 385–391.
- (76) McClements, D. J. Nanoemulsions versus Microemulsions: Terminology, Differences, and Similarities. *Soft Matter* **2012**, *8* (6), 1719–1729.
- (77) Leong, T. S. H.; Wooster, T. J.; Kentish, S. E.; Ashokkumar, M. Minimising Oil Droplet Size Using Ultrasonic Emulsification. *Ultrason. Sonochem.* **2009**, *16* (6), 721–727.
- (78) Mahdi Jafari, S.; He, Y.; Bhandari, B. Nano-Emulsion Production by Sonication and Microfluidization - A Comparison. *Int. J. Food Prop.* **2006**, *9* (3), 475–485.
- (79) Calligaris, S.; Plazzotta, S.; Bot, F.; Grasselli, S.; Malchiodi, A.; Anese, M. Nanoemulsion Preparation by Combining High Pressure Homogenization and High Power Ultrasound at Low Energy Densities. *Food Res. Int.* **2016**, *83*, 25–30.
- (80) Solans, C.; Solé, I. Nano-Emulsions: Formation by Low-Energy Methods. *Curr. Opin. Colloid Interface Sci.* **2012**, *17* (5), 246–254.
- (81) Anton, N.; Vandamme, T. F. The Universality of Low-Energy Nano-Emulsification. *Int. J. Pharm.* **2009**, *377* (1–2), 142–147.
- (82) Anton, N.; Gayet, P.; Benoit, J. P.; Saulnier, P. Nano-Emulsions and Nanocapsules by the PIT Method: An Investigation on the Role of the Temperature Cycling on the Emulsion Phase Inversion. *Int. J. Pharm.* **2007**, *344* (1–2), 44–52.
- (83) Fernandez, P.; André, V.; Rieger, J.; Kühnle, A. Nano-Emulsion Formation by Emulsion Phase Inversion. *Colloids Surfaces A Physicochem. Eng. Asp.* **2004**, *251* (1–3), 53–58.
- (84) Miller, C. A. Spontaneous Emulsification Produced by Diffusion - A Review. *Colloids and Surfaces* **1988**, *29* (1), 89–102.
- (85) Solans, C.; Morales, D.; Homs, M. Spontaneous Emulsification. *Curr. Opin. Colloid Interface Sci.* **2016**, *22*, 88–93.
- (86) López-Montilla, J. C.; Herrera-Morales, P. E.; Pandey, S.; Shah, D. O. Spontaneous Emulsification: Mechanisms, Physicochemical Aspects, Modeling, and Applications. *J. Dispers. Sci. Technol.* **2002**, *23* (1–3), 219–268.

- (87) Ruschak, K. J.; Miller, C. A. Spontaneous Emulsification in Ternary Systems with Mass Transfer. *Ind. Eng. Chem. Fundam.* **1972**, *11* (4), 534–540.
- (88) Shahidzadeh, N.; Bonn, D.; Meunier, J.; Nabavi, M.; Airiau, M.; Morvan, M. Dynamics of Spontaneous Emulsification for Fabrication of Oil in Water Emulsions. *Langmuir* **2000**, *16* (25), 9703–9708.
- (89) Shahidzadeh, N.; Bonn, D.; Meunier, J. A New Mechanism of Spontaneous Emulsification: Relation to Surfactant Properties. *Europhys. Lett.* **1997**, *40* (4), 459–464.
- (90) Greiner, R. W.; Evans, D. F. Spontaneous Formation of A Water-Continuous Emulsion from a W/O Microemulsion. *Langmuir* **1990**, *6* (12), 1793–1796.
- (91) Kunieda, H.; Fukui, Y.; Uchiyama, H.; Solans, C. Spontaneous Formation of Highly Concentrated Water-in-Oil Emulsions (Gel-Emulsions). *Langmuir* **1996**, *12* (9), 2136–2140.
- (92) Forgiarini, A.; Esquena, J.; González, C.; Solans, C. Formation of Nano-Emulsions by Low-Energy Emulsification Methods at Constant Temperature. *Langmuir* **2001**, *17* (7), 2076–2083.
- (93) Foster, L. M.; Worthen, A. J.; Foster, E. L.; Dong, J.; Roach, C. M.; Metaxas, A. E.; Hardy, D.; Larsen, E. S.; Bollinger, J. A.; Truskett, T. M.; et al. High Interfacial Activity of Polymers “Grafted through” Functionalized Iron Oxide Nanoparticle Clusters. *Langmuir* **2014**, *30*, 10188–10196.
- (94) Erni, P.; Fischer, P.; Windhab, E. J.; Kusnezov, V.; Stettin, H.; Läger, J. Stress- and Strain-Controlled Measurements of Interfacial Shear Viscosity and Viscoelasticity at Liquid/Liquid and Gas/Liquid Interfaces. *Rev. Sci. Instrum.* **2003**, *74* (11), 4916–4924.
- (95) Krägel, J.; Derkatch, S. R. Interfacial Shear Rheology. *Curr. Opin. Colloid Interface Sci.* **2010**, *15* (4), 246–255.
- (96) Krägel, J.; Derkatch, S. R.; Miller, R. Interfacial Shear Rheology of Protein-Surfactant Layers. *Adv. Colloid Interface Sci.* **2008**, *144* (1–2), 38–53.
- (97) Verwijlen, T.; Leiske, D. L.; Moldenaers, P.; Vermant, J.; Fuller, G. G. Extensional Rheometry at Interfaces: Analysis of the Cambridge Interfacial Tensiometer. *J. Rheol. (N. Y. N. Y.)* **2012**, *56* (5), 1225.
- (98) Jones, D. B.; Middelberg, A. P. . Direct Determination of the Mechanical Properties of an Interfacially Adsorbed Protein Film. *Chem. Eng. Sci.* **2002**, *57* (10), 1711–1722.

- (99) Dimitrijevic-Dwyer, M.; Middelberg, A. P. J. The Extensional Viscoelasticity of Protein-Coated Interfaces. *Soft Matter* **2011**, *7* (17), 7772–7781.
- (100) Evans, E. A. Bending Elastic Modulus of Red Blood Cell Membrane Derived from Buckling Instability in Micropipet Aspiration Tests. *Biophys. J.* **1983**, *43* (1), 27–30.
- (101) Evans, E.; Rawicz, W. Entropy-Driven Tension and Bending Elasticity in Condensed-Fluid Membranes. *Phys. Rev. Lett.* **1990**, *64* (17), 2094–2097.
- (102) Döbereiner, H. G. Properties of Giant Vesicles. *Curr. Opin. Colloid Interface Sci.* **2000**, *5* (3–4), 256–263.
- (103) Cervantes Martinez, A.; Rio, E.; Delon, G.; Saint-Jalmes, A.; Langevin, D.; Binks, B. P. On the Origin of the Remarkable Stability of Aqueous Foams Stabilised by Nanoparticles: Link with Microscopic Surface Properties. *Soft Matter* **2008**, *4* (7), 1531–1535.
- (104) Freer, E. M.; Yim, K. S.; Fuller, G. G.; Radke, C. J. Interfacial Rheology of Globular and Flexible Proteins at the Hexadecane/Water Interface: Comparison of Shear and Dilatation Deformation. *J. Phys. Chem. B* **2004**, *108*, 3835–3844.
- (105) Ganzevles, R. A.; Zinoviadou, K.; van Vliet, T.; Cohen Stuart, M. A.; de Jongh, H. H. J. Modulating Surface Rheology by Electrostatic Protein / Polysaccharide Interactions. *Langmuir* **2006**, *108* (16), 10089–10096.
- (106) Monteux, C.; Fuller, G. G.; Bergeron, V. Shear and Dilational Surface Rheology of Oppositely Charged Polyelectrolyte/Surfactant Microgels Adsorbed at the Air-Water Interface . Influence on Foam Stability. *J. Phys. Chem. B* **2004**, *108*, 16473–16482.
- (107) Bhattacharyya, A.; Monroy, F.; Langevin, D.; Argillier, J. F. Surface Rheology and Foam Stability of Mixed Surfactant-Polyelectrolyte Solutions. *Langmuir* **2000**, *16* (23), 8727–8732.
- (108) Rao, C. N. R.; Kulkarni, G. U.; Agrawal, V. V.; Gautam, U. K.; Ghosh, M.; Tumkurkar, U. Use of the Liquid-Liquid Interface for Generating Ultrathin Nanocrystalline Films of Metals, Chalcogenides, and Oxides. *J. Colloid Interface Sci.* **2005**, *289* (2), 305–318.
- (109) Hu, L.; Chen, M.; Fang, X.; Wu, L. Oil-Water Interfacial Self-Assembly: A Novel Strategy for Nanofilm and Nanodevice Fabrication. *Chem. Soc. Rev.* **2012**, *41* (3), 1350–1362.
- (110) Raaijmakers, M. J. T.; Benes, N. E. Current Trends in Interfacial Polymerization Chemistry. *Prog. Polym. Sci.* **2016**, *63*, 86–142.

- (111) Manor, O.; Chau, T. T.; Stevens, G. W.; Chan, D. Y. C.; Grieser, F.; Dagastine, R. R. Polymeric Stabilized Emulsions: Steric Effects and Deformation in Soft Systems. *Langmuir* **2012**, *28* (10), 4599–4604.
- (112) Lazaridis, N.; Alexopoulos, A. H.; Chatzi, E. G.; Kiparissides, C. Steric Stabilization in Emulsion Polymerization Using Oligomeric Nonionic Surfactants. *Chem. Eng. Sci.* **1999**, *54* (15–16), 3251–3261.
- (113) Halperin, A.; Pincus, P. Polymers at a Liquid-Liquid Interface. *Macromolecules* **1986**, *19* (1), 79–84.
- (114) Gragson, D. E.; Jensen, J. M.; Baker, S. M. Characterization of Predominantly Hydrophobic Poly(Styrene)-Poly(Ethylene Oxide) Copolymers at Air/Water and Cyclohexane/Water Interfaces. *Langmuir* **1999**, *15* (19), 6127–6131.
- (115) Netz, R. R.; Andelman, D. Neutral and Charged Polymers at Interfaces. *Phys. Rep.* **2003**, *380* (1–2), 1–95.
- (116) Kawaguchi, M.; Tohyama, M.; Mutoh, Y.; Takahashi, A. Ellipsometric Study of Polymer Monolayers Spread at the Air-Water Interface. 1. Thickness of Monolayers. *Langmuir* **1988**, *4* (2), 407–410.
- (117) Rother, G.; Findenegg, G. H. Monolayer Films of PS-b-PEO Diblock Copolymers at the Air/Water- and an Oil/Water-Interface. *Colloid Polym. Sci.* **1998**, *276* (6), 496–502.
- (118) Taddese, T.; Carbone, P.; Cheung, D. L. Thermodynamics of Linear and Star Polymers at Fluid Interfaces. *Soft Matter* **2015**, *11* (1), 81–93.
- (119) Peleshanko, S.; Jeong, J.; Gunawidjaja, R.; Tsukruk, V. V. Amphiphilic Heteroarm PEO-b-PS MStar Polymers at the Air–Water Interface: Aggregation and Surface Morphology. *Macromolecules* **2004**, *37*, 6511–6522.
- (120) Francis, R.; Skolnik, A. M.; Carino, S. R.; Logan, J. L.; Underhill, R. S.; Angot, S.; Taton, D.; Gnanou, Y.; Duran, R. S. Aggregation and Surface Morphology of a Poly(Ethylene Oxide)-Block-Polystyrene Three-Arm Star Polymer at the Air/Water Interface Studied by AFM. *Macromolecules* **2002**, *35* (17), 6483–6485.
- (121) Schwenke, K.; Isa, L.; Cheung, D. L.; Del Gado, E. Conformations and Effective Interactions of Polymer-Coated Nanoparticles at Liquid Interfaces. *Langmuir* **2014**, *30* (42), 12578–12586.
- (122) Quan, X.; Peng, C. W.; Dong, J.; Zhou, J. Structural Properties of Polymer-Brush-Grafted Gold Nanoparticles at the Oil-Water Interface: Insights from Coarse-Grained Simulations.

Soft Matter **2016**, *12* (14), 3352–3359.

- (123) Gao, H.; Matyjaszewski, K. Synthesis of Functional Polymers with Controlled Architecture by CRP of Monomers in the Presence of Cross-Linkers: From Stars to Gels. *Prog. Polym. Sci.* **2009**, *34* (4), 317–350.
- (124) Gao, H.; Matyjaszewski, K. Synthesis of Star Polymers by A New “Core-First” Method: Sequential Polymerization of Cross-Linker and Monomer. *Macromolecules* **2008**, *41* (4), 1118–1125.
- (125) Gao, H.; Matyjaszewski, K. Arm-First Method as a Simple and General Method for Synthesis of Miktoarm Star Copolymers. *J. Am. Chem. Soc.* **2007**, *129* (38), 11828–11834.
- (126) Matyjaszewski, K.; Xia, J. Atom Transfer Radical Polymerization. *Chem. Rev.* **2001**, *101* (9), 2921–2990.
- (127) Matyjaszewski, K. Atom Transfer Radical Polymerization (ATRP): Current Status and Future Perspectives. *Macromolecules* **2012**, *45* (10), 4015–4039.
- (128) Riley, J. K. Friction Control by Adsorption of Polymer Brush Nanoparticles, Carnegie Mellon University, 2016.
- (129) Zhang, M.; Liu, L.; Zhao, H.; Yang, Y.; Fu, G.; He, B. Double-Responsive Polymer Brushes on the Surface of Colloid Particles. *J. Colloid Interface Sci.* **2006**, *301* (1), 85–91.
- (130) Bonkovoski, L. C.; Martins, A. F.; Bellettini, I. C.; Garcia, F. P.; Nakamura, C. V.; Rubira, A. F.; Muniz, E. C. Polyelectrolyte Complexes of Poly[(2-Dimethylamino) Ethyl Methacrylate]/Chondroitin Sulfate Obtained at Different PHs: I. Preparation, Characterization, Cytotoxicity and Controlled Release of Chondroitin Sulfate. *Int. J. Pharm.* **2014**, *477* (1–2), 197–207.
- (131) Binks, B. P.; Lumsdon, S. O. Catastrophic Phase Inversion of Water-in-Oil Emulsions Stabilized by Hydrophobic Silica. *Langmuir* **2000**, *16* (6), 2539–2547.
- (132) Stauffer, C. E. The Measurement of Surface Tension by the Pendant Drop Technique. *J. Phys. Chem.* **1965**, *69* (6), 1933–1938.
- (133) Kralchevsky, P. A.; Eriksson, J. C.; Ljunggren, S. Theory of Curved Interfaces and Membranes: Mechanical and Thermodynamical Approaches. *Adv. Colloid Interface Sci.* **1994**, *48* (C), 19–59.
- (134) Kaoui, B.; Ristow, G. H.; Cantat, I.; Misbah, C.; Zimmermann, W. Lateral Migration of a

- Two-Dimensional Vesicle in Unbounded Poiseuille Flow. *Phys. Rev. E - Stat. Nonlinear, Soft Matter Phys.* **2008**, *77* (2), 1–9.
- (135) Kotula, A. P.; Anna, S. L. Regular Perturbation Analysis of Small Amplitude Oscillatory Dilatation of an Interface in a Capillary Pressure Tensiometer. *J. Rheol.* **2015**, *59* (1), 85–117.
- (136) Zuidema, H.; Waters, G. Ring Method for the Determination of Interfacial Tension. *Ind. Eng. Chem. Anal. Ed.* **1941**, *13* (5), 312–313.
- (137) Cupples, H. L. Interfacial Tension by the Ring Method: The Benzene-Water Interface. *J. Phys. Chem.* **1947**, *51* (6), 1341–1345.
- (138) Beaglehole, D. Ellipsometric Study of the Surface of Simple Liquids. *Physica B C* **1980**, *100* (2), 163–174.
- (139) Benjamins, J. W.; Jönsson, B.; Thuresson, K.; Nylander, T. New Experimental Setup to Use Ellipsometry to Study Liquid-Liquid and Liquid-Solid Interfaces. *Langmuir* **2002**, *18* (16), 6437–6444.
- (140) Azzam, R. M. A.; Bashara, N. M. *Ellipsometry and Polarized Light*, 1st ed.; North-Holland: Amsterdam, 1987.
- (141) De Feijter, J.; Benjamins, J.; Veer, F. Ellipsometry as a Tool to Study the Adsorption Behavior of Synthetic and Biopolymers at the Air Water Interface. *Biopolymers* **1978**, *17* (7), 1759–1772.
- (142) Barnett, C. E. Some Applications of Wave-Length Turbidimetry in the Infrared. *J. Phys. Chem.* **1942**, *46* (1), 69–75.
- (143) Cao, B. H.; Kim, M. W. Molecular Weight Dependence of the Surface Tension of Aqueous Poly(Ethylene Oxide) Solutions. *Faraday Discuss.* **1994**, *98*, 245–252.
- (144) Fleeer, G. J.; Cohen Stuart, M. A.; Scheutjens, J. M. H. M.; Cosgrove, T.; Vincent, B. *Polymers at Interfaces*, 1st ed.; Chapman & Hall: London, 1993.
- (145) Petkov, J. T.; Gurkov, T. D.; Campbell, B. E.; Borwankar, R. P. Dilatational and Shear Elasticity of Gel-like Protein Layers on Air/Water Interface. *Langmuir* **2000**, *16* (8), 3703–3711.
- (146) Erni, P.; Fischer, P.; Windhab, E. J. Sorbitan Tristearate Layers at the Air/Water Interface Studied by Shear and Dilatational Interfacial Rheology. *Langmuir* **2005**, *21* (23), 10555–10563.

- (147) Safouane, M.; Langevin, D.; Binks, B. P. Effect of Particle Hydrophobicity on the Properties of Silica Particle Layers at the Air-Water Interface. *Langmuir* **2007**, *23* (23), 11546–11553.
- (148) Díez-Pascual, A. M.; Monroy, F.; Ortega, F.; Rubio, R. G.; Miller, R.; Noskov, B. A. Adsorption of Water-Soluble Polymers with Surfactant Character. Dilational Viscoelasticity. *Langmuir* **2007**, *23* (7), 3802–3808.
- (149) Cao, B. H.; Kim, M. W. Adsorption Layer Effects on Surface Waves at the Polyethyleneoxide (PEO) Solution/Air Interface. *Europhys. Lett.* **1995**, *29* (7), 555–560.
- (150) Dunér, G.; Thormann, E.; Dédinaïté, A.; Claesson, P. M.; Matyjaszewski, K.; Tilton, R. D. Nanomechanical Mapping of a High Curvature Polymer Brush Grafted from a Rigid Nanoparticle. *Soft Matter* **2012**, *8*, 8312–8320.
- (151) Pagac, E. S.; Prieve, D. C.; Solomentsev, Y.; Tilton, R. D. A Comparison of Polystyrene-Poly(Ethylene Oxide) Diblock Copolymer and Poly(Ethylene Oxide) Homopolymer Adsorption from Aqueous Solutions. *Langmuir* **1997**, *13* (11), 2993–3001.
- (152) Kapilashrami, A.; Malmsten, M.; Eskilsson, K.; Benjamins, J. W.; Nylander, T. Ellipsometric Studies of Nonionic Block Copolymers Adsorbed at the Solid/Water and Oil/Water Interfaces. *Colloids Surfaces A Physicochem. Eng. Asp.* **2003**, *225* (1–3), 181–192.
- (153) Flood, C.; Cosgrove, T.; Howell, I.; Revell, P. Effects of Electrolytes on Adsorbed Polymer Layers: Poly (Ethylene Oxide)-Silica System. *Langmuir* **2006**, *22* (16), 6923–6930.
- (154) Trens, P.; Denoyel, R. Conformation of Poly(Ethylene Glycol) Polymers at the Silica/Water Interface: A Microcalorimetric Study. *Langmuir* **1993**, *9* (2), 519–522.
- (155) Chremos, A.; Camp, P. J.; Glynos, E.; Koutsos, V. Adsorption of Star Polymers : Computer Simulations. *Soft Matters* **2010**, *6*, 1483–1493.
- (156) Good, R. J.; Girifalco, L. a. A Theory for Estimation of Surface and Interfacial Energies. I. Derivation and Application to Interfacial Tension. *J. Phys. Chem.* **1960**, *24* (13), 561–565.
- (157) Lord, D. L.; Demond, A. H.; Hayes, K. F. Effects of Organic Base Chemistry on Interfacial Tension, Wettability, and Capillary Pressure in Multiphase Subsurface Waste Systems. *Transp. Porous Media* **2000**, *38* (1), 79–92.
- (158) Demond, A. H.; Lindner, A. S. Estimation of Interfacial Tension between Organic Liquids

- and Water. *Environ. Sci. Technol.* **1993**, 27 (12), 2318–2331.
- (159) Alvarez, N. J.; Walker, L. M.; Anna, S. L. A Microtensiometer to Probe the Effect of Radius of Curvature on Surfactant Transport to a Spherical Interface. *Langmuir* **2010**, 26 (16), 13310–13319.
- (160) Shahidzadeh, N.; Bonn, D.; Aguerre-Chariol, O.; Meunier, J. Spontaneous Emulsification: Relation to Microemulsion Phase Behaviour. *Colloids Surfaces A Physicochem. Eng. Asp.* **1999**, 147 (3), 375–380.
- (161) Nylander, T.; Hamraoui, A.; Paulsson, M. Interfacial Properties of Whey Proteins at Air/Water and Oil/Water Interfaces Studied by Dynamic Drop Tensiometry, Ellipsometry and Spreading Kinetics. *Int. J. Food Sci. Technol.* **1999**, 34 (5–6), 573–585.
- (162) Dong, Z.; Wei, H.; Mao, J.; Wang, D.; Yang, M.; Bo, S.; Ji, X. Synthesis and Responsive Behavior of Poly(N,N-Dimethylaminoethyl Methacrylate) Brushes Grafted on Silica Nanoparticles and Their Quaternized Derivatives. *Polymer (Guildf)*. **2012**, 53 (10), 2074–2084.
- (163) Schepelina, O.; Zharov, I. Poly (2-(Dimethylamino) Ethyl Methacrylate)-Modified Nanoporous Colloidal Films with PH and Ion Response. *Langmuir* **2008**, 24 (28), 14188–14194.
- (164) Zhou, L.; Yuan, W.; Yuan, J.; Hong, X. Preparation of Double-Responsive SiO₂-g-PDMAEMA Nanoparticles via ATRP. *Mater. Lett.* **2008**, 62 (8–9), 1372–1375.
- (165) Kusumo, A.; Bombalski, L.; Lin, Q.; Matyjaszewski, K.; Schneider, J. W.; Tilton, R. D. High Capacity, Charge-Selective Protein Uptake by Polyelectrolyte Brushes. *Langmuir* **2007**, 23 (8), 4448–4454.
- (166) Cohen Stuart, M. A.; Hoogendam, C. W.; de Keizer, A. Kinetics of Polyelectrolyte Adsorption. *J. Phys. Condens. Matter* **1997**, 9 (37), 7767.
- (167) Stefaniu, C.; Chanana, M.; Wang, D.; Novikov, D. V.; Brezesinski, G.; Möhwald, H. Biocompatible Magnetite Nanoparticles Trapped at the Air/Water Interface. *ChemPhysChem* **2010**, 11 (17), 3585–3588.
- (168) Stubenrauch, C.; Miller, R. Stability of Foam Films and Surface Rheology: An Oscillating Bubble Study at Low Frequencies. *J. Phys. Chem. B* **2004**, 108 (20), 6412–6421.
- (169) Fruhner, H.; Wantke, K. D.; Lunkenheimer, K. Relationship between Surface Dilational Properties and Foam Stability. *Colloids Surfaces A Physicochem. Eng. Asp.* **2000**, 162 (1–3), 193–202.

- (170) Wantke, K.; Malysa, K.; Lunkenheimer, K. A Relation between Dynamic Foam Stability and Surface Elasticity. *Colloids Surfaces A Physicochem. Eng. Asp.* **1994**, *82* (2), 183–191.
- (171) Yim, H.; Kent, M.; Matheson, A.; Ivkov, R.; Satija, S.; Majewski, J.; Smith, G. S. Adsorption of Polystyrene Sulfonate to the Air Surface of Water by Neutron Reflectivity. *Macromolecules* **2000**, *33* (16), 6126–6133.
- (172) Petkova, R.; Tcholakova, S.; Denkov, N. D. Foaming and Foam Stability for Mixed Polymer-Surfactant Solutions: Effects of Surfactant Type and Polymer Charge. *Langmuir* **2012**, *28* (11), 4996–5009.
- (173) Georgieva, D.; Schmitt, V.; Leal-Calderon, F.; Langevin, D. On the Possible Role of Surface Elasticity in Emulsion Stability. *Langmuir* **2009**, *25* (10), 5565–5573.
- (174) Santini, E.; Liggieri, L.; Sacca, L.; Clause, D.; Ravera, F. Interfacial Rheology of Span 80 Adsorbed Layers at Paraffin Oil-Water Interface and Correlation with the Corresponding Emulsion Properties. *Colloids Surfaces A Physicochem. Eng. Asp.* **2007**, *309* (1–3), 270–279.
- (175) Lucassen-Reynders, E. H.; Cagna, A.; Lucassen, J. Gibbs Elasticity, Surface Dilational Modulus and Diffusional Relaxation in Nonionic Surfactant Monolayers. *Colloids Surfaces A Physicochem. Eng. Asp.* **2001**, *186* (1–2), 63–72.
- (176) Daniel-David, D.; Pezron, I.; Clause, D.; Dalmazzone, C.; Noik, C.; Komunjer, L. Interfacial Properties of a Silicone Copolymer Demulsifier at the Air/Water Interface. *Phys. Chem. Chem. Phys.* **2004**, *6* (7), 1570–1574.
- (177) Bos, M. A.; Van Vliet, T. Interfacial Rheological Properties of Adsorbed Protein Layers and Surfactants: A Review. *Adv. Colloid Interface Sci.* **2001**, *91* (3), 437–471.
- (178) Sun, H. Q.; Zhang, L.; Li, Z. Q.; Song, X. W.; Cao, X. L.; Zhao, S.; Zheng, L.; Yu, J. Y. Effect of Alkyl Chain Length on the Surface Dilational Rheological and Foam Properties of N-Acyltaurate Amphiphiles. *Colloid Polym. Sci.* **2012**, *290* (1), 31–40.
- (179) Bouchemal, K.; Briançon, S.; Perrier, E.; Fessi, H. Nano-Emulsion Formulation Using Spontaneous Emulsification: Solvent, Oil and Surfactant Optimisation. *Int. J. Pharm.* **2004**, *280* (1–2), 241–251.
- (180) Komaiko, J.; McClements, D. J. Low-Energy Formation of Edible Nanoemulsions by Spontaneous Emulsification: Factors Influencing Particle Size. *J. Food Eng.* **2015**, *146*, 122–128.

- (181) Wulff-Pérez, M.; Martín-Rodríguez, A.; Gálvez-Ruiz, M. J.; De Vicente, J. The Effect of Polymeric Surfactants on the Rheological Properties of Nanoemulsions. *Colloid Polym. Sci.* **2013**, *291* (3), 709–716.
- (182) Tadros, T.; Izquierdo, P.; Esquena, J.; Solans, C. Formation and Stability of Nano-Emulsions. *Adv. Colloid Interface Sci.* **2004**, *108–109*, 303–318.
- (183) Lee, G. W. J.; Tadros, T. F. Formation and Stability of Emulsions Produced by Dilution of Emulsifiable Concentrates. Part II. The Influence of Surfactant Concentration on the Stability of Oil-in-Water Emulsions. *Colloids and Surfaces* **1982**, *5* (2), 117–127.
- (184) Lamaallam, S.; Bataller, H.; Dicharry, C.; Lachaise, J. Formation and Stability of Miniemulsions Produced by Dispersion of Water/Oil/Surfactants Concentrates in a Large Amount of Water. *Colloids Surfaces A Physicochem. Eng. Asp.* **2005**, *270–271* (1–3), 44–51.
- (185) Pouton, C. W. Formulation of Self-Emulsifying Drug Delivery Systems. *Adv. Drug Deliv. Rev.* **1997**, *25* (1), 47–58.
- (186) Wang, L.; Dong, J.; Chen, J.; Eastoe, J.; Li, X. Design and Optimization of a New Self-Nanoemulsifying Drug Delivery System. *J. Colloid Interface Sci.* **2009**, *330* (2), 443–448.
- (187) Kommuru, T. R.; Gurley, B.; Khan, M. A.; Reddy, I. K. Self-Emulsifying Drug Delivery Systems (SEDDS) of Coenzyme Q10: Formulation Development and Bioavailability Assessment. *Int. J. Pharm.* **2001**, *212* (2), 233–246.
- (188) Yoo, J. H.; Shanmugam, S.; Thapa, P.; Lee, E. S.; Balakrishnan, P.; Baskaran, R.; Yoon, S. K.; Choi, H. G.; Yong, C. S.; Yoo, B. K.; et al. Novel Self-Nanoemulsifying Drug Delivery System for Enhanced Solubility and Dissolution of Lutein. *Arch. Pharm. Res.* **2010**, *33* (3), 417–426.
- (189) Kaminski, A.; McBain, J. W. Spontaneous Emulsification of Pure Xylene in an Aqueous Solution through Mere Adsorption of a Detergent in the Interface. *Proc. R. Soc. London. Ser. A. Math. Phys. Sci.* **1949**, *198* (1055), 447–454.
- (190) Komaiko, J.; McClements, D. J. Optimization of Isothermal Low-Energy Nanoemulsion Formation: Hydrocarbon Oil, Non-Ionic Surfactant, and Water Systems. *J. Colloid Interface Sci.* **2014**, *425*, 59–66.
- (191) Gallová, J.; Uhríková, D.; Hanulová, M.; Teixeira, J.; Balgavý, P. Bilayer Thickness in Unilamellar Extruded 1,2-Dimyristoleoyl and 1,2-Dierucoyl Phosphatidylcholine Vesicles: SANS Contrast Variation Study of Cholesterol Effect. *Colloids Surfaces B Biointerfaces* **2004**, *38* (1–2), 11–14.

- (192) Kučerka, N.; Kiselev, M. A.; Balgavý, P. Determination of Bilayer Thickness and Lipid Surface Area in Unilamellar Dimyristoylphosphatidylcholine Vesicles from Small-Angle Neutron Scattering Curves: A Comparison of Evaluation Methods. *Eur. Biophys. J.* **2004**, *33* (4), 328–334.
- (193) Nawroth, T.; Conrad, H.; Dose, K. Neutron Small Angle Scattering of Liposomes in the Presence of Detergents. *Phys. B Phys. Condens. Matter* **1989**, *156–157* (C), 477–480.
- (194) Balgavý, P.; Dubničková, M.; Kučerka, N.; Kiselev, M. A.; Yaradaikin, S. P.; Uhríková, D. Bilayer Thickness and Lipid Interface Area in Unilamellar Extruded 1,2-Diacylphosphatidylcholine Liposomes: A Small-Angle Neutron Scattering Study. *Biochim. Biophys. Acta - Biomembr.* **2001**, *1512* (1), 40–52.
- (195) McKelvey, C. A.; Kaler, E. W. Characterization of Nanostructured Hollow Polymer Spheres with Small-Angle Neutron Scattering (SANS). *J. Colloid Interface Sci.* **2002**, *245* (1), 68–74.
- (196) Reynolds, P. A.; Gilbert, E. P.; White, J. W. High Internal Phase Water-in-Oil Emulsions Studied by Small-Angle Neutron Scattering. *J. Phys. Chem. B* **2000**, *104* (30), 7012–7022.
- (197) Reynolds, P. A.; Gilbert, E. P.; White, J. W. High Internal Phase Water-in-Oil Emulsions and Related Microemulsions Studied by Small Angle Neutron Scattering. 2: The Distribution of Surfactant. *J. Phys. Chem. B* **2001**, *105* (29), 6925–6932.
- (198) Staples, E.; Penfold, J.; Tucker, I. Adsorption of Mixed Surfactants at the Oil–Water Interface. *J. Phys. Chem. B* **2000**, *104* (3), 606–614.
- (199) Larson-Smith, K.; Jackson, A.; Pozzo, D. C. Small Angle Scattering Model for Pickering Emulsions and Raspberry Particles. *J. Colloid Interface Sci.* **2010**, *343* (1), 36–41.
- (200) Pisarchick, M. L.; Gesty, D.; Thompson, N. L. Binding Kinetics of an Anti-Dinitrophenyl Monoclonal Fab on Supported Phospholipid Monolayers Measured by Total Internal Reflection with Fluorescence Photobleaching Recovery. *Biophys. J.* **1992**, *63* (1), 215–223.